DOCTOR OF PHILOSOPHY

Investigating the potential of remote sensing for long-term limnological analysis at pan-continental scales

Politi, Eirini

Award date:
2010

DOCTOR OF PHILOSOPHY

Investigating the potential of remote sensing for long-term limnological analysis at pan-continental scales

Eirini Politi

2010

University of Dundee

Chapter I.

INTRODUCTION

1.1 Definition and importance of lakes

Lakes are microcosms of life with a distinctive structure (Horne & Goldman, 1994) and dynamic ecosystems that vary greatly in their characteristics. According to Reid (1961), "Lakes defy precise definition, chiefly because of the diversity of ways in which they originate, because they change with age, and because numerous features of them differ latitudinally" (Reid, 1961, p.13). Generally, lakes are relatively large bodies of standing water, known as lentic environments, occupying a basin and have a surface area larger than 0.01 km^2 (1 ha) and water depth of at least 1 m (US EPA, 2008; CEN, 2010). They are typically deep enough to stratify thermally (Welch, 1935). A lake could be also defined as a body of water in which the residence time is long, varying from a few years up to thousands of years (Hickling, 1975), though many have considerably shorter residence times (e.g. Bennion *et al*., 2005). Although lakes fall into the category of standing water systems, a certain amount of water movement occurs driven by processes, such as wave action, internal currents and/or coherent flow in the vicinity of inlets and outlets (Welch, 1935).

Lakes are important to people for their ecological, economic and cultural values (UNEP, 2000; Sawaya *et al*., 2003). On one hand, lakes are rich and dynamic ecosystems that support various forms of aquatic and terrestrial life, including large migrating bird populations, providing us at the same time with considerable amounts

of drinking water. On the other hand, they host multiple socioeconomic activities (EUROPA WFD, 2009). In fact, the majority of anthropogenic activities are accumulated in areas where land neighbours water, such as lakes. For example, fishing, industrial and urban development, water sports and other leisure activities are some of the main activities that usually take place in and around lakes (UNEP, 2000).

1.2 European lakes as indicators of environmental change

The above mentioned values of lakes can sometimes be threatened because lakes undergo changes through time, common with all dynamic environmental systems (Welch, 1935). Changes in lakes occur due to (a) natural drivers and (b) anthropogenic drivers.

1.2.1 Natural drivers of lake change

Several factors may influence the morphology, the physico-chemical and biological conditions in lakes as they age with time, altering the lake characteristics and even leading to their destruction. The main destructive forces are (a) scouring of the basin due to the action of water, sand and gravel movement, and (b) natural tendency towards infilling by autochthonous organic material and incoming soil and sediment (Maitland, 1990). These processes occur at varying yet long temporal scales, for example, in small lakes infilling can take place in less than a century, but it takes thousands of years in larger lakes (Hickling, 1975).

Natural climatic fluctuations can also affect lake ecosystems. In the past, the Earth's climate has undergone periodic natural fluctuations where alternating cool and warm periods have occurred over time scales ranging from hundreds to thousands of years, depending on the causative factors (e.g. variations in the Earth's orbital characteristics) (e.g. Bonan, 2002; Houghton, 2004). Several studies have shown that lakes are sensitive indicators of climate fluctuations (e.g. De Stasio *et al*., 1996). Lakes that are located in different climatic regions and many kilometres apart, can be shown to exhibit similar response to synoptic-scale meteorological forcing, i.e. large-area patterns of pressures and wind (Livingstone & Padisak, 2007). The thermal structure of lakes has been demonstrated to follow fluctuations in four weather elements, more specifically, air temperature, cloud cover, water vapour pressure (relative humidity) and wind speed (Livingstone & Dokulil, 2001).

Also, short-term climatic fluctuations, such as variability in the North Atlantic Oscillation (NAO), can affect the ecology of lakes at continental and regional scales (e.g. Weyhenmeyer *et al*., 1999; Gerten & Adrian, 2000; Straile, 2000; Straile & Adrian, 2000; Gerten & Adrian, 2001; Livingstone & Dokulil, 2001; Weyhenmeyer *et al*., 2002). The NAO is a climatic phenomenon that occurs due to fluctuations in the differences between the Icelandic Low and the Azores High semi-permanent centres of sea-level atmospheric pressure. The phenomenon is related to the speed and direction of westerly winds and the wintertime mid-latitude storminess that affect the North Atlantic Ocean and Europe. Being the dominant atmospheric mode in the North Atlantic throughout the year, the NAO index is a key indicator of weather variability in Eurasia and North America. Since the NAO is most pronounced in winter, the winter NAO index is often used in climatic studies. The

winter NAO index is calculated for the months December-March and is believed to be strongly associated with changes in the thermal characteristics of temperate European lakes (e.g. Gerten *et al*., 2001; Livingstone & Dokulil, 2001).

A positive winter NAO index causes cooling over the oceans and warming over the continents in the regions where it occurs and *vice versa* (Hurrell, 1995). Despite the regional signature of the NAO, general temperature patterns related to the specific phenomenon have been observed and it has been shown that temperate European lakes in different geographical locations have been similarly affected by fluctuations in air temperature, which may well be attributed to variations in the NAO index (Livingstone & Padisák, 2007).

1.2.2 Anthropogenic drivers of lake change

The hydrological and geomorphological conditions in lakes are also sensitive to anthropogenic impacts. Since the Industrial Revolution in the 19th century, the exploitation of lakes has intensified and has been rather extensive, and this had immediate effects on these vulnerable ecosystems (ILEC, 2010). At a global scale, pollution from industry, urban waste, shipping, aquaculture and runoff from agricultural land has changed directly the chemical and physical, and indirectly the biological, conditions of lake water. Numerous elements that are toxic for many aquatic species have been introduced into the hydrological cycle and waters have tended to become more eutrophic and undrinkable, whilst toxic algal blooms occur more often (e.g. George 1997b). Moreover, the lakeshore operation of power plants imparts a local increase in the thermal conditions of lakes and can have an impact on the life cycle and habits of many aquatic species, such as benthic fauna and fish

(ILEC, 2010). Apart from pollution, management plans and lakeshore constructions have also altered the natural geomorphological character of numerous lakes, changing the habitats and altering the life cycles of several aquatic and terrestrial species (Foley *et al*., 2005). The above factors influence each lake individually depending on its specific characteristics and the degree of human intervention. Nevertheless, human-induced climate change has both direct and indirect impacts on all surface waters (Hickling, 1975), which need to be quantified and accounted for.

According to the UN Framework Convention on Climate Change, "Climate change is the change of climate that is attributed directly or indirectly to human activity that alters the composition of the global atmosphere and which is, in addition to natural climate variability, observed over comparable time periods" (UNFCCC, 1992, p. 3). Therefore, climate change should not be confused with climatic variability, which has been taking place for millennia, rather than being a newly introduced environmental phenomenon.

Scientific research on historical and recent climate change has shown that in the last 150 years climatic changes have occurred more rapidly than in the past (e.g. Hardy, 2003; Houghton, 2004). In fact, these changes seem to be outwith the natural variation (when compared to past historical trends) and are characterized by recent unusually warm, dry and wet climate extremes (Munasinghe & Swart, 2005). Such changes include global increases in the Earth's lower atmosphere average temperature by about 0.6 ± 0.2°C since the late 19th century (Pittock, 2005). The latter has a direct effect on the global sea-surface temperature that has increased at a rate of 0.14°C per decade in the relatively short period between 1976 and 2000

(IPCC, 2001). As a result, changes in the Earth's biota have been observed, including alterations to plant species composition, for example (Houghton, 2004). Due to increased temperatures, the water volume has expanded and with the contribution of melting polar ice, there has been an average global sea-level rise of approximately 2.4 cm per decade. In temperate regions, the frost-free season has increased and snow and ice cover have decreased. Glaciers in the European Alps are melting rapidly and have lost more than half their volume since 1850 (Hardy, 2003).

The actual effect and attribution of both natural and human-induced changes can be estimated only through thoughtful examination of simultaneous patterns of change over space and time (Page, 2006). For example, Hardy (2003) suggests that local and regional decade-long climate trends are a direct effect of human-induced climate change.

1.2.2.1 Effects of changing climate on lake water quality

The degree of lake response to climate change depends to some extent on the time scale under consideration. For example, changes in the last decade may seem insignificant when compared to those over the past million years (Hardy, 2003). Nevertheless, lakes are widely considered sensitive indicators of climate change with the potential to reveal changes and homogeneous trends even at relatively short (i.e. decadal) scales (e.g. Livingstone, 2003; Arhonditsis *et al*., 2004a). Despite that, the responsiveness of different systems owes much to their site-specific characteristics, such as the thermal structure and mixing type (Gerten & Adrian, 2001).

A range of parameters are influenced by climate change and variability, such as water temperature (e.g. Livingstone, 2003), concentrations of dissolved gases and lake water levels (e.g. Schindler *et al*., 1996), primary production (e.g. Straile, 2000) and duration of winter ice cover (e.g. Palecki & Barry; 1986; Weyhenmeyer *et al*., 2004). Lake surface temperature is considered the parameter most directly affected by climate, exhibiting strong response to climate forcing (e.g. Kondratyev & Filatov, 1999; Livingstone & Dokulil, 2001; Livingstone *et al*., 2005; Livingstone & Padisák, 2007). Important features such as stratification and mixing patterns may vary due to climatic fluctuations (e.g. Livingstone, 1997; Elo *et al*., 1998; Livingstone & Lotter, 1998), according to the degree of increase of surface water warming. Chlorophyll *a* is considered an equally important climate change indicator (e.g. Straile & Adrian, 2000; Weyhenmeyer *et al.,* 2002), as it is strongly dependant on temperature, dissolved oxygen and nutrients, whose distribution is influenced by thermal structures within the lake body, such as mixing and stratification, and upwellings (e.g. Gerten & Adrian, 2000; Jankowski *et al*., 2006; Peeters *et al*., 2007). Increases in water temperature can influence the ecological characteristics of lakes and, thus, strongly affect aquatic life. Warming can change the species composition, distribution, growth and dynamics of aquatic vegetation (Hardy, 2003; Munasinghe & Swart, 2005). Also, oxygen solubility decreases at increased temperatures affecting the aquatic biota, while changes in precipitation, evaporation patterns and stream inflows due to climatic fluctuations may also have a direct effect on the chemistry of lake water (Hardy, 2003; Munasinghe & Swart, 2005) that in turn influences water transparency (Welch, 1935; Fraser, 1998).

1.2.2.2 Possible future changes in European temperate lakes

According to future global climate prediction models, winter lake temperature is not expected to change greatly. However, summer temperatures are predicted to increase by 3 to 4°C (Hardy, 2003). Also, climatic changes are not predicted to occur homogeneously across the globe. For example, Southern and Eastern Europe is expected to suffer the most from water shortage in future years (Munasinghe & Swart, 2005), while warming is likely to be greater at higher latitudes and in mid-continental regions (Hardy, 2003). This is likely to lead to a variable response in lakes at a continental scale and requires operational systems that can identify and monitor lake response to climate change at a finer scale in order to inform international management plans and European Union policies.

1.3 The need for monitoring lakes

Due to the dynamic and variable character of lake ecosystems, their repeated monitoring is considered vital for sustainability and robust lake management, to protect them from pollution, overexploitation and ecosystem destruction (EUROPA WFD, 2009). At a European level, the EU Water Framework Directive (WFD) was introduced in 2000 to satisfy requirements for freshwater assessment and monitoring. According to this, European lakes (and other surface water bodies of Europe) have to be mapped and monitored as to their status and condition. By 2015, the ecological status of all European Union Member States lakes has to be assessed and national actions for the effective management and sustainable use of lake ecosystems need to be put into place (EUROPA WFD, 2009). The international character of the WFD has introduced the need for methods that can be widely applied over large spatial and

temporal scales and produce comparable results. As a result, reliable, transparent and transferable methodologies are needed.

1.4 The potential of remote sensing in limnological studies

Lakes have been monitored using point measurements during field sampling campaigns, but these traditional techniques usually offer limited spatial and often temporal resolution. Remote sensing has been employed at local and regional scales for lake studies, due to its ability to estimate lake properties covering large spatial scales (e.g. Gitelson *et al*., 1993; George, 1997b; Pulliainen *et al*., 2001). While the traditional methods for *in situ* lake survey are time-consuming and expensive, remote sensing techniques can acquire systematic data across wide study areas. These digital data sources are not prone to subjectivity, unlike surveyors' observations. However, the spatial and temporal reliability, and transferability of methods and relationships observed remains untested. In addition, a project studying lake response to climate change at a pan-European scale has rarely, if ever, been undertaken. Dekker and Peters (1993) suggest that accurate mapping of a small number of lakes with a wide range of characteristics, for example ranging from the clearest to the most turbid, is sufficient to map other lakes in the surrounding area, provided that atmospheric conditions are the same, or that atmospheric correction techniques are relatively accurate (i.e. the accuracy is greater than the standard deviation of the algorithms used). A similar suggestion was made by Kutser *et al*. (2005), who devised an algorithm to map water quality in lakes with different optical characteristics and in different geographic locations. The above suggest that it is possible to design a

universal methodology for the estimation of water quality parameters for European lakes using remotely sensed data.

1.5 Project rationale

This project is based on the idea of using remote sensing data in systematic limnological research over large spatial scales. The development of an operational methodology for the study of the water quality of European lakes could provide very useful information in conjunction with the study of climate change and its immediate effect upon sensitive habitats and environmental systems. The ability to study multiple sites despite the large distance separating them and the extreme differences in their ecological characteristics could offer an insight to some of the interregional drivers of change in European lakes. It could also provide feedback for the update and extension of ecological databases already containing environmental information related to European lakes and hence aid the development of management strategies.

1.6 Aims and Objectives

This project seeked to develop an operational methodology based on remote sensing that can be used to extract current and former water quality information from European lakes. The aim was to demonstrate the applicability of remote sensing with existing water quality estimation algorithms in mapping and monitoring three lake water quality parameters (temperature, chlorophyll *a* and Secchi disk depth) in European lakes with different physical, chemical, biological and geomorphological characteristics. The NERC Earth Observation Data Acquisition and Analysis Service (NEODAAS) Dundee Satellite Receiving Station (DSRS) archive was utilized for

the acquisition of historic remotely sensed data from the last three decades. Then, water quality parameters from past years were extracted from the satellite data to identify spatial and temporal patterns in the water quality of various European lakes and perform trend analysis to test for coherent changes in water quality and the ecological behaviour of the study sites.

Consequently, the objectives of the project were:

- To specify the temporal and spatial variability of the parameters under consideration in this study and, thus, to decide on the frequency of field and satellite data required
- To identify and select appropriate methodologies and algorithms to estimate water quality parameters from remotely sensed data based upon an extensive study of published literature
- To test the spatial and temporal transferability of predictive relationships defined at one site to other lakes across Europe and compare the results between lakes with different ecological characteristics
- To test the potential of NOAA AVHRR and Terra/Aqua MODIS to offer accurate estimates of the parameters under consideration within individual lakes
- To investigate trends in water quality parameters for large lakes across Europe in the past 30 years and provide reasons as to why such trends have been observed
- To make recommendations as to the required sensor characteristics, data and appropriate methods to provide an operational remote sensing-based monitoring system for lakes across regional and continental scales

1.7 Thesis outline

The thesis outline is illustrated in flowchart form in Figure 1-1.

Chapter 2 illustrates the degree of variability between lake systems focusing on hydromorphological characteristics, such as origin and shape, and other characteristics, such as water quality. The spatial distribution and temporal variability of the three water quality parameters studied in this project are presented and that knowledge was used in later chapters to make decisions on the frequency and type of field and satellite data required to fulfil the purpose of the study. Despite their differences, lakes can be classified into broad categories based on their thermal, chemical, biological or other characteristics (such as geographical position and altitude) and thus the most common classification schemes are also presented. Then, the optical properties of water and the principles of remote sensing of water quality are presented with respect to various water components (e.g. chlorophyll *a*, suspended and dissolved matter). A review of published literature on limnological studies that employed remote sensing techniques to estimate lake water quality follows and leads to a comparison between different remote sensing platforms and sensors. Finally, the potential of two sensors to estimate lake water quality is discussed.

Chapter 3 describes the type of field measurements that were obtained from various researchers and research institutes across Europe for various European lakes. The quantity of field data obtained determined the study sites, which were then described in terms of their ecology, hydromorphology, catchment land cover and land use and any issues of pollution or ecosystem disturbance they face due to anthropogenic

activities. Then, the lakes were categorized according to their mixing type, eutrophication status and regional climate, and grouped according to similarities in their ecology. Spatial and temporal analysis of the field data revealed patters and helped identify the timing of important changes or critical thresholds that were used in subsequent analysis to determine the frequency and volume of satellite data needed in order to study these phenomena with remote sensing.

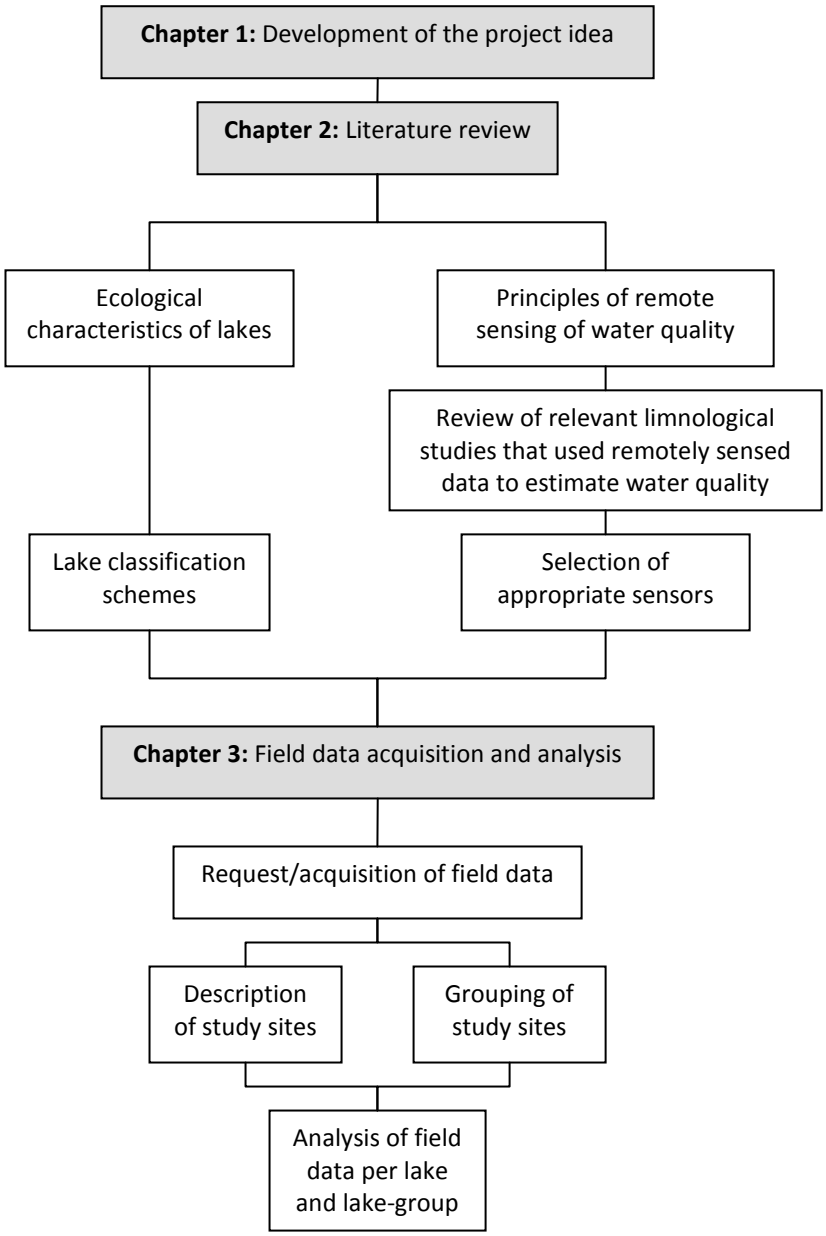

Figure 1-1: Thesis outline.

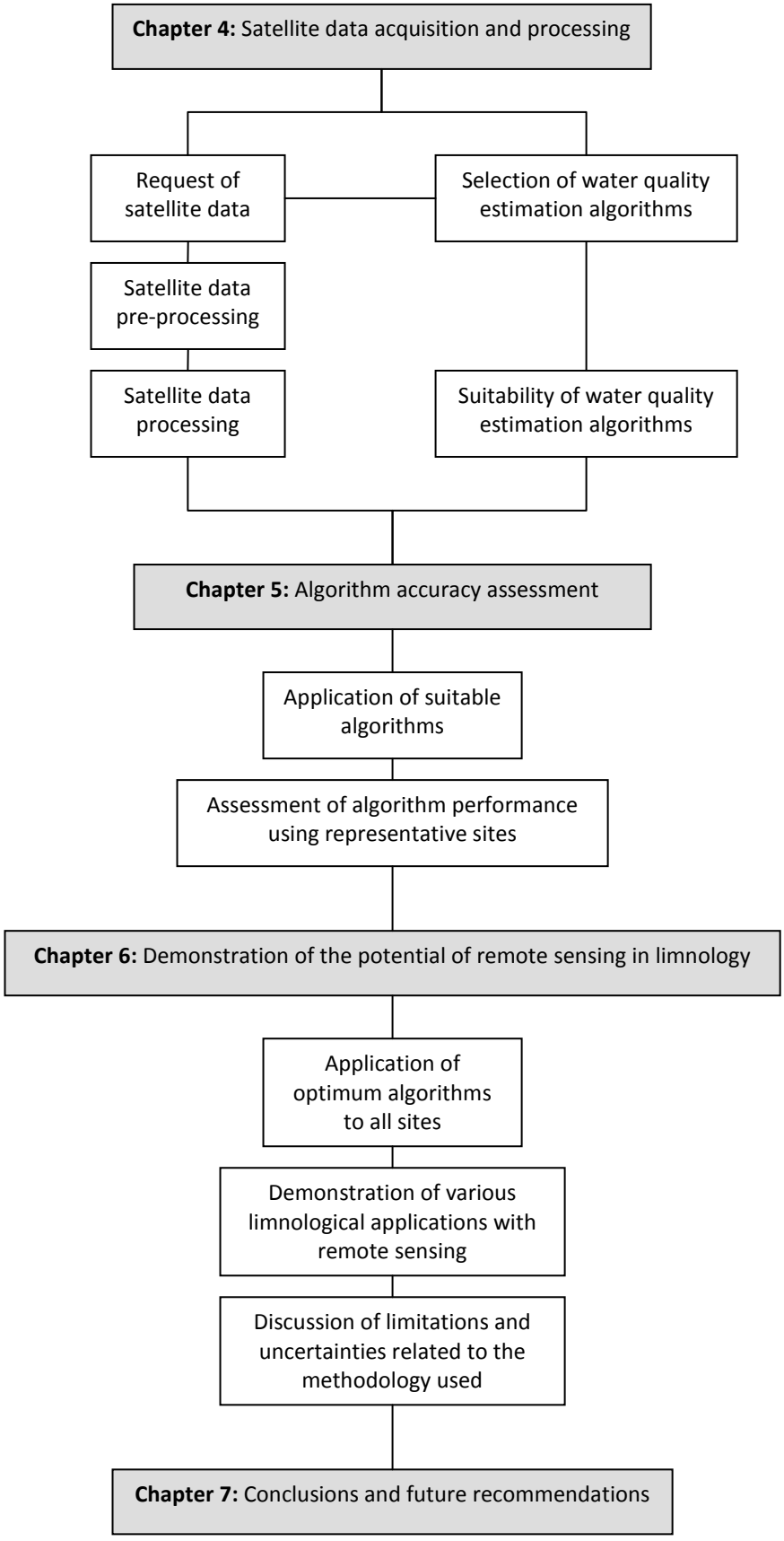

Figure 1-1: (cont.)

Chapter 4 covers the procedure followed for the acquisition of the satellite data used in this project. First, the study periods were determined based on the frequency and volume of field data. Then, the selection of cloud-free satellite data that coincided with field measurements is described and the data pre-processing is presented. A bank of suitable algorithms was created using operationally used algorithms and existing algorithms from published literature. The selection of appropriate algorithms was very important and rather crucial in terms of the accuracy achieved in this project, since the wide spatial and temporal scale of the project suggest that only a transferable and repeatable methodology would provide accurate results. In the literature, there are numerous limnological studies that have applied various empirical algorithms to map lake water quality at local scales using remote sensing. However, the selection of the algorithms for this project depended on factors such as the spectral characteristics of the sensors employed and the accuracy of results obtained. The bank of algorithms provided information on the type of remote sensing products needed (e.g. processing level of data, number and spectral width of wavebands) and the level of data preparation that was necessary for the application of the algorithms. Finally, the suitability of algorithms from the published literature was tested.

Once the preparation of satellite images was completed all suitable algorithms were applied to four contrasting study sites. This was intended to be the pilot phase of the project. The algorithms were applied to each lake pixel resulting in the construction of thematic maps of water quality parameters. The thermal characteristics of lakes were estimated using NOAA AVHRR and Terra/Aqua MODIS data, whilst Secchi

disk depth and chlorophyll *a* concentrations were estimated using Terra/Aqua MODIS data.

Chapter 5 presents the accuracy assessment of all algorithms that were tested. The algorithms that produced significant results in more than one lake and seasons were flagged as promising and were calibrated using data from other sites. In the case where none of the algorithms exhibited strong predictive accuracy for a water quality parameter, regression analysis between satellite and field data took place to develop new algorithms.

Chapter 6 aims to demonstrate the potential or remote sensing in limnological studies. The set of optimum algorithms was applied to all study sites to model their behaviour using satellite data from the NEODAAS DSRS remote sensing archive. The estimation of water quality parameters on several images from the long NEODAAS DSRS satellite archive was performed to analyze trends and potentially highlight patterns in lake properties. The interaction of these parameters and their spatial variability across Europe were also discussed.

Chapter 7 discusses the conclusions and the advantages and disadvantages of the methods used. The processing chain is also described with guidelines and recommendations for future studies.

Chapter II.

LITERATURE REVIEW

2.1 Introduction

Ecological processes in lake systems are variable and dynamic due to their dependence on factors such as hydromorphology, landscape setting, impacts of anthropogenic activities and the biogeographic and environmental history of the site (Moss, 1998). Lakes are greatly influenced by natural fluctuations in the local and global climate, but also undergo anthropogenically-induced changes. Recent advances in lake water sampling techniques, such as the incorporation of estimates of water quality from remote sensing instruments, have revolutionised the monitoring of lacustrine systems (Kondratyev & Filatov, 1999; Odermatt *et al*., 2008a). In this chapter, a review of the ecology and characteristics of lakes is given, with particular attention to temperate European systems and water quality. The potential of remote sensing to yield information relevant to the key issues of water quality is then addressed.

2.2 A review of basic lake characteristics

The response of lakes to climate change and other anthropogenic drivers of change (e.g. land use change within the catchment and/or changes in lake management) might not be homogeneous or equally pronounced between different lake bodies, because it depends on the specific characteristics of the lake (Livingstone & Padisák, 2007). Characteristics such as the origin, shape, morphology and water quality of

lakes determine their ecology (and thus their response to drivers of change), but may vary between sites (Reid, 1961; Maitland, 1990).

2.2.1 Origin of lakes

Lakes may be formed in a multitude of ways (Hutchinson, 1957). Some are water-filled depressions formed by movements in the Earth's crust (*tectonic* lakes), or depressions caused by solution of the bedrock (*solution* lakes). Others occupy calderas of old volcanoes (*volcanic* lakes) or they are formed in glacial regions by erosional scouring that deepens valleys which are then dammed by terminal moraines, ice or by deposition of sediments around wasting ice producing kettle holes (*glacial* lakes). Common causes of stream damming that form lakes are *wind* and *stream action*; the former by carrying fine, light materials that block the streams, and the latter by depositing materials in suspension where smaller streams join larger streams. *Landslides* and *flows of lava* may also block stream valleys, resulting in lake formations. Lakes are also developed from *shoreline activities*, where currents move masses of water carrying suspended sediments that are then deposited opposite a small embayment, forming a lake. In addition, along sea coasts, sand carried by currents may effectively block a lagoon or bay, thereby creating a lake. Of *organic* origin are basins that result from depressions formed within organic materials (peats) produced from the activities of living organisms. Finally, lake basins can have a *meteoritic* origin, whilst a few have origins that have yet to be established (Reid, 1961; Hickling, 1975; Maitland, 1990).

2.2.2 Shape of lakes

The origin of lakes determines their shape and morphology. Even though the latter are greatly modified through time, in many cases they may reveal the mechanisms responsible for the formation of the lake basin. In general, *circular* basins have meteoritic or volcanic origin, being craters or calderas of inactive volcanoes. Scouring from glacial drift forms *irregular*-shaped lakes, whereas tarns created in mountainous areas of glacial valleys by freezing and thawing ice action have a *subcircular* (amphitheatre-like) shape. The damming of branched channel networks can create lakes of *dendritic* shape. Channel migration in mature rivers creates oxbows and *lunate* basins. Tectonic movements in the Earth's crust may develop *rectangular* lakes. Coastal lakes, formed when a stream is blocked by sand and sediment and its continuity with the sea is cut, are usually *triangular*. Finally, there are *elliptical* lakes, whose origin is less clear, though multiple mechanisms are likely (Reid, 1961).

2.2.3 Lake water quality

The water quality of lakes is naturally controlled by their morphology and some of the basic parameters include maximum and mean depth, length, breadth[1], area, volume, extent and development of shoreline, water level and the altitude of the lake (Reid, 1961). There are many parameters that are used by limnologists and hydrologists to describe the water quality and ecology of lakes (Table 2-1).

[1] Breadth is the distance from shore to shore measured at right angles to the longitudinal axis. Often the mean breadth is used, which is defined as the ratio of the surface area to the length of the lake (Reid, 1961).

Table 2-1: Physical, chemical and biological parameters used in limnological studies.

Properties	Parameter
Physical	Electric conductivity [μScm^{-1}]
	Secchi disk depth or transparency [m]
	Turbidity [FNU or NTU]
	Mixing properties of water, e.g. thermal stratification and mixing
	Temperature (°C)
	Wind-induced oscillations (waves, seiches)
	Circulation patterns, e.g. eddies, internal currents, upwelling and downwelling
	Turbulence
Chemical	Oxygen saturation (%) and concentration
	Chemical Oxygen Demand (COD) and Biological Oxygen Demand (BOD) [mg L^{-1} O_2]
	Alkalinity [$meqL^{-1}$] and salinity
	Total Organic Carbon (TOC) [mg L^{-1} C]
	Nitrate and nitrite nitrogen (oxidised nitrogen), ammonia nitrogen, total nitrogen, nitrite and nitrate [mg L^{-1} N]
	Total phosphorus [mg L^{-1} P] and orthophosphate
	Other limiting nutrients: lead, zinc, mercury, cadmium and copper
	pH
	Dissolved Organic Matter (DOM)
	Dissolved Organic Carbon (DOC)
	Suspended sediment
	CO_2 and O_2 in stratification and turnover
	Particulate Organic Matter (POM)
Biological	Chlorophyll *a* [$\mu g\ L^{-1}$] and phytoplankton
	Fluorescent DOM
	Bacterioplankton composition

Amongst the most commonly studied parameters in limnological research are temperature, transparency (or Secchi disk depth) and chlorophyll *a*. Temperature is one of the most important factors in an aquatic environment (e.g. Welch, 1935; Livingstone & Lotter, 1998; Livingstone & Dokulil, 2001). In fact, the thermal

properties of lakes can have a profound direct (and indirect) influence on the speed and range of lake processes, making temperature one of the most important (and hence widely studied) water quality parameters (e.g. Rajadurai *et al*., 2005; De Stasio *et al*., 2009). Also, one of the most obvious and familiar properties of water is its transparency, which is inversely related to turbidity and therefore both parameters have been studied interchangeably. Finally, phytoplankton community structure and abundance are key biotic indicators of water quality (Baban, 1993) and hence, they are frequently monitored in lakes that provide drinking water to human populations (EUROPA WFD, 2009). All phytoplanktonic species use chlorophyll *a* during photosynthesis, but there are also other photosynthetically active pigments, such as chlorophyll *c*, *d*, *e*, carotenoids and phycobilins. However, chlorophyll *a* alone is considered a reasonable indicator of the phytoplankton in natural waters (Jensen, 2000) and, therefore, is used widely in algae monitoring (Vos *et al*., 2003).

2.2.4 Distribution and characteristics of key parameters

Lake temperature, transparency and chlorophyll *a* concentrations exhibit spatial and temporal variations, depending on a range of environmental factors, such as wind-induced advection and diffusion, variability in catchment nutrient loading and primary and secondary production (Hedger *et al*., 1996). These variations may have an ephemeral nature (Figure 2-1), varying over short (i.e. hours to days) or long temporal scales (i.e. weeks to months) or may be more structural, being determined by hydromorphological features (e.g. the shape and origin of the basin) or catchment characteristics (e.g. land use and land cover) (Schofield *et al*., 1999; Hedger *et al*., 1996). Temperature, transparency and chlorophyll *a* are most profoundly influenced by seasonal changes (Horne & Goldman, 1994; Schwarz *et al*., 2005) and these

changes have been observed with satellite data (Bussières *et al*., 2002). In addition to seasonal variation, however, water quality parameters (e.g. temperature) also fluctuate over shorter temporal scales depending on their diurnal cycle and the response of the lake to meteorological forcing (Bussières *et al*., 2002). As a result, different sampling strategies (varying from field measurements to satellite observations) are appropriate for the study of different phenomena at different temporal and spatial scales (Figure 2-1).

The spatial patterns of water quality parameters and ecological processes differ as well within different lakes (e.g. Kallio *et al*., 2003; Steissberg *et al*., 2005) and in many cases, the spatial variation of a water quality parameter is low at small scales (e.g. meters), but high over large scales (e.g. hundreds or thousands of meters) (Hedger *et al*., 1996).

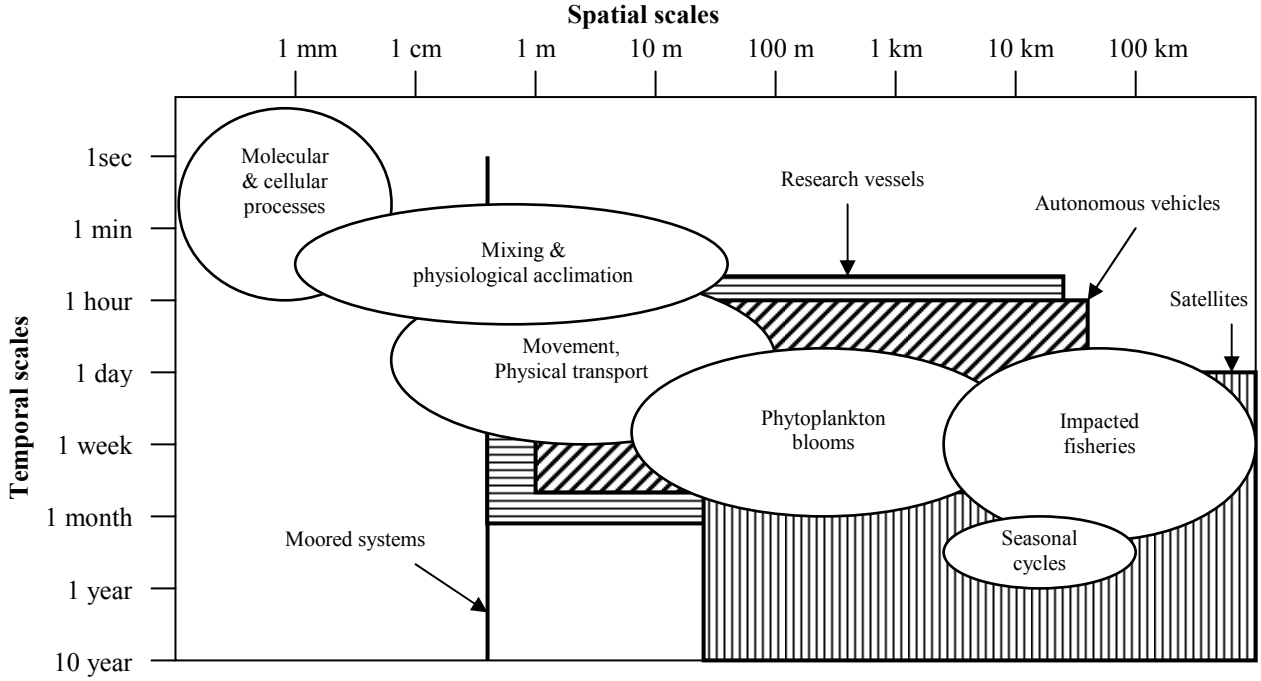

Figure 2-1: The relevant temporal and spatial scales of critical processes regulating phytoplankton ecology (in circles) and the sampling capabilities of the diverse sampling platforms available (in squares) (Adapted from Schofield *et al.,* 1999).

2.2.4.1 Temperature and stratification

Temperature varies between and within lakes, according to the mixing conditions of each water body. Regionally, temperature also varies according to factors such as latitude, altitude, local meteorological conditions and the physiographic character of lakes (Welch, 1935).

Generally, sunlight heats the surface water of lakes and, due to the poor conductivity of water, a relatively warm upper layer is formed. Since warm water is less dense than the underlying cool water a condition of stability is set up and the lake water is separated into layers; a phenomenon called stratification. During stratification, the lake is divided into three distinct zones; the *epilimnion*, which is the warm surface layer; the *thermocline* or *metalimnion*, the transition zone of intermediate-density; and the *hypolimnion*, the cool bottom layer (Hickling, 1975; Horne & Goldman, 1994; Steissberg *et al*., 2005). The thermocline is the region where temperature changes rapidly with depth and can be greater than 1 °C per metre (Horne & Goldman, 1994). The thermocline acts as a barrier against mixing and diffusion processes between the epilimnion and hypolimnion (Hickling, 1975). The conditions under which stratification occurs can be spatially complex even across a single lake, where a lake is large enough, due to irregularities in mixing caused by inflows and other processes that take place within the lake, and/or wind and wave action (Moss, 1988).

The stable conditions during stratification end when wind-induced mixing of the water column takes place. At the same time, cooling of the surface waters, due to lower sun-angles, may add to increased instability and thus lead to the breakdown of

the stratification (Moss, 1988). In general, lakes in temperate zones (mid-latitudes) stratify in spring-summer when lakes effectively receive increased solar radiation and the wind action is less than in winter. In winter, on the other hand, lakes usually mix (Steissberg *et al*., 2005, Reid, 1961). However, this seasonal pattern might change in very shallow lakes or in lakes that are covered with ice in winter. As a result, temperate lakes may mix more than once per year (Horne & Goldman, 1994).

In addition to stratification there are other thermal phenomena that take place at finer spatial and temporal scales. For example, vertical movements (upwelling/ downwelling) in the epilimnion occur throughout the stratification season locally, changing the surface temperature at specific points within the lake (Horne & Goldman, 1994). Seiches may result from extended periods of wind blowing from a given direction. These phenomena may occur intermittently or more regularly depending on the frequency of the causative factors (e.g. periods of strong and sustained winds) (Steissberg *et al*., 2005). Finally, river discharge or warm water from power stations may also locally distort the surface temperature of lake water from ambient levels.

2.2.4.2 Transparency

Transparency is a measure of water clarity and the degree of water opacity. It is not uniform within a lake and is determined by the relative amounts of three major water components; suspended sediment, particulate organic matter and algal cells (Welch, 1935; Fraser, 1998). Generally, lake transparency is influenced by the levels of both *allochthonous* and *autochthonous* suspended particulate matter. Allochthonous matter is produced outside the lake, for example in the lake catchment due to erosion,

and it is transported into the lake by inflowing streams and surface runoff. As a consequence, the highest concentrations of allochthonous matter are expected next to the shore (due to runoff) and around estuaries (Horne & Goldman, 1994) and include various grades of humus, silt, organic detritus, colloidal matter, plants and animals (Reid, 1961). Autochthonous matter is produced within the lake itself, key amongst which is biological material (e.g. plankton), but also re-suspended bottom sediment due to wind-driven mixing that occurs throughout the entire water column in shallow lakes (Reid, 1961; Baban, 1993). As a result, changes in transparency follow the seasonal variations in quality and quantity of such water constituents. Increases in stream discharge due to intense rainfall may introduce considerable amounts of sediments and other materials, altering the colour and degree of transparency of lakes (Reid, 1961). In fact, sediment transport is higher during the wetter seasons (Nellis *et al*., 1998). Moreover, partial upwelling, when intermediate depth water reaches the surface, generally decreases water clarity; whereas total upwellings, when bottom water surfaces, can increase clarity (Steissberg *et al*., 2005). However, it is worth noting that while the clarity of surface water decreases with increasing amounts of suspended components, the dissolved components of water (e.g. mineral salts, gases and organic substances) do not influence lake transparency (Reid, 1961).

2.2.4.3 Phytoplankton and chlorophyll *a*

The distribution of plankton in lakes exhibits high spatial variability both horizontally and vertically, due to various factors that control and influence the planktonic life cycle and growth. The horizontal distribution is rather irregular and transient (Horne & Goldman, 1994). Wind-induced drifts of the surface waters and currents may lead to temporary shifts of the floating planktonic populations and

cause irregularities in the population distribution (Welch, 1935). Inflowing streams can play an important role in controlling the quality and quantity of plankton in a lake through new planktonic species introduced to the lake from the catchment or by dilution effects where inflowing waters are plankton-free. Streams may also cause physico-chemical alteration of the lake water that in turn may influence the growth and distribution of planktonic species (Welch, 1935). For instance, the introduction of high concentrations of suspended sediment from estuaries results in a decrease in water transparency reducing primary production. Another prominent factor that controls primary production is the wind conditions (Moss, 1988; Horne & Goldman, 1994). In calm periods algae float to the surface until they are (locally) depleted by grazers, turbulence or strong wind conditions (Welch, 1935; Horne & Goldman, 1994).

The vertical distribution of planktonic populations within lakes is influenced by four major factors, which are: (a) light penetration and the level of transparency, (b) stratification, (c) nutrient load, and (d) benthic macrophytes and their contribution of organic detritus to the benthos and water body (Moss, 1988). Certain planktonic species have been observed to populate areas where nutrients are abundant and to generally avoid the lake surface during periods of strong sunlight (Welch, 1935). Such vertical movements, referred to as migration, cause diurnal changes in the density of plankton within the water column. For example, most cyanobacteria sink in the morning and float to the surface at night (Horne & Goldman, 1994).

Temperature and thermal stratification in lakes also influence the vertical distribution of plankton. The epilimnion receives incident sunlight and is therefore the only layer

where photosynthesis can take place. In the hypolimnion, the potential abundance of nutrients is trapped due to the overlying thermocline. However, in this layer lack of sunlight does not allow growth of phytoplankton (Hickling, 1975). Moreover, the temperature gradient with depth and the variation of temperature within the lake body control the growth of certain planktonic species and favour areas of high concentrations (Welch, 1935). Motile phytoplankton (e.g. the blue-green algae and cryptomonads) tend to accumulate near the thermocline where turbulence is minimal (Horne & Goldman, 1994).

The origin, landscape position and shape of lakes also determines the amount and distribution of phytoplankton. Rock basins of glacial, volcanic or tectonic origin are typically oligotrophic, because they have base-poor catchment lithology and rocky or stony shorelines and thus, few nutrients and sediments (Maitland, 1990). In contrast, shallower lakes on sedimentary rocks, especially if calcareous, are naturally eutrophic with nutrient-rich bottom sediments and considerable mineral flux introduced from the catchment (Maitland, 1990). Within lakes, protected bays may provide more favourable conditions for developing plankton than open water. Also, certain species prefer deep waters than shallow areas in certain seasons (e.g. diatoms). In addition, productivity generally increases with the age of a lake (Welch, 1935). Latitude and altitude also play an important role, with northern lakes at low altitudes tending to be highly productive in contrast to alpine lakes that tend to be oligotrophic, although exceptions apply in both cases (Welch, 1935).

The temporal distribution of planktonic populations in temperate lakes is dominated by seasonal changes (Horne & Goldman, 1994). In general, the seasonal variability

of phytoplankton in temperate lakes follows a general pattern (Figure 2-2) that is determined by high concentrations in late spring and autumn (two maxima accordingly), and reach minimum concentrations in summer and winter (two minima accordingly) (Welch, 1935; Arhonditsis *et al.*, 2004b). Seasonal variations in different years may cause the dates of the maxima and minima to shift somewhat, however, while the relative sizes of maxima and minima follow no fixed rule, the spring maximum commonly exceeds the autumn maximum, and the winter minimum is usually lower than the summer minimum (Welch, 1935). During the stratification period in summer, concentrations of phytoplankton decrease, due to nutrient limitation and zooplankton grazing (Horne & Goldman, 1994).

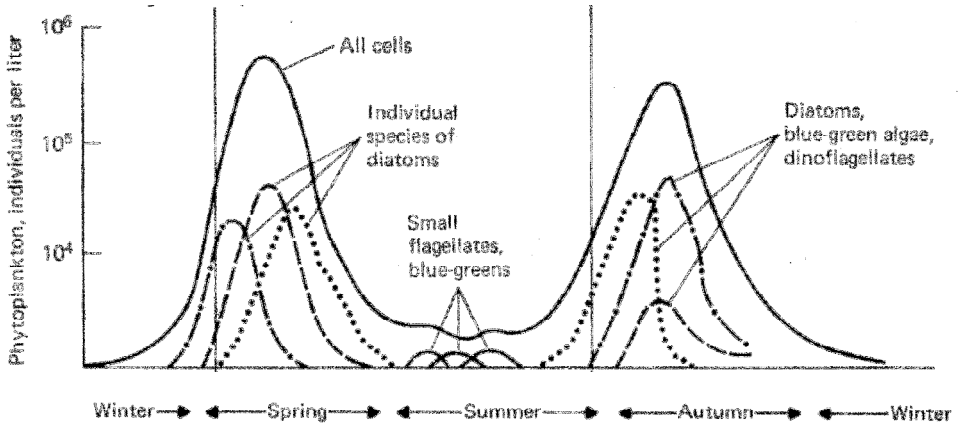

Figure 2-2: Typical seasonal variability of phytoplankton concentrations and species in the temperate zone (Horne & Goldman, 1994; p. 237).

Each species of plankton has different seasonal cycles. For example, *holoplanktonic* species spend their entire life in the water column as part of the plankton, whereas *meroplanktonic* species spend only the larval or early stages of their lives as part of the plankton. Holoplankton dominates the spring bloom in lakes, because of its faster

growth rates in comparison to competing algae. However, cyanobacterial blooms and red tides are caused by meroplanktonic species. For example, the holoplanktonic diatom *Asterionella formosa* usually blooms in spring (Figure 2-3A), as opposed to the meroplanktonic diatom *Melosira italica* that blooms during the mixing period in winter and spring (Figure 2-3B). Both groups may be found in the same lake and their domination over competing species depends on limiting physical (e.g. light), chemical (e.g. nutrients) and biological (e.g. grazers) parameters. The latter enhances the need for inter-seasonal monitoring rather than inter-annual mapping during one or two seasons (Allee & Johnson, 1999).

2.3 Classification of lakes

Lakes evolve and change through time. As a consequence of their ephemeral character the classification of lakes is considered to be a rather difficult task (Reid, 1961). In addition, lake systems are so variable that lakes with different origins might have the same ecological characteristics and *vice versa* (Maitland, 1990). Following on from above, there have existed various schemes for the classification of lakes, all taking into account different parameters, such as latitude, altitude, surface area, volume, mean or maximum depth, salinity, mixing conditions or the eutrophication status of lakes. Three common schemes divide lakes into categories according to their thermal, chemical and biological characteristics.

(A)

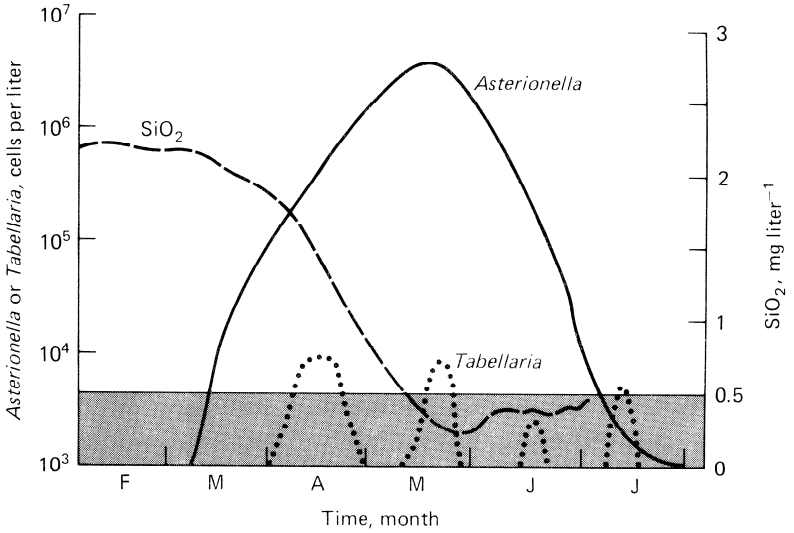

(B)

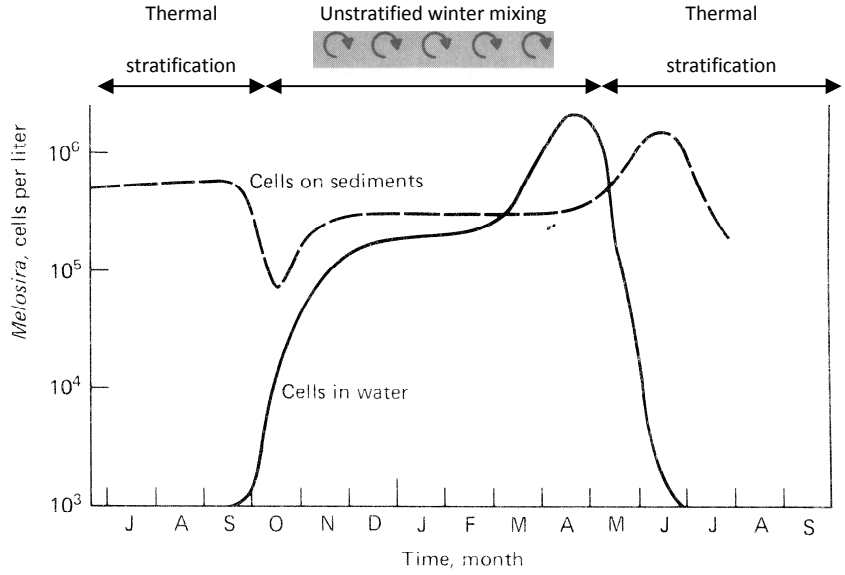

Figure 2-3: (A) The spring bloom in the North Basin of Windermere, England is dominated by the holoplanktonic diatom *Asterionella Formosa*, while (B) the meroplanktonic diatom *Melosira italica* dominates only in unstratified conditions during the winter and early spring in Blelham Tarn, English Lake District (Horne & Goldman, 1994; p. 239 & 243). *Notice the difference in time scales between the two figures*.

2.3.1 Thermal classification

According to Forel (1982), lakes can be divided into three categories according to their surface temperature; *polar* lakes, whose surface temperature never exceeds 4

°C; *temperate* lakes, with surface temperatures sometimes below and at other times above 4 °C; and *tropical* lakes, whose surface temperature is always above 4 °C (Kondratyev & Filatov, 1999). Moreover, and according to their depth, the aforementioned categories can be all subdivided into *shallow* lakes, with variable bottom temperature, and *deep* lakes, with constant bottom temperature (Maitland, 1990).

A rather commonly used classification of lakes based on their thermal characteristics but also taking into consideration altitude, geographical location (with respect to latitude) and the depth of the basin, is the scheme suggested by Hutchinson and Loffler (1956) that divides them into amictic, cold monomictic, dimictic, warm monomictic and oligomictic (Kondratyev & Filatov, 1999).

Amictic (polar) lakes are found in the Antarctic and in high altitudes that are always covered with ice, therefore insulated and protected from weather and other influences. As a result, amictic lakes never mix. *Cold monomictic* (arctic) lakes are also found in polar regions and are also covered with ice. They mix only once, at temperatures that do not exceed 4 °C in summer. The third category includes *dimictic* (temperate) lakes that mix twice a year; in autumn before ice cover and in spring after ice melt (Figure 2-4A). Dimictic lakes are typical in the temperate zone (e.g. Europe) and in high altitudes in subtropical regions. *Warm monomictic* (tropical) lakes are found in warmer regions and exhibit water temperatures that never fall below 4 °C at any depth. Warm monomictic lakes are also common in temperate regions and are not (or only ever partially) covered with ice in winter. They continuously mix in late autumn and throughout the winter due to wind action, until

they stratify in late spring and summer (Figure 2-4B). *Oligomictic* (equatorial) lakes are warm lakes in which water circulation occurs rarely and at irregular periods. These are mostly found at low elevations in tropical zones. Finally, *polymictic* lakes are shallow and exposed to strong winds that mix whenever storms break down the thermal stratification. Such successive phenomena can take place every few days to a few weeks, depending on the frequency of storm events. Such lakes are more widely distributed on high mountains in the equatorial regions (e.g. Reid, 1961; Horne & Goldman, 1994), however polymictic lakes are also found within temperate regions, such as Lake Balaton in Hungary and Lake Müggelsee in Germany (e.g. Ministry of Environmental Protection and Water Management, Hungary, 2009; Adrian *et al*., 1999). Lakes that never stratify throughout the year also fall into this category.

Finally, with respect to the extent of circulation in the entire water column, lakes might completely mix from top to bottom (*holomictic*) or mix partially (*meromictic*) (e.g. Reid, 1961; Hickling, 1975; Horne & Goldman, 1994).

2.3.2 Chemical classification

Thermally similar lakes might have different chemical characteristics, and thus, a categorization based on the alkalinity of lake water also exists. According to that scheme, lakes can be *nutrient-poor*, with less than 15 mg L^{-1} of calcium carbonate ($CaCO_3$); *moderately rich*, 15-60 mg L^{-1} $CaCO_3$; or *nutrient-rich*, with more than 60 mg L^{-1} $CaCO_3$ (Maitland, 1990).

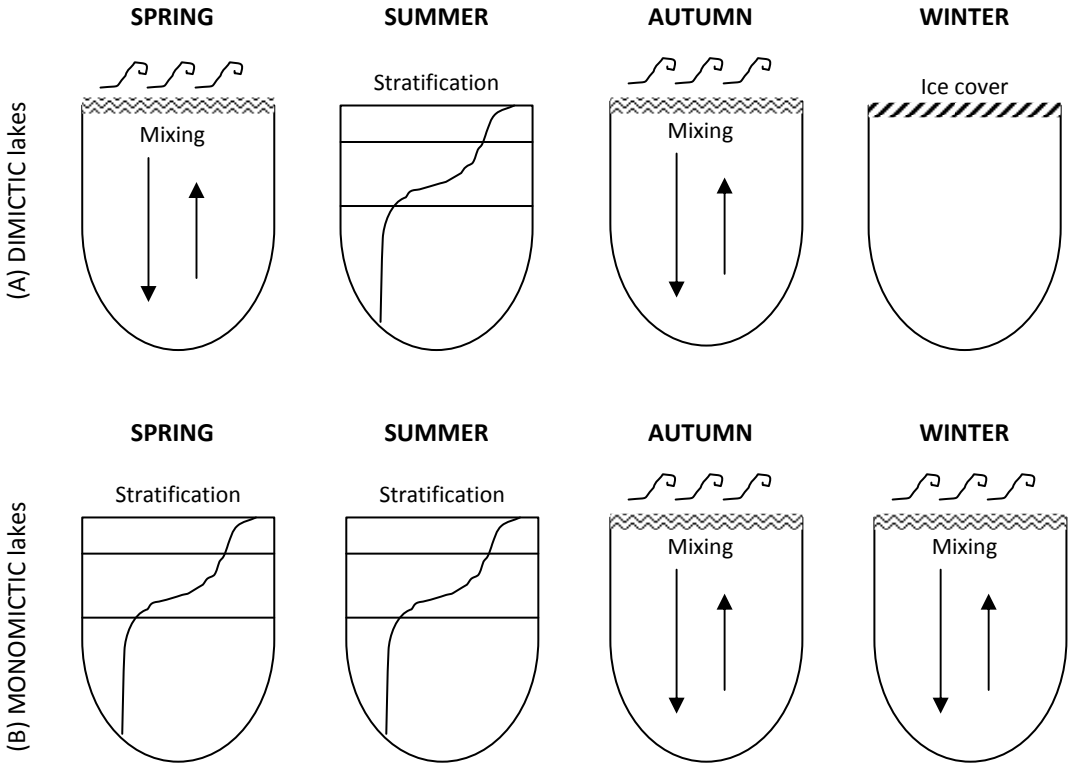

Figure 2-4: Two types of lakes are mainly found in Europe: (A) Dimictic lakes that mix twice per year, in early spring after the ice cover breaks down and in autumn after the thermocline breaks and before the lake is covered with ice; (B) Monomictic lakes that are not covered with ice and mix after the thermocline breaks in autumn and throughout winter.

2.3.3 Biological classification

One of the most commonly used classification schemes is based on the biological characteristics of lake bodies (Table 2-2). In this scheme, lakes are divided into three main groups, as follows (Welch 1935; Maitland, 1990):

- *Oligotrophic* lakes are nutrient-poor, usually deep and clear water bodies with oxygen abundance.
- *Eutrophic* lakes are nutrient-rich, usually shallow and turbid lakes that may have oxygen deficiency in deeper water at some times of year.

- *Dystrophic* lakes that have variable amounts of nutrients and large amounts of humus. They are usually shallow or moderately deep and may show oxygen deficiency in the deep water layers.

Table 2-2: Principal characteristics of oligotrophic, eutrophic and dystrophic lakes (adapted from Welch, 1935; p 312-313 and Maitland, 1990; p. 89).

Parameter	**Lake type**		
	Oligotrophic	**Eutrophic**	**Dystrophic**
Basin type; thermal characteristics	Narrow and deep; volume of hypolimnion greater than epilimnion	Broad and shallow; volume of hypolimnion smaller than epilimnion	Small and shallow
Lake substrate	Stones & inorganic silt	Fine organic silt	Peaty silt
Lake shoreline	Stony	Weedy	Stony or peaty
Transparency	High	Low	Low
Water colour	Blue to green	Green to yellow and brownish green	Yellow to brown
Dissolved solids	Low, poor in N	High, much N and Ca	Low, poor in Ca
Suspended solids	Low	High	Low
Oxygen	High	High at surface, low under ice or thermocline	High
Phytoplankton	Many species, low numbers	Few species, high numbers	Few species, low numbers
Macrophytes	Few species, some in deep water	Many species, abundant in shallow water	Few species, some abundant in shallow water
Zooplankton	Many species, low numbers	Few species, high numbers	Few species, low numbers
Zoobenthos	Many species, low numbers	Few species, high numbers	Few species, low numbers
Fish	Few species	Many species	Very few species, often none
Succession	Into eutrophic type	Into pond, swamp, meadow moor	Into peat bog

The Organization of Economic Cooperation and Development (OECD) introduced certain criteria for the classification of lakes into five distinct trophic status categories, ranging from ultra-oligotrophic to hypertrophic (or dystrophic) lakes (OECD, 1982). The criteria are based on the critical values (minimum, mean and maximum) of three water quality parameters: the concentration of total phosphorus and chlorophyll *a*, and Secchi disk depth (Table 2-3).

Table 2-3: OECD criteria for trophic status of lakes (OECD, 1982).

Trophic status	Total P	Chlorophyll *a*		Secchi disk depth	
	Mean (µg L^{-1})	Mean (µg L^{-1})	Max (µg L^{-1})	Mean (m)	Min (m)
Ultra-oligotrophic	< 4	< 1	< 2.5	> 12	> 6
Oligotrophic	< 10	< 2.5	< 8	> 6	> 3
Mesotrophic	10-35	2.5-8	8-25	6-3	3-1.5
Eutrophic	35-100	8-25	25-75	3-1.5	1.5-0.7
Hypertrophic	> 100	> 25	> 75	< 1.5	< 0.7

2.3.4 Other classification schemes

The Water Framework Directive (WFD) has set two systems to standardize the characterization and classification of European water bodies, including lake waters (Directive 2000/60/EC, 2000; CEN, 2010). These two systems ('System A' and 'System B') are very similar, the difference being that the first employs the idea of ecoregions, while the second uses geographic latitude and longitude instead, plus additional environmental parameters (e.g. lake shape, residence time, mean air temperature, mixing characteristics, *etc*.) (EC Guidance Document No 10, 2003). However, both systems are based on natural abiotic characteristics of lakes (Table 2-

4), including altitude, mean depth, surface area and geology of the lake (Kolada *et al*., 2005).

In addition, lake waters can be divided into *Case I* or *Case II* according to their dominant components. Water bodies mostly dominated by phytoplankton, similar to open oceanic water, are Case I waters. Other water substances such as biological debris, dissolved organic matter (DOM) and other small organisms (e.g. flagellates, bacteria, viruses) are also present in Case I waters. On the other hand, coastal areas, estuaries and most lakes are Case II waters, because they contain considerable amounts of particulate inorganic matter (suspended sediment) and/or coloured DOM (CDOM, also called yellow substances or Gelbstoffe) in the water column in addition to phytoplankton (IOCCG, 2000).

Table 2-4: WFD lakes typology; obligatory parameters used in System A and System B (Directive 2000/60/EC, 2000; CEN, 2010).

Parameter	Description
Altitude	Lowland: < 200 m a.s.l
	Mid-altitude: 200-800 m a.s.l
	High: > 800 m a.s.l
Mean depth	Very shallow: < 3 m
	Shallow: 3-15 m
	Deep: > 15 m
Surface area	Small: 0.5-1 km^2
	Medium: 1-10 km^2
	Large: 10-100 km^2
	Very large: > 100 km^2
Geology	Organic
	Siliceous
	Calcareous

2.4 Remote sensing of water quality principles

Since the 1840s, when photographs were first used for topographic surveying, the science of remote sensing has progressed (Lillesand *et al*., 2008). Following the launch of the first artificial satellite (Sputnik) in 1957 numerous satellite instruments have orbited the Earth acquiring vast amounts of observations for a wide variety of applications. The scientific community quickly realized the potential for remote sensing in water applications. Instruments dedicated to oceanography have been launched onboard satellite platforms, such as the NASA Nimbus-7 Coastal Zone Color Scanner (CZCS) in 1978 and the NASA Orbview-2 Sea-viewing Wide Field-of-view Sensor (SeaWiFS) in 1997, revolutionising operational oceanography and global water studies (Kondratyev & Filatov, 1999). The basic principles of water remote sensing are based on the optical and thermal properties of water and on the different ways the medium interacts with solar radiation depending on its variable characteristics.

2.4.1 Optical properties of water

Much of the solar radiation received at the top of the Earth's atmosphere is scattered, reflected or absorbed within and by the atmosphere, until a relatively small amount finally reaches the Earth's surface (Moss, 1988). Completely pure water absorbs all light, but the rate of attenuation is wavelength dependant. For example, long wavelengths are attenuated more than shorter wavelengths, which penetrate deeper in the water column (Figure 2-5). In very clear waters, light can sometimes reach great depths, i.e. up to 100 m (Liceaga-Correa & Euan-Avila, 2002).

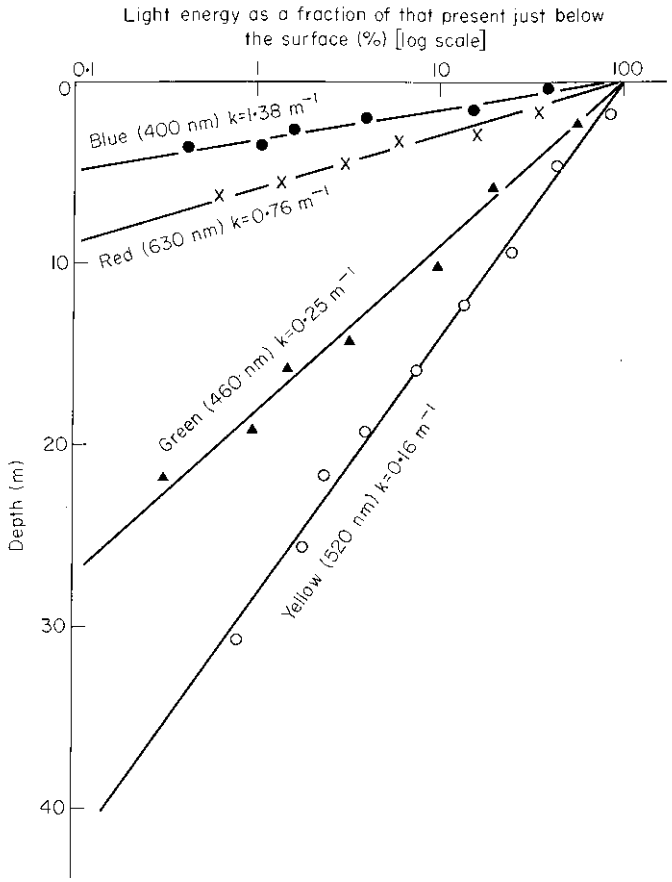

Figure 2-5: Absorption of light at various wavelengths in a typical lake (Moss, 1988; p. 162).

Freshwater and the oceans show great differences in the degree to which they permit light penetration because they contain certain optically active components that interact with solar radiation (Figure 2-6). Particulate organic matter (POM) determines light attenuation by both scattering and absorption and includes living organisms (i.e. phytoplankton and zooplankton) and non-living particles (e.g. dead organisms, detritus, colloidal substances). Particulate inorganic matter (suspended sediment) also scatters and absorbs light. On the other hand, DOM only absorbs radiation, and includes proteins, fats, carbohydrates and their break-down derivatives (Reid, 1961; Moss, 1988). The way water and its optically active components affect

light attenuation is referred to as the Inherent Optical Properties (IOPs) of water (Koponen *et al*., 2002) and its immediate effect, detected by remote sensing (or a human eye), is water colour.

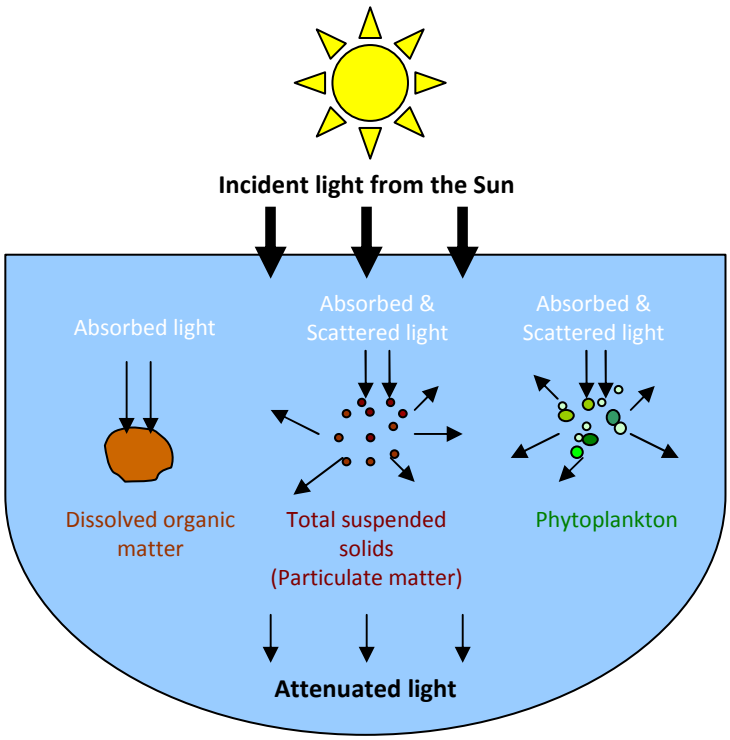

Figure 2-6: Light attenuation in natural waters is determined by the amount of absorption and scattering caused by major water components, such as dissolved organic matter, suspended matter and phytoplankton.

The study of water colour offers information related to the IOPs and the chemical characteristics of water bodies (Figure 2-7). Natural lake waters that only contain small amounts of suspended matter (i.e. the IOPs are dominated by pure water) appear *blue* (Reid, 1961), due to the fact that suspended matter absorbs least in the blue and green wavelengths (400–500 nm) (Moss, 1988). In waters where the amount of CDOM and fulvic acids (tannins from decaying vegetation), is high all

blue light is absorbed and lakes look *yellowish to brown* (Hirtle & Rencz, 2003). Finally, peaty waters and water with high amounts of inorganic suspended matter and detritus generally scatter light at higher rates than they absorb it and appear *brown* (Moss, 1988).

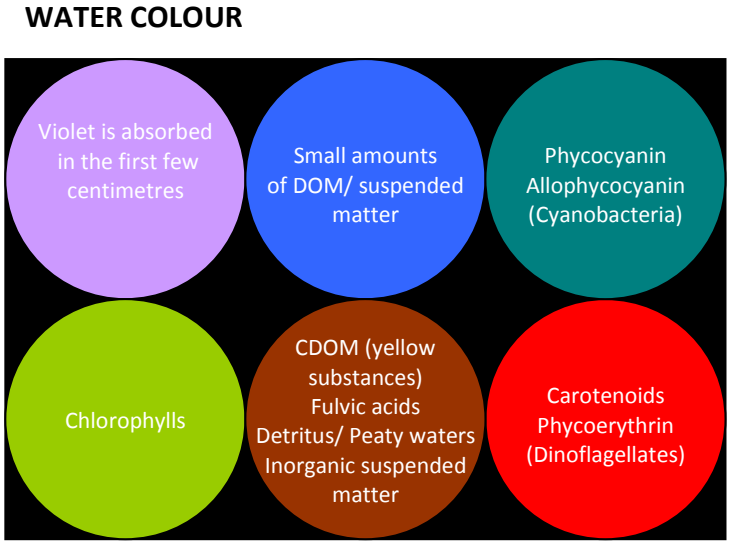

Figure 2-7: The colour of water varies according to the predominant water components (Moss, 1988).

If there is a moderate amount of dissolved matter and some phytoplankton then the lake will probably appear *green*. However, different phytoplankton species contain a range of pigments during their growth cycle that absorb at different wavelengths and water colour changes accordingly (Figure 2-7). For example, when the predominant phytoplanktonic species contain chlorophylls, then the water appears *green*. Other pigments used by phytoplankton result in different water colour if the species dominate in a water body. Species that contain carotenoids or phycoerythrin colour the water *orange-red to brownish* as often observed during the 'red tides' caused by dinoflagellates, while the blue pigments (phycocyanin and allophycocyanin) found in

blue-green algae (cyanobacteria) absorb in the yellow and green parts of the visible spectrum, giving the water a *dark green*, *milky*, or even *brown* colour, depending on species and their health (Moss, 1988; Horne & Goldman, 1994; Jensen, 2000). In cases where more than one phytoplanktonic species dominate and the phytoplankton community is mixed, the colour of water depends on the attenuation rate at different wavelengths and therefore it usually appears *yellow-green* as these two regions of the spectrum are usually least absorbed (Moss, 1988).

The degree of light attenuation, and therefore water colour, is determined largely by seasonal variations in the quantity and quality of the optically active components of water. As a result, the colour of natural waters may change periodically (Reid, 1961). It is this fact that complicates mapping of water colour, especially in optically complex waters, and introduces high levels of uncertainty if not monitored at very high temporal resolution.

2.4.2 Remote sensing of water quality parameters

In turbid lake waters, low water clarity often discourages estimations of physical and biological characteristics, such as bathymetry and benthos (e.g. Bijaoui *et al*., 1995; George, 1997a; Lafon *et al*., 2002; Liceaga-Correa & Euan-Avila, 2002). However, an important number of other useful water quality parameters have been estimated in lake waters, and provide a good reference for the assessment of the ecological status of lakes. Thermal remote sensing data can provide estimations of surface temperature (e.g. Bussières *et al*., 2002; Oesch *et al*., 2005), and thermal features, such as vertical (e.g. upwellings) and horizontal (e.g. eddies, thermal currents) circulation patterns (Steissberg *et al*., 2005). Transparency (or Secchi disk depth) has been estimated

with moderate to high accuracy in freshwaters (e.g. Dekker & Peters, 1993; Allee & Johnson, 1999; Sawaya *et al*., 2003) and turbidity levels have been estimated with promising estimation accuracy in lake waters (e.g. Fraser, 1998; Vincent *et al*., 2004). The winter ice coverage of northern lakes can also be mapped with optical remote sensing (e.g. Wynne *et al*., 1998; Latifovic & Pouliot, 2007). The estimation of chemical parameters, such as the concentration of CDOM, Dissolved Organic Carbon (DOC), suspended sediment and dissolved solids (e.g. total phosphorus) has also shown promising results using remotely sensed data (e.g. Dekker *et al*., 2002; Hirtle & Rencz, 2003; Kutser *et al*., 2005). Finally, chlorophyll *a* and phytoplankton are two major biological parameters that have been successfully mapped in many lake studies (e.g. George, 1997b; Vos & Rijkeboer, 2000; Kallio *et al*., 2003; Vos *et al*., 2003). All the above suggest that remote sensing is a promising tool for lake studies.

Of the three key water quality parameters studied in this project, water surface temperature is the least complex and the most reliable parameter to map and estimate (Cracknell, 1997; Kondratyev & Filatov, 1999). The thermal properties of water are well understood and therefore temperature mapping is a relatively simple procedure. Generally, temperature estimation models are based on the principle that water has an emissivity (ε) very close to 1, meaning that the radiant temperature detected by the remote sensing instrument approximates closely to the true kinetic temperature of water bodies, (assuming appropriate atmospheric corrections have been applied to the data). It is, therefore, possible to estimate water surface temperature to a very high accuracy (Jensen, 2000).

On the other hand, the estimation of Secchi disk depth (referred to as SDD hereafter) and chlorophyll *a* has proved more complicated (IOCCG, 2000). A distinction should be made here between Case I and Case II waters because they exhibit different inherent optical properties and are, therefore, studied with different methods, depending on the purpose of the investigation.

In Case I waters, where phytoplankton dominates as a major contributor to the water optical properties, the estimation of chlorophyll *a* is straightforward and generally accurate (IOCCG, 2000). Chlorophyll *a* strongly absorbs blue light between 400-500 nm and red light at approximately 675 nm. On the other hand, chlorophyll *a* reflects light at 550 nm and at around 695 nm (Figure 2-8A) (e.g. Horne & Goldman, 1994; Jensen, 2000). Chlorophyll *a* estimation algorithms that have been developed for Case I waters (oceanic or lacustrine) usually employ the blue (450-500 nm) and green (500-580 nm) regions of the spectrum (George, 1997b). The algorithms for the estimation of chlorophyll *a* in Case I waters are sensor-specific, but are used operationally to map phytoplankton abundance in oceanic waters (NASA Ocean Colour, 2009).

In Case II waters, where suspended matter and CDOM are also present, the spectral response of chlorophyll *a* differs. Chlorophyll *a* in lakes containing suspended sediments can be measured using the ratio between the near infrared (nIR) reflectance peak (at around 690-700 nm) and the red absorption maximum (at approximately 675 nm), as this is independent of the suspended sediment concentration (Han *et al*., 1994) (Figure 2-8B). The same ratio has been also used to estimate chlorophyll *a* in lakes with high amounts of CDOM (Kallio *et al*., 2003)

because it avoids the use of a blue waveband, where chlorophyll *a* absorbs, as this part is also absorbed by CDOM and might impart a certain amount of confusion (Thiemann & Kaufmann, 2000). Consequently, the nIR/red ratio has been used in various studies to estimate chlorophyll *a* in Case II waters (e.g. Dekker & Peters, 1993; Thiemann & Kaufmann, 2000; Kallio *et al*., 2003). However, the above ratio works best for the estimation of chlorophyll *a* at low concentrations, whereas at relatively high concentrations a single band algorithm using the nIR reflectance peak at 690 nm is preferable (Jensen, 2000).

The red region of the spectrum is considered to give the best predictive ability when used to establish correlations between remotely sensed reflectance and turbidity (Nellis *et al*., 1998). SDD is inversely correlated with turbidity and, by extension, to the amount of suspended sediment in water. Hence, it is the type and amount of suspended sediments in waters that determines the spectral reflectance of turbid waters. According to Jensen (2000), the 580-690 nm region of the spectrum (yellow-red) is used when the type of suspended sediment in water bodies is under investigation, whereas the near infrared range of 714-880 nm provides useful information on the amount of suspended sediment in Case II waters.

Despite the difficulties due to the complexity of the optical properties of Case II waters, several algorithms have been proposed for lake waters and many attempts have observed promising results (e.g. Baban, 1993; Gitelson *et al*., 1993; Kloiber *et al*., 2002b; Dall'Olmo *et al*., 2005). These are discussed in the following section.

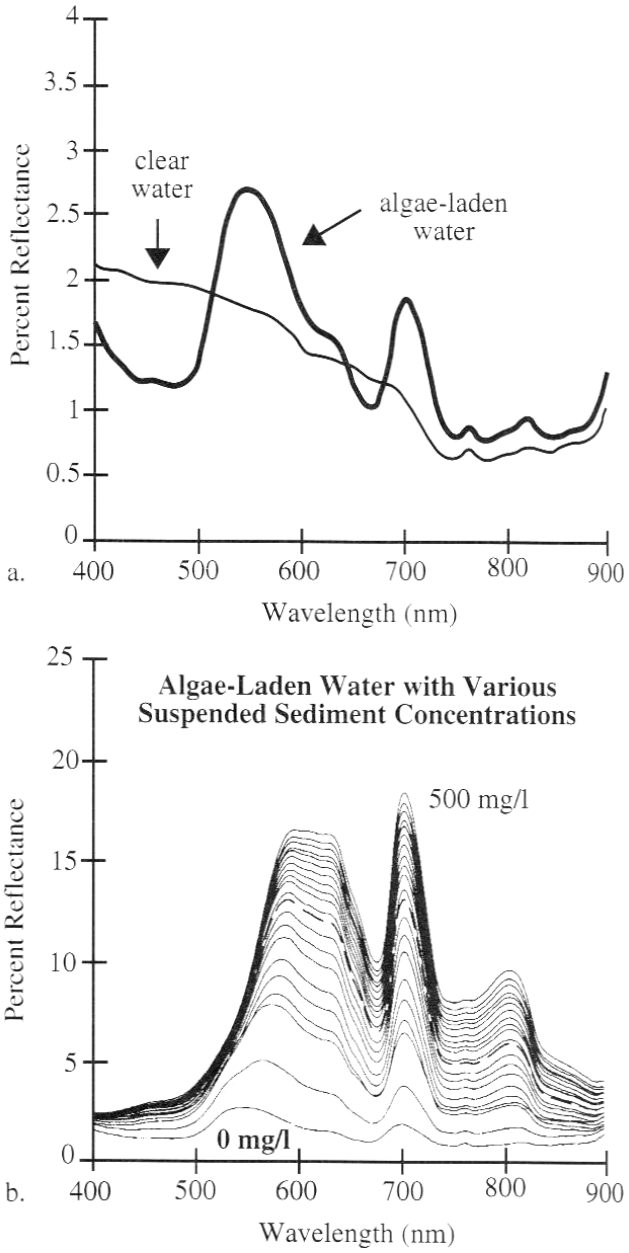

Figure 2-8: (A) Reflectance of clear and algae-laden water based on *in situ* spectroradiometer measurements and (B) Reflectance of algae-laden water with various concentrations of suspended sediment ranging from 0-500 mg L^{-1} (Han, 1997).

2.4.3 Sources of uncertainty in remotely sensed estimates

There are known (but not always easily detected and/or quantified) sources of uncertainty that affect the accuracy of water quality parameter estimations

(Cracknell, 1997). These uncertainties broadly belong to two categories; namely atmospheric effects and water surface effects, such as skin effect and specular reflection (Hepplewhite, 1989).

2.4.3.1 Atmospheric effects

The remote sensing observations of LST are influenced by atmospheric absorption caused primarily by water vapour (H_2O) in the lower atmosphere, ozone (O_3) at greater heights (20-30 km) and carbon dioxide (CO_2) that is distributed uniformly through the atmosphere. Aerosols also affect the accuracy of LST estimates (Hepplewhite, 1989). Water vapour varies with latitude and season across large horizontal areas (1000 km), ozone varies diurnally and carbon dioxide varies seasonally (Robinson, 1985). Such variations in the main absorbers of radiation in the atmosphere cause variable uncertainty in the estimation of LST. Even though the NOAA AVHRR thermal bands are designed to fall within the atmospheric absorption windows, the latter are not completely transparent (Robinson, 1985) and water vapour absorption may reduce brightness temperatures by as much as 5 °C (Cracknell, 2001). Atmospheric corrections account for the effect of water vapour, which is the largest source of error in the estimation of water surface temperature after cloud contamination (Kondratyev & Filatov, 1999), but the effect of absorbing aerosols is difficult to quantify (Hepplewhite, 1989).

Optical images used for the estimation of chlorophyll *a* and Secchi disk depth also need to be atmospherically corrected, when quantitative estimations of water parameters are performed (Kutser *et al.*, 2005). In this project the transferability and repeatability of the non-standard algorithms from published literature that were

tested was very low. One cause for the latter could be the fact that most methodologies used non-atmospherically corrected data that limits their applicability over the site and the season for which they were developed, where and when the atmospheric effects do not vary significantly between images. A disadvantage of using the red and nIR wavebands for the estimation of chlorophyll *a* in Case II waters is that the signal detected at the sensor is weaker, as the penetration of light in water is poor and that might reduce the accuracy of chlorophyll *a* estimations (George, 1997b).

Interestingly, the atmospherically corrected Terra/Aqua MODIS data available in this project were very weakly correlated with field measurements, suggesting that the atmospheric corrections applied to the data were potentially not sufficient. In fact, the main limiting factor for the development of an effective algorithm to estimate water quality parameters from satellite data over Case II waters is widely recognised to be the lack of a robust atmospheric correction (e.g. IOCCG, 2000; Odermatt *et al*., 2008b; Odermatt *et al*., 2010).

2.4.3.2 Surface effects

The remote sensing instruments detect radiation that is emitted from the uppermost layer of the water surface whose thickness depends on the wavelength used for detection. For NOAA AVHRR data that cover the spectral region of 3-14 μm that surface layer is thinner than 0.1 mm (Robinson, 1985). The temperature of that thin uppermost layer differs from the bulk temperature (the layers that stretch from a few centimetres to a few metres below the surface) and that difference is called the skin effect. Skin temperature can be affected by the diurnal thermocline which is similar

to the seasonal thermocline in lakes, but with an ephemeral character. It is created when daytime solar heating causes the surface temperature to rise. Short-wave solar radiation warms the upper metre of the water that gets locally warmer, while the deeper layers are not directly affected (Robinson, 1985). Under low wind conditions this warming creates an afternoon temperature maximum a few millimetres below the surface. Below this shallow temperature maximum lie mixed layers of lower temperatures, while above it the temperature drops from the shallow maximum to create the cool skin of the water body (Cracknell, 1997). On sunny days, with calm weather, the effect of a diurnal thermocline is maximised, whilst at night the surface temperature decreases and this maximum is erased by vertical mixing (Robinson, 1985).

Uncertainty in the accuracy assessment of LST estimation algorithms is introduced by the fact that remotely sensed skin temperature estimates are compared to bulk temperatures measured *in situ* at depths ranging from a few centimetres to a few metres (buoys and ship measurements) (Robinson, 1985). The difference between the skin and bulk temperature can be between 0.1-0.5 °C and it is a highly recognized limitation in LST estimations with remote sensing (Robinson, 1985). In fact, it is probably the main cause of the bias observed in the NOAA AVHRR estimates of LST in this project (Cracknell, 1997). Unfortunately, the skin effect is quite variable (Reinart & Reinhold, 2008), which means it cannot be easily modelled and thus successfully removed from NOAA AVHRR water surface temperature estimates (Cracknell, 1997). However, at large spatial scales (e.g. larger than 150 km) it is expected that variations in the skin temperature reflect variations in the bulk temperatures. Thus the former have been used to validate *in situ* measurements of the

latter with more confidence in recent studies (e.g. Reinart & Reinhold, 2008). At smaller spatial scales (e.g. 20 km) the later is not always true (Cracknell, 1997).

The existence of specular reflection (i.e. sun-glint) on the surface of water is a common problem in both optical and thermal remote sensing unless appropriate corrections are made (Lillesand *et al*., 2008). The effect of specular reflection is that the estimation of the parameter under consideration is much different than its true value/concentration and thus the effect should be accounted for. However, areas of specular reflection can sometimes provide useful information during the visual interpretation of an image. For example, internal waves appear on the lake surface in the form of low frequency surface waves and are easily identified in areas of sun-glint (Kondratyev & Filatov, 1999). In this project areas of specular reflection that were identified visually in satellite scenes were omitted from analysis.

2.5 Sensors and methods to estimate lake water quality

Many lake studies have employed spaceborne and/or airborne remote sensing for the estimation of water parameters as shown in the following sections. Hand-held field spectroradiometers have also been employed to study in detail the spectral response of water constituents and their correlation with field measurements. Several key studies are explored here as they provide the basis for algorithm selection in a later chapter. The selected algorithms are presented in Chapter 4; Tables 4-5 to 4-8.

2.5.1 Limnological studies with spaceborne sensors

The most popular spaceborne sensor to estimate water quality parameters, even though originally developed for geological applications, is the Landsat Thematic Mapper (TM) and in some cases the Enhanced TM (ETM+) or the Multispectral Scanner (MSS). However, other sensors, such as Orbview-2 SeaWiFS, NOAA Advanced Very High Resolution Radiometer (AVHRR), Terra/Aqua Moderate Resolution Imaging Spectroradiometer (MODIS), Terra Advanced Spaceborne Thermal Emission and Reflection Radiometer (ASTER) and Envisat Medium Resolution Imaging Spectrometer (MERIS) have also been used.

2.5.1.1 Landsat MSS, TM and ETM+

Landsat TM has been employed to estimate chlorophyll *a* concentrations and SDD in a monomictic and oligotrophic reservoir in Arkansas, USA (Allee & Johnson, 1999). Two season-specific chlorophyll *a* estimation algorithms were developed for the months July and December of the same year and exhibited promising results. Two algorithms were also developed for SDD for the months July and February of two consecutive years. The first was rejected due to sampling bias (Allee & Johnson, 1999). The second algorithm (February) exhibited a strong coefficient of determination ($R^2 = 0.96$), but was developed from only a small sample size ($n = 14$) and the relationship was incapable of detecting changes of SDD of less than 1 m, whilst the actual field data range was only 1-4 m. The accuracy assessment of the chlorophyll *a* algorithms with historic data from the same season in different years showed that, when the algal composition was the same, the predictions were promising (Allee & Johnson, 1999). In fact, the authors highlighted that the

composition of the algal species (which varies seasonally) is a key issue to the development of algorithms for the prediction of chlorophyll *a* concentrations. On one hand, the type of species determines the wavelength at which absorption and reflectance of radiation exhibit a maximum. For example, the phycobiliproteins present in cyanobacteria absorb all visible light above 500 nm, but different phycobiliproteins exhibit different absorption maxima (Bennett & Bogorad, 1973). Phycoerythrin (also found in marine red algae) shows an absorption maximum at 562 nm and phycocyanin (found in cyanobacteria) at 615 nm (Bennett & Bogorad, 1973). On the other hand, the size of the species determines the characteristics of the backscattered light that is detected by remote sensing. For example, small coccolithophore (< 5 μm) scatter light which is wavelength-dependant, whereas coccospheres that are much larger (~ 22 μm) scatter light which is wavelength-independent. This phenomenon affects the reliability of chlorophyll *a* estimations if the same method is used for algal species of different sizes (Balch *et al*., 1989). The latter suggests that the development of a chlorophyll *a* algorithm, which is applicable in different seasons and in different lakes, may be difficult.

Another study where Landsat TM images were employed to map lake water quality was carried out by Dekker and Peters (1993). In this case, two images of ten eutrophic temperate lakes in the Netherlands were analyzed to provide estimations of chlorophyll *a* and SDD. Landsat TM bands 1, 2 and 3 were used in single band algorithms that were developed for small sample sizes (n = 9 in June and n = 10 in July). The authors showed that variability in the concentrations of water constituents may influence the predictive accuracy of regression analyses. It was shown that the best fit could be exponential at low to intermediate concentrations of water

constituents and may approach a linear relationship at higher concentrations (Dekker & Peters, 1993), which suggests that the optimum method for the estimation of different eutrophication levels in lakes might be the development of group-specific algorithms after the lakes are grouped with respect to their chlorophyll *a* concentrations.

Baban (1993) used Landsat TM data and multiple linear regression analysis to estimate various water quality parameters, including chlorophyll *a*, SDD and temperature, in fourteen very small (0.01-1.2 km^2) and shallow lakes of the Norfolk Broads, in England. The algorithms produced realistic predictions of summer concentrations and values of the three parameters under consideration both within the study sites and in neighbouring lakes, where extrapolated models were applied. However, small sample sizes were used for the development of the algorithms (n = 12 for chlorophyll *a*, n = 9 for SDD and n = 8 for lake surface temperature). The author used the green/red and red/blue ratios in the chlorophyll *a* estimation algorithm and the blue band in the SDD estimation algorithm.

Kloiber *et al*. (2002b) used thirteen scene-specific algorithms to estimate SDD within a Minnesota (USA) lake district in approximately 500 lakes over a period of 25 years. The surface area of the lakes varied between 0.1-7.5 km^2. Using historic field and a mixture of Landsat MSS and TM data, the authors mapped SDD in all 500 lakes and performed trend analysis that revealed temporal trends in forty nine of the sites. The remotely sensed data were not atmospherically corrected and as a result the regression equation was calibrated for each scene individually. The varying coefficients of the equation were found to result from the varying atmospheric

conditions and the differences between the view and Sun angles (Kloiber *et al*., 2002b). However, all regression equations had the same form and employed the same bands and band ratios, suggesting that if atmospherically calibrated data had been used instead of DN values, the coefficients would have been consistent.

The same combination of Landsat TM bands proposed by Kloiber *et al*. (2002a, 2002b) were used by Sawaya *et al*. (2003) to map SDD variations in small lakes in Minnesota, USA, in late summer (August-September). First, field data were regressed against Landsast TM radiances employing band 1 and the ratio band 1/band 3 to develop a SDD algorithm. Using the latter, SDD was mapped in the study sites with a prediction accuracy of $R^2 = 0.76$ and then these estimates were used as input to the development of a new algorithm based on IKONOS data. The authors suggest that remotely sensed estimates from one sensor could be used for the accuracy assessment of the estimates of another sensor, when field measurements are insufficient (Sawaya *et al*., 2003). The use of remote sensing sensors with high spatial resolution (e.g. IKONOS) in limnology offers the possibility to study very small lakes (minimum lake surface area 800 m^2). However, the high cost of such data and their relatively small geographic coverage make them inappropriate for the purposes of this project.

Vincent *et al*. (2004) detected water colour, especially the phycocyanin pigment, and mapped cyanobacterial blooms in a large eutrophic lake with frequent algal blooms (Lake Erie, the Laurentian Great Lakes) using both Landsat TM and ETM+ data. The advantage of combining the two sensors is the more frequent revisit capability, which is 8 days, instead of 16 days for one sensor. Water colour was sufficiently mapped

using Landsat EMT+ data, despite the relatively coarse spectral resolution of the sensor. The correlation coefficient was not as strong for Landsat TM data due to the noisier bands of the sensor in comparison to Landsat ETM+. The authors recommend the use of band ratios over single bands for the algorithm development, as they appeared to produce more robust and reliable results between the two sensors and with different solar angles (seasons) and atmospheric conditions (Vincent *et al*., 2004).

Tyler *et al*. (2006) studied chlorophyll *a* in a shallow polymictic temperate lake (Lake Balaton) using an algorithm developed for Landsat TM and ETM+ data that incorporates information on the spectral end members of suspended sediment, chlorophyll *a* concentrations and clear water. The authors produced a robust algorithm ($R^2 = 0.95$) that performed well in the lake under consideration estimating chlorophyll *a* with an accuracy of ± 4 µg L^{-1}. The lower limit of detection was approximately 10 µg L^{-1}, which suggests that the algorithm is not suitable for oligotrophic lakes. However, the application of the same approach to sensors with finer spectral and radiometric resolution than the Landsat TM/ETM+ is expected to decrease the lower limit of chlorophyll *a* detection (Tyler *et al*., 2006).

2.5.1.2 Other spaceborne sensors

Water quality parameters have been mapped in Case II waters using instruments such as Orbview-2 SeaWiFS even though the instrument was originally developed for Case I water applications, where emphasis is given to the blue and green parts for the spectrum (Vos & Rijkeboer, 2000). Vos and Rijkeboer (2000) developed a two-step method to map total suspended matter (TSM) and chlorophyll *a* in a large shallow

lake in the Netherlands with high concentrations of chlorophyll *a*. In the first step TSM was estimated using Orbview-2 SeaWiFS bands 3, 4, 5 and 6 and incorporating *in situ* estimates of chlorophyll *a* and CDOM. The TSM output was then used in an algorithm for the estimation of chlorophyll *a* incorporating again an estimate of CDOM. The chlorophyll *a* algorithm performed well only for high chlorophyll *a* concentrations (> 30 $\mu g\ L^{-1}$) with a stated accuracy of 20-30%, which was considered good given the high optical complexity of the lake for which it was developed (Vos & Rijkeboer, 2000). However, the exact form of the algorithm was not presented in the published study.

Vos *et al*. (2003) also used a similar method in two large shallow and eutrophic lakes in the Netherlands and found that it worked well only when the concentration of chlorophyll *a* was much higher than that of the TSM and high enough to mask out any variations caused by absorption due to CDOM at 440 nm. The authors also suggested the use of a multiplatform approach in the study of large lakes because water quality in such systems is highly heterogeneous and satellite remote sensing alone is incapable to study phenomena that occur at spatial scales smaller than the spatial resolution of the sensor used. Also, due to frequent cloud cover, spaceborne remote sensing data can only provide information on phenomena that occur at large temporal scales, for example seasonal variability. As a result, the authors used two types of remote sensing sensors: multispectral spaceborne (Orbview-2 SeaWiFS) and hyperspectral airborne (EPS-A Hyperspectral Mapper) remote sensing data. Due to their fine spatial resolution, airborne data are suited to the study of small scale phenomena (e.g. river plumes, fronts) while spaceborne data are capable of producing synoptic views for an entire lake in one overpass (Vos *et al*., 2003).

Envisat MERIS has been used in limnological studies in recent years with promising results (e.g. Gons *et al*., 2002; Odermatt *et al*., 2008a; Giardino *et al*., 2010). For example, Odermatt *et al*. (2008a) used Envisat MERIS data in conjunction with field spectroscopy data to map chlorophyll *a* concentrations in Lake Constance. They used a program called Modular Inversion and Processing System (MIP) that consists of various algorithms based on physical inversion models to generate water quality estimations (Heege & Fischer, 2004). The approach produced promising results, but it was limited by uncertainty in the atmospheric correction and especially due to the adjacency effect (Odermatt *et al*., 2008a). Gons *et al*. (2002) developed an Envisat MERIS specific algorithm to map chlorophyll *a* concentrations in various inland and coastal bodies. The approach worked well in mesotrophic to eutrophic Case II waters and employed Envisat MERIS bands 7 (red) and 9 (nIR). Finally, Giardino *et al*. (2010) produced an empirical algorithm for the estimation of chlorophyll *a* in a European lagoon that employed the ratio of MERIS bands 7 and 9 and produced very promising results (R^2 = 0.94) in spring and summer. The authors found that the empirical algorithm (used with atmospherically corrected data) produced more accurate results than the Case 2 Regional processor (C2R), assuming that atmospheric correction plays an important role in the estimation of water quality (Giardino *et al*., 2010).

Studies have also used processors that were specifically designed for the estimation of water quality parameters from Envisat MERIS data. For example, Odermatt *et al*. (2010) compared field chlorophyll *a* measurements with C2R chlorophyll products and found that the latter were relatively accurate over seven peri-alpine lakes varying from oligotrophic to mesotrophic. Also, Alikas *et al*. (2010) have used the Maximum

Chlorophyll Index (MCI) with Envisat MERIS data to map the seasonal and spatial distribution of chlorophyll *a* concentrations in two eutrophic European lakes. The MCI employs MERIS bands 8, 9 and 10 and produced promising results in the two study sites in different seasons. It was found that submerged aquatic vegetation affected the accuracy of the MCI estimates. Also, the composition of phytoplankton affects the concentration of chlorophyll *a* and, thus, the chlorophyll *a* estimates when different species are dominant in the same lake in different seasons (Alikas *et al*., 2010). The latter agrees with the findings of others (e.g. Bennett & Bogorad, 1973; Balch *et al*., 1989; Allee & Johnson, 1999).

Other sensors that have been employed in lake studies include NOAA AVHRR, Terra/Aqua MODIS and Terra ASTER. Temperature is a parameter commonly studied with these instruments. Bussières *et al*. (2002) used NOAA AVHRR thermal data to map water temperatures in spring and summer over 132 boreal lakes in Canada with surface areas greater than 100 km^2. An empirical quadratic polynomial algorithm was calibrated for each study site separately. Once temperature was mapped in all study sites, the thermal cycles of the lakes were studied with respect to the individual geographical and morphological characteristics of the sites (i.e. latitude, water body area and perimeter) in order to provide information on lake thermal behaviour. The authors found that latitude and water body area are critical parameters that affect the lake water temperature cycle. However, the latter was found to be independent of the perimeter of lakes. Further analysis showed a strong agreement between air temperature and water temperatures. The same has been concluded by other studies as well (e.g. Livingstone & Padisák, 2007; Arhonditsis *et al*., 2004; Peeters *et al*., 2002; Livingstone & Dokulil, 2001). According to Bussières

et al. (2002), slow seasonal changes in temperature values in boreal lakes can be adequately mapped with NOAA AVHRR data, despite any gaps due to cloud cover and other operational problems. The latter suggests that NOAA AVHRR is a good candidate for the study of the thermal distribution and patterns of European lakes across large spatial scales.

Thermal Terra ASTER, MODIS and Landsat ETM+ data have been used to map surface temperatures, and thus, determine upwellings and surface circulation in lakes (Steissberg *et al*., 2005). While Landsat ETM+ has only one thermal band (band 6), Terra ASTER carries five thermal bands (bands 10-14) and Terra MODIS carries three (bands 29, 31-32). It was found that the horizontal distribution of surface temperature was clearly shown in Landsat ETM+ and Terra ASTER images that have a relatively fine spatial resolution (30 x 30 m and 90 x 90 m respectively), but Terra MODIS data (1 x 1 km) were incapable of reproducing detail at small scales of thermal phenomena, such as upwellings. However, Terra MODIS data are available at shorter time scales (every 2 days) whereas Terra ASTER and Landsat ETM+ provide data every 16 days, which are too infrequent for the study of upwellings and other thermal features with life spans of a only few days. Steissberg *et al*. (2005) suggest that a combination of higher spatial resolution sensors, such as ASTER and Landsat ETM+, and data from sensors with higher revisit capability, such as Terra/Aqua MODIS, is optimum for the study of relatively small spatial and temporal scale thermal processes in lake waters.

Oesch *et al*. (2005) employed NOAA AVHRR and Terra/Aqua MODIS thermal data over lakes Geneva, Constance and Mond to test three algorithms for lake surface

temperature mapping. The NASA standard NOAA AVHRR multi-channel sea surface temperature (MCSST) and non-linear sea surface temperature (NLSST) algorithms and the NASA standard Terra/Aqua MODIS SST algorithm were tested. Night-time data from both sensors were found to be more reliable than data collected during the day because they are not affected by the diurnal variability in SST, offering better estimations of lake surface temperature (Oesch *et al*., 2005). However, in most limnological studies, where field data are essential for the accuracy assessment of the remotely sensed estimates, the correspondence of timings of the two datasets is a key factor and therefore day-time satellite data are used to match the timings of the field campaigns.

2.5.2 Limnological studies with airborne sensors

Airborne sensors have also been used for the estimation and mapping of lake water quality parameters. Among these the Airborne Imaging Spectrometer for Applications (AISA) has often been used, as well as the Deadalus 1268 Airborne Thematic Mapper (ATM).

2.5.2.1 AISA

AISA data have been used to predict chlorophyll *a* concentrations (e.g. Pulliainen *et al*., 2001; Kallio *et al*., 2003), turbidity and SDD (e.g. Kallio *et al*., 2001; Koponen *et al*., 2002); while Deadalus 1268 ATM has been used in lake waters to map chlorophyll *a* (e.g. Hedger *et al*., 1996; George, 1997b). Pulliainen *et al*. (2001) developed a chlorophyll *a* estimation algorithm using AISA data and field measurements from a small number of south Finnish lakes and applied it to

neighbouring lakes with similar characteristics (where field data were unavailable) to produce estimations of mean chlorophyll *a* concentrations. In total, eleven lakes were studied that ranged from oligotrophic to eutrophic and humic with various turbidity levels. Due to the additive effect of turbidity on the spectral signature of chlorophyll *a* in Case II waters a chlorophyll *a* estimation algorithm that works well in Case II waters should incorporate spectral wavebands that are independent of changes in turbidity, such as the nIR/red ratio at around 665-675 nm (red) and 700-710 nm (nIR) (e.g. Quibell, 1991; Gitelson *et al*., 1993; Han *et al*., 1994). Pulliainen *et al*. (2001) used two different spectral ratios that approximate the nIR/red ratio to produce the best results in different seasons. In that way, they highlighted the advantage of hyperspectral data over multispectral data as the former have a large number of narrow wavebands in the red and nIR that offers the possibility to identify optimum bands in the estimation of water quality in different seasons. The authors recommend an *a priori* grouping of the lakes according to their eutrophication status and the calibration of the algorithm separately for each group of lakes in order to improve the accuracy of the technique (Pulliainen *et al*., 2001).

Kallio *et al*. (2001) tested band ratios and combinations recommended in published literature to develop optimal algorithms for the estimation of water quality in eleven south Finnish lakes with variable ecological characteristics. They employed AISA band combinations that approximated Envisat MERIS channels, showing the applicability of the first and the potential for the second in lake studies. Their findings suggest that the best band ratio for the estimation of chlorophyll *a* depends on the chlorophyll *a* concentration. Shorter wavelengths (685-691 nm) in the red region are more appropriate for low chlorophyll *a* concentrations (oligotrophic and

mesotrophic lakes) and longer wavelengths (699-705 nm) are necessary to map high concentrations (eutrophic lakes) (Kallio *et al*., 2001). The latter agrees with observations made by others. For example, Gitelson (1992) found that the maximum reflectance peak of chlorophyll *a* shifts from approximately 680 nm to 715 nm with increasing chlorophyll *a* concentrations from 1 to 100 μg L^{-1}. George (1997b) reached a similar conclusion for Case I lake waters. He found that the blue waveband is more appropriate for the study of Case I oligotrophic waters; whereas the green was more suitable for more productive Case I waters. Kallio *et al*. (2001) produced reliable season-specific algorithms to map water quality parameters in the lakes and found that the use of reflectance data over radiance improved the accuracy of SDD estimation algorithms, but the same was not observed for chlorophyll *a* (Kallio *et al*., 2001). Even though the algorithms produced by Kallio *et al*. (2001) are not transferable in different seasons, they were developed for a range of chlorophyll *a* concentrations, which suggests a potential for transferability between sites in the same season.

Kallio *et al*. (2003) demonstrated that AISA data can reliably predict ($R^2 > 0.96$) chlorophyll *a* concentrations in two mesotrophic to eutrophic lakes in late summer (August) and suggest that, as long as the dominant phytoplankton species are the same, the same algorithms can be applied again in the same sites and in the same season in different years. The same band ratio was used for both sites, but the regression coefficients were calibrated for each site separately. The latter suggests that the development of a universal algorithm that predicts chlorophyll *a* concentrations in all European lakes despite their eutrophication status is not feasible. Moreover, it seems rather difficult to produce a chlorophyll *a* estimation

algorithm that is applicable in all seasons. The authors studied a ratio of wavebands that can also be applicable to Envisat MERIS data showing the potential of that sensor in limnological studies.

Apart from chlorophyll *a,* turbidity and SDD have also been accurately mapped using AISA data (Koponen *et al*., 2002) with the most successful algorithm relating to SDD, while turbidity and chlorophyll estimations were also well characterized (Koponen *et al*., 2002). The authors used field data from eleven south Finnish lakes with variable characteristics. The advantage of using band ratios over single bands in the estimation of water quality parameters is that it corrects part of the atmospheric effects (Koponen *et al*., 2002). Moreover, they subtracted a nIR band (centred at 781 nm) from the radiance bands used in the SDD and chlorophyll *a* estimation algorithms, which works as an atmospheric correction. Even though in turbid lake waters the reflectance of water at the nIR wavelengths is not always zero, the authors found that the method improved the predictive accuracy of the algorithms. The authors spectrally simulated Envisat MERIS data using AISA data and found that the results were very similar to those with AISA. Envisat MERIS could therefore replace the use of AISA data, especially because the latter are very expensive and cover small areas. However, the atmospheric effects are stronger in satellite imagery and that might reduce the accuracy of the methods. Despite that, another advantage of spaceborne remote sensing over the airborne is that the solar angle and weather conditions are constant in the image, as it takes less time for the acquisition of the data, which is thought to increase the accuracy of the estimation method. Finally, the method presented was not tested for temporal reliability (i.e. in other seasons), but

the authors believe that it should provide reliable estimates of water quality parameters in other Finnish lakes with similar characteristics.

2.5.2.2 Daedalus ATM

Daedalus 1268 ATM airborne data have been successfully used to map chlorophyll *a* concentrations in six large lakes in the English Lake District though necessitating the application of different algorithms in lakes with different levels of productivity and eutrophication status (George, 1997b). The lakes are Case I waters and thus the green/blue ratio was used to estimate low chlorophyll *a* concentrations (< 10 μg L^{-1}) and only the green band to estimate higher chlorophyll *a* concentrations (10-66 μg L^{-1}). The author has concluded that algorithms based on band ratios have the advantage to reduce problems caused by variations in the sun angle, whereas single band algorithms are more sensitive to such effects. However, the combination of bands in the development of an algorithm introduces more noise than when single bands are used (George, 1997b).

Hedger *et al*. (1996) argued that band ratios are inappropriate when comparing water quality parameters in different lakes, because spatial and temporal variations in the quality of light in different images might introduce errors when ratios are used. The latter can be a barrier towards the development of an interregional methodology for the estimation of water quality parameters in European lakes. Hedger *et al*. (1996) used Daedalus 1268 ATM radiance data in conjunction with algorithms developed by Bennet (1995) to estimate chlorophyll *a* concentrations in two British lakes (Loch Lomond and Loch Leven). The authors used the blue/green ratio for the oligotrophic

lake (Loch Lomond) and the green/red ratio for the mesotrophic lake (Loch Leven) (Hedger *et al*., 1996).

2.5.3 Limnological studies with field spectroscopy

Several researchers have employed hand-held field spectroradiometers in studies of lake water quality.

Thiemann & Kaufmann (2000) used field spectroscopy to estimate chlorophyll *a* in lake waters. The study, carried out in five German temperate lakes, demonstrated a strong correlation between the nIR/red ratio for field reflectance data and field chlorophyll *a* measurements (Thiemann & Kaufmann, 2000). Strömbeck and Pierson (2001) employed reflectance measurements from a field spectroradiometer in a meso-eutrophic Swedish lake (Lake Mälaren) to create a chlorophyll *a* estimation algorithm based on the nIR/red ratio, using a band combination that approximates two Envisat MERIS bands. The algorithm produced inaccurate estimations for chlorophyll *a* concentrations less than 20 μg L^{-1} (oligotrophic and mesotrophic lakes) due to the variable influence of other heterogeneously distributed water constituents, such as suspended matter and CDOM. It was concluded that chlorophyll *a* estimation algorithms should follow a two-step approach incorporating information on the amount of suspended matter and CDOM in water to maximise their performance (Strömbeck & Pierson, 2001).

Dall'Olmo *et al*. (2005) studied the extent to which the nIR/red ratio, where the absorption by other optical active water constituents such as CDOM and suspended matter is negligible, can be accurately used to estimate chlorophyll *a* concentrations

in Case II waters and how this ratio is affected by uncertainties in atmospheric correction. In clear waters (Case I) the nIR wavelengths are completely absorbed and the only signal that returns to the sensor is due to atmospheric effects. Atmospheric corrections in Case I waters are based on this principle (IOCCG, 2000). However, in turbid waters (Case II) suspended particles scatter light back to sensor and so the atmospheric effects are not easily quantified (Vidot & Santer, 2005). Dall'Olmo *et al*. (2005) used field spectrometer data to simulate Orbview-2 SeaWiFS and Terra/Aqua MODIS data and showed that both sensors have the potential to produce promising results, but they highlighted that the lack of an accurate and robust atmospheric correction method is a major problem in the estimation of chlorophyll *a* concentrations when employing the two sensors (Dall'Olmo *et al*., 2005). Even though they are currently used operationally only for Case I waters, Orbview-2 SeaWiFS and Terra/Aqua MODIS both produced promising results, despite the lower signal-to-noise ratio of the former. Other studies have also demonstrated the potential for Orbview-2 SeaWiFS to estimate water quality parameters in Case II waters (e.g. Vos & Rijkeboer, 2000). The combination of Terra/Aqua MODIS 667 nm and 748 nm exhibited higher predictive accuracy than the combination of 678 nm and 748 nm (Dall'Olmo *et al*., 2005). In another study, lower red wavelengths have been shown to work well in oligo-mesotrophic lake waters, while higher red wavelengths perform better in eutrophic lakes (Kallio *et al*., 2001). However, the chlorophyll *a* concentration of the water bodies studied by Dall'Olmo *et al*. (2005) varied from 4-236.5 μg L^{-1} with an average of 38.5 μg L^{-1}, which means the study sites were highly eutrophic. The NASA standard SeaWiFS OC4 (version 4) algorithm was also tested with field data from turbid lakes and the results showed

that the algorithm is incapable to produce reliable estimates of chlorophyll *a* in Case II waters.

Finally, Gitelson *et al*. (1993) studied lake systems and other inland water bodies in different geographical areas of Eastern Europe (Russia, Hungary, Bulgaria) and Central Europe (Germany) that encompass a wide range of ecological characteristics. They used reflectance measured by a field spectrometer and tested different band combinations finding that shorter wavelengths (blue, green) are suitable for oligotrophic waters, while longer wavelengths (red, nIR) are more appropriate for eutrophic waters. This agrees with the findings of others (e.g. Gitelson, 1992; George, 1997b; Kallio *et al*., 2001). They also found that the ratios nIR/green and nIR/red work best in chlorophyll *a* estimation algorithms with the second giving a predictive accuracy of less than ± 2 μg L^{-1} (Gitelson *et al*., 1993). They overcame the problem of inconsistent algorithm coefficients, when the same algorithm is calibrated separately in lakes with different eutrophication status, by using a local correction based on the average chlorophyll *a* concentration of each lake under consideration (Gitelson *et al*., 1993). This could provide the basis of a universal model that can be applied to all European temperate lakes.

2.5.4 Comparison of different platforms: spaceborne, airborne and field spectroscopy data

Field spectroscopy is a very promising method in water applications and it has been used in the establishment of a theoretical basis on the principles of interaction between water components and the detected signal (e.g. Quibell, 1991; Han *et al*.,

1994). Field spectroscopy collects data that do not require atmospheric correction as the measurements originate directly above the water body. The latter is a major advantage in the estimation of water quality parameter estimations in lakes because the low accuracy of these algorithms is partly due to uncertainties associated with atmospheric corrections over lake bodies (Dall'Olmo *et al*., 2005). However, field spectroscopy cannot provide wide spatial and temporal coverage of lakes and therefore it cannot be used in the real-time estimation of water quality parameters. Moreover, like traditional field campaigns, it is time-consuming and requires a lot of effort in the field. Despite these problems, field spectroscopy does not suffer from scaling issues (unlike airborne and spaceborne data), as a point field measurement of any water quality parameter is directly compared to a point field reflectance measurement. In conclusion, field spectroscopy is useful in the sophisticated study of the inherent optical properties of individual lakes and therefore it can be incorporated in the development of accurate algorithms that are compatible with the specifications of satellite sensors (e.g. Strömbeck & Pierson, 2001; Dall'Olmo *et al*., 2005).

Hyperspectral data have fine spectral resolutions, and are often flown on aircrafts so also offer high spatial resolution, that offer the opportunity to study very small lakes and also phenomena that occur at small spatial scales. The large number of narrow wavebands offers the possibility to optimize water quality estimation algorithms for different lake types and different seasons when individual absorption maxima and reflection peaks occur (Kallio *et al*., 2001; Pulliainen *et al*., 2001). In addition, airborne hyperspectral data can be collected simultaneously to field measurements and as many times as desired, but for limited time periods due to their high cost. As a result, hyperspectral data are unsuitable for the study of wide temporal scale

phenomena. Moreover, they are unsuitable for the study of large lake systems (or large areas in general) due to their narrow swath and thus inappropriate for the real-time study of European lakes.

Multispectral remote sensing has the advantage of synoptic viewing; it is affordable and has a frequent revisit capability (e.g. Baban, 1993; Fraser, 1998). For that reason, many lake studies have used Landsat TM/ETM+ data in past and recent years (e.g. Dekker & Peters, 1993; Allee & Johnson, 1999; Kloiber *et al*., 2002b; Vincent *et al*., 2004). The merit of Landsat TM/ETM+, compared to other multispectral sensors, is the long archive of data (since July 1972) and the continuity of data collection due to future Landsat satellites (LDCM, 2010). The sensor has an acceptable spatial resolution, but its low spectral and radiometric resolution is a limiting factor in limnological studies (Dekker & Peters, 1993). By contrast, two sensors that were developed for water applications are now considered inappropriate for operational use either because they have been discontinued or they are considered unreliable due to technical issues. Specifically, the Nimbus-7 CZCS archive covers only 7.5 years (October 1978 - June 1986) and the Orbview-2 SeaWiFS (launched in August 1997) has a potential for lake studies (Vos & Rijkeboer, 2000; Dall'Olmo *et al*., 2005), but its operation has been irregularly interrupted with significant failures in 2008 and 2009 (Personal Communication with Dr. Feldman G. C., NASA).

2.5.4.1 Requirements of a suitable sensor for the estimation of lake water quality

Dekker and Peters (1993) note that the technical characteristics of sensors, such as the radiometric and spectral resolution, may limit the quantitative mapping of water quality parameters. Not all sensors can be used to map water quality, as the low

sensitivity in bands that are crucial for mapping water characteristics is the main limiting factor. The relatively poor spatial resolution also limits their use in similar applications over small water bodies and/or when small spatial scale phenomena are to be studied (Vos *et al*., 2003). Moreover, changes in atmospheric and weather conditions influence the measurements, but a robust atmospheric correction has not been yet developed for lake waters (e.g. Dall'Olmo *et al*., 2005; Odermatt *et al*., 2010).

In summary, a suitable sensor for the implementation of this project should satisfy most (if not all) of the following criteria:

- Frequent revisit capability (e.g. every day or a few days)
- Large swath to cover large spatial scales (hundreds of kilometres), but relatively fine spatial resolution (tens or a few hundreds of metres)
- Relatively narrow spectral wavebands that cover regions of the visible and nIR parts of the spectrum where key water components (e.g. chlorophyll *a* and suspended matter) absorb and reflect radiation and wavebands in the TIR for the estimation of temperature
- Fine radiometric resolution (e.g. 10-bit or more)
- Automated facilities for real-time data pre-processing and robust methods for atmospheric correction of the satellite data
- Long archive of images to permit use of historical data for the study of long-term trends and patterns
- Continuation of mission that will supply satellite data in the future
- Free or low cost data supply

- Successfully applied in other studies for the estimation of lake water quality and/or recommended in published literature

2.6 The potential of NOAA AVHRR and Terra/Aqua MODIS for estimating lake water quality

The NOAA AVHRR and Terra/Aqua MODIS have potential for estimating and monitoring lake water quality as they satisfy most of the above mentioned criteria.

Oesch *et al*. (2005) suggest that NOAA AVHRR data are suitable for the estimation of lake water surface temperature. The potential of frequent cloud-free NOAA AVHRR data to map temperature and thermal circulation features in lake waters throughout a year has been demonstrated at one site (Oesch *et al*., 2008), but the need to study more sites simultaneously is essential for international policies and management plans. According to Bussières *et al*. (2002), slow seasonal changes in temperature values in boreal lakes can be adequately mapped with NOAA AVHRR data, despite any gaps due to cloud cover. In addition, Terra/Aqua MODIS data are potentially useful for the study of thermal phenomena that occur over short temporal scales (Steissberg *et al*., 2005) and are suitable for lake surface temperature estimations (Oesch *et al*., 2005). The above suggest that NOAA AVHRR and Terra/Aqua MODIS are good candidates for the study of the thermal distribution and patterns of European lakes across large spatial scales.

Also, Dall'Olmo *et al*. (2005) suggest that Terra/Aqua MODIS data can be used to map chlorophyll *a* concentrations in Case II waters. The Terra/Aqua MODIS data

also cover spectral regions that are used in the correction of atmospheric scattering and absorption, which means that there is a possibility to develop methods for adequate atmospheric corrections over Case II waters (Kloiber *et al*., 2002a).

2.6.1 The NOAA Advanced Very High Resolution Radiometer

The Advanced Very High Resolution Radiometer (AVHRR) was developed by NASA as part of the Polar-Orbiting Operational Environmental Satellites (POES) project and is carried on the NOAA satellite series, which have been operating since late 1978 (initially named TIROS satellites) (Table 2-5).

Table 2-5: NOAA series characteristics: name, orbit, number of channels and operational dates (NEODAAS DSRS, 2009).

Platform	Orbit	Number of channels	Operational dates
NOAA 6	Day	4	07/1979-07/1986
7	Night	5	06/1981-01/1985
8	Day	4	06/1982-10/1985
9	Night	5	12/1984-01/1995
10	Day	4	10/1986-10/1994
11	Night	5	10/1988-09/1994
12	Day	5	07/1991-date
13	-	-	(failed)
14	Night	5	01/1995-date
15	Day	6[+]	05/1998-07/2000
16	Night	6[+]	09/2000-date
17	Day	6[+]	06/2002-date
18	Night	6[+]	05/2005-date

[+]Transmit only channel 3A or 3B, and thus, in total 5 channels

NOAA satellites are in a sun-synchronous orbit at an altitude of approximately 833 km above the Earth's surface. The NOAA AVHRR is an across-track (whiskbroom) scanner (Figure 2-9A) with a field-of-view (FOV) of ± 55.4° off nadir, providing a swath width of 2400 km and a spatial resolution of 1.1 x 1.1 km. The radiometric resolution of AVHRR is 10-bit and it senses in five wavebands (the first three day-time sensors in the series (NOAA-6, -8 and -10) had only four channels). At any time, two NOAA satellites are operational; one day-time and one night-time satellite. The equatorial crossing times are 1.30 to 2.30 a.m. for NOAA-7, -9, -11, -14 and -16, and 7.30 a.m. for NOAA-6, -8, -10, -12, -15 (10 a.m. for NOAA-17). Each satellite covers the globe every 24 hours, with a revisit time of 12 hours when both satellites are used (Jensen, 2000), and hence, daily visible data and twice-daily thermal data can be obtained (Lillesand *et al*., 2008).

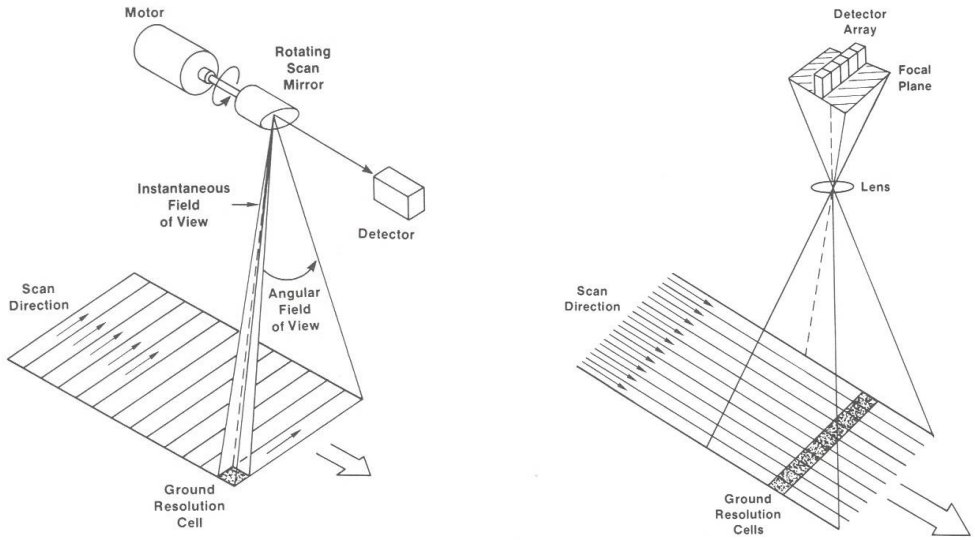

(A) Across-track (whiskbroom) scanner (B) Along-track (pushbroom) scanner

Figure 2-9: Two types of scanning systems for acquiring remotely sensed images: (A) Across-track scanner and (B) Along-track scanner (Sabins, 1997; p. 7).

The AVHRR sensor has been successfully employed for hydrologic and oceanographic applications (NESDIS, 2009). In fact, the NOAA AVHRR thermal infrared bands were designed for the estimation of sea surface temperature and are calibrated for that purpose (Cracknell, 1997). In addition, AVHRR data are regularly used to map vegetation, soil moisture, snow cover, volcanic eruptions, floods, fires, and geological features (Table 2-6) (Jensen, 2000; Lillesand *et al*., 2008).

Table 2-6: NOAA AVHRR spectral channels and their primary use (Adapted from Jensen, 2000; NASA, 2009; NESDIS, 2009).

Band	Bandwidth (μm)			Application/ Primary use
	AVHRR/1[1]	AVHRR/2[2]	AVHRR/3[3]	
1 (Red)	0.58-0.68	0.58-0.68	0.58-0.68	Day-time cloud, snow, ice and vegetation mapping
2 (nIR)	0.725-1.10	0.725-1.10	0.725-1.00	Land-water interface delineation; snow, ice and vegetation mapping
3a (mIR)	-	-	1.58-1.63	Monitoring hot targets (forest fires, volcanoes); night cloud mapping
3b (TIR)	3.55-3.93	3.55-3.93	3.55-3.93	Day and night cloud and surface temperature mapping
4 (TIR)	10.5-11.5	10.3-11.3	10.3-11.3	Cloud and surface temperature, day and night cloud mapping; removal of atmospheric water vapour path radiance
5 (TIR)	-	11.5-12.5	11.5-12.5	

[1]AVHRR/1 onboard TIROS-N and NOAA-6, -8, -10

[2]AVHRR/2 onboard NOAA-7, -9, -11, -12, -14

[3]AVHRR/3 onboard NOAA-15, -16, -17, -18

2.6.2 The Terra/Aqua Moderate Resolution Imaging Spectroradiometer

NASA's Moderate Resolution Imaging Spectro-Radiometer (MODIS) is one of many sensors onboard the Terra and Aqua satellite platforms developed by NASA

during the Earth Observing System (EOS) project. The mission aims to study the Earth's environment and especially the impacts of anthropogenic activities and natural events. MODIS was developed to address many applications over land, the ocean, ice surfaces and the atmosphere. Thus, the sensor incorporates wavebands (Table 2-7) suitable to provide observations of vegetation structure and dynamics, cloud and aerosol properties, concentrations of greenhouse gases and surface processes (e.g. volcanic eruptions) (Lillesand *et al*., 2008). The visible and nIR wavebands 8-16 on MODIS enable collection of information regarding ocean colour and the concentration of chlorophyll *a* in Case I waters.

The Terra and Aqua satellites are in a sun-synchronous orbit at an altitude of 705 km above the Earth's surface. Terra has an equatorial crossing time of 10.30 a.m., while Aqua follows with an equatorial crossing time of 13.30 p.m. MODIS is an across-track (whiskbroom) scanner with a set of linear detector arrays (Figure 2-9A). It has a FOV of ± 55° off nadir, providing a swath width of 2330 km. The instrument employs 36 spectral channels at a radiometric resolution of 12-bit. The spatial resolution of MODIS ranges from 250 x 250 m (bands 1-2), to 500 x 500 m (bands 3-7) and 1000 x 1000 m (bands 8-36).

The operational use of the Terra and Aqua platforms started in April 2000 and May 2002 respectively and thus, no MODIS data are available before these dates. However, the frequency of data acquisition for Terra/Aqua MODIS is high, as the capacity of the satellites to provide data over a specific area can be up to two days depending on cloud cover. Also, Terra/Aqua MODIS have the advantage to offer

many more and relatively narrower wavebands than other multispectral sensors (e.g. Landsat TM, Orbview-2 SeaWiFS) that have been used in limnological studies.

Table 2-7: MODIS spectral bands and specifications and their primary use (modified from Jensen, 2000; p. 232 and Lillesand *et al*., 2008; p. 474).

Band	Bandwidth (μm)	Spatial resolution at nadir (m)	Application/ Primary use
1	0.620-0.670	250	Land/cloud boundaries, land cover classification and chlorophyll absorption
2	0.841-0.876	250	
3	0.459-0.479	500	Land, cloud and aerosol properties
4	0.545-0.565	500	
5	1.230-1.250	500	
6	1.628-1.652	500	
7	2.105-2.155	500	
8	0.405-0.420	1000	Ocean colour, phytoplankton, biogeochemistry
9	0.438-0.448	1000	
10	0.483-0.493	1000	
11	0.526-0.536	1000	
12	0.546-0.556	1000	
13	0.662-0.672	1000	
14	0.673-0.683	1000	
15	0.743-0.753	1000	
16	0.862-0.877	1000	
17	0.890-0.920	1000	Atmospheric water vapour
18	0.931-0.941	1000	
19	0.915-0.965	1000	

Table 2-7: (cont.)

Band	Bandwidth (μm)	Spatial resolution at nadir (m)	Application/ Primary use
20	3.660-3.840	1000	Surface-cloud temperature
21[a]	3.929-3.989	1000	
22	3.929-3.989	1000	
23	4.020-4.080	1000	
24	4.433-4.498	1000	Atmospheric temperature
25	4.482-4.549	1000	
26[b]	1.360-1.390	1000	Cirrus clouds
27	6.538-3.895	1000	Water vapour
28	7.175-7.475	1000	
29	8.400-8.700	1000	
30	9.580-9.880	1000	Ozone
31	10.780-11.280	1000	Surface-cloud temperature
32	11.770-12.270	1000	
33	13.185-13.485	1000	Cloud top altitude
34	13.485-13.758	1000	
35	13.785-14.085	1000	
36	14.085-14.385	1000	

[a]Bands 21 and 22 are similar, but band 21 saturates at 500 K versus 328 K

[b]Wavelength out of sequence due to change in sensor design

2.7 Summary

This chapter has demonstrated that lakes are variable ecosystems and because of that their monitoring with remote sensing is not always a straight-forward procedure. The

type of lakes (i.e. Case I or Case II) and their ecological characteristics (e.g. trophic status, mixing conditions, local climatic regime, geographical location) should be taken into account in studies of multiple lakes across wide spatial and temporal scales, in order to identify all factors that influence the behaviour and optical properties of the lakes under consideration. Because of the complexity of lake optical characteristics, season- and site-specific algorithms are common for the estimation of key lake water quality parameters, which suggests that the need for a universal algorithm is high, but its development challenging. NOAA AVHRR and Terra/Aqua MODIS have potential for estimating water quality in lakes but their reliability in limnological studies of wide temporal and spatial scales has yet to be tested.

Chapter III.

METHODOLOGY PART I: FIELD DATA ACQUISITION AND ANALYSIS

3.1 Introduction

The aim of this chapter is to present the source, frequency and volume of the field data and provide information on each study site. In total 23 European lakes were studied including eleven sites in Scandinavia, nine in the European mainland and three in Britain. Apart from varying in their ecological characteristics, the lakes also span a wide range of physical types, varying from small (surface area ~ 5 km^2) up to the third largest lake in Europe (surface area > 5,000 km^2). Field data from various collaborating Environmental Institutes were used in the construction of an extensive database. Individual characteristics of the study sites and similarities in their ecological behaviour could then be explored, thus providing a basis for their grouping.

3.2 Field data request

Field observations for 23 lakes were requested for a period extending back 30 years, comparable to the length of the NERC Earth Observation Data Acquisition and Analysis Service (NEODAAS) Dundee Satellite Receiving Station (DSRS) satellite archive. Field measurements of lake surface temperature (referred to as LST hereafter) and chlorophyll *a* concentrations at the lake surface were requested. The lake surface generally represents the upper 0.5 m part of the water body, but data

from as deep as 1 m below the surface were also acquired when shallower measurements were not available. SDD measurements for the same sampling stations and sites were also requested along with the coordinates of each sampling station. In order to study lakes across as large an area as possible, field data were requested from limnological institutes and environmental organisations across Europe, including the European mainland, Scandinavia and Britain.

For each lake for which data were requested two criteria had to be met. First, the surface area of the lake should be large enough with respect to the spatial resolution of satellite sensors to be used. As a result, lakes with surface areas greater then 3 km^2 were requested. Second, the total sample of lakes should vary in their ecological and hydromorphological characteristics (e.g. mixing type, eutrophication status, formation and duration of winter ice cover), and/or be subject to a range of climatic conditions and/or a spectrum of management practices in order to test the reliability of algorithms in different types of lakes within various geographical settings.

3.2.1 Data sources

Most of the field data were obtained during the first year of the project. Data for the British lakes were obtained in the second year, due to delays. A letter was sent to potential data suppliers explaining the aims and objectives of the project and requesting field measurements of three water quality parameters in the past three decades from lakes around Europe. In total, ten suppliers replied positively and provided field data. The data sources included Environmental Agencies, Institutes and Universities that have studied environmental issues, but also other relevant

organizations and legal bodies that have been involved in limnological research (Table 3-1).

Table 3-1: Collaborating institutes and agencies from the European countries and sites for which data were acquired.

Country	Institute/ Agency	Lake
Sweden	Swedish Environmental Protection Agency	Vänern Vättern Mälaren Hjälmaren
Finland	Finnish Environment Institute (SYKE)	Päijänne Inarijärvi Oulujärvi Pielinen Haukivesi Kallavesi Nasijärvi
Germany	Institute of Coastal Research (GKSS) & Society for the Utilisation of Atomic Energy in Shipbuilding and Shipping Ltd	Constance
	Leibniz Institute of Freshwater Ecology and Inland Fisheries (IGB)	Müggelsee
Hungary	Ministry of Environmental Protection and Water Management, Ministry of Health	Balaton Tisza Velence
Switzerland	International Commission for the Protection of Lake Geneva (CIPEL)	Geneva
France	Syndicate Mixte du Lac d'Annecy (SILA)	Bourget
	Comité Intercommunal pour le suivi et l'assainissement du lac du Bourget (CISALB)	Annecy Aiguebelette
Britain	Environmental Change Network (ECN)	Lomond Windermere Leven

Table 3-2a: Sampling period and frequency for each of the parameters in the study sites: Scandinavia.

Lake	Parameter		
	Temperature	**Chlorophyll *a***	**SDD**
Vänern	1973-2008 monthly in Apr-Aug	1973-2008 monthly in Apr-Oct	1973-2008 monthly; Apr-Oct
Vättern	1969-2003 monthly in Apr-Oct	1967-2003 monthly in Apr-Oct	1967-2003 monthly; Apr-Nov
Mälaren	1964-2008 monthly in Mar & May-Oct	1965-2008 monthly in Feb-Nov	1964-2008 monthly; Mar-Oct
Hjälmaren	1965-1995, 2003-2004 monthly; Mar & May-Oct	1966-1995 monthly in Mar-Oct	1965-1995 monthly; Mar-Oct
Päijänne	1965-2005 monthly; bimonthly	1975-2005 weekly; biweekly; monthly	(no data)
Inarijärvi	1965-2005 3-4 months per year; usually Mar & Aug	1974-2005 Jun-Sep; usually only Aug	(no data)
Oulujärvi	1960-2005 biweekly; monthly; seasonally	2001-2005 monthly in May-Aug (1 station only)	(no data)
Pielinen	1960-2005 bimonthly; seasonally usually Mar & Aug	1977-2005 biweekly; monthly in May-Oct	(no data)
Haukivesi	1961-2005 Monthly; bimonthly; seasonally	1976-2005 monthly; bimonthly in May-Oct	(no data)
Kallavesi	1962-2005 monthly; seasonally	1978-2005 monthly in Jun-Sep	(no data)
Nasijärvi	1962-2005 monthly; bimonthly	1975-2005 biweekly, monthly; summer months	(no data)

Table 3-2b: Sampling period and frequency for each of the parameters in the study sites: the European mainland and Britain.

Lake	Parameter		
	Temperature	**Chlorophyll *a***	**SDD**
Constance	1989-1997 daily, weekly, biweekly; all months	1980-1997 daily, weekly, biweekly; all months	1980-1996 daily, weekly, biweekly; usually all months
Müggelsee	1978-2005 weekly, biweekly, monthly; all months	2002-2005 daily; most months	1979-2005 weekly, biweekly; most months
Balaton	2000-2006 weekly; mid May-mid Sep	2000-2009 weekly; mid May-mid Sep	(no data)
Tisza	2001-2008 monthly; Mar-Oct	2001-2008 monthly; Mar-Oct	(no data)
Velence	2000-2006 weekly; mid May-mid Sep	2000-2007 weekly; mid May-mid Sep	(no data)
Geneva	1984-2004 biweekly, monthly; all months	1984-2004 biweekly, monthly; all months	1984-2004 biweekly, monthly; all months
Bourget	1984-2005 weekly, biweekly; usually all months	(no data)	(no data)
Annecy	1999-2005 biweekly, monthly; all months	1999-2005 biweekly, monthly; all months	(no data)
Aiguebelette	1988-2005 weekly, biweekly; usually all months	(no data)	(no data)
Lomond	Jun 2000-Nov 2003 seasonally (monthly in summer)	(no data)	2000-2003 seasonally (monthly in summer)
Windermere	May 2000-Dec 2004 biweekly	2000-2002 biweekly	May 2000-Dec 2004 biweekly
Leven	Jul 2000-Apr 2005 seasonally	2000-2001 seasonally	2000-2005 seasonally

3.2.2 Parameters, volume and frequency

Not all parameters were available for all the study sites or for the entire 30-year period. The data sampling frequency and volume varied according to the needs of the institute or agency that collected them. However, long datasets were available for most study sites, allowing for pattern and trend analysis to take place. The sampling frequency and period for the measured parameters in each lake are given in Tables 3-2a and 3-2b.

All data were imported into a common database and the study sites were categorized according to their mixing type and trophic status (Table 3-3). The classification of lakes into different trophic levels was performed in accordance to the OECD criteria regarding the trophic levels of lake waters (OECD, 1982).

Table 3-3: Categorization of study sites according to their trophic status and mixing type.

Trophic status / Mixing type	Unknown	Oligotrophic	Mesotrophic	Eutrophic
Unknown				Tisza, Velence/ Leven
Monomictic	Bourget, Aiguebelette	Annecy/Lomond	Geneva/Constance/ Windermere	
Dimictic		Vänern, Vättern/ Inarijärvi	Päijänne, Pielinen Oulujärvi, Haukivesi, Kallavesi, Nasijärvi	Mälaren
Polymictic				Balaton/Müggelsee
Always mixing				Hjälmaren

3.3 Study sites

The 23 study sites cover a wide geographical area and landscape settings; they are therefore affected by different hydrogeology, soil and climatic conditions that influence their water quality. The lakes were categorized according to the climate zone they belong to (Table 3-4) and are also presented scaled according to their surface area (Figure 3-1).

Table 3-4: Categorization of the study sites according to the climate zone they belong to.

Temperate Maritime with Cool Summer	Temperate Continental Humid with Warm Summer	Temperate Continental Humid with Cool Summer	Temperate Continental to Subarctic	Subarctic
Geneva	Balaton	Müggelsee	Päijänne	Inarijärvi
Constance	Tisza	Vänern	Nasijärvi	Pielinen
Bourget	Velence	Vättern		Oulujärvi
Annecy		Mälaren		Haukivesi
Aiguebelette		Hjälmaren		Kallavesi
Lomond				
Windermere				
Leven				

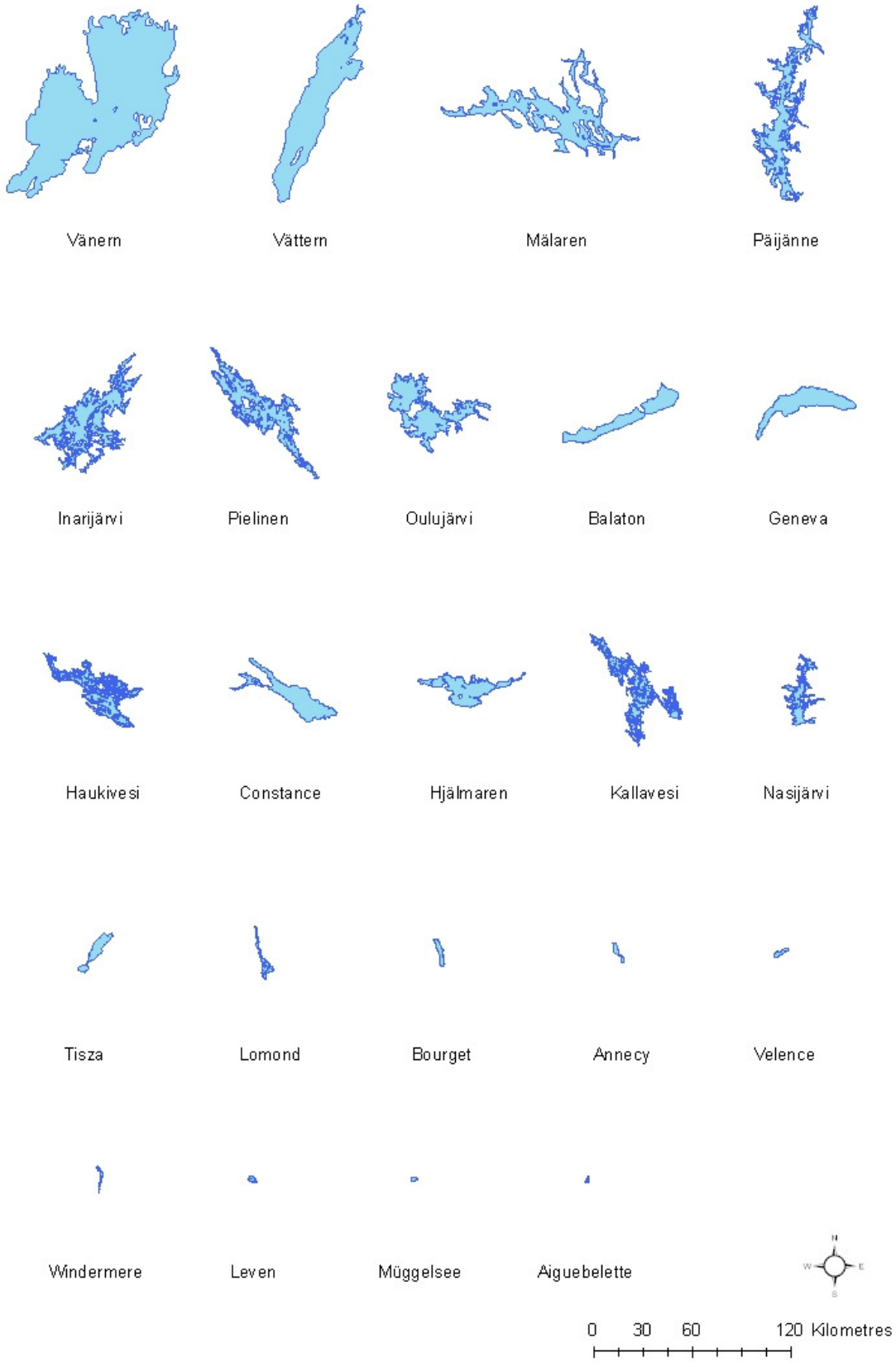

Figure 3-1: Study sites scaled according to their surface area.

The main morphological characteristics of the lakes are summarized in Table 3-5, while information about the main islands, the major outflowing and inflowing tributaries and the catchment area (where available) are presented in Appendix I. The WFD abiotic typology used in the following sections to characterise lakes is based on three key parameters recommended in 'System A' in Annex II of the Directive; altitude, surface size and mean depth (Directive 2000/60/EC, 2000) (Chapter 2, Table 2-4). Detailed information on the fourth key abiotic parameter (geology of lakes with respect to alkalinity, water colour, conductivity and content of calcium (Kolada *et al*., 2005)) was unavailable. In this project, fifteen very large (surface area > 100 km^2) lakes were studied, six large lakes (10-100 km^2) and two medium-sized lakes (1-10 km^2). Small lakes were not considered, because of the relatively coarse spatial resolution of the satellite sensors used. Moreover, eighteen lakes are situated below 200 m a.s.l. (lowland) and five at mid altitudes (200-800 m a.s.l.). There were no high altitude lakes (> 800 m a.s.l.). Finally, two lakes were very shallow with mean depth < 3 m, eight lakes were shallow with mean depth between 3-15 m and nine lakes were deep with mean depth > 15 m. Mean depth information for four of the study sites was unavailable.

The information on each study site that is provided in the following sections derived from the World Lakes Database (WLD) of the International Lake Environment Committee (ILEC, 2010), unless explicitly stated.

Table 3-5: Main morphological characteristics of the 23 study sites (Source: ILEC, 2010; LakeNet, 2009; Finland's Environmental Administration, 2009).

Lake	Surface area (km^2)	Volume (km^3)	Maximum depth (m)	Mean depth (m)	Altitude (m a.s.l.)	Shoreline length (km)
Vänern	5,648	153	106	27	44	1,940
Vättern	1,856	74	128	40	89	642
Mälaren	1,096	14	64	12.8	0.3	1,410
Hjälmaren	478	2.9	22	6	22	428
Päijänne	1,080	17.8	98	17	78	1,140
Inarijärvi	1,040	15.1	86	14.4	119	2,776
Pielinen	894	8.5	60	10	94	610
Oulujärvi	887	6.2	38	7	122	
Haukivesi	562				< 200	
Kallavesi	473				82	
Näsijärvi	256		63		95	
Geneva	584	88.9	310	153	372	167
Constance	476	48.5	254	90	396	255
Bourget	44.5	3.8	145	85	232	
Annecy	27	1.1	65	41.5	447	35
Müggelsee	7.4	0.04	8	4.9	34	
Aiguebelette	5.4		71		391	
Balaton	593	1.9	12	3.2	105	236
Tisza	127	0.17	17	1.3	< 200	
Velence	26	0.04		1.6	< 200	28.5
Lomond	71	2.6	190	37	8	154
Windermere	15	0.32	64	25.1	39	52.1
Leven	13.3	0.05	25.5	4	107	23

3.3.1 Scandinavia

Four Swedish and seven Finnish lakes were studied in this project.

3.3.1.1 Sweden

Figure 3-2: Map of the Swedish study sites; Lakes Vänern, Vättern, Mälaren and Hjälmaren.

Lake Vänern is the largest Swedish lake and the fourth largest freshwater body (third largest lake) in Europe. It is located in south-western Sweden (Figure 3-2) and was formed when ice melted after the last ice age 10,000 years ago. The lake forms numerous bays along its shoreline and there are numerous small islands in the lake, mostly situated close to the lakeshore, leaving an island-free open water body. Due to its great depth (the maximum depth is 106 m) the open lake water in spring warms up later than the shallow coastal waters, resulting in thermal variability (Kondratyev

& Filatov, 1999). However, eventually in spring and autumn the water mixes completely (dimictic). Lake Vänern freezes partially in winter.

The bedrock and drift deposits of the catchment area are nutrient-poor, and the lake is naturally oligotrophic, although some bays locally exhibit eutrophication problems. Low concentrations of nutrients, low densities of phytoplankton and clear waters are expected in the lake. However, the industrial establishments (mostly pulp and paper industries) on the northern part of the lake used to act as important sources of organic matter and mercury contaminants until recently. That came to an end when many mills closed down in the 1970s, while the remainder adopted purification techniques. Also, management policies concerning the urban sewage treatment were introduced at the same time and nitrogen levels are now being regulated. As a result, the water quality of Lake Vänern is nowadays very good and the lake water is used for drinking purposes for over 800,000 people. The lake biota has also recovered and activities like commercial and recreational fishing in the lake are now very popular. Other land uses and land cover features within the catchment area include natural woodland, agriculture and animal breeding, while the inhabited areas around the lake are few and rather sparse (Lake Vänern Society for Water Conservation, 2009).

Lake Vättern is Sweden's second largest lake and is located in southern Sweden (Figure 3-2). The lake was also formed approximately 10,000 years ago after the last glacial period and was connected to an adjacent lake basin until 8,000 years ago, when on-going isostatic rebound separated the two bodies again to delimit the current lake basin. The point of maximum depth (128 m) is located in the southern part of the water body, while the lake is shallower in the central and northern parts.

There are numerous small islands within the lake, mostly situated close to the lakeshore. The largest island is found on the south of the lake. Lake Vättern freezes partially in winter.

The nutrient loading from the surrounding land is relatively low, suggesting Lake Vättern is a naturally oligotrophic water body. In fact, the lake has such an excellent water quality that it is considered to be the largest body of potable water in the World, as its water requires either very little or no treatment at all. The main land cover category within the catchment area is natural forest, while agriculture covers about a quarter of the total area. There are also a few towns around the lakeshore and some industrial development, namely mining, manufacturing, forestry and paper mills. The lake itself is used for commercial fishing.

Lake Mälaren is situated in south-eastern Sweden (Figure 3-2) and is the third largest lake in the country. The lake is connected to Lake Hjälmaren, which lies to its west via a canalized inlet (fresh water inflow). The shoreline of Lake Mälaren is very complex, forming numerous narrow bays and sub-basins that give rise to variability in the biochemical characteristics of the water. High eutrophication levels have been observed in some of the enclosed shallow bays, especially in the western part of the lake, and generally the lake is meso-eutrophic (Strömbeck & Pierson, 2001). There are many large islands within the lake. Lake Mälaren is dimictic and freezes for about four months in winter.

The catchment area is mostly covered by natural woodland. The deposits of the catchment area are suitable for cultivation and, therefore, agriculture has developed

around the lake contributing to nutrient loading of the water body. Apart from agriculture, the area is also highly populated, with major cities situated around the lake (including the city of Stockholm, which is located in the eastern part of the lake), and partially occupied by industrial establishments. Sewage treatment plants have operated in the area since the 1970s to control pollution within the lake.

Lake Hjälmaren is Sweden's fourth largest lake and is located in south-eastern Sweden (Figure 3-2). It is rather shallow (maximum depth is 22 m) and it never stratifies with a freezing period of about four months. Alongside the shoreline there are many bays, while islands and narrow sounds divide the lake into four distinct basins.

The catchment area is quite large and it is mostly covered by natural woodland, but also agriculture, which contributes to high nutrient loading in the main lake body. Lake Hjälmaren is eutrophic. Urban sewage discarded into the lake has added to the eutrophic character of Hjälmaren in recent years, especially in the western part, where the town Örebro is situated. Despite that, the lake water is treated for drinking purposes.

3.3.1.2 Finland

Lake Päijänne is the second largest lake in Finland and also the deepest lake in the country (98 m). It is situated in southern Finland (Figure 3-3) and was formed 8,000 years ago when the ice from the last glacial period melted and isostatic re-adjustment cut the lake's connection with the sea. It is 120 km long and up to 28 km wide in places. The lake has numerous bays formed along the shore and has several sub-

basins. The lake is dimictic with the freezing period extending from December to May. There are many islands within the lake.

Figure 3-3: Map of the Finnish study sites; Lakes Inarijärvi, Oulujärvi, Pielinen, Kallavesi, Haukivesi, Päijänne and Näsijärvi.

The catchment area is mainly forested, but also used as farmland (agriculture, animal breeding) and for urban and industrial development. Lake Päijänne is mesotrophic with its northern part being more affected by nutrient loading than the southern part. However, regulations and strict control have improved the water quality in recent years following the increasing need for drinking water from the neighbouring city of Helsinki.

Lake Inarijärvi is the most northern lake of all the study sites of this project. It is the third largest Finnish lake, located in the northern part of Lapland (Figure 3-3) and is of tectonic origin. The location of Lake Inarijärvi in combination with its relatively high altitude results in a long freezing period that may last up to seven months (from November to early June) depending on the meteorological conditions. The shoreline of the lake forms many enclosed bays and there are more than 3,000 islands in the lake.

The catchment area is mostly forested with a few sparse habitations and remote industries. There are no major cities located in the proximity of the lake and most of the catchment area is used for the breeding of semi-domestic reindeers. Generally, the lake is oligotrophic with a few local points of elevated nutrient loading due to wastewater discharge. Despite the good state of water quality the operation of the Kaitakoski hydroelectric power plant on the eastern part of the catchment area has affected the lake biota, such as the benthic fauna and fish (e.g. lake trout and arctic char) due to a slight increase (0.5 m) in the natural water level of the lake.

Lake Pielinen is the fourth largest lake in Finland and located in the eastern part of the country (Figure 3-3). It was formed after the last ice age, when ice retreated and isostatic rebound of the land surface occurred. Lake Pielinen has a length of 100 km and maximum width about 10 km. It is a dimictic lake that freezes between late November and mid May. There are numerous islands in the lake and many bays along the shoreline.

The catchment area of Lake Pielinen is shared by two countries, Russia and Finland. It is mainly covered by natural woodland, but there are also large areas of swamps. Koli National Park is situated in the western shore of the lake. The water quality of Lake Pielinen is in a moderate state and the lake is mesotrophic (locally eutrophic) due to wastewater discharge mostly from two major cities on the eastern and northern part of the water body. The operation of industries at those locations as well nutrient loading from the surrounding land have also added to the elevated eutrophication levels of the lake. The water concentration of humic material in the water is also high, giving a brownish colour to the water.

Lake Oulujärvi is the fifth largest lake in Finland (Figure 3-3). Due to its shape the main water basin is divided into three distinct sub-basins. There are numerous islands within Lake Oulujärvi and a few enclosed bays. The lake is mesotrophic and dimictic.

Lake Haukivesi is located in south-eastern Finland (Figure 3-3) and is one of the seven major basins that form the largest lake in the country, Lake Saimaa, with a total surface area of 4,400 km^2. Lake Haukivesi is of glacial origin. There are numerous islands in the lake, including the island Linnansaari in the middle of the lake that is a National Park and hosts the endangered Saimaa Ringed Seal, which lives only at Saimaa Lake and is one of only three species of freshwater seals. The lake is mesotrophic and dimictic.

Lake Kallavesi is one of the six large basins that form Lake Iso-Kalla with a total surface area of 890 km^2. It is located in the south-eastern part of Finland, just north

of Lake Haukivesi (Figure 3-3). The long shoreline of Lake Kallavesi forms many enclosed bays and there are numerous small islands within the lake.

Lake Näsijärvi is another large Finnish lake, located in the southern part of the country (Figure 3-3). It is dimictic, usually freezing completely between February and March. There are numerous small islands within the lake as well as many enclosed bays. The main pressure within the catchment area is silviculture (forestry) that has caused degradation of the water quality in past years. However, the control of wastewater discharged into the lake has helped the lake recover. There is only one major human settlement along the shoreline, which is situated in the south shore of the lake.

3.3.2 The European mainland

Three French, one German and three Hungarian lakes, and two lakes that are shared between countries were studied.

3.3.2.1 Switzerland

Lake Geneva is shared between Switzerland and France (Figure 3-4) and is the second largest Central European lake. It is very deep (maximum depth is 310 m), which means that full mixing does not happen in all years (Livingstone, 1993), and it is monomictic and of glacial origin. Stratification is established between April and October, while in the rest of the year the lake (partially) mixes responding to meteorological forcing, whilst the vertical stability within the water column is low (Livingstone, 1993). There are no islands in the lake. Numerous urban centres are

located within the large catchment area, including two major cities (Geneva and Lausanne). Industrial and domestic waste water and contributions to nutrient loads from the mountainous Alpine areas around the lake have increased the trophic state of Lake Geneva and affected its naturally high levels of transparency in the past years. Between the 1960s and the 1980s the lake biota was strongly affected by heavy pollution and high eutrophication levels. However, the quality of lake water has been recently under strict control due its use as a drinking-water source and a host for recreational activities.

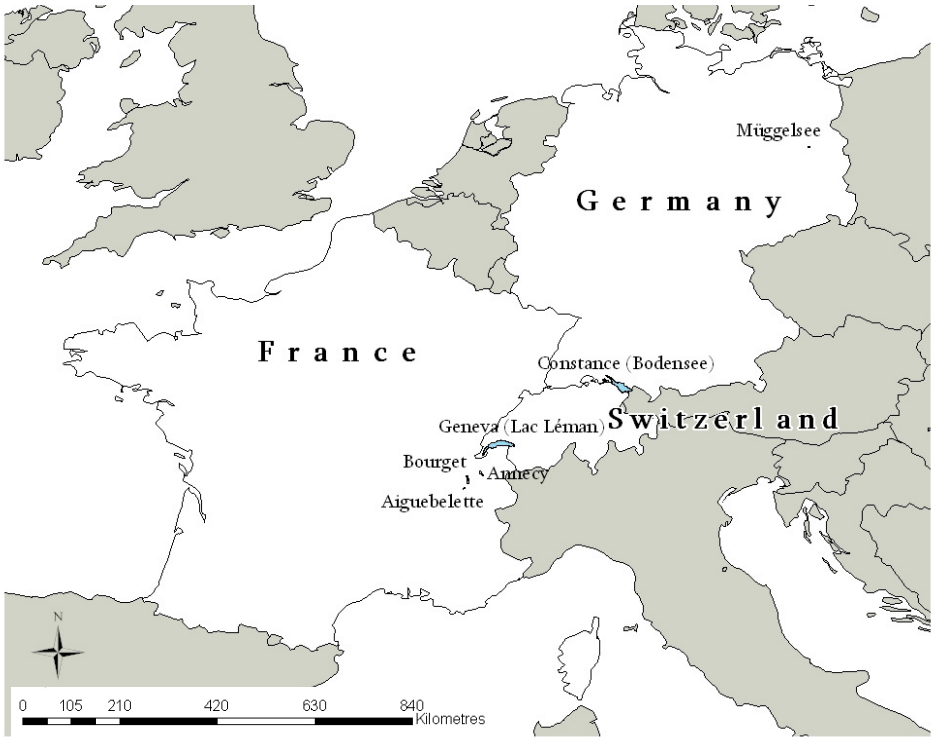

Figure 3-4: Map of the western European mainland study sites; Lakes Müggelsee (Germany), Constance (Germany, Switzerland, Austria), Geneva (France, Switzerland), Bourget, Annecy and Aiguebelette (France).

3.3.2.2 France

Lake Bourget is the largest and deepest lake in France, situated in the central-eastern part of the country (Figure 3-4). It has a maximum length of 18 km and maximum width 3.5 km. It is a Ramsar site surrounded by few small urban establishments.

Lake Annecy is a 14.6 km long lake located in France, 30 km south of the city Geneva (Figure 3-4). As the second largest lake in France it is a relatively small water body, yet moderately deep (maximum depth is 65 m). It is monomictic, with the thermocline forming between May and November. The lake basin is physically separated into two sub-basins of which the northern one is the largest, accounting for approximately 80% of the whole lake area and volume. There are no enclosed bays along the shore and no islands.

The catchment area is characterized by steep mountain slopes that are located to the west and east sides of the lake. There are numerous inflowing rivers and tributaries. There are also small settlements in the catchment area and the installation of a sewage treatment plant in 1967 has maintained the originally oligotrophic character of the lake in recent years.

Lake Aiguebelette is one of the largest natural lakes in France and is located in the eastern part of the country, just a few kilometres south of Lake Bourget (Figure 3-4). There are a few small urban developments around the lake, but no major cities. The lake is warm monomictic, but it has frozen in the past (1909, 1929, 1941, 1942 and 1956).

3.3.2.3 Germany

Lake Constance is a glacial lake that is shared between Germany, Switzerland and Austria (Figure 3-4). It is the largest lake in Germany and the third largest in Central Europe. The lake is 63 km long and up to 14 km wide and morphologically divided into two main parts, the deep central-eastern part and the shallow western part (Peeters *et al*., 2007). There are three islands in the lake, all situated close to the shoreline, leaving an island-free open water body. The lake is warm monomictic; however, it has frozen partially or completely in past years with the most recent report of full ice cover in 1963 (Table 3-6).

Table 3-6: Years when Lake Constance has partially or completely frozen.

Year	Ice cover	Year	Ice cover
1077	(n/a)	1573	Complete
1326	Partial	1600	Partial
1378	Partial	1684	Complete
1435	Complete	1695	Complete
1465	Partial	1709	Partial
1477	Partial	1795	Complete
1491	Partial?	1830	Complete
1517	Partial	1880	Partial
1571	partial	1963	Complete

Lake Constance is naturally oligotrophic with high water transparency. However, intense human activities such as agriculture and sewage discharge from human settlements and industries within the large catchment area resulted in an eutrophication peak in the 1970s (Odermatt *et al*., 2008). Nevertheless, since then the establishment of a sewage water treatment plant has helped the lake recover (Peeters

et al., 2007). Nowadays, Lake Constance provides fresh water to many cities in south Germany.

Lake Müggelsee is a relatively small lake for this project, but still the largest of the Berlin lakes. It is situated at 34 m a.s.l. in eastern Germany, southeast of the city of Berlin (Figure 3-4) (Wilhelm *et al*., 2006). It is 4.3 km long and up to 2.6 km wide and there are no islands within the lake. Lake Müggelsee is highly eutrophic and freezes in winter (Gerten & Adrian, 2000). The freezing period may vary from 0 days in mild winters (e.g. 1988-89 and 1989-90) up to almost four months in severe winters (e.g. 1995-96) (Adrian *et al*., 1999). It is a polymictic lake and due to its shallowness the temperature at the surface approximates the average temperature of the entire water body (Straile & Adrian, 2000). In recent years changes in the catchment have influenced the water quality of the lake. A decrease in external nutrient loading has changed the composition and abundance of phytoplankton within the lake (Köhler *et al*., 2005).

3.3.2.4 Hungary

Lake Balaton is the largest lake in Hungary and also in Central Europe, located in western Hungary (Figure 3-5). It is a tectonic lake and is 78 km long and up to 14 km wide (Padisák, 1992). There are no islands in the lake and due to its shallowness it is strongly affected by wind action that causes high turbulence due to bed sediment resuspension. As a result, the suspended sediment concentrations within the lake are high and heterogeneous (Tyler *et al*., 2006). Lake Balaton is polymictic and never stratifies, so the temperature measured at the surface is considered representative of the column as a whole (Livingstone & Padisak, 2007). It has a freezing period of two

months in winter. The main inflowing tributary is located in the south-west, River Zala, which drains the catchment area of intense human activities such as cultivation, farming and urban development (Sváb *et al*., 2005). As a result, the nutrient load input and sewage discharge has increased the eutrophication levels of the lake water in past years. The lake was originally mesotrophic, but eutrophication peaked in the 1970's and management policies, such as an eutrophication control programme and sewage treatment, have been introduced to help the lake recover. It is currently meso-eutrophic with local algal blooms mostly at the western part (Padisák, 1992; Ministry of Environmental Protection and Water Management, Hungary, 2009) and the last significant algal bloom occurred in autumn 2000 (Tyler *et al*., 2006).

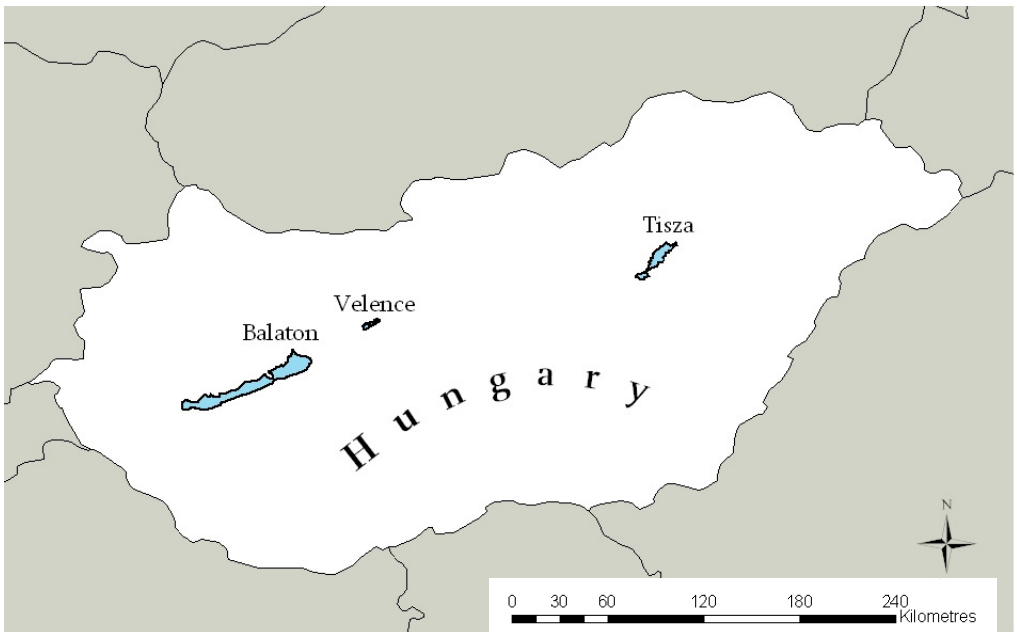

Figure 3-5: Map of the Hungarian study sites; Lakes Balaton, Velence and Tisza.

Lake Tisza is the other name for Kisköre Reservoir and is the largest artificial lake in eastern Hungary (Figure 3-5). It was built between 1973-1990s to fulfil the need

for flood control and management in the River Tisza. The lake is 27 km long. Fast urban growth for recreational purposes followed the completion of the reservoir, however, the lake water quality has been constantly monitored to ensure a good-to-excellent ecological status (Ministry of Environmental Protection and Water Management, Hungary, 2009).

Lake Velence is the third largest lake in Hungary located in the north-east of Lake Balaton in central Hungary (Figure 3-5). One third of its surface area is covered by reeds. It is 10.8 km long and up to 3.3 km wide. It is very shallow and freezes in winter for an average period of two months. There are no islands in the lake. The lake is surrounded by small habitations, but there are no major cities (Ministry of Environmental Protection and Water Management, Hungary, 2009).

3.3.3 Britain

Loch Lomond is the second largest standing water body in Britain and is situated in the south-west of Scotland, north of the city of Glasgow (Figure 3-6). The lake is of glacial origin and part of the Loch Lomond and Trossachs National Park. The catchment covers an area of 696 km^2 and includes hill ranges, forested areas and designated special nature conservation sites. The northern part of Loch Lomond is very narrow (1 km width), but the southern part is wider and reaches a maximum width of 8 km. The lake is 34 km long. The water level in the lake is regulated and the number of islands depends on the water level at each specific time. Loch Lomond is oligotrophic and monomictic. However, it occasionally freezes in winter.

The catchment area of the southern basin is mostly arable nutrient-rich land that contributes to the nutrient loading of the lake. The area around the northern basin is covered by steep terrain and there is also a much smaller area dedicated to agriculture. The population around the lake is sparse and the area is characterized by discontinuous urban developments located mostly in the southern bank (ECN, 2009).

Figure 3-6: Map of the British study sites; Lochs Lomond and Leven and Lake Windermere.

Lake Windermere is located in north-western England (Figure 3-6) and is the largest natural lake in England. It is part of the Lake District National Park and is a long, narrow lake that was formed by glacial action. Lake Windermere is a relatively small system compared to the rest study sites being 17 km long and up to 1.5 km wide. There is one large island in the lake and numerous small ones. It is monomictic with the thermocline forming from June to early November and rarely freezes in

winter (Blenckner *et al*., 2007). The main basin is naturally divided into two halves by a shallow area located approximately in the centre of the lake. The northern sub-basin is deeper than the southern (ECN, 2009).

The catchment area supports various land uses, mostly farmland and cultivated areas, but also woodlands and sparse residential areas. Lake Windermere is mesotrophic, but tends to reach eutrophic levels due to high nutrient inflows from the neighbouring land. The lake water is used for drinking purposes (ECN, 2009)

Loch Leven is located in central-eastern Scotland, north of the Scottish capital, city of Edinburgh (Figure 3-6). It has a circular shape. There are a few small islands in the lake, most of them exposed during low water levels. The lake is naturally eutrophic with the major part of its catchment being covered by agricultural land.

3.4 Field data analysis

The temporal variability of water quality parameters determined the frequency of desired satellite data acquisition. As a result, the temporal scale of the three parameters was investigated to provide rough estimates of the number of satellite images required to adequately describe phenomena related to temperature, chlorophyll *a* and SDD in the lakes. Time series were plotted for the extensive datasets of field measurements for each lake. From those plots features such as the timing of ice break-up completion, the timing of significant changes or critical thresholds and other lake behavioural features were identified. According to the timing of such phenomena for each study site, adequate numbers of satellite images were processed. Descriptive statistics were also calculated to determine typical

monthly, seasonal and annual characteristics of the parameters in each study site. For instance, mean values, the range of values (as a measure of spread) and the standard deviation (as a measure of central tendency in the data) were calculated (Clark-Carter, 2004). One-sample T-test was used to test the significance in the difference between the sample mean and the all-year mean for each parameter. The method was used to reveal any anomalies in the datasets related to cooling or warming trends in lake temperature.

3.4.1 Lake surface temperature

Due to irregularities in sampling intervals (ranging from daily to seasonal) historical limnological data are normally standardised by averaging prior to analysis (Livingstone, 2003). All daily, weekly and biweekly measurements were averaged into monthly values (calendar months) for all years available. In some cases only one measurement was available per month and that was assumed to be representative of the entire month. Those monthly averages will be referred to as monthly LSTs hereafter.

In lakes with more than one sampling station, the monthly LSTs were computed by averaging data from all stations within each lake. The mean value was assumed to be representative of the whole lake as the data from each station within each individual lake were highly correlated with each other (Pearson's $r > 0.90$). There was more than one sampling station in all Swedish, Finnish, Hungarian lakes and in one of the British lakes, whereas only one station in two British and all German, Swiss and French lakes. The location of the station(s) in each lake is shown in Appendix II.

The field data were used to estimate the minimum, maximum and mean annual temperatures from monthly means in all years available (Table 3-7) and to identify important timings in the seasonal variability of lake surface temperature in all study sites. For example, the timing/periods of (a) temperatures lower than 4 °C, (b) complete ice break-up and spring warming onset, (c) maximum temperature rise in spring, (d) maximum annual temperature and (e) maximum temperature drop in autumn were identified (Table 3-8).

The above mentioned analysis of the field data illustrated that whilst lakes showed individual characteristics there were also many similarities in their ecological behaviour. For example, all seven Finnish lakes generally remain below 4 °C in winter and early spring. The highest monthly mean temperature rise occurs between April and May reaching a maximum in July (in August in Inärijärvi). Temperature decreases slightly in August with the maximum temperature drop being observed in all lakes between September and October.

In the four Swedish lakes the temperature remains below 4 °C in winter and early spring. The temperature rises in early spring with the highest monthly mean temperature rise occurring between May and June and the temperature maximum between July-August. In late summer the temperature decreases with the maximum monthly mean temperature drop occurring between August and October.

Table 3-7: Minimum and maximum values of lake surface temperature in each study site calculated from monthly means for all available years.

Lake	Temperature (°C)		
	Min	Max	Mean
Vänern	(n/a)	17.9	(n/a)
Vättern	(n/a)	16.2	(n/a)
Mälaren	(0.5)	19.1	(n/a)
Hjälmaren	(0.4)	18.9	(n/a)
Päijänne	0.5	18.5	7.5
Inarijärvi	(0.2)	13.2	(n/a)
Pielinen	0.2	18.0	6.5
Oulujärvi	0.3	17.9	6.5
Haukivesi	0.3	18.7	7.9
Kallavesi	0.4	18.2	7.0
Näsijärvi	0.4	17.6	7.1
Geneva	6.09	21.85	12.75
Constance	4.63	21.53	11.68
Bourget	5.74	22.95	13.41
Annecy	5.30	21.94	13.35
Müggelsee	2.1	20.6	10.9
Aiguebelette	4.87	24.09	13.76
Balaton	(n/a)	23.52	(n/a)
Tisza	0.4	23.8	12.8
Velence	(n/a)	24.1	(n/a)
Lomond	(n/a)	17	(n/a)
Windermere	5.4	19.3	11.4
Leven	(2.9)	(17.1)	(n/a)

Note: Due to lack of data in certain months the annual minimum, maximum and mean could not always be accurately determined; indicative values (available data) are presented in parentheses.
(n/a) stands for not available and denotes lack of field data

Table 3-8: Important timings/periods in the seasonal variability of lake surface temperature in all study sites for all available years.

Lake	Temp ≤ 4 °C	Spring warming onset	Spring maximum temperature rise	Max temp	Autumn maximum temperature drop
Vänern	(Jan)-Apr	(n/a)	May-Jun: 5.6 °C	Aug	Aug-Sep: -4.3 °C
Vättern	(Jan)-Apr	(n/a)	May-Jun: 5.5 °C	Aug	Aug-Sep: -3.5 °C
Mälaren	(Jan)-Feb-Mar, Dec	Mar	May-Jun: 7.3 °C	Jul	Sep-Oct: -5 °C
Hjälmaren	(Jan)-Feb-Mar, Nov-(Dec)	Mar	Apr-May: 7.6 °C (May-Jun: 6.1 °C)	Aug	Sep-Oct: -5.9 °C
Päijänne	Jan-Apr, Dec	Apr	Apr-May: 7.2 °C (May-Jun: 6.4 °C)	Jul	Sep-Oct: -5 °C
Inarijärvi	(n/a)	(n/a)	(n/a)	Aug	(n/a)
Pielinen	Jan-Apr, Nov-Dec	Apr	Apr-May: 7.1 °C May-Jun: 7.1 °C	Jul	Sep-Oct: -5.7 °C
Oulujärvi	Jan-Apr, Nov-Dec	Apr	Apr-May: 6.9 °C	Jul	Sep-Oct: -5.3 °C
Haukivesi	Jan-Apr, (Dec?)	Apr	Apr-May: 8 °C	Jul	Sep-Oct: -7.9 °C
Kallavesi	Jan-Apr, Dec	Apr	(Apr-May: 6.4 °C) Jun-Jul: 6.9 °C	Jul	Sep-Oct: -7.1 °C
Näsijärvi	Jan-Apr, Dec	Apr	Apr-May: 6.3 °C May-Jun: 6.3 °C	Jul	Sep-Oct: -6 °C
Geneva	NEVER	NO	Apr-May: 5 °C	Aug	Oct-Nov: -4.2 °C
Constance	NEVER	NO	Apr-May: 5.5 °C	Aug	Aug-Sep: -4.7 °C
Bourget	NEVER	NO	Apr-May: 5.8 °C	Aug	Oct-Nov: -5.2 °C
Annecy	NEVER	NO	Apr-May: 6.3 °C (May-Jun: 5.8 °C)	Aug	Oct-Nov: -5.2 °C
Müggelsee	Jan-Feb, Dec	NO	Apr-May: 6.6 °C	Aug	Sep-Oct: -5 °C Oct-Nov: -5.4 °C
Aiguebelette	Sometimes in Feb	NO	Apr-May: 5.9 °C	Aug	Oct-Nov: -5.4 °C
Balaton	2 months in winter	NO	(n/a)	Aug	(n/a)
Tisza	(n/a)	NO	Apr-May: 7.8 °C (May-Jun: 5.2 °C)	Jul	(n/a)
Velence	(n/a)	NO	(n/a)	Jul	(n/a)
Lomond	(n/a)	NO	(n/a)	Jul	Oct-Nov: -3.8 °C
Windermere	(NEVER)	NO	Apr-May: 4.2 °C	Aug	Sep-Oct: -3.6 °C
Leven	Jan (maybe others?)	NO	(n/a)	(n/a)	(n/a)

The thermal characteristics of the Continental and British lakes were also quite similar. In these lakes the temperature gradient is generally smaller than the Scandinavian lakes and the temperature in most lakes never falls below 4 °C throughout the year. Exceptions to the latter are three lakes for which winter temperature is usually lower than 4 °C; namely Lake Müggelsee, Lake Aiguebelette and Loch Leven. It was impossible to study the winter patterns in the three Hungarian lakes and in Loch Lomond, due to lack of winter LST data. In Lake Constance there have been a few events of total or partial ice cover in winter in the past (Table 3-6). However, the field data from Lake Constance in the period 1989-1997 showed no temperatures below 4 °C, with exception of one day, when the temperature was measured at 3.88 °C (04/02/1997). In the lakes for which monthly data were available, it was observed that the maximum mean monthly temperature rise occurs between April and May, reaching a maximum in July or August. In autumn, temperatures decrease with the maximum mean monthly temperature drop occurring in most cases between October and November.

The monthly LSTs from lakes within the same climate zone were highly correlated with each other for all corresponding years (Pearson's $r > 0.90$). As a result, the 23 lakes were grouped into Central European, British, Hungarian, Swedish and Finnish lakes to facilitate further analysis. These five zones corresponded directly to five ecoregions described in Map A, Annex XI of the WFD (Directive 2000/60/EC, 2000); namely Alps, Great Britain, Hungarian lowlands, Central plains and Fenno-Scandian shield respectively. This grouping allowed the group monthly LST (computed as the arithmetic mean of the individual monthly LSTs for lakes in the same group) to be constructed for each group (Livingstone & Padisak, 2007). Lake

Müggelsee (northern Germany) belongs to the same ecoregion as the four Swedish lakes (Central plains), but the Müggelsee monthly LSTs were closer to the Alpine group monthly LSTs instead. However, Lake Müggelsee exhibited different temporal patterns to both Swedish and Alpine lakes and it was therefore excluded from both groups. Lake Inärijärvi is the most northern lake and belongs to the subarctic climate zone. The lake also exhibited individual behaviour and was excluded from the Fenno-Scandian shield group. Therefore, lakes Müggelsee and Inärijärvi were treated separately.

The individual lake LST series were in some cases incomplete in some or all of the years. During the calculation of the group monthly LSTs, it was assumed that those missing LST values did not influence significantly the group monthly LST. The latter was based on the facts that (a) the individual lake LSTs were strongly correlated with each other within each group ($p < 0.1$), and (b) the standard deviation for each group mean LST was equal to or less than 1.5 °C in 88% of cases, assuming strong thermal similarity in corresponding months within the lakes of the same group. However, only the months for which data were available from at least two-thirds of the number of lakes in each group were considered for the analysis so that the group statistics are representative of an adequate number of lake bodies. Figure 3-7 shows the temporal patterns that represent each of the five lake groups. The temporal patterns of Lake Müggelsee and Inärijärvi are also presented. The key point illustrated is that the monthly LST records show different levels of completeness. In many cases field measurements are restricted to summer and autumn months only (Figure 3-7).

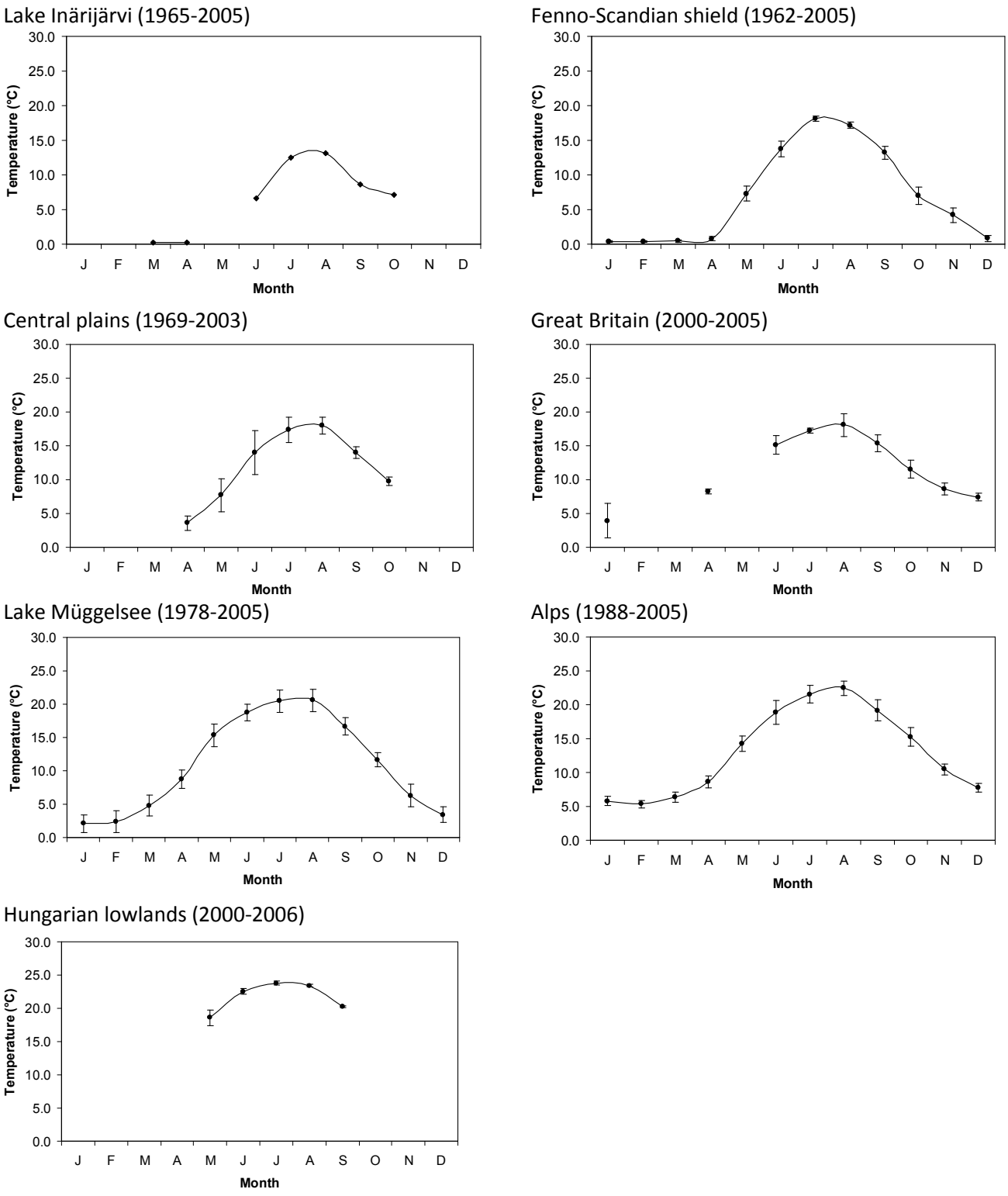

Figure 3-7: Temporal patterns of monthly LST within five lake groups (ecoregions) and two individual lakes for all years available (shown in brackets).

The group monthly LSTs for each available year were used for the computation of the group seasonal LSTs; in winter (DJF), spring (MAM), summer (JJA) and autumn (SON). The seasonal means were computed when data from all three months or the first and third months of the season were available. The time series of the seasonal LSTs per group/ecoregion are shown in Appendix III. Linear regression was applied to the seasonal LST series on calendar years to determine whether any evidence of long-term warming (or cooling) could be found in the lakes (Livingstone & Dokulil, 2001). Data from the Great Britain group/ecoregion were inadequate for this analysis. No significant trends were observed within the group-specific time periods for two groups/ecoregions; namely Hungarian lowlands and Central plains. However, data from the first group/ecoregion (Hungarian lowlands) were limited to a seven-year period and only in summer. Data from the second group/ecoregion (Central plains) extended to a 25-year period, but only in summer and two-thirds of autumn (September-October) (Appendix III).

More complete datasets showed significant ($p < 0.01$) warming trends in certain seasons. In particular, the Fenno-Scandian shield lakes showed a significant warming trend in spring (Figure 3-8), Lake Inärijärvi showed a significant warming trend in summer (Figure 3-9), and the Alpine lakes and Lake Müggelsee showed a significant warming trend in autumn months (Figure 3-10). Among these, the most pronounced warming trends were exhibited in the high-altitude Alpine lakes and the most northern lake, Lake Inärijärvi. In fact, Livingstone and Padisák (2007) suggested that due to similarities in their physical behaviour, high-altitude and high-latitude lakes should respond similarly to meteorological forcing (Livingstone & Padisák, 2007).

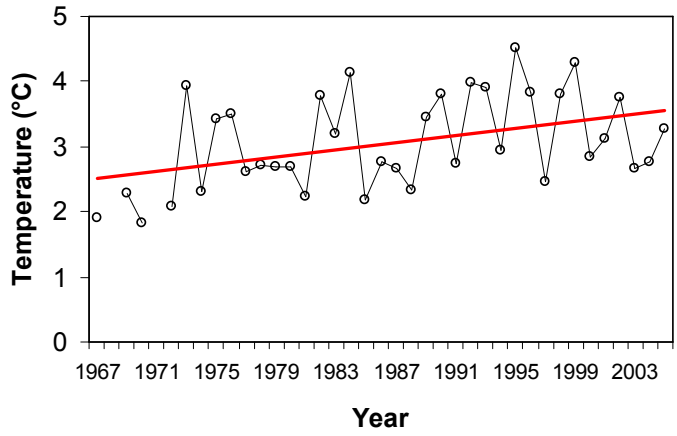

Figure 3-8: Spring mean LST values in the Fenno-Scandian shield lakes in 1967-2005. The red line was determined by linear regression.

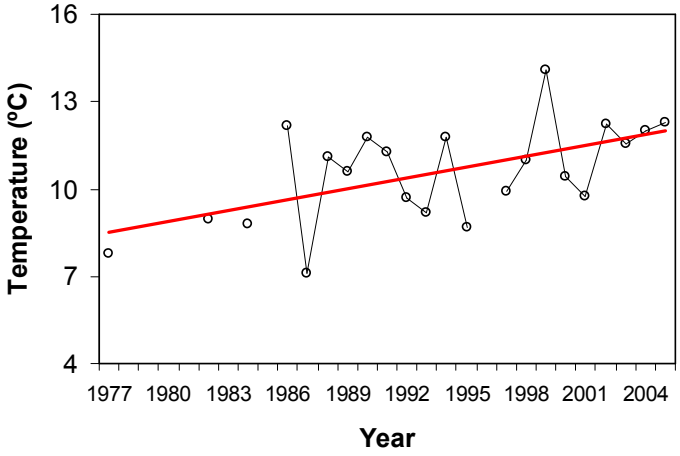

Figure 3-9: Summer mean LST values in Lake Inarijarvi in 1977-2005. The red line was determined by linear regression.

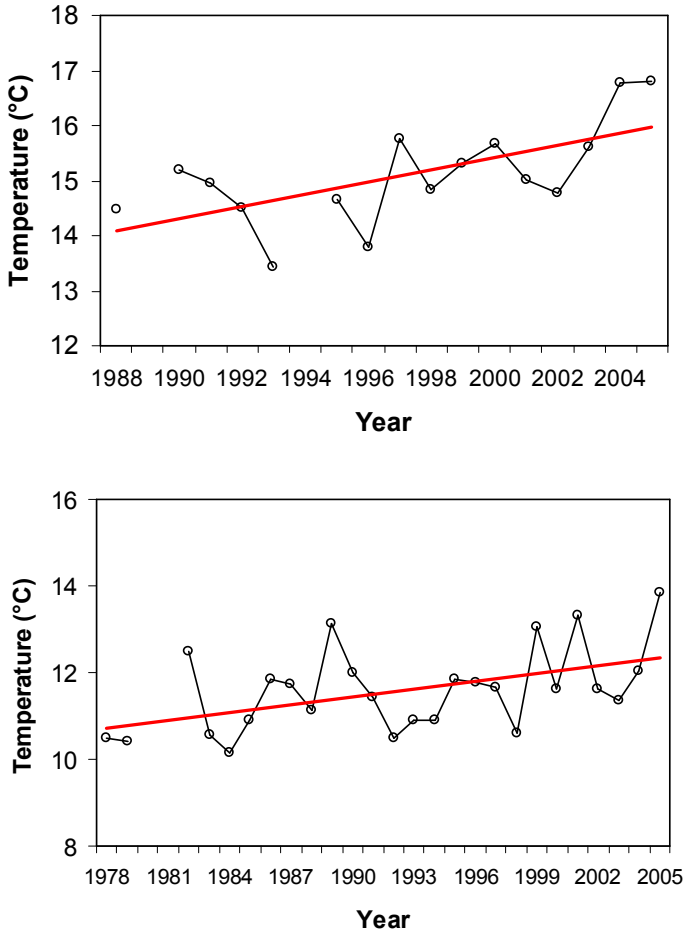

Figure 3-10: Autumn mean LST values in the Alpine lakes in 1988-2005 (top) and Lake Muggelsee in 1978-2005 (bottom). The red lines were determined by linear regression.

3.4.2 Chlorophyll *a* and Secchi disk depth

The temporal pattern of chlorophyll *a* and SDD in most study sites was difficult to determine from the available field dataset because the sampling frequency was much lower compared to temperature. Phytoplankton in temperate lakes generally peaks in spring and in late summer or early autumn (Horne & Goldman, 1994), but exhibited great variability between the study sites and within the same groups of lakes. The latter was also true for SDD, which appeared to be strongly site-dependant. However,

in some cases it was possible to extract the annual minimum, maximum and mean values of chlorophyll *a* concentrations and SDD (Table 3-9).

Table 3-9: Minimum and maximum values of chlorophyll *a* and SDD in each study site calculated from monthly means for all available years.

Lake	Chlorophyll *a* (µg L^{-1})			SDD (m)		
	Min	Max	Mean	Min	Max	Mean
Vänern	(n/a)	(3.55)	(n/a)	(3.5)	(4.1)	(n/a)
Vättern	(n/a)	1.17	(n/a)	(9.8)	(11.9)	(n/a)
Mälaren	(1.77)	17.35	(10.05)	(1.2)	(2.2)	(1.9)
Hjälmaren	(n/a)	34.33	(n/a)	(1.2)	(2.8)	(n/a)
Päijänne	0.55	(11.42)	(4.75)	(n/a)	(n/a)	(n/a)
Inarijärvi	(n/a)	(1.57)	(n/a)	(n/a)	(n/a)	(n/a)
Pielinen	(n/a)	(6.66)	(n/a)	(n/a)	(n/a)	(n/a)
Oulujärvi	(n/a)	(8.30)	(n/a)	(n/a)	(n/a)	(n/a)
Haukivesi	(n/a)	15.17	(n/a)	(n/a)	(n/a)	(n/a)
Kallavesi	(0.5)	(9.98)	(n/a)	(n/a)	(n/a)	(n/a)
Näsijärvi	(1.9)	(4.50)	(n/a)	(n/a)	(n/a)	(n/a)
Geneva	1.21	9.60	4.93	4.2	13.1	7.6
Constance	0.80	13.41	5.30	4.35	14.68	8.86
Bourget	(n/a)	(n/a)	(n/a)	(n/a)	(n/a)	(n/a)
Annecy	0.61	1.91	1.21	(n/a)	(n/a)	(n/a)
Müggelsee	3.90	35.6	13.7	1.3	3.1	2.0
Aiguebelette	(n/a)	(n/a)	(n/a)	(n/a)	(n/a)	(n/a)
Balaton	(n/a)	(27.64)	(n/a)	(n/a)	(n/a)	(n/a)
Tisza	1.00	20.6	10.29	(n/a)	(n/a)	(n/a)
Velence	(n/a)	(25.77)	(n/a)	(n/a)	(n/a)	(n/a)
Lomond	(n/a)	(n/a)	(n/a)	(2.8)	(4.0)	(n/a)
Windermere	1.3	25.8	9.0	3.5	5.2	4.3
Leven	(11.1)	(66.45)	(n/a)	(2.1)	(1.1)	(n/a)

Note: Due to lack of data in certain months the annual minimum, maximum and mean could not always be accurately determined (n/a); indicative values (from available data) are presented in parentheses.

Chlorophyll *a* data for Lakes Bourget and Aiguebelette were unavailable in this project. The other three sites of the same group (Alpine lakes) exhibited various timings of phytoplankton peaks. Lakes with lower productivity levels generally showed a later increase in phytoplankton concentrations (e.g. May) than more productive lakes that usually showed an algal increase in April (Thiemann & Kaufmann, 2000). Indeed, the mesotrophic Geneva and Constance showed two peaks with the maximum in spring (April and May respectively), whereas oligotrophic Annecy exhibited three peaks with the maximum in autumn (October). The two British lakes for which chlorophyll *a* data were available (Windermere and Leven) both showed a peak in April and a second much higher peak in autumn (September and October respectively). The chlorophyll *a* dataset for the Hungarian lowlands lakes was insufficient to determine all maximum peak timings, but both Balaton and Velence showed peaks in August. There were more frequent data for Tisza that exhibited three peaks; a maximum in May and two smaller ones in July and September. Lake Müggelsee is the only lake (according the present dataset) that showed a maximum peak much earlier in spring (March) than any other lake studied in the project. It also showed a peak in July and September, in a similar manner to other European mainland lakes.

Insufficient data in the early spring months made it impossible to determine the exact spring peak timings (if any) in most Fenno-Scandian shield lakes, apart from Kallavesi that exhibited a maximum peak in May. However, all lakes of the Fenno-Scandian shield ecoregion showed a phytoplankton peak in August. The Central plains lakes exhibited similar behaviour in pairs. Lakes Vänern and Hjälmaren showed a maximum peak in April and then two more peaks in June and August. On

the other hand, phytoplankton in Lakes Vättern and Mälaren appeared to peak only twice in late spring (May), which is the maximum, and then again in August.

The SDD is influenced by the amount of phytoplankton (and suspended sediment concentrations) within the water bodies and this was obvious in the temporal patterns of SDD in the lake sites for which data were available. In many cases, the minimum SDDs coincided with or followed major phytoplankton peaks in the lakes, such as in Lakes Vänern, Vättern, Hjälmaren, Geneva, Constance, Müggelsee and Windermere. This is illustrated here for Lake Geneva (Figure 3-11). The maximum SDDs mostly appeared in the winter season, when phytoplankton populations were small, or just before and after phytoplankton peaks in early spring and autumn respectively. Similar SDD patterns between lakes of the same group or between groups were not observed.

3.5 Summary

This chapter described the field data acquisition process. The field data included measurements of lake surface temperature, chlorophyll *a* and SDD from 23 lakes at variable frequencies and for different time periods. The study sites were then presented and also categorized according to their specific ecological characteristics and geographical settings. Analysis of the data facilitated the grouping of lakes with similar ecological behaviours and the specification of timings and periods in which important ecological events take place within the lakes. This information was then used to determine the amount and type of satellite data needed to fulfil the purposes of this project, as described in the next chapter.

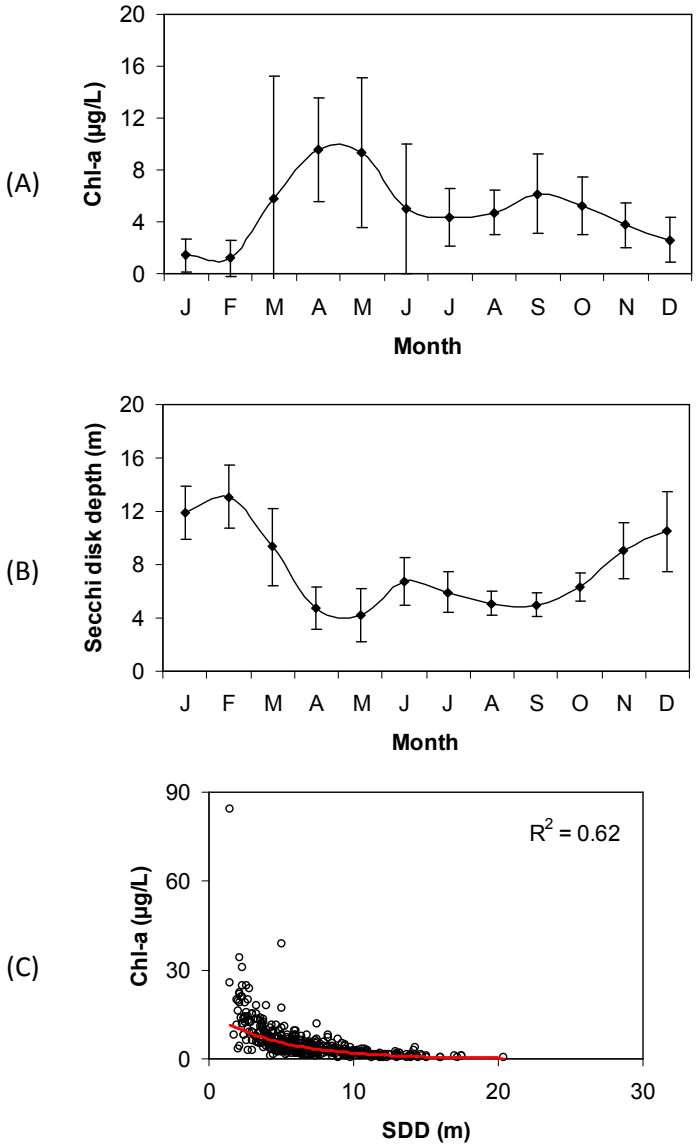

Figure 3-11: Temporal patterns of (A) chlorophyll *a* and (B) SDD in Lake Geneva calculated from monthly means in 1984-2004. (C) Scatter plot between all chlorophyll *a* and SDD field measurements in Lake Geneva on corresponding dates and times in 1984-2004; the red line was determined by an exponential model.

Chapter IV.

METHODOLOGY PART II: SATELLITE DATA ACQUISITION AND PROCESSING

4.1 Introduction

This project utilised field measurements and remotely sensed data from various lakes across Europe for a range of time periods. Field observations for 23 lakes were supplied for a period extending back 30 years, which is the length of the NERC NEODAAS DSRS satellite archive. Following the field data acquisition, a request was made to NEODAAS for satellite images that coincided with specific time periods when field measurements were available. The following sections outline the approach to satellite data acquisition and describe the quantity and quality of satellite data obtained. Also, the applicability of existing water quality estimation algorithms is discussed and the procedure followed to prepare the satellite data for the application of these algorithms is presented. Finally, the techniques for the accuracy assessment of the algorithms are presented.

4.2 Study period selection

The original aim of the project was to investigate the entire thirty year NOAA AVHRR archive. However, due to the large volume of data and the amount of data processing this proved excessively time-consuming despite the automated facilities at NEODAAS Plymouth Marine Laboratory (PML) for data pre-processing. A 12-month delay in NEODAAS PML providing the satellite data requested (and

originally granted) restricted the amount of data used in this project to two four-year periods.

The study periods were determined after the field data acquisition was completed, designed to coincide with periods of field data richness. A large number of frequent field sampling dates increased the possibility of coinciding cloud-free satellite overpasses, despite the frequent cloud cover in Europe. To determine which periods would be suitable, a field data quantity and quality assessment took place. This revealed that the optimum periods were the four-year periods of 1993-96 and 2001-04.

The two four-year study periods include years when significant air-temperature related weather phenomena occurred in Europe. Livingstone (1997) describes a climate-driven structure referred to as “sawtooth”, which is essentially a phenomenon of a few consecutive warm winters, which results in gradual air temperature increase, followed by an abrupt decrease. The phenomenon is directly linked to the winter NAO index inter-annual variability and has been observed during 1992-96 in Europe (Hurrell, 1995). During that period, the 1994-95 winter NAO index was strongly positive (+2.44) and led to a relatively warm and mild winter in 1995. That year was then followed by an equally strongly negative 1995-96 winter NAO index (-2.32) that caused a severe winter in 1996 (CRU, 2008). Also, the decade 1998-2007 has been the warmest since 1850, and especially the years 2002, 2003 and 2004 were among the top five warmest years since 1890, the other two being 1998 and 2005 (WMO, 2008).

The ability of remotely sensed data to accurately document the expected response of lake water bodies to the thermal anomalies described above was investigated. The potential link of thermal changes to corresponding variability in chlorophyll *a* concentrations and consequently in SDD was also assessed.

4.3 Satellite data selection

The acquisition of satellite images that are cloud-free on dates when the field sampling took place was an absolute necessity for this project. As a result, a cloud detection model was used to calculate the cloud cover of each study site on all desired dates.

4.3.1 Cloud detection

The NEODAAS DSRS employed a cloud-percentage calculation model using a list of all overpasses that matched sampling dates in all lakes and for all three water quality parameters. First, the percentage of cloud-cover over each lake was calculated for all available NOAA AVHRR scenes. After the calculation was completed, all images that coincided with field sampling dates and in which the study sites were covered by clouds in less than two-thirds (67%) of their surface area were listed. Images that fell within ± 1-2 days from the field sampling date and exhibited less than 33% cloud-cover (one-third of their surface area) were also listed. According to Kloiber *et al.* (2002a), the correlation strength between field measurements and satellite data decreases with increasing time windows between the collection of field data and the satellite overpass. As a result, the same authors suggest the use of images acquired only within ± 1 days from the field data collection

date to ensure optimum results. Only daytime scenes were selected assigning priority to morning-to-early-afternoon overpasses, as this was when most field data sampling took place. In cases where the exact field sampling time was known, the satellite scenes selected were the ones close to that time. Unfortunately, very few data pairs (i.e. field data and remote measurements of the three parameters) coincided exactly at the same location at the same instant of time. In most cases the separation between the field sampling time and satellite overpass varied between a few minutes to a few hours. Finally, Terra/Aqua MODIS scenes that coincided with cloud-free AVHRR scenes were listed. The AVHRR and MODIS lists of cloud-free and almost cloud-free images were then forwarded to the PML, where appropriate satellite data products were produced.

In total, 947 dates of satellite images matching field sampling dates from 13 lakes in 1993-96 and 1322 dates in 2001-04 for 18 lakes were sent to the NEODAAS DSRS. The model was then used to calculate the cloud percentage over all 18 lakes for all dates, which increased the time of processing (to four months) and the amount of output data (Personal communication with the DSRS team). A total of 23,396 overpass dates for 1993-96 and 48,611 dates for 2001-04 were returned. These were then checked to identify dates for each lake when (a) the remotely sensed data coincided with field data collection, and (b) the lakes were partially or totally cloud-free. Only 39% in 1993-96 and 40% in 2001-04 of the total number of scenes exhibited a cloud cover percentage of less than 66% (i.e. two-thirds of the lake surface area), while only 15% and 18% respectively were completely cloud-free (0% cloud coverage of the lake surface) above the lake. Interestingly, 44% of the total

images in 1993-96 and 43% in 2001-04 were completely cloud covered (100% cloud coverage of the lake surface).

Figure 4-1 illustrates the increase in the number of completely cloudy days as the geographical latitude increases. Generally, most of the lakes in warm temperate climates, such as the European mainland lakes, exhibit lower numbers of cloudy days than lakes in cold and subarctic climates, such as the Swedish and Finnish lakes. Within the subarctic climate zone (Haukivesi, Kallavesi, Pielinen, Oulüjärvi and Inärijärvi) the number of cloudy days reaches a maximum of over 200 days per year. In fact, linear regression analysis between the number of completely cloudy days and latitude showed a significantly high coefficient of determination ($R^2 = 0.68$, $p < 0.01$, $n = 18$). On the other hand, the completely clear (cloud-free) days remain almost constant in number with increasing latitude.

It is also noted that the average number of days per year on which the cloud cover over each lake is less than 66% decreases with latitude. As expected, it is higher for lakes in the European mainland and lower for lakes in Scandinavia (Figure 4-1).

The upshot of all of this is that there were more cloudy days than clear for all 23 study sites on days when satellite images coincided with the field data collection period. In a large lake study carried out in the Netherlands, Vos *et al*. (2003) underlined the problem of frequent cloud-cover, but suggested that 10 images per year are sufficient to show the main seasonal variations of chlorophyll *a*. Moreover, Bussières *et al*. (2002) have suggested that slow seasonal changes in temperature in

boreal lakes can be adequately mapped with remote sensing data, despite any gaps due to cloud cover and other problems.

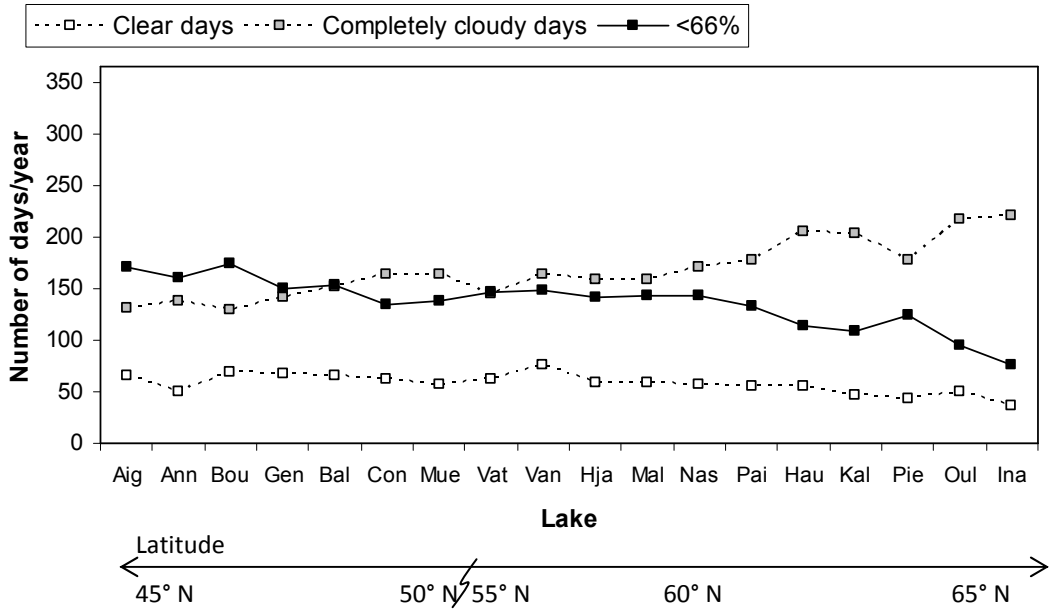

Figure 4-1: The number of (a) completely cloud-free days (white squares), (b) completely cloudy days (grey squares) and (c) days on which the cloud cover above each lake is less than 66% (black squares) in an average year calculated per lake from data in the periods 1993-96 and 2001-2004. Lakes are listed with increasing latitude (Notice the break of scale between 50° and 55° N).

4.4 Satellite data pre-processing

Generally, raw satellite images are corrected before most applications take place in order to remove systematic errors (Rees, 1990). This satellite data pre-processing procedure includes radiometric, atmospheric, geometric and topographic corrections. Furthermore, any other noise and distortions, such as banding and striping, may also be reduced or removed before further data analysis (Campbell, 2002; Lillesand *et al*., 2008). However, the need to perform corrections and rectifications to the satellite

data depends upon the particular application as not all corrections are always appropriate (Lillesand *et al*., 2008) and thus, in this project only certain corrections took place as described below.

4.4.1 Radiometric and atmospheric correction

The satellite data for this project were radiometrically and atmospherically corrected prior to receipt exploiting the PML automated facilities. Radiance, which is the signal detected by the remote sensing instrument, is a function of (a) the reflected or emitted radiation of an object at the Earth's surface and (b) the amount of distortions that are caused by several factors, such as the sensor response characteristics, system noise and malfunctions, the intensity and direction of illumination, the orientation and position of the object being observed and local atmospheric conditions (Campbell, 2002; Lillesand *et al*., 2008). Generally, systematic distortions are automatically calibrated onboard (Rees, 1990). The at-satellite spectral radiance[2] was calibrated in order to account for non-linear sensor response between wavebands and scaled to enhance weak detected signals. Other corrections included calibration for the Sun's elevation and the Earth-Sun distance which was performed to normalize for different solar illumination angles and seasonal changes in the Earth-Sun distance. Also, raw DN values were converted into absolute radiance; a process which is necessary in quantitative applications where satellite data are correlated with field observations (Lillesand *et al*., 2008), such as in this research project.

[2] At-satellite spectral radiance is the total radiance detected by the sensor when observing an object, including the light leaving the object and the effect of the atmosphere between the object and the sensor (Lillesand *et al*., 2008)

Part of the radiometric correction is a process called *atmospheric correction*, which accounts for distortions due to the interaction of radiation with the atmosphere. Since these atmospheric effects are wavelength dependant, the procedure should be applied to each band individually. Scattering is reduced with increasing wavelengths, while absorption takes place in longer wavelengths. According to that principle, satellite images obtained in the optical and nIR parts of the spectrum need to be atmospherically corrected for scattering, while thermal data need to be corrected for the effect of water vapour (Campbell, 2002). Kutser *et al*. (2005) suggest that when quantitative estimations of water parameters are to be performed, atmospheric correction is of great importance. For the purposes of this project, the NOAA AVHRR optical and near optical data were atmospherically corrected for Rayleigh scattering and the thermal data for water vapour absorption (personal communication with PML, 2007). The Terra/Aqua MODIS data were atmospherically corrected using the standard NASA Arnone model (personal communication with PML, 2007). The latter is a near-IR correction model based on the reflectance in the 670 nm region of the spectrum that estimates backscatter and it is specifically proposed for applications where chlorophyll *a* concentrations are mapped (NASA Ocean Colour, 2009).

4.4.2 Geometric correction

Geometric correction rectifies systematic and non-systematic distortions primarily caused by the motion of sensor while scanning and the forward motion of the satellite platform (Sabins, 1997), but also by the Earth's curvature and rotation, and other factors. During geometric correction, an undistorted output is matched to the original distorted image and the pixel values are re-sampled to fill in the

corresponding pixels of the rectified output (Figure 4-2). Since the re-sampling methods spatially and/or numerically alter the original values and their statistical characteristics, such as the mean, variance and covariance, and, hence, influence the uncertainty of the accuracy assessment process (Campbell, 2002), they were not applied in this project (personal communication with PML, 2007). However, a geolocation file was appended to each dataset to facilitate the comparison of satellite data pixel values to field data from sampling stations of known coordinates.

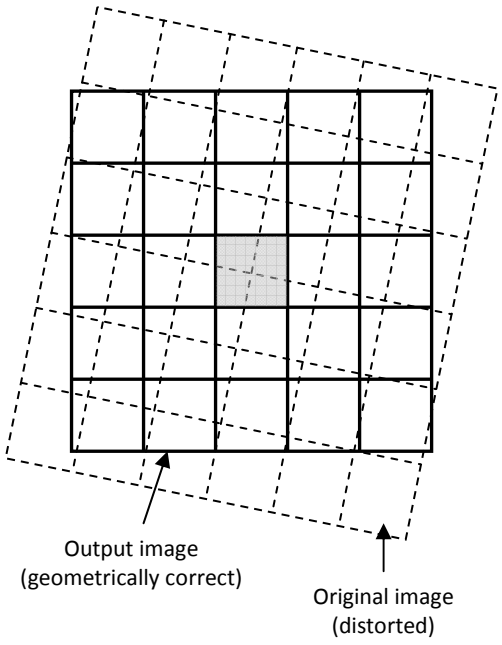

Figure 4-2: Geometrically corrected output image superimposed on original distorted image. The value of the shaded pixel in the output may vary according to the re-sampling method used, generally being a new averaged output value that many have not existed in the original image (Redrawn from Lillesand *et al*., 2008; p. 488).

4.4.3 Data products

The type of satellite products used in this project depended on the algorithms applied. Usually, normalized water-leaving radiance[3] is used in regression analysis, but raw DN values and at-satellite radiance/reflectance[4] have also been employed (e.g. Baban, 1993; Dekker & Peters, 1993; Allee & Johnson, 1999). For NOAA AVHRR, the brightness temperature (i.e. the apparent temperature of a surface/object detected by the radiometer) of bands 4 and 5 were acquired to serve as inputs to the LST estimation algorithms. At the same time, information regarding the land and cloud pixels was provided to facilitate the construction of a land-cloud mask model by the author (see Section 4.7.1). The cloud pixel information provided by the NEODAAS PML was reasonably good, but it was developed for ocean purposes and thus its accuracy over inland waters is uncertain (Personal Communication, PML). Regarding the Terra/Aqua MODIS data, a wider range of product levels was requested, including Level 1B and Level 2 data. Level 1B data products are calibrated and geolocated at-satellite radiances (L_{toa}) for all 36 MODIS bands (i.e. radiance for bands 1-19 and 26 and emissive radiance for bands 20-25 and 27-36) and at-satellite reflectance[5] (R_{toa}) for the reflective solar bands (i.e. MODIS bands 1-19 and 26). MODIS Level 2 data comprise calibrated, geolocated and atmospherically corrected remote sensing reflectance (R_{rs}) and normalized water-leaving radiances (nL_w) for bands 1-16. Also, the products of a NASA standard bio-optical (OC3) and physical (SST) model were incorporated in MODIS Level 2 data (NASA Ocean Colour, 2009).

[3] Normalized water-leaving radiance is the radiance which would exit the water surface if the Sun were at the zenith and if the atmosphere were absent (Gordon *et al*., 1988)
[4] At-satellite reflectance is the ratio of the amount of light leaving an object to the amount of incident light upon the object
[5] Remote sensing reflectance is reflectance measured at the water surface if the atmosphere were absent

4.5 Satellite data volume

A total of 111 cloud-free (or almost cloud-free) NOAA AVHRR scenes were requested and acquired for the period 1993-96 and 246 for the period 2001-04. The data consisted of the full swath of the original scenes and hence each included more than one study site.

Table 4-1: Number of Aqua MODIS subsets and Terra MODIS scenes acquired for each region and year.

AQUA	Year	Number of subsets	
		Level 1B	Level 2
Finland	2002	273	273
	2003	591	591
	2004	606	606
	Total:	**1470**	**1470**
Sweden	2002	294	296
	2003	615	615
	2004	615	615
	Total:	**1524**	**1526**
Switzerland	2002	217	217
	2003	434	434
	2004	445	445
	Total:	**1096**	**1096**
TERRA	**Year**	**Number of scenes**	
		Level 1B	**Level 2**
	2001	9	9
	2002	19	19
	2003	26	26
	2004	14	14
	Total:	**68**	**68**

The Terra/Aqua MODIS archive dates back to 2000, which limits the study period for MODIS data to the most recent period only (2001-04). A total of 8,318 Terra and Aqua MODIS Level 1B and Level 2 products were acquired (Table 4-1). The large amount of scenes delivered was because of two main reasons. First, the Aqua MODIS data were delivered in subsets of the original images each covering one of a total five lakes; Inarijärvi (Finland), Vänern, Vättern and Hjälmaren (Sweden) and Geneva (France-Switzerland). Second, one or two Aqua MODIS subsets were delivered for each of the five lakes on each day of 2.5 consecutive years, which included cloudy scenes despite the initial request for cloud-free (or almost cloud-free) scenes on specific dates. Aqua MODIS data before May 2002 (when the satellite was launched) are unavailable, so data from this sensor only covered the period between the second half of 2002 up until 2004.

The Terra MODIS data acquired coincided with the dates for which data were originally ordered. The Terra MODIS Level 1B and 2 products covered the full geographical extent of the original scenes and, hence, each included more than one study site. Fewer Terra MODIS data were acquired in 2001 compared to the rest of the years (i.e. 2002-04) probably due to frequent cloud cover of the study sites on the requested dates.

Approximately 500 GB of data were acquired from PML either on dvds and an external hard disk drive or via an online server.

4.5.1 Satellite data processing

Once radiometrically and atmospherically corrected satellite images were acquired from the PML, the data were further processed by the researcher to derive the desired water quality parameter products. Three image processing software packages were used during the data handling and analysis; ERDAS Imagine 9.1 was used to process the NOAA AVHRR images, while ENVI 4.5 and SeaDAS 5.2.0 were used for the Terra/Aqua MODIS images.

As mentioned above, the original NOAA AVHRR scenes that were acquired covered a wide area of Europe and, thus, each included several study sites. Image subsetting is a typical procedure when very large satellite images are used (both in size and number), because it minimizes computer storage, time and effort (Campbell, 2002). Thus, the pre-processed NOAA AVHRR scenes were imported and displayed on ERDAS Imagine 9.1 and the study sites on each scene were located. Spatial subsets of each lake were created for all images, while the number of spectral channels remained unchanged.

On the other hand, the Terra/Aqua MODIS Level 1B products were already subset when acquired to minimize data volume. The Level 2 data were acquired in their original size, but subsetting was unnecessary at this stage.

4.6 Water quality estimation algorithms

The selection of appropriate algorithms to estimate water quality is very important as it determines the accuracy achieved, since the wide spatial and temporal scale of the

project suggest that only transferable and repeatable algorithms will provide reliable results. This section lists and describes all standard and non-standard algorithms investigated in this project. Standard algorithms are used operationally to estimate water quality parameters (e.g. by NASA), while non-standard algorithms are empirical algorithms proposed in the published literature and their spatial and temporal transferability has not been tested.

4.6.1 Temperature estimation algorithms

Three NASA standard temperature estimation algorithms were tested in this project; two for NOAA AVHRR data and one for Terra/Aqua MODIS data. There was also a non-standard algorithm from published literature that was tested for Terra/Aqua MODIS data.

4.6.1.1 The NOAA AVHRR MCSST and NLSST algorithms

For NOAA AVHRR, the split window approach combines an effective atmospheric correction of the thermal radiance emitted by a water body with the advantage of taking into consideration the variation of atmospheric path length with changing satellite zenith angles (Oesch *et al*., 2005). In this project the linear multichannel SST estimation (MCSST) and non-linear SST estimation (NLSST) approaches of the split window algorithm were used to estimate LST. Oesch *et al*. (2005) tested the accuracy of both AVHRR operational algorithms in three European alpine lakes; namely Lakes Constance, Geneva and Mond (in Austria) in 2002 and 2003. They found that the MCSST algorithm provided more accurate estimations of lake surface temperature than the NLSST and that data collected at night generally showed more

reliable results, as the day-time algorithms overestimated surface temperature especially in warm summer months (due to solar insolation of the surface film). The applicability of both algorithms in lake water bodies was suggested for the first time (Oesch *et al*., 2005). In this project only day-time satellite data were used due to the unavailability of coinciding night-time *in situ* LST measurements.

The general form of the MCSST and NLSST equations is given below:

$$\text{MCSST [°C]} = A_1 (T_4) + A_2 (T_4 - T_5) + A_3 (T_4 - T_5)(\sec(\theta)-1) - A_4 \quad (4.1)$$

$$\text{NLSST [°C]} = B_1 (T_4) + B_2 (T_4 - T_5)\, \text{Tsfc} + B_3 (T_4 - T_5)(\sec(\theta)-1) - B_4 \quad (4.2)$$

where T_4 and T_5 are the brightness temperatures of AVHRR bands 4 and 5 in degrees Kelvin; Sec(θ) is the secant of the satellite zenith angle θ; MCSST and NLSST are the linear multi-channel and the non-linear SST algorithms respectively in degrees Celsius; $A_{1,2,3,4}$ and $B_{1,2,3,4}$ are constant coefficients; and Tsfc is an *a priori* estimate of the water surface temperature in degrees Celsius. The constant coefficients in the Equations 4.1 and 4.2 are estimated either from model simulations or correlations with field measurements (Jensen 2000) and for each satellite are given in Tables 4-2 and 4-3. Since the input brightness temperatures (T_4 and T_5) were acquired from PML in degrees Celsius (ºC), the last constants in Equations 4.1 and 4.2 (A_4 and B_4) which are used as converters from degrees Kelvin to Celsius, were omitted. The Tsfc value can be a LST estimation derived from AVHRR data using one of the MCSST equations (Oesch *et al*., 2005). In this project, the MCSST values were used in the non-linear NLSST algorithm rather than *a priori* LST estimates obtained from analysis of past satellite LST data.

Table 4-2: Operational day-time linear multi-channel sea surface temperature (MCSST) estimation algorithm using a split window approach for AVHRR data (NOAA MOST, 2009).

Period of validation	NOAA	SST equation
01/01/1984-31/12/9999	7	$1.0346\ T_4 + 2.5779\ (T_4-T_5)\ -283.21$
30/03/1988-31/12/9999	9	$T_4 + 2.6084\ (T_4-T_5) - 0.0269\ T_5\ -265.479$
11/06/1993-31/12/9999	11	$0.979224\ T_4 + 2.361743\ (T_4-T_5) + 0.33084\ (T_4-T_5)(\sec(\theta)-1) - 267.029$
08/04/1994-31/12/9999	12	$0.963563\ T_4 + 2.579211\ (T_4-T_5) + 0.242598\ (T_4-T_5)(\ \sec(\theta)-1) - 263.006$
20/03/1995-31/12/9999	14	$1.017342\ T_4 + 2.139588\ (T_4-T_5) + 0.779706\ (T_4-T_5)(\ \sec(\theta)-1) - 278.43$
13/05/1998-31/12/9999	15	$0.964243\ T_4 + 2.71296\ (T_4-T_5) + 0.387491\ (T_4-T_5)(\ \sec(\theta)-1) - 262.443$
21/09/2000-31/12/9999	16	$0.999314\ T_4 + 2.30195\ (T_4-T_5) + 0.628976\ (T_4-T_5)(\ \sec(\theta)-1) - 273.768$
27/07/2002-31/12/9999	17	$0.992818\ T_4 + 2.49916\ (T_4-T_5) + 0.915103\ (T_4-T_5)(\ \sec(\theta)-1) - 271.206$
20/05/2005-31/12/9999	18	$1.02453\ T_4 + 2.10044\ (T_4-T_5) + 0.784059\ (T_4-T_5)(\ \sec(\theta)-1) - 280.43$

Table 4-3: Operational day-time non-linear sea surface temperature (NLSST) estimation algorithm using a split window approach for AVHRR data (NOAA MOST, 2009).

Period of validation	NOAA	SST equation
06/11/1993-31/12/9999	11	$0.92323\ T_4 + 0.082523\ (T_4-T_5)\ \text{Tsfc} + 0.463038\ (T_4-T_5)(\sec(\theta)-1) - 250.109$
08/04/1994-31/12/9999	12	$0.876992\ T_4 + 0.083132\ (T_4-T_5)\ \text{Tsfc} + 0.349877\ (T_4-T_5)(\sec(\theta)-1) - 236.667$
20/03/1995-31/12/9999	14	$0.939813\ T_4 + 0.076066\ (T_4-T_5)\ \text{Tsfc} + 0.801458\ (T_4-T_5)(\sec(\theta)-1) - 255.165$
13/05/1998-31/12/9999	15	$0.913116\ T_4 + 0.0905762\ (T_4-T_5)\ \text{Tsfc} + 0.47694\ (T_4-T_5)(\sec(\theta)-1) - 246.887$
21/09/2000-31/12/9999	16	$0.914471\ T_4 + 0.0776118\ (T_4-T_5)\ \text{Tsfc} + 0.668532\ (T_4-T_5)(\sec(\theta)-1) - 248.116$
27/07/2002-31/12/9999	17	$0.936047\ T_4 + 0.083867\ (T_4-T_5)\ \text{Tsfc} + 0.920848\ (T_4-T_5)(\sec(\theta)-1) - 253.951$
20/05/2005-31/12/9999	18	$0.934004\ T_4 + 0.0724457\ (T_4-T_5)\ \text{Tsfc} + 0.748044\ (T_4-T_5)(\sec(\theta)-1) - 253.308$

Note: NLSST equations have not been developed for NOAA-7 and NOAA-9 AVHRR data

The satellite zenith angle (θ) was calculated for the central point of each lake according to the following procedure. The satellite zenith angle depends on the satellite location during the overpass in relation to the study site being observed and the distance of the site from the satellite nadir (Figure 4-3). It was calculated for each lake and for each satellite image using known information, such as the tangent of θ, which is given by the following equation:

$$\tan(\theta) = \frac{x}{H} \tag{4.3}$$

where θ is the satellite zenith angle, x is the distance of the central point of each lake from the satellite nadir of each scene and H is the altitude of the satellite (H = 833 km for NOAA AVHRR).

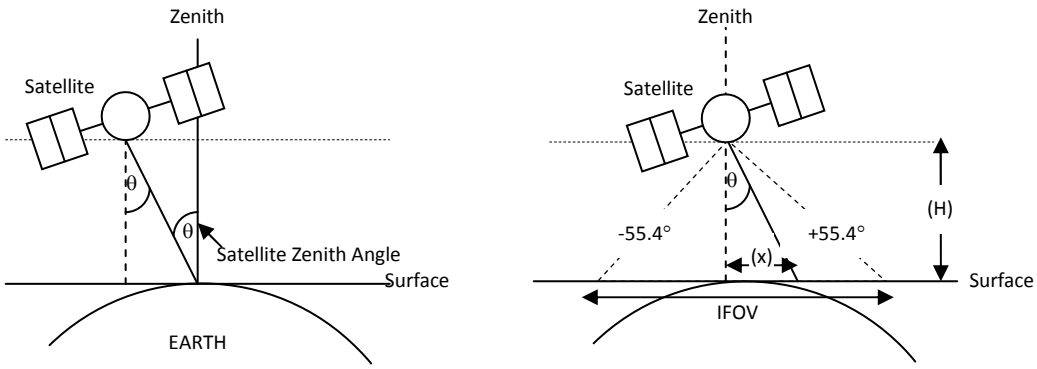

Figure 4-3: Calculation of the satellite zenith angle (θ).

Distance x was estimated using the following procedure. In total, an AVHRR image has 2048 columns (i.e. number of pixels on the x-axis), so the nadir of any AVHRR scene is assumed to be the centre of those, i.e. at the 1024th pixel (Figure 4-4A). By

extracting the x-axis coordinate (in pixels) of the lake central point (Figure 4-4B) and subtracting that from 1024, the *x* distance (in pixels) from the satellite nadir is found. In this approach, distance *x* was calculated by approximation because the curvature of the Earth was not accounted for as shown in Figure 4-3B. Then, by multiplying the *x* distance (in pixels) with the pixel size (IFOV = 1.1 km) the *x* distance in kilometres is calculated. After tan(θ) is calculated for each lake using Equation 4.3, the angle θ is easily computed.

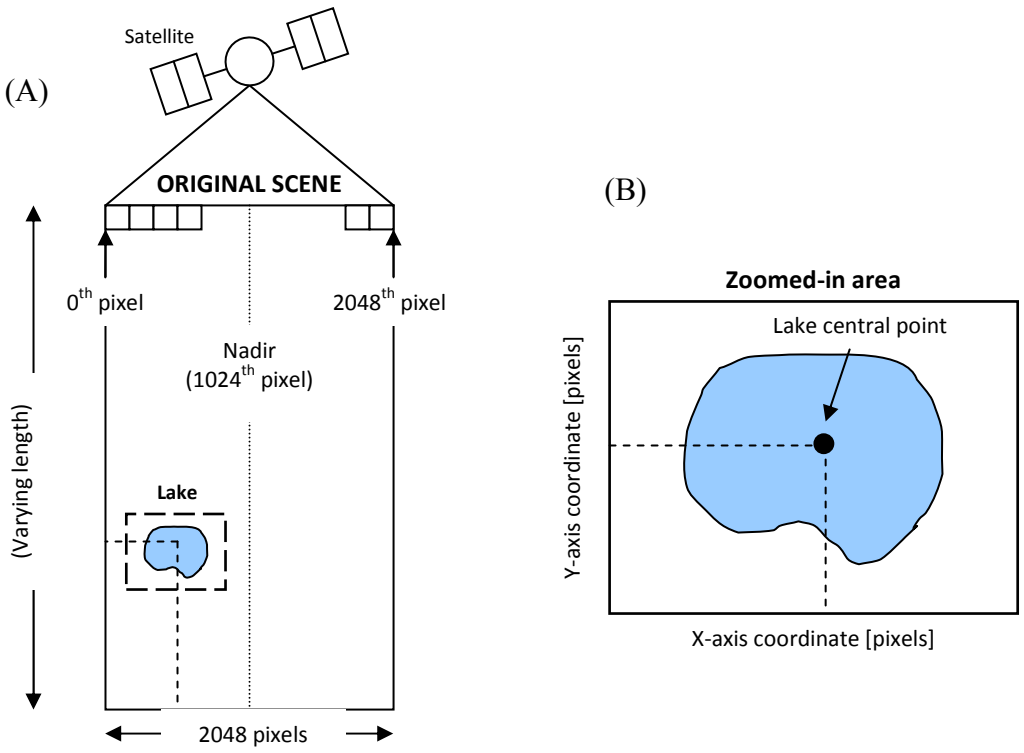

Figure 4-4: The figure shows (A) a hypothetical AVHRR scene, its dimensions in pixels and the location of the zenith point (1024th pixel in the centre of the scene), and (B) a zoomed-in area of the scene around a study site and its central point from which the X-axis coordinate is extracted for the calculation of distance *x* (refer to text for details).

Uncertainty in LST estimations may be introduced due to distortions in the image pixels viewed at large viewing angles, because an increase in the atmospheric path

length causes greater attenuation of the surface radiance. At nadir, the IFOV is equal to 1.1 km and increases with distance from the satellite nadir to 5 km (along track) and 6.8 km (across track) at the scanning extreme of 55.4° (Latifovic & Pouliot, 2007). Due to this distortion adjacent off-nadir pixels overlap and cause the off-nadir observations to be highly redundant (Cracknell, 1997). Oesch *et al*. (2005) suggested that pixels viewed with a satellite zenith angle greater than 53° should be excluded from analysis, in order to maintain high accuracy in the LST estimations. In this project, geometric correction was not applied to the images and pixels viewed with a satellite zenith angle greater than 50° were excluded from analysis due to the distortion caused at the edges of the images.

4.6.1.2 The Terra/Aqua MODIS SST algorithm

The MODIS SST estimation algorithm is based on the same principle as the AVHRR split window approach and takes the following general form:

$$SST\ [°C] = C_1 + C_2\,(T_{31}) + C_3\,(T_{32} - T_{31}) + C_4\,(\sec(\theta)-1)(T_{32} - T_{31}) \qquad (4.4)$$

where T_{31} and T_{32} are the brightness temperatures at MODIS bands 31 and 32 (*cf.* AVHRR bands 4 and 5 respectively); $C_{1,2,3,4}$ are constant coefficients and $\sec(\theta)$ is secant of the satellite zenith angle (θ). The values of the constant coefficients for the MODIS bands 31 and 32 SST estimation algorithm depend on the difference $T_{32} - T_{31}$ as shown in Table 4-4.

Table 4-4: Coefficients for the MODIS SST algorithm (NASA Ocean Colour, 2009).

Coefficients	$T_{32} - T_{31} \leq 0.7$	$T_{32} - T_{31} > 0.7$
C_1	1.11071	1.196099
C_2	0.9586865	0.9888366
C_3	0.1741229	0.1300626
C_4	1.876752	1.627125

4.6.1.3 A non-standard LST estimation algorithm

Baban (1993) developed an algorithm for the estimation of lake surface temperature in the Norfolk Broads, UK, using Landsat TM raw DN data in June. The algorithm exhibited a high coeffiecient of determination (R^2 = 0.83, n = 8) and is presented below:

$$\text{Temperature } [^{\circ}\text{C}] = -23.4 + 0.35\, B_6 \qquad (4.5)$$

where B_6 are DN values at Landsat TM band 6.

4.6.2 Chlorophyll *a* estimation algorithms

One NASA standard and 35 non-standard chlorophyll *a* estimation algorithms were tested in this project.

4.6.2.1 The Terra/Aqua MODIS OC3 algorithm

For chlorophyll *a* estimations in Case I waters the OC3 algorithm has been developed specifically for Terra/Aqua MODIS data (NASA Ocean Colour, 2009). The algorithm incorporates MODIS bands 9, 10 and 12 with waveband centres at 443, 488 and 551 nm respectively:

$$C_{chl-a}\left[\mu\text{g/lt}\right] = 10^{(0.283-2.753R+1.457R^2+0.659R^3-1.403R^4)}$$
$$\text{where } R = \log_{10}\left(\frac{R_{rs}443 > R_{rs}488}{R_{rs}551}\right) \tag{4.6}$$

where $R_{rs}443$, $R_{rs}488$ and $R_{rs}551$ is the remote sensing reflectance at MODIS bands 9, 10 and 12 respectively. The algorithm employs the greater of either ratio $R_{rs}443/R_{rs}551$ or $R_{rs}488/R_{rs}551$.

The OC3 algorithm works within a range of chlorophyll *a* concentrations between 0-100 μg L^{-1}; outside that range, the algorithm fails. Also the algorithm fails when $R_{rs}551 < 0$ or $R_{rs}443$ or $R_{rs}488 < 0$ or $R > 10$.

4.6.2.2 Non-standard chlorophyll *a* estimation algorithms

The 35 chlorophyll *a* estimation algorithms that were selected from published literature are presented in this section (Tables 4-5 to 4-7).

Table 4-5: List of chlorophyll *a* estimation algorithms developed for Landsat TM and Daedalus 1268 ATM raw DN data or L_{toa}.

Author(s)	Lake(s)	Sensor	Data	Period	Algorithm	R^2	*n*	Code
Dekker & Peters (1993)	10 eutrophic (Netherlands)	TM	DN	Jun	$C_{chl\text{-}a}$ [µg L^{-1}] = – 4764.54 + 51.87 B_1	0.70	9	DchlB1jun
					$C_{chl\text{-}a}$ [µg L^{-1}] = – 1437.54 + 43.41 B_2	0.95	9	DchlB2jun
					$C_{chl\text{-}a}$ [µg L^{-1}] = – 1028.43 + 38.33 B_3	0.85	9	DchlB3jun
					$\ln(C_{chl\text{-}a})$ = – 88.32 + 25.95 $\ln(B_2)$	0.70	9	DlnB2jun
					$\ln(C_{chl\text{-}a})$ = – 63.65 + 20.08 $\ln(B_3)$	0.72	9	DlnB3jun
				Jul	$C_{chl\text{-}a}$ [µg L^{-1}] = – 1137.52 + 48.93 B_2	0.87	10	DchlB2jul
					$C_{chl\text{-}a}$ [µg L^{-1}] = – 913.83 + 51.52 B_3	0.81	10	DchlB3jul
					$\ln(C_{chl\text{-}a})$ = – 55.37 + 18.39 $\ln(B_2)$	0.87	10	DlnB2jul
					$\ln(C_{chl\text{-}a})$ = – 43.54 + 15.97 $\ln(B_3)$	0.91	10	DlnB3jul
Baban (1993)	14 eutrophic (England, UK)	TM	DN	Jun	$C_{chl\text{-}a}$ [µg L^{-1}] = – 770 + 4768 (B_3/B_1) – 24.6 [(B_2/B_3)/2]	0.55	12	BchlB123
Allee & Johnson (1999)	1 monomictic, oligotrophic (Arkansas, USA)	TM	L_{toa}	Jul	$\ln(C_{chl\text{-}a})$ = [(0.70 – 3.63) $\ln(B_1$dev.)] + 1.83 $\ln(B_2$dev.) + 4.08 $\ln(B_3$dev.) – 0.15 $\ln(B_5$dev.^{3})	0.80	30	AchlaJuly
				Dec	$\ln(C_{chl\text{-}a})$ = [(1.47 – 2.08) $\ln(B_2$dev.^{3})] – 0.61 $\ln(B_3$dev.) + 0.65 $\ln(B_3$dev.^{3})	0.84	30	AchlaDec
Hedger *et al.* (1996)	1 oligotrophic 1 mesotrophic (Scotland, UK)	ATM	L_{toa}	May	$C_{chl\text{-}a}$ [µg L^{-1}] = 7.5672 – 4.6973 (B_1/B_3)	(n/a)	(n/a)	HchlB13
					$C_{chl\text{-}a}$ [µg L^{-1}] = – 7.545 + 6.9684 (B_3/B_5)	(n/a)	(n/a)	HchlB35

where B_x is Landsat TM or Daedalus 1268 ATM band x, ln is the natural logarithm, 'dev.' indicates deviation from the mean and (n/a) indicates that the information was not included in the publication

Table 4-6: List of chlorophyll *a* estimation algorithms developed for Daedalus 1268 ATM and AISA L_{toa} or nL_w data.

Author(s)	Lake type	Sensor	Data	Period	Algorithm	R^2	*n*	Code
George (1997b)	15 Case I, various* (England, UK)	ATM	L_{toa}	Jul-Aug	$C_{chl\text{-}a}$ [µgL^{-1}] = – 7.14 + 16.78 (B_3/B_2)	0.83	9	GeochlB32lo
					$C_{chl\text{-}a}$ [µgL^{-1}] = – 4.30 + 1.44 B_3	0.50	9	GeochlB3lo
					$C_{chl\text{-}a}$ [µg L^{-1}] = – 28.82 + 59.41 (B_3/B_2)	0.69	9	GeochlB32hi
					$C_{chl\text{-}a}$ [µg L^{-1}] = – 41.63 + 6.91 B_3	0.96	9	GeochlB3hi
Pulliainen *et al.* (2001)	11 lakes, various* (Finland)	AISA	L_{toa}	May	$C_{chl\text{-}a}$ [µg L^{-1}] = – 136.34 + 164.68 (L_{688}/L_{680})	0.93	20	PchlMay
				Aug	$C_{chl\text{-}a}$ [µg L^{-1}] = – 68.96 + 105.25 (L_{702}/L_{665})	0.94	38	PchlAug
Kallio *et al.* (2001)	11 lakes, various* (Finland)	AISA	L_{toa}	May	$C_{chl\text{-}a}$ [µg L^{-1}] = – 51.0 + 69.0 ($L_{699\text{-}705}/L_{670\text{-}677}$)	0.76	19	KalMay01
					$C_{chl\text{-}a}$ [µg L^{-1}] = – 102.0 + 129.0 ($L_{685\text{-}691}/L_{670\text{-}677}$)	0.93	19	KalMay02
				Aug	$C_{chl\text{-}a}$ [µg L^{-1}] = – 62.6 + 89.0 ($L_{699\text{-}705}/L_{670\text{-}677}$)	0.91	88	KalAug01
					$C_{chl\text{-}a}$ [µg L^{-1}] = – 192.1 + 250.0 ($L_{685\text{-}691}/L_{670\text{-}677}$)	0.86	88	KalAug02
				May,Aug	$C_{chl\text{-}a}$ [µg L^{-1}] = – 64.8 + 90.2 ($L_{699\text{-}705}/L_{670\text{-}677}$)	0.90	107	KalMA01
					$C_{chl\text{-}a}$ [µg L^{-1}] = – 187.0 + 241.0 ($L_{685\text{-}691}/L_{670\text{-}677}$)	0.79	107	KalMA02
Koponen *et al.* (2002)	11 lakes, various* (Finland)	AISA	nL_w	Aug	$C_{Chl\text{-}a}$ [µg L^{-1}] = – 33.79 + 65.66 [($L_{700} - L_{781}$)/($L_{662} - L_{781}$)]	0.94	80	Kopchla
Kallio *et al*. (2003)	2 meso-eutrophic (Finland)	AISA	nL_w	Aug	$C_{chl\text{-}a}$ [µg L^{-1}] = 108.5 (L_{705}/L_{662}) – 68.7	0.98	12	Kalchl01
					$C_{chl\text{-}a}$ [µg L^{-1}] = 112.1 (L_{705}/L_{662}) – 77.1	0.96	15	Kalchl02

where B_x is Daedalus 1268 ATM band x, L_{xyz} is the AISA band centred at xyz nm and $L_{abc\text{-}xyz}$ is the AISA band with spectral range abc-xyz nm

* Various indicates lakes with various trophic status and mixing characteristics

Table 4-7: List of chlorophyll *a* estimation algorithms developed field spectroradiometer (FSR) R_{toa} or R_{rs} data.

Author(s)	Lake type	Sensor	Data	Period	Algorithm	R^2	*n*	Code
Gitelson *et al*. (1993)	1 meso-eutrophic (Hungary)	FSR	R_{toa}	Summer	$C_{Chl\text{-}a}$ [µg L^{-1}] = a_1 (R_{700}/R_{560})^{b1} where a_1 = 1.46 MEAN($C_{Chl\text{-}a}$) + 44.25 and b_1 = – 0.013 MEAN($C_{Chl\text{-}a}$) + 2.9	0.63	103	Gitchl01
					$C_{Chl\text{-}a}$ [µg L^{-1}] = a_2 (R_{700}/R_{675})^{b2} where a_2 = 0.473 MEAN($C_{Chl\text{-}a}$) + 1.68 And b_2 = – 0.013 MEAN($C_{Chl\text{-}a}$) + 3.5	0.9	103	Gitchl02
Thiemann & Kaufmann (2000)	16 lakes, various* (Germany)	FSR	R_{toa}	May-Jun, Sep	$C_{Chl\text{-}a}$ [µg L^{-1}] = – 52.9 + 73.6 (R_{705}/R_{678})	0.89	28	Thiemchla
Strömbeck & Pierson (2001)	1 dimictic, eutrophic (Sweden)	FSR	R_{toa}	Late summer	$C_{Chl\text{-}a}$ [µg L^{-1}] = [($R_{700\text{-}710}/R_{678\text{-}685}$) – 0.81]/0.0076	0.47	732	Strömchla
Dall'Olmo *et al.* (2005)	8 Case II, various* (Nebraska, USA)	FSR	R_{rs}	Spring-Autumn	$C_{chl\text{-}a}$ [µg L^{-1}] = $10^{[2.048 + 1.38 \log(R(748)/R(667))]}$	0.90	136	Dallchl01
					$C_{chl\text{-}a}$ [µg L^{-1}] = $10^{[2.046 + 1.49 \log(R(748)/R(678))]}$	0.85	136	Dallchl02

where R_{xyz} is the field spectroradiometer band centred at xyz nm and $R_{abc\text{-}xyz}$ is the field spectroradiometer band with spectral range abc-xyz nm

* Various indicates lakes with various trophic status and mixing characteristics

4.6.3 Secchi disk depth estimation algorithms

There are no standard algorithms for the estimation of SDD. However, eleven non-standard algorithms were tested (Table 4-8).

The non-standard chlorophyll *a* and SDD estimation algorithms were assigned a code name, based on the initial of the first author, the parameter used, the remote sensing bands employed and (if applicable) the month of application for quick reference (Tables 4-5 to 4-8).

The ecological type and hydrological status of the lakes studied in published literature varies and the sites cover a wide range of geographical areas. Thus, the water quality estimation algorithms listed here were investigated in the search for a universal algorithm that can be applied at wide spatial and temporal scales. However, it should be noted that most algorithms are site- and season-specific, which means that they might not be transferable through space and time.

4.7 Application of algorithms

Once the satellite data pre-processing was complete, the standard and non-standard algorithms were applied to the satellite data as appropriate. Specifically, the operational MCSST and NLSST algorithms were applied to the AVHRR data and the non-standard chlorophyll *a* and SDD estimation algorithms were applied to the Terra/Aqua MODIS data. The MODIS SST and OC3 algorithm products were provided by PML within the Level 2 images so no algorithm application was necessary in that case.

Table 4-8: List of SDD estimation algorithms developed for Landsat TM and AISA raw DN data or L_{toa}.

Author(s)	Lake(s)	Sensor	Data	Period	Algorithm	R^2	*n*	Code
Dekker & Peters (1993)	10 eutrophic (Netherlands)	TM	DN	Jun	$\ln(SDD) = 54.97 - 15.13 \ln(B_3)$	0.81	9	DlnSecB3jun
				Jul	$SDD\ [cm] = 1199.93 - 55.90\ B_3$	0.66	10	DSecB3jul
					$\ln(SDD) = 42.75 - 11.95 \ln(B_2)$	0.68	10	DlnSecB2jul
					$\ln(SDD) = 37.36 - 11.15 \ln(B_3)$	0.86	10	DlnSecB3jul
Baban (1993)	14 eutrophic (England, UK)	TM	DN	Jun	$SDD\ [m] = 5.41 - 0.0748\ B_1$	0.69	9	BSecB1
Allee & Johnson (1999)	1 monomictic, oligotrophic (Arkansas, USA)	TM	L_{toa}	Feb	$SDD\ [m] = [(1.67 - 0.62)\ B_3dev.] + 1.27\ B_3dev.^2 - 0.87\ B_3dev.^3$	0.96	30	ASecFeb
Sawaya *et al*. (2003)	Multiple lakes (Minnesota, USA)	TM	L_{toa}	Aug	$\ln(SDD) = 1.493\ (B_1/B_3) - 0.035\ B_1 - 1.956$	0.76	94	SlnSDTB13
Kallio *et al.* (2001)	11 lakes, various* (Finland)	AISA	L_{toa}	May	$SDD\ [m] = -1.442 + 3.94\ [(L_{488\text{-}496} - L_{747\text{-}755})/(L_{618\text{-}625} - L_{747\text{-}755})]$	0.95	19	KalSDD01
				Aug	$SDD\ [m] = -0.935 + 2.60\ [(L_{488\text{-}496} - L_{747\text{-}755})/(L_{618\text{-}625} - L_{747\text{-}755})]$	0.86	103	KalSDD02
				May,Aug	$SDD\ [m] = -0.909 + 2.66\ [(L_{488\text{-}496} - L_{747\text{-}755})/(L_{618\text{-}625} - L_{747\text{-}755})]$	0.84	122	KalSDD03
Koponen *et al.* (2002)	11 lakes, various* (Finland)	AISA	L_{toa}	Aug	$SDD\ [m] = -0.4298 + 1.0926\ [(L_{521} - L_{781})/(L_{700} - L_{781})]$	0.93	102	KopSDD

where B_x is Landsat TM band x, ln is the natural logarithm, 'dev.' indicates deviation from the mean, L_{xyz} is the AISA band centred at xyz nm, and $L_{abc\text{-}xyz}$ is the AISA band with spectral range abc-xyz nm

4.7.1 NOAA AVHRR data

The MCSST and NLSST algorithms were applied to the NOAA AVHRR subsets to estimate LST, which was performed using the spatial modeller function of ERDAS Imagine 9.1. First, water surface temperature maps were constructed by applying the algorithms to each pixel of the satellite subsets. Then a land and cloud mask was created by incorporating information provided by the PML within each scene, which was essentially a classified image, where land, water and cloud pixels represented distinct classes. Visual interpretation of the original scenes and direct comparison of those to the corresponding classified images took place and the classes that represented non-water pixels were identified. In addition, the thermal properties of water were taken into account to confirm the distinction between water and land pixels using the LST maps produced in an earlier step. The land and cloud mask model was then applied to remove the land and cloud pixels from all subsets. Boundary and mixed pixels were identified during the same procedure and were also masked out. In addition to that, the adjacency effect was accounted for as it is often observed in near-shore pixels due to radiation scattering from neighbouring land pixels (Odermatt *et al*., 2008; *Ruiz*-Verdú *et al*., 2008). Near-shore pixels are often omitted to avoid contamination due to the adjacency effect (e.g. Lavender *et al*., 2004, Bussières *et al*., 2002) and, as a result, only unmixed and cloud-free off-shore water temperature pixels appeared in the processed scenes that were used in subsequent analysis (Figure 4-5).

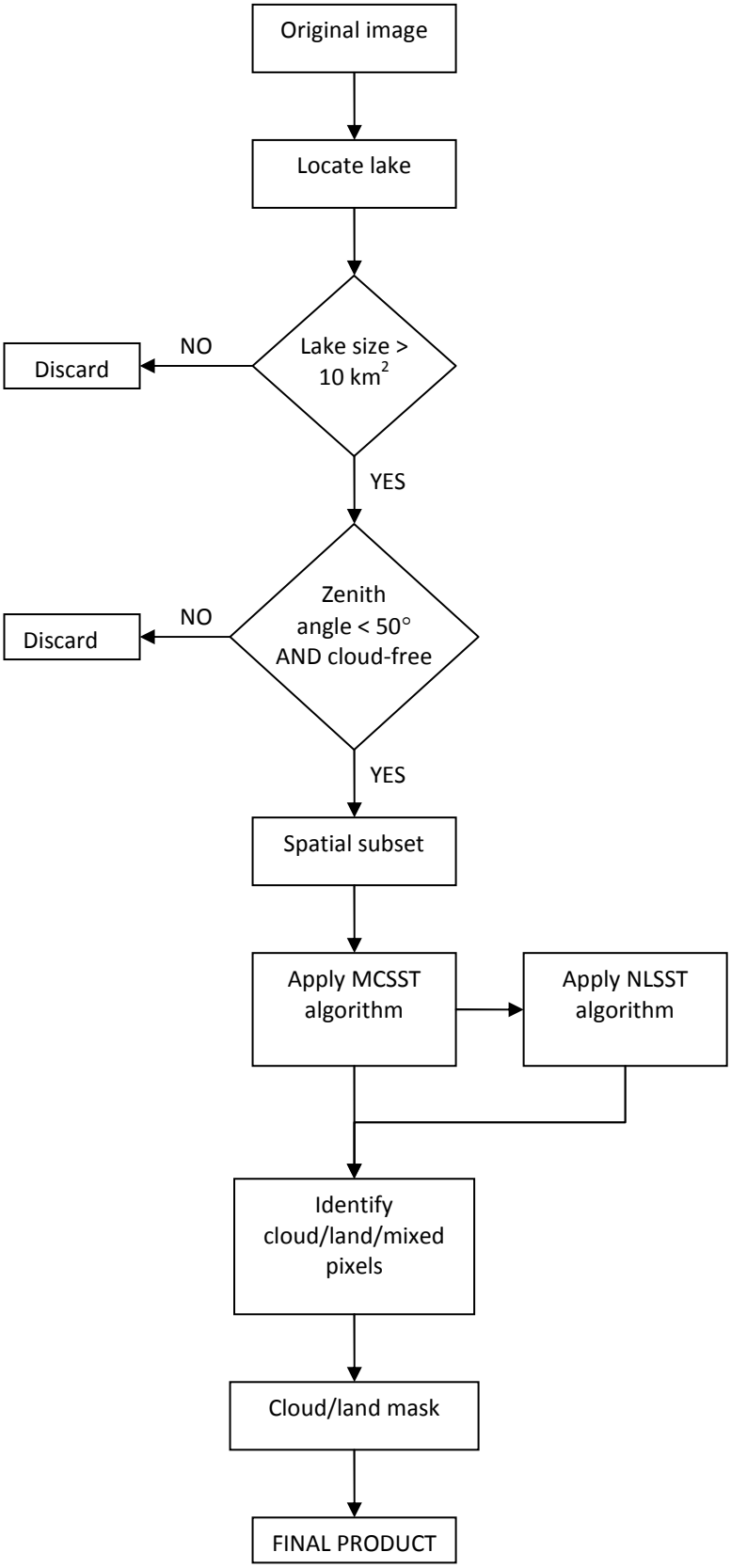

Figure 4-5: Flowchart of the NOAA AVHRR data preparation and algorithm application.

4.7.2 Terra/Aqua MODIS data

The Terra/Aqua MODIS data preparation differed from the procedure described above. Since the standard OC3 and SST algorithm products were obtained within each Level 2 scene, there was no data processing needed prior to data extraction and statistical analysis for these two algorithms. In contrast, some preparation was required for the MODIS Level 1B and Level 2 data before the application of the non-standard algorithms.

Algorithms selected from published literature and used in this project were originally developed for sensors other than Terra/Aqua MODIS. The most commonly employed multispectral sensors for lake studies was the Thematic Mapper (TM) and its successor, the Enhanced TM Plus (ETM+) onboard the Landsat satellite series. They have been used to map water quality in four out of the total 14 studies presented here. However, instruments such as the Airborne Imaging Spectrometer for Applications (AISA) (four studies) and Daedalus 1268 Airborne Thematic Mapper (ATM) (two studies) were also employed. Finally, field reflectance measured by spectroradiometers has provided the basis for the development of water quality estimation algorithms in a further four studies presented earlier. Despite the fact that water quality estimation algorithms are sensor-specific, data obtained from one sensor (e.g. Terra/Aqua MODIS) can be transformed to simulate the specifications of another sensor (i.e. the above mentioned sensors) and thus used with relatively high accuracy (Koponen *et al*., 2002).

During data transformation (simulation), data from one sensor are effectively rescaled to simulate the spatial, spectral and radiometric characteristics of another

sensor. However, the method is not always applicable, as it depends on the specifications of both sensors. For example, coarse multispectral data are usually inappropriate to simulate fine spectral resolution data (hyperspectral), especially when the hyperspectral channels employed in the algorithm are (almost) contiguous. Thus, certain non-standard algorithms that exhibited promising results (e.g. Kallio *et al*., 2001; Pulliainen *et al*., 2001; Koponen *et al*., 2002) could not be applied here, due to such limitations.

In this project, Terra/Aqua MODIS data were used to simulate data from Landsat TM/ETM+, Daedalus 1268 ATM, AISA and four field spectroradiometers in order to use the water quality estimation algorithms developed for these sensors. The sensors characteristics are presented in the following section.

4.7.2.1 Sensor characteristics

Landsat TM is an across-track (whiskbroom) scanner that employs seven spectral bands covering the visible, nIR, middle IR and TIR regions of the electromagnetic spectrum at a spatial resolution of 30 m and 120 m for thermal band 6 (Table 4-9). Data are collected at a radiometric resolution of 8-bit, which resolves to a possible 256 grey levels. The Landsat ETM+ sensor has the same specifications as the TM, with the difference that it employs an extra band; band 8 (520-900 nm), and the thermal band 6 has a spatial resolution of 60 m.

The Daedalus 1268 ATM is a multispectral scanner with eleven bands that approximate those of Landsat TM (Table 4-9) and a radiometric resolution of 8-bit. The spatial resolution depends on the altitude of the aircraft during data collection.

Finally, the AISA is an along-track (pushbroom) scanner that collects data in the spectral range 450-900 nm at a maximum number of 288 contiguous bands each programmable to range in width from approximately 1.6 to 9.4 nm. The radiometric resolution of AISA is 12-bit, which means it records up to 2048 grey levels. When the AISA is operated at an altitude of 1 km above the Earth's surface it yields a ground pixel size at nadir of approximately 1 x 1 m. However, the aircraft altitude is adjusted to the application and so the spatial resolution varies accordingly.

The portable field spectrometers used in the lake water quality studies presented in this project were:

- ASD FieldSpec FR spectrometer (Thiemann & Kaufmann, 2000), with a 350-2500 nm spectral range, 10 nm spectral resolution and 12-bit radiometric resolution
- Ocean Optics USB2000 radiometer (Dall'Olmo *et al*., 2005), with a 200-1100 nm spectral range and 12-bit radiometric resolution
- GER 1500 spectroradiometer (Strömbeck & Pierson, 2001), with a spectral range of 350-1050 nm, 512 channels and radiometric resolution of 16-bit
- Unknown (Gitelson *et al*., 1993)

Table 4-9: Landsat TM/ETM+ and Daedalus 1268 ATM specifications (adapted from Lillesand *et al*., 2008; p.401 and Jensen, 2000; p. 186).

Landsat TM/EMT+			Daedalus 1268 ATM		
Band	**Bandwidth (nm)**	**Spectral region**	**Band**	**Bandwidth (nm)**	**Spectral region**
			1	420-450	Violet
1	450-520	Blue	2	450-520	Blue
2	520-600	Green	3	520-600	Green
			4	600-620	Red
3	630-690	Red	5	630-690	Red
			6	690-750	nIR
4	760-900	nIR	7	760-900	nIR
			8	910-1050	nIR
5	1550-1750	mid IR	9	1550-1750	mid IR
6	10400-12500	TIR	10	2080-2350	mid IR
7	2080-2350	mid IR	11	850-1300	nIR

4.7.2.2 Simulation procedure

Radiometric rescaling of the AISA data, the FieldSpec FR spectrometer and Ocean Optics USB2000 radiometer data was not necessary, as the three sensors measure at 12-bit like the Terra/Aqua MODIS. The other three sensors measure at different radiometric resolutions to the Terra/Aqua MODIS, however, radiometric rescale for the simulation of these sensors was unnecessary (and was not performed) as in this project only radiance and reflectance data (i.e. R_{toa}, L_{toa}, R_{rs} and nL_w) were used. In addition, re-projection of the spatially coarse Terra/Aqua MODIS data into finer spatial scales to match the spatial resolutions of the sensors to be simulated was considered unnecessary as it would not add extra information to the dataset, and was therefore omitted (Figure 4-6).

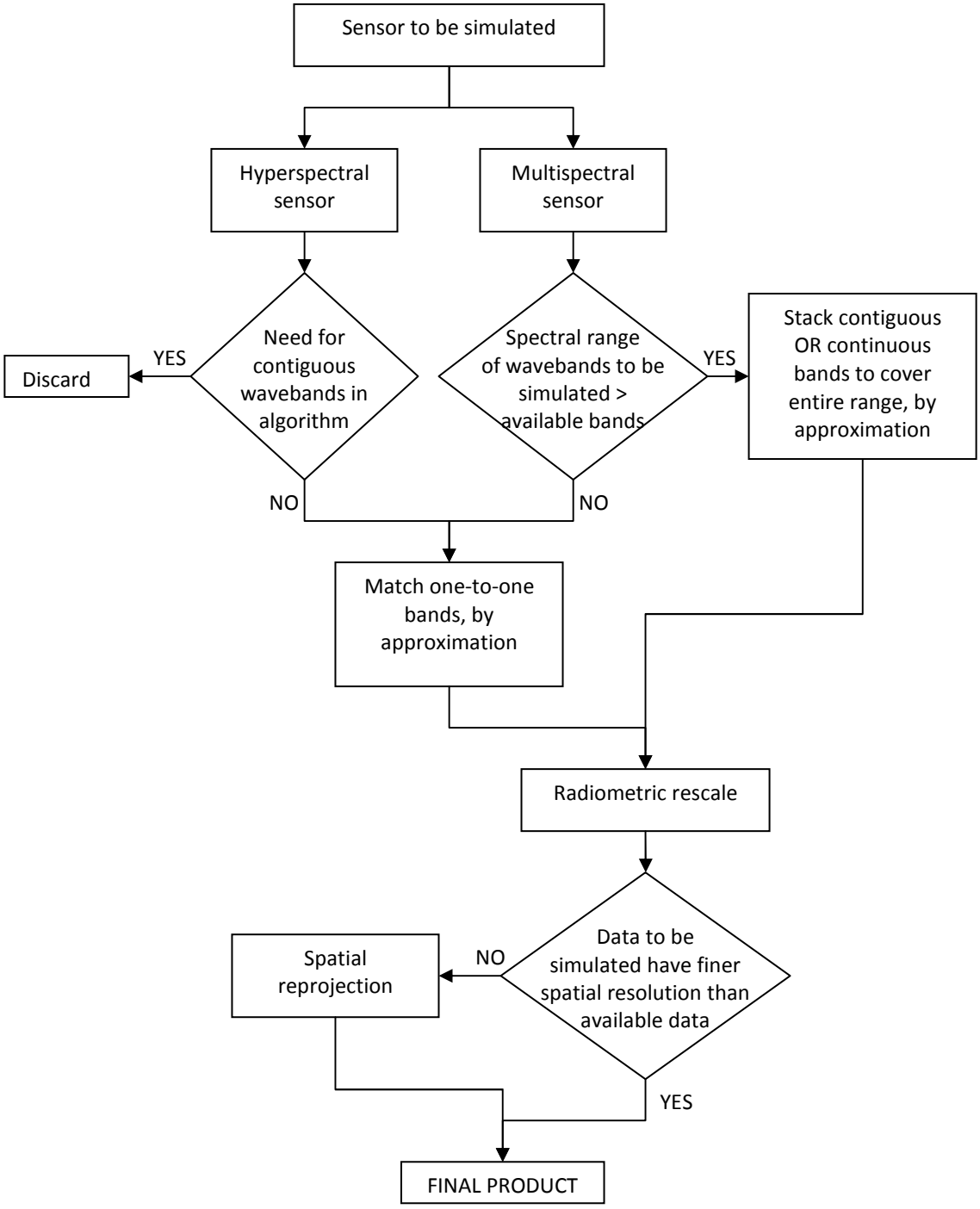

Figure 4-6: Flowchart of the simulation of multispectral or hyperspectral data using other multispectral data.

As a result, only spectral simulation was performed to the data. The Terra/Aqua MODIS wavebands that best reflect the range of each Landsat TM/ETM+ and

Daedalus 1268 ATM multispectral wavebands were identified (Table 4-10). Terra/Aqua MODIS bands are relatively narrow and not contiguous, so only one Terra/Aqua MODIS band was used for the simulation of a particular Landsat TM or Daedalus 1268 ATM band in the optical and nIR parts of the spectrum. The wide range of Landsat TM band 6 necessitated the use of two non-contiguous Terra/Aqua MODIS thermal wavebands to cover its full range, whose mean variance was calculated during the simulation procedure.

Table 4-10: Adaptation of MODIS spectral bands to simulate Landsat TM/ETM+ and Daedalus 1268 ATM bands used in this project.

Landsat TM/ETM+ bands			**Corresponding Terra/Aqua MODIS bands**		
Band	**Bandwidth (nm)**	**Band centre (nm)**	**Band**	**Bandwidth (nm)**	**Band centre (nm)**
1	450-520	485	10	483-493	488
2	520-600	560	4	545-565	555
3	630-690	660	13	662-672	667
4	760-900	830	2	841-876	859
5	1550-1750	1650	6	1628-1652	1640
6	10400-12500	11450	31	10780-11280	11030
			32	11770-12270	12020
Daedalus 1268 ATM bands			**Corresponding Terra/Aqua MODIS bands**		
Band	**Bandwidth (nm)**	**Band centre (nm)**	**Band**	**Bandwidth (nm)**	**Band centre (nm)**
1	420-450	435	9	438-448	443
2	450-520	485	10	483-493	488
3	520-600	560	4	545-565	555
5	630-690	660	13	662-672	667

All Terra/Aqua MODIS bands used for the simulation fully fell within the spectral range of each corresponding Landsat TM and Daedalus 1268 ATM band (Figure 4-7). The latter was important because the upper and lower edges of the spectral range that a waveband covers exhibit lower sensitivity than the central part of the band, where generally the response is at peak (Figure 4-8). The latter is based on the fact that the radiation signal measured by any remote sensing instrument is not uniformly detected throughout the full spectral range of each band (Clark, 1999). As a result, during simulation it is important to ensure that the band centres (and if possible also the spectral ranges) of the original (i.e. Terra/Aqua MODIS) and the simulated (i.e. Landsat TM and Daedalus 1268 ATM) bands coincide (Clark, 1999).

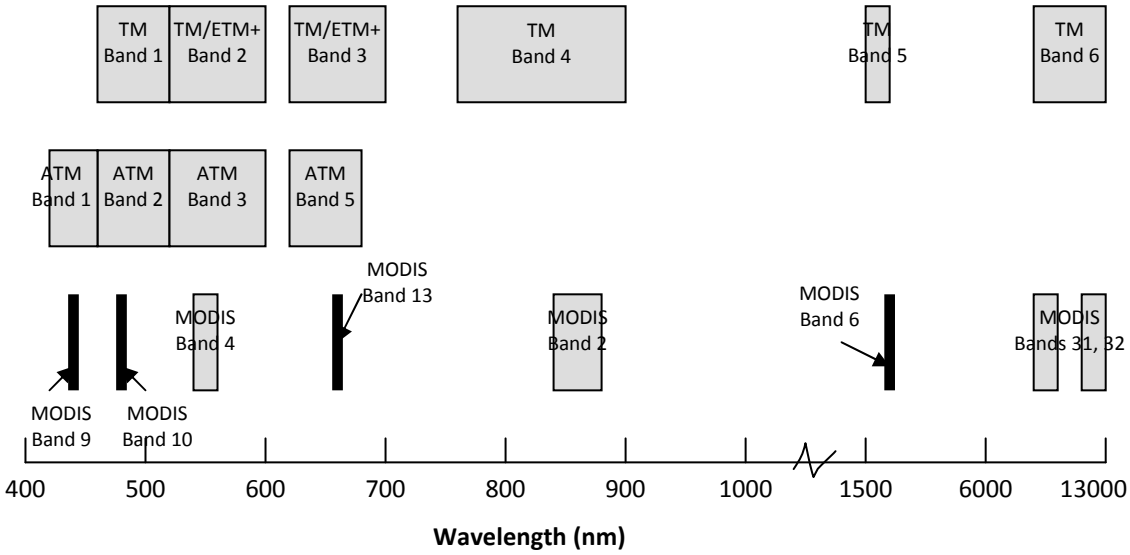

Figure 4-7: Spectral range of simulated Landsat TM/ETM+ and Daedalus 1268 ATM wavebands, and Terra/Aqua MODIS wavebands. *Notice the change in scale for wavelengths over 1000 nm.*

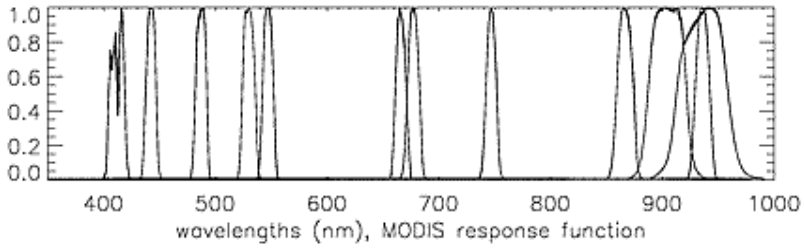

Figure 4-8: The spectral response of MODIS bands 8-19 (MUMM Ocean Colour, 2009).

Only the Landsat TM/ETM+ and Daedalus 1268 ATM bands needed for the application of algorithms were simulated to avoid unnecessary effort. Following that, only TM bands 1-6 were simulated, while TM band 7 was omitted from the simulation procedure. The ETM+ bands 2 and 3 are exactly the same as the TM bands 2 and 3 so the simulation was performed only once for both sensors. The Daedalus 1268 ATM bands 2, 3 and 5 needed for the application were exactly the same (in terms of their spectral and radiometric resolution) as Landsat TM bands 1, 2 and 3 accordingly so the simulation was performed only once for both sensors in this case too. The Daedalus 1268 ATM band 1 was also simulated.

The MODIS bands that best matched the AISA and field spectroradiometer data were used as an approximation, where applicable. Figures 4-9 and 4-10 show the hyperspectral channels (AISA and field spectroradiometers respectively) used in the non-standard algorithms in comparison to the Terra/Aqua MODIS bands 8-16. Some of the non-standard algorithms could not be applied due to lack of appropriate Terra/Aqua MODIS data to approximate certain AISA and field spectrometer bands. In this category fell all algorithms developed be Kallio *et al*. (2001), the May chlorophyll *a* estimation algorithm by Pulliainen *et al*. (2001) ('PchlMay') and the

chlorophyll *a* and SDD estimation algorithms by Koponen *et al*. (2002) ('Kopchla' and 'KopSDD').

A distinct feature of the Terra/Aqua MODIS sensor is the existence of MODIS band 13 low and 13 high (and 14 low and 14 high) that measure at the same wavelength, but saturate at different temperatures. The choice of low or high waveband depends on the application. Here, MODIS bands 13 low and 14 low were used as in most cases the values were either very similar or the same and because in some scenes the 13 high and 14 high values were missing.

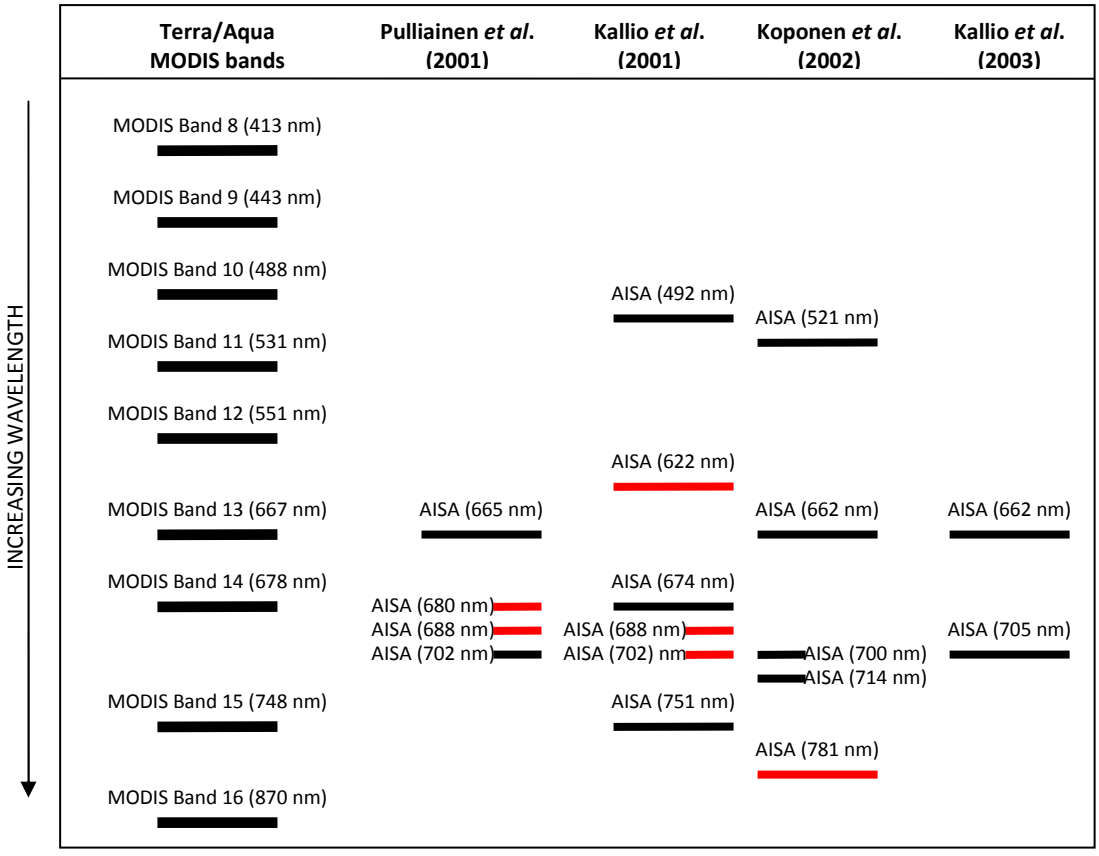

Figure 4-9: AISA band centres and corresponding Terra/Aqua MODIS band centres used in approximation. In red the hyperspectral channels that approximated with the same MODIS band as another hyperspectral channel used in the same algorithm (or did not approximate any MODIS band) and therefore were not used.

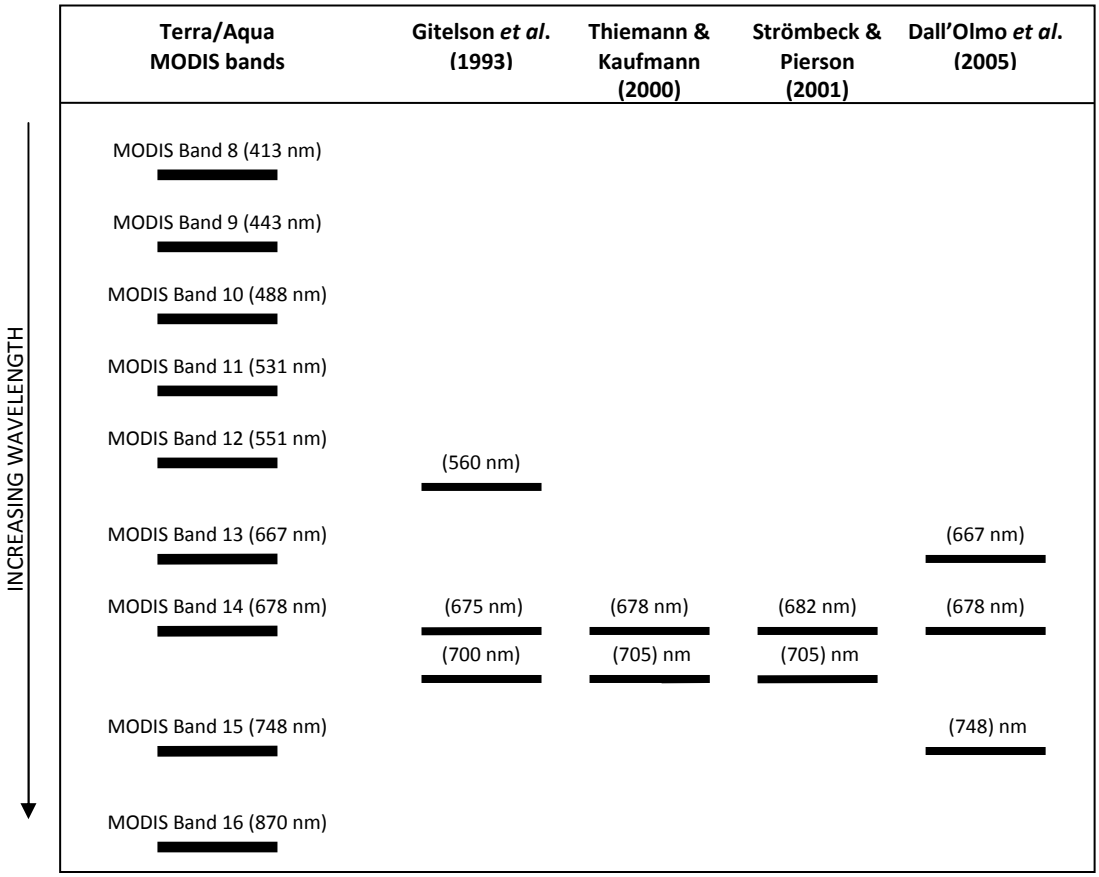

Figure 4-10: Band centres of field spectroradiometer data and corresponding Terra/Aqua MODIS band centres used in approximation.

4.8 Suitability of non-standard algorithms

Prior to the application of the non-standard algorithms the suitability of the algorithms for use with the available satellite data was assessed. First, the range of *in situ* chlorophyll *a* concentrations, SDD and temperature values for lakes Geneva and Vättern were identified using the field dataset. Then the maximum and minimum field values were used in the inverted non-standard algorithms to generate the range of required remote sensing data (henceforth referred to as '*required inputs*') for each simulated Landsat TM/ETM+, Daedalus 1268 ATM, AISA and field spectroradiometer bands in order to produce the expected range of field

measurements (as identified above). Then, 9-pixel means of the appropriate remote sensing products (e.g. L_{toa}, R_{toa}, nL_w or R_{rs}) centred on the location of the station(s) in lakes Geneva and Vättern were extracted from all images on dates when field data were available. The range of the latter (henceforth referred to as '*available inputs*') was compared to the range of the required inputs and the percentage of overlap between the two ranges was calculated for each algorithm. This procedure showed whether the available data were appropriate for the use of the non-standard algorithms and was therefore used to determine the suitability of the algorithms for further application.

In total, 27 chlorophyll *a*, seven SDD and one LST estimation algorithms were selected from the published literature and tested for their suitability. Three algorithms ('BtempB6', 'DchlB1jun' and 'DchlB3jun') proved unsuitable because the range of required data failed to overlap with any available simulated data in this project (Tables 4-11 and 4-12); hence, these algorithms were excluded. Also, it was impossible to determine the range of required inputs per band for five algorithms, so these algorithms were marked 'Pot' to show that they are potentially suitable and they were applied to the simulated satellite data anyway (Tables 4-11 and 4-12).

The rest of the non-standard algorithms required input satellite data that overlapped to some extent with the simulated remote sensing data (derived from either Terra/Aqua MODIS or both) available in this project. The percentage of this overlap for all algorithms was then calculated. Tables 4-13 and 4-14 show that for some algorithms only a small fraction of the available simulated data actually fell within the range of required inputs, meaning that the rest of the data were expected to result

in outputs outside the range of field data in lakes Geneva and Vättern. Algorithms for which the overlap percentage was less than 33% for simulated data derived from both Terra and Aqua MODIS data and both lakes were omitted from further analysis.

Table 4-11: Suitability of the non-standard LST and SDD estimation algorithms tested for LST values 0-30 °C and SDD 0-30 m respectively, using simulated Landsat TM and AISA data for lakes Geneva and Vättern (2001-04).

Algorithm code	The required inputs…		Available – Required overlap	
	.. are atmospherically corrected	.. cover a narrow range	Terra	Aqua
Temperature				
BtempB6	NO	NO	NO	NO
Secchi disk depth				
DlnSecB3jun	NO	NO	YES	YES
DSecB3jul	NO	NO	YES	YES
DlnSecB2jul	NO	NO	YES	NO
DlnSecB3jul	NO	NO	YES	YES
BSecB1	NO	NO	YES	YES
ASecFeb	NO	Pot	Pot	Pot
SlnSDTB13	NO	Pot	Pot	Pot

Table 4-12: Suitability of the non-standard chlorophyll *a* estimation algorithms tested for chlorophyll *a* concentrations 0-300 µg L^{-1} using simulated Landsat TM, Daedaulus 1268 ATM, AISA and field spectroscopy data for lakes Geneva and Vättern (2001-04).

Algorithm code	The required inputs…		Available – Required overlap	
	.. are atmospherically corrected	.. cover a narrow range	Terra	Aqua
DchlB1jun	NO	YES	NO	NO
DchlB2jun	NO	YES	YES	NO
DchlB3jun	NO	YES	NO	NO
DlnB2jun	NO	NO	YES	NO
DlnB3jun	NO	NO	YES	YES
DchlB2jul	NO	YES	YES	NO
DchlB3jul	NO	YES	YES	YES
DlnB2jul	NO	NO	YES	NO
DlnB3jul	NO	NO	YES	YES
BchlB123	NO	Pot	Pot	Pot
AchlaJuly	NO	Pot	Pot	Pot
AchlaDec	NO	Pot	Pot	Pot
PchlAug	NO	NO	YES	YES
Kalchl01	NO	NO	YES	YES
Kalchl02	NO	NO	YES	YES
HchlB13	NO	NO	YES	YES
HchlB35	NO	NO	YES	YES
GeochlB32lo	NO	NO	YES	YES
GeochlB3lo	NO	NO	YES	NO
GeochlB32hi	NO	NO	YES	NO
GeochlB3hi	NO	NO	YES	NO
Gitchl01	NO	NO	YES	YES
Gitchl02	NO	NO	YES	YES
Thiemchla	NO	NO	YES	YES
Strömchla	NO	NO	YES	YES
Dallchl01	YES	NO	YES	YES
Dallchl02	YES	NO	YES	YES

Table 4-13: Required range of inputs for each SDD estimation algorithm to estimate SDD values between 0-30 m, and percentage (%) of available simulated Landsat TM data that fall within that range for lakes Geneva and Vättern (2001-04).

Algorithm code	Required range of inputs*	% of available R/S data that fall within the required range						Suitable
		Terra MODIS			Aqua MODIS			
		Gen	Vät	Both	Gen	Vät	Both	
DlnSecB3jun	22 – 38	8	0	**6**	0	50	**22**	NO
DSecB3jul	-32 – 21	92	100	**94**	100	50	**82**	YES
DlnSecB2jul	18 – 36	67	100	**75**	0	0	**0**	YES
DlnSecB3jul	14 – 29	33	25	**31**	14	50	**27**	NO
BSecB1	-329 – 72	100	100	**100**	100	100	**100**	YES
ASecFeb	(n/a)	(n/a)	(n/a)	**(n/a)**	(n/a)	(n/a)	**(n/a)**	Pot
SlnSDTB13	(n/a)	(n/a)	(n/a)	**(n/a)**	(n/a)	(n/a)	**(n/a)**	Pot

* For both lakes (L_{toa}, R_{toa}, nL_w or R_{rs} according to the algorithm specifications)

[+] The algorithm uses band ratios

Table 4-14: Required range of inputs for each algorithm to estimate chlorophyll *a* concentrations 0-300 µg L^{-1} and percentage (%) of available simulated Landsat TM, Daedaulus 1268 ATM, AISA and field spectroscopy data that fall within that range for lakes Geneva and Vättern (2001-04).

Algorithm code	Required range of inputs*	% of available R/S data that fall within the required range						Suitable
		Terra MODIS			Aqua MODIS			
		Gen	Vät	Both	Gen	Vät	Both	
DchlB2jun	33 – 40	33	0	**25**	0	0	**0**	NO
DlnB2jun	25 – 37	50	100	**63**	0	0	**0**	YES
DlnB3jun	19 – 32	8	0	**6**	0	50	**18**	NO
DchlB2jul	23 – 29	33	50	**38**	0	0	**0**	Pot
DchlB3jul	18-24	8	0	**6**	14	25	**18**	NO
DlnB2jul	16 – 28	42	25	**38**	0	0	**0**	Pot
DlnB3jul	11 – 22	75	100	**82**	71	50	**63**	YES
BchlB123	(n/a)	(n/a)	(n/a)	**(n/a)**	(n/a)	(n/a)	**(n/a)**	Pot
AchlaJuly	(n/a)	(n/a)	(n/a)	**(n/a)**	(n/a)	(n/a)	**(n/a)**	Pot
AchlaDec	(n/a)	(n/a)	(n/a)	**(n/a)**	(n/a)	(n/a)	**(n/a)**	Pot
PchlAug+	0.655 – 3.506	50	100	**63**	44	100	**62**	YES
Kalchl01+	0.633 – 3.398	67	100	**75**	78	100	**85**	YES
Kalchl02+	0.688 – 3.364	25	50	**31**	22	75	**38**	YES
HchlB13+	-62.256 – 1.611	8	0	**6**	100	100	**100**	YES
HchlB35+	1.083 – 44.134	100	100	**100**	14	0	**11**	YES
GeochlB32lo+	0.426 – 18.304	100	100	**100**	43	0	**33**	YES
GeochlB3lo	3 – 211	100	100	**100**	0	0	**0**	YES
GeochlB32hi+	0.485 – 5.535	100	100	**100**	0	0	**0**	YES
GeochlB3hi	6 – 49	100	100	**100**	0	0	**0**	YES
Gitchl01+	0 – 1.716	100	100	**100**	100	100	**100**	YES
Gitchl02+	0 – 4.144	100	100	**100**	100	100	**100**	YES
Thiemchla+	0.719 – 0.923	100	100	**100**	100	100	**100**	YES
Strömchla+	0.81 – 3.09	60	100	**70**	43	100	**63**	YES
Dallchl01	0 – 2.046	100	100	**100**	100	(n/a)	**100**	YES
Dallchl02	0 – 1.947	100	100	**100**	100	(n/a)	**100**	YES

* For both lakes (L_{toa}, R_{toa}, nL_w or R_{rs} according to the algorithm specifications)

+ The algorithm uses band ratios

An illustration of the above results is presented below, by using as an example an unsuitable algorithm (Figure 4-11), a potentially suitable (Figure 4-12), and two suitable algorithms (Figure 4-13). The four graphs present the range of required satellite data in order to produce a chlorophyll *a* concentration between 0-300 μg L^{-1}. They also present the range of available satellite data in this project and indicate the degree of overlap with the required data.

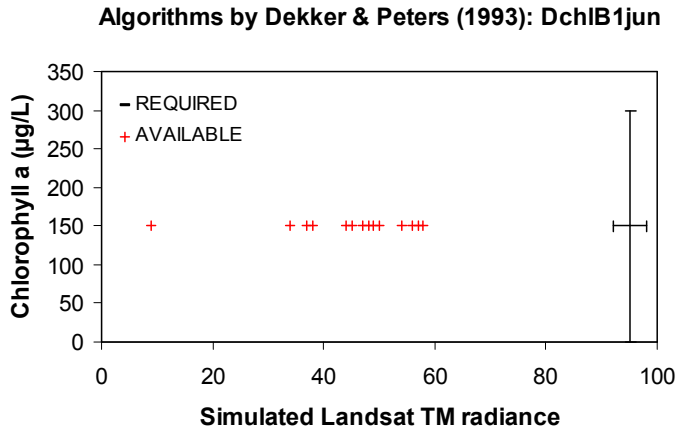

Figure 4-11: The 'DchlB1jun' algorithm exhibited 0% overlap between the 'available' and 'required' satellite data and was considered unsuitable.

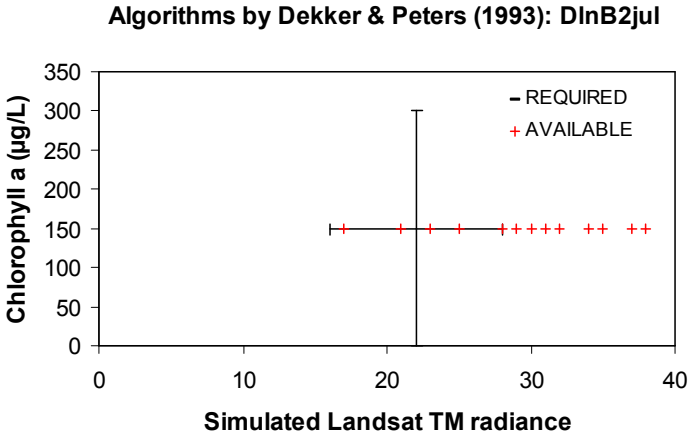

Figure 4-12: The 'DlnB2jul' algorithm exhibited 38% overlap between the 'available' and 'required' satellite data and was considered potentially suitable.

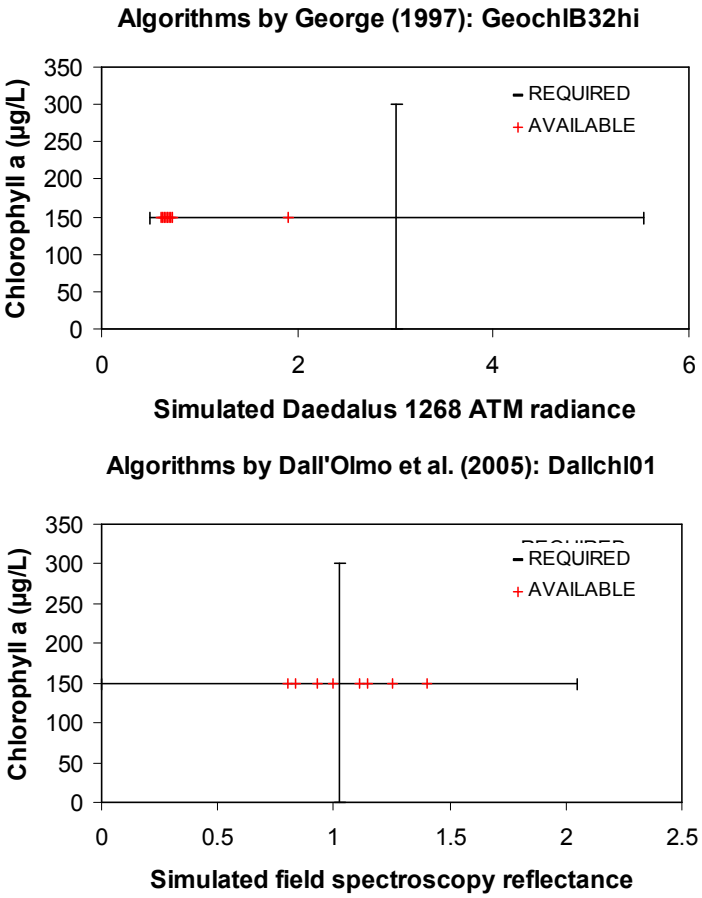

Figure 4-13: The 'GeochlB32hi' and 'Dallchl01' algorithms exhibited 100% overlap between the 'available' and 'required' satellite data and were considered suitable.

In conclusion, five non-standard algorithms exhibited very low percentages of overlap and were therefore considered unsuitable. Twenty algorithms exhibited very high percentages of overlap for either Terra MODIS-derived simulated data, Aqua MODIS-derived simulated data or both. Two algorithms ('DchlB2jul' and 'DlnB2jul') exhibited 38% overlap for the Terra MODIS-derived simulated data but 0% overlap for the Aqua MODIS-derived simulated data and they were marked as potentially suitable ('Pot') and were included in further analysis. Including the five algorithms that could not be tested and the one that is potentially suitable, 27 non-

standard water quality estimation algorithms were applied to the Terra/Aqua MODIS-derived simulated data to estimate chlorophyll *a* and SDD.

4.9 Algorithm accuracy assessment

Following the application of the algorithms, the outputs were checked to ensure that the algorithms did not produce spurious results, such as negative or extreme values (i.e. extremely high or low values in respect to the expected temperature, SDD and chlorophyll *a* ranges for each season) (Dekker & Peters, 1993). The presence of extreme values within the data may affect the outputs of statistical tests (Kinnear & Gray, 2008) and in some cases need to be removed before statistical analysis. In order to identify extreme values, the *z*-scores for both field and satellite datasets were calculated by subtracting the dataset mean from each individual dataset value and then dividing the difference by the dataset standard deviation (Kinnear & Gray, 2008). This calculation derives a dimensionless score, the *z*-score, which indicates how many standard deviations a value is above or below the mean (Wheeler *et al*., 2004). All values that laid more than three standard deviations above or below the mean were identified as extremes (Wheeler *et al*., 2004).

In addition, all field and satellite datasets were tested for normality. In the parametric statistical tests used in this project normality is an essential prerequisite and therefore, was tested in advance. The Kolmogorov-Smirnov (K-S) test was performed to test the datasets for normality of distribution. The K-S test is a common approach to test the goodness-of-fit of a dataset. It essentially compares the cumulative probabilities of observations in the sample under investigation with the cumulative probabilities of the same values in a specified theoretical distribution

(e.g. normal, Poisson, *etc*.) (Kinnear & Gray, 2008). In the case where datasets were not normally distributed, parametric tests were omitted and the results of non-parametric tests were considered instead or logarithmic transformations were applied to the data as necessary (Kinnear & Gray, 2008).

Accuracy assessment and test of performance for all algorithms was then performed. During this step, lists of coinciding field data and remotely sensed estimates of the three water quality parameters were produced for each lake and year. The remotely sensed data were averaged values of the parameters calculated from a 9-pixel squared grid centred around the pixel where the sampling station was located to avoid issues of geometric distortion and consequent imprecise determination of the location of sampling points in the images. The assumption was made that a point measurement from the sampling station was representative of the average value of the parameter studied for a 9 km^2 area containing the sample (Lavender *et al*., 2004), but clearly this would depend upon the intrinsic scale of variation of the parameter under consideration. In fact, Kloiber and colleagues (2002a) used a 9-pixel average as a minimum and showed that the accuracy of water quality estimations in 20 lakes significantly improved when the number of pixels (used for the computation of the average) increased from one to nine. Baban (1993) similarly found that the use of a 3 x 3 pixel average when comparing Landsat TM data to field measurements was the optimum, as opposed to a smaller or larger grid, because it reduced noise in the data or biased pixel values.

The relationship between estimated and observed water quality parameters was assessed using correlation analysis. The product-moment (Pearson's) correlation

coefficient (r) was used, which assumes that (a) the data are measured on interval or ratio scales (such as temperature, SDD and chlorophyll *a*), (b) the two variables correlated come from a normal distribution (Wheeler *et al*., 2006), and (c) each of the samples in each dataset are independent to the rest in the same set (Clark-Carter, 2004). Pearson's correlation coefficient tests the ability of the dependant variable to vary according to the variations observed in the independent variable. However, in cases where the datasets were not normally distributed or were relatively small and due to the fact that correlation coefficients are influenced by sample size (n), non-parametric Spearman's rho correlation coefficient (ρ) was also performed (Wheeler *et al*., 2006). Spearman's rho tests the ability of the dependant to rank the variables in the same order as the independent variable. Since there are no established rules about what makes a sample size small, both correlation coefficients were computed for all datasets with sample sizes between six and thirty for comparison. For datasets with n less than six only non-parametric tests were applied. For datasets with n greater than thirty the choice of test depended upon normality.

Three statistical terms were calculated for each water quality estimation algorithm that produced promising results to test its performance; namely, the coefficient of determination (R^2), the root mean square error (RMSE) and the systematic error (bias) of prediction. The RMSE is a measure of accuracy (Atkinson & Foody, 2002) and it was calculated as shown below:

$$\text{RMSE} = \sqrt{\frac{1}{n}\sum_{i=1}^{n}\left(x[pred]_i - x[true]_i\right)^2}$$

where RMSE = root mean square error of prediction; n = number of observations (sample size); $x[pred]_i$ = predicted value of observation i; and $x[true]_i$ = true value of observation i.

Bias is an expectation of over- or under-estimation and a measure of the systematic errors associated with the estimation (Atkinson & Foody, 2002). Bias was calculated according to the following equation, which is essentially the mean error of the estimation:

$$\text{bias} = \frac{1}{n}\sum_{i=1}^{n}\left(x[pred]_i - x[true]_i\right)$$

The significance of all statistical tests was calculated at the 99% (0.01) level of significance (2-tailed), unless otherwise stated.

4.9.1 Selection of sites for the algorithm accuracy assessment

Four lakes were chosen for the algorithm accuracy assessment. Satellite data from the rest of the study sites were used to demonstrate the potential of remote sensing by applying to them only the algorithms that performed best (Chapter 6).

NOAA AVHRR images of lakes Geneva, Balaton and Vättern were used for the accuracy assessment of MCSST and NLSST algorithms in the study period (1993-96 and 2001-04). Terra/Aqua MODIS scenes of lakes Geneva, Balaton, Vättern and Vänern were used in the years 2001-04 to assess the accuracy of all standard and non-standard algorithms for the estimation of all three water quality parameters. The selection of these four lakes was based on the fact that (a) they represent three major

groups of lakes (Central European, Hungarian and Finnish) at different geographical areas, and (b) their characteristics cover the entire range of mixing and eutrophication conditions; Lake Geneva is monomictic and mesotrophic, Lake Balaton is polymictic and eutrophic and lakes Vättern and Vänern are dimictic and oligotrophic. Also, they all have large enough surface areas to allow for adequate numbers of unmixed water pixels after the removal of mixed land-water pixels around the perimeter of the water bodies.

In total, 87 NOAA AVHRR images were used for the accuracy assessment of the MCSST and NLSST algorithms; 20 Terra MODIS and 24 Aqua MODIS Level 2 images were used for the accuracy assessment of the MODIS SST and OC3 algorithms; 28 Terra/Aqua MODIS Level 1B and 28 Terra/Aqua MODIS Level 2 images were used for the accuracy assessment of the non-standard algorithms (Table 4-15).

Table 4-15: Number of satellite images used during the accuracy assessment of existing algorithms.

Accuracy assessment of:	NOAA AVHRR	Terra MODIS		Aqua MODIS	
		Level 1B	Level 2	Level 1B	Level 2
NOAA AVHRR MCSST and NLSST	87	0	0	0	0
Terra/Aqua MODIS SST and OC3	0	0	20	0	24
Non-standard algorithms	0	14	14	14	14

4.9.1.1 Balaton

In 2001-04, 34 NOAA AVHRR images were available that matched the sampling dates and were cloud-free above at least one of the four stations (Figure 4-14A). As a result, a total of 110 pairs of field and satellite estimations were available for the accuracy assessment process. There were no field data available in 1993-96.

4.9.1.2 Geneva

In 1993-96 and 2001-04 a total of 58 NOAA AVHRR images were available that matched the sampling dates and were cloud-free above the sampling station (Figure 4-14B). As a result, 58 pairs of field and satellite estimations were available for the accuracy assessment process.

In 2001-2004 37 Level 2 Terra/Aqua MODIS scenes coincided with field temperature data and 25 Level 2 Terra/Aqua MODIS images coincided with field chlorophyll *a* data on the exact dates and were used for the accuracy assessment of the standard SST and OC3 algorithms respectively (Figure 4-15A). In the same study period, 21 Level 1-b Terra/Aqua MODIS scenes coincided with field temperature and chlorophyll *a* data on the exact dates and were used for the accuracy assessment of the non-standard algorithms (Figure 4-16A).

(A)

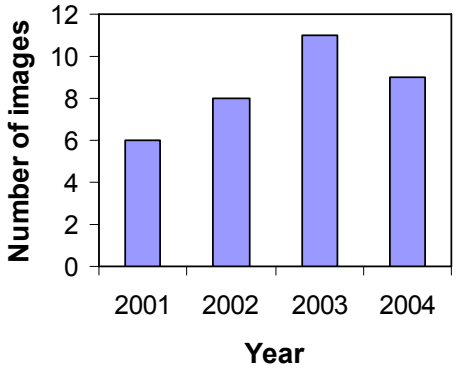

(B)

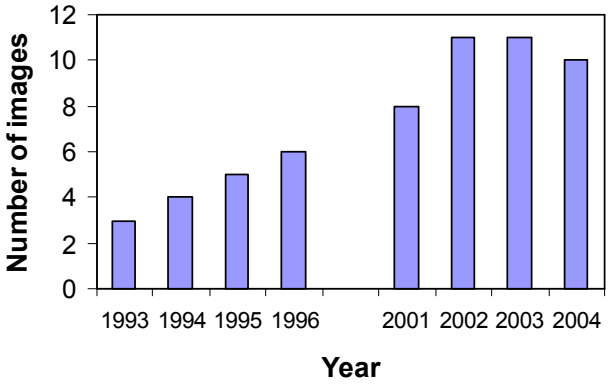

(C)

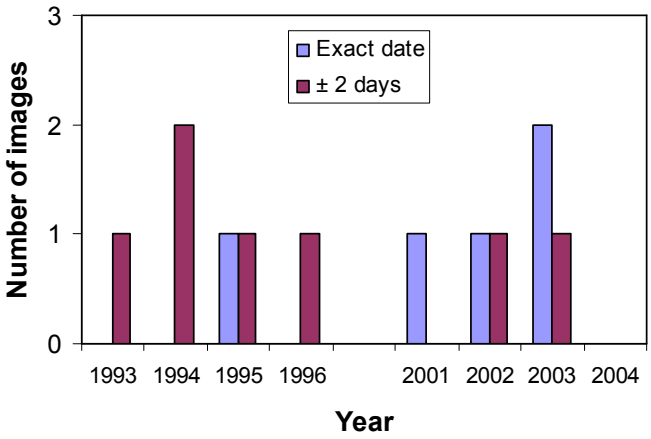

Figure 4-14: Number of cloud-free NOAA AVHRR images that coincided with field data in (A) Lake Balaton (2001-04), (B) Lake Geneva (1993-96 and 2001-04) and (C) Lake Vättern (1993-96 and 2001-04).

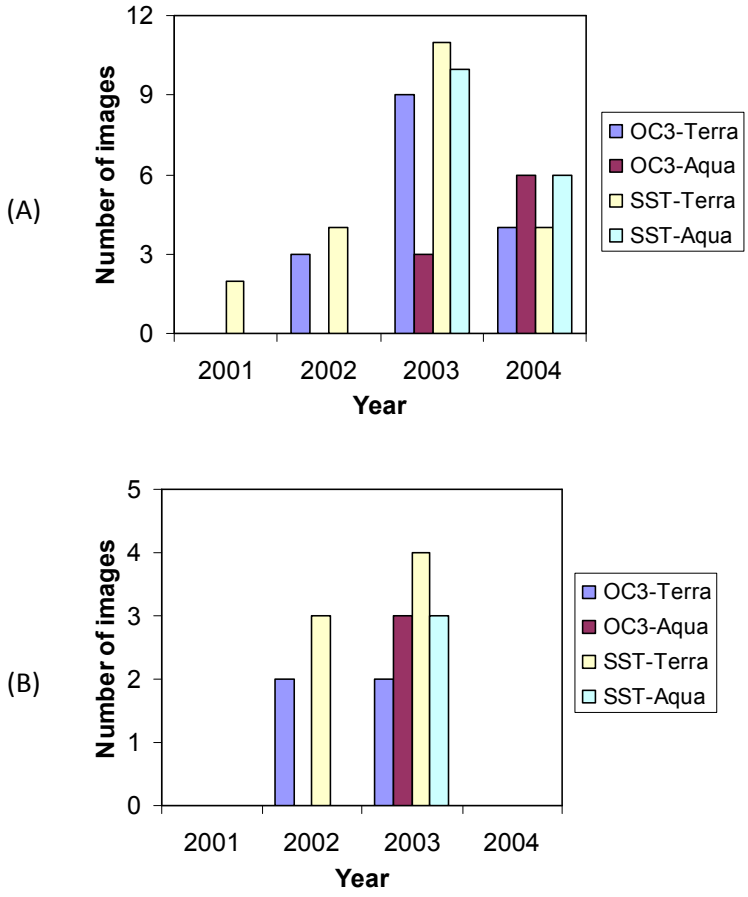

Figure 4-15: Number of cloud-free Terra/Aqua MODIS Level 2 images that coincided with field LST and chlorophyll *a* data in (A) Lake Geneva and (B) Lake Vättern in 2001-04.

4.9.1.3 Vättern

In 1993-96 and 2001-04 there were a total of five NOAA AVHRR images available that matched the sampling dates and were cloud-free above at least one of the two stations. Because of the smaller number of available images, seven more scenes acquired ± 2 days of the field sampling date were also used to increase the sample size. For the latter, the assumption was made that the variability in temperature was not significant within a period of 1-2 days (Kloiber *et al*., 2002a). As a result, a total

of 17 pairs of field and satellite estimations were available for the accuracy assessment process (Figure 4-14C).

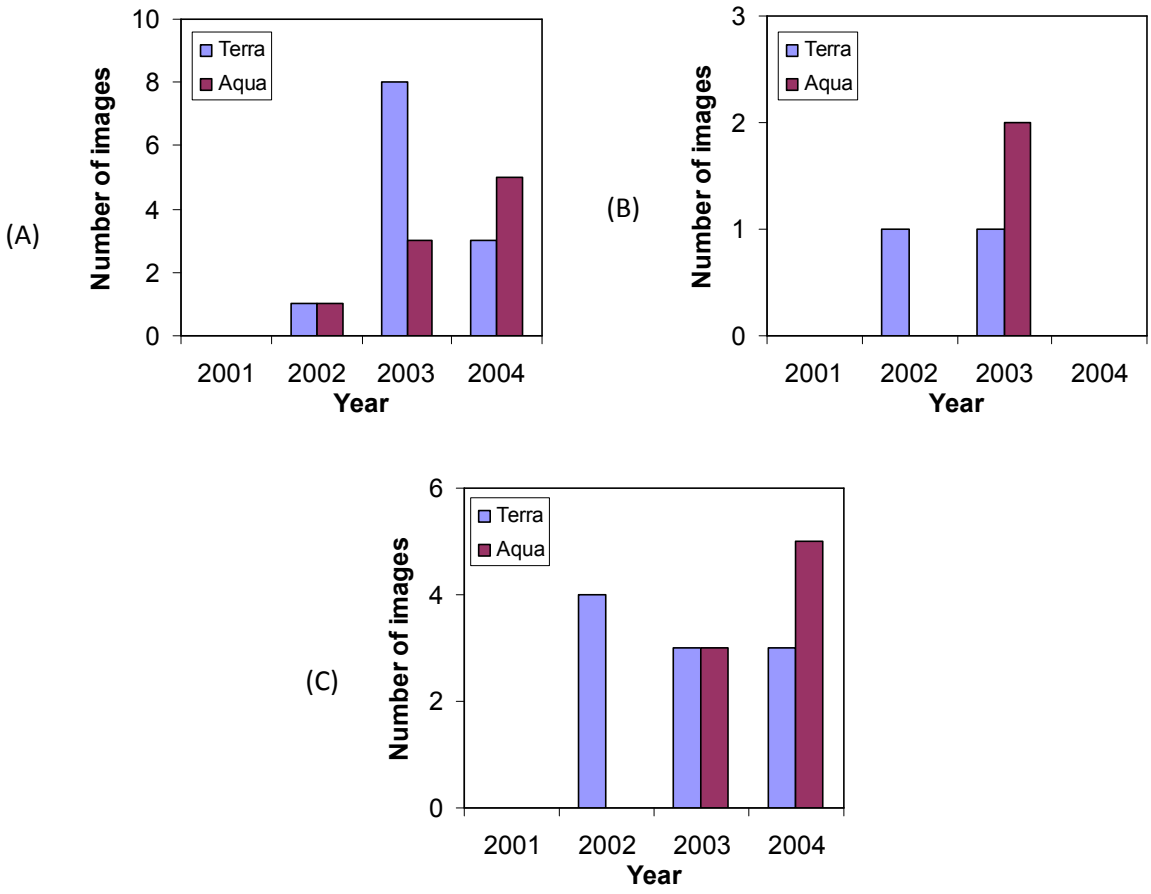

Figure 4-16: Number of cloud-free Terra/Aqua MODIS Level 1B images that coincided with field LST and chlorophyll *a* data in (A) Lake Geneva, (B) Lake Vättern and (C) Lake Vänern in 2001-04.

In 2001-04 ten Level 2 Terra/Aqua MODIS scenes coincided with field temperature data and seven Level 2 Terra/Aqua MODIS images coincided with field chlorophyll *a* data on the exact dates and were used for the accuracy assessment of the standard SST and OC3 algorithms respectively (Figure 4-15B). In the same study period, four

Level 1-b Terra/Aqua MODIS scenes coincided with field temperature and chlorophyll *a* data on the exact dates and were used for the accuracy assessment of the non-standard algorithms (Figure 4-16B).

Figure 4-16B presents a very good example of the limitations of remote sensing. In 2001 Aqua MODIS data were unavailable. In 2002 satellite data from only the second half of the year were available, but all dates coinciding with field data were cloudy. In 2003 most Aqua MODIS scenes that coincided with field data were cloud-free and used in the project. In 2004 Aqua MODIS data were available, but field data were not. However, when there is no need to match satellite overpasses to field sampling dates for accuracy assessment purposes, the completely cloud-free days in Lake Vättern are approximately 60 (Figure 4-1), which suggests an almost weekly coverage of the lake.

4.9.1.4 Vänern

Satellite data from Lake Vänern were unavailable for 2001. However, 18 scenes, where at least one of the stations was cloud-free, were available in the remaining years (2002-04) adding up to 25 pairs of corresponding field and satellite data that were used for further analysis (Figure 4-16C).

4.10 Summary

This chapter has presented the procedure followed for the selection, pre-processing and acquisition of appropriate NOAA AVHRR and Terra/Aqua MODIS data. It has also listed four operationally used (standard) algorithms and 47 algorithms from the published literature (non-standard) with potential for estimating lake surface

temperature, chlorophyll *a* and SDD. After a suitability test, the non-standard algorithms were reduced to 27. The preparation of the satellite data for the application of all suitable algorithms was also presented and in the end 31 standard and non-standard algorithms were applied to the satellite data and their accuracy assessment is discussed in the following chapter.

Chapter V.

ALGORITHM ACCURACY ASSESSMENT

5.1 Introduction

In this chapter the best performing algorithms for estimating lake water quality parameters across European large lake systems were identified. Even though many algorithms have been proposed in the published literature their spatial and temporal transferability has not been tested. In this chapter NOAA AVHRR data for lakes Geneva, Balaton and Vättern from 1993-96 and 2001-04, and Terra/Aqua MODIS data for lakes Geneva, Balaton, Vänern and Vättern from 2001-04 were used to assess the accuracy of existing water quality estimation algorithms. The lakes are representative of three major groups with varying trophic levels, and different mixing regimes and other abiotic characteristics (e.g. morphology, latitude, altitude, *etc*.). All algorithms were tested for each category separately and then for all combined to test for transferability in various sites and the level of accuracy of the parameters estimates in each and all of the three trophic level categories. In addition, regression analysis was performed combining field and Terra/Aqua MODIS data.

5.2 Temperature

Temperature was estimated using two standard algorithms for NOAA AVHRR and one standard algorithm for Terra/Aqua MODIS data.

5.2.1 Accuracy of the NOAA AVHRR MCSST and NLSST algorithms

The field LST data from lakes Balaton, Geneva and Vättern were strongly correlated with both NOAA AVHRR MCSST and NLSST estimates on corresponding dates (Table 5-1; Figure 5-1). Field LST data from Lake Geneva showed the strongest correlation with satellite estimates, followed closely by data from Lake Vättern, while Lake Balaton was ranked third. These results show that both MCSST and NLSST algorithms have a strong potential in lakes with different characteristics. In fact, field data from all three lakes (combined into a common dataset) were strongly correlated with corresponding NOAA AVHRR MCSST and NLSST estimates for all available years (Table 5-1; Figure 5-2).

Table 5-1: Correlation of field LST data with the NOAA AVHRR MCSST and NLSST estimates in lakes Balaton, Geneva and Vättern in 1993-96 and 2001-04.

Lake	Sample size (n)	Pearson's coefficient (r)		Spearman's rho (ρ)	
		MCSST	NLSST	MCSST	NLSST
Balaton	110	0.731(**)	0.725(**)	-	-
Geneva	58	0.952(**)	0.952(**)	-	-
Vättern	17	0.948(**)	0.921(**)	0.931(**)	0.912(**)
Combined data	185	-	-	0.891(**)	0.890(**)

(**) Result is significant at the 0.01 level (2-tailed)

For the combined dataset, the MCSST algorithm had a slightly larger bias (1.22 ºC) than the NLSST algorithm (-0.89 ºC). The accuracy (measured with the root mean square error, RMSE) of the MCSST algorithm was 2.29 °C and the accuracy of the NLSST algorithm was 2.22 °C.

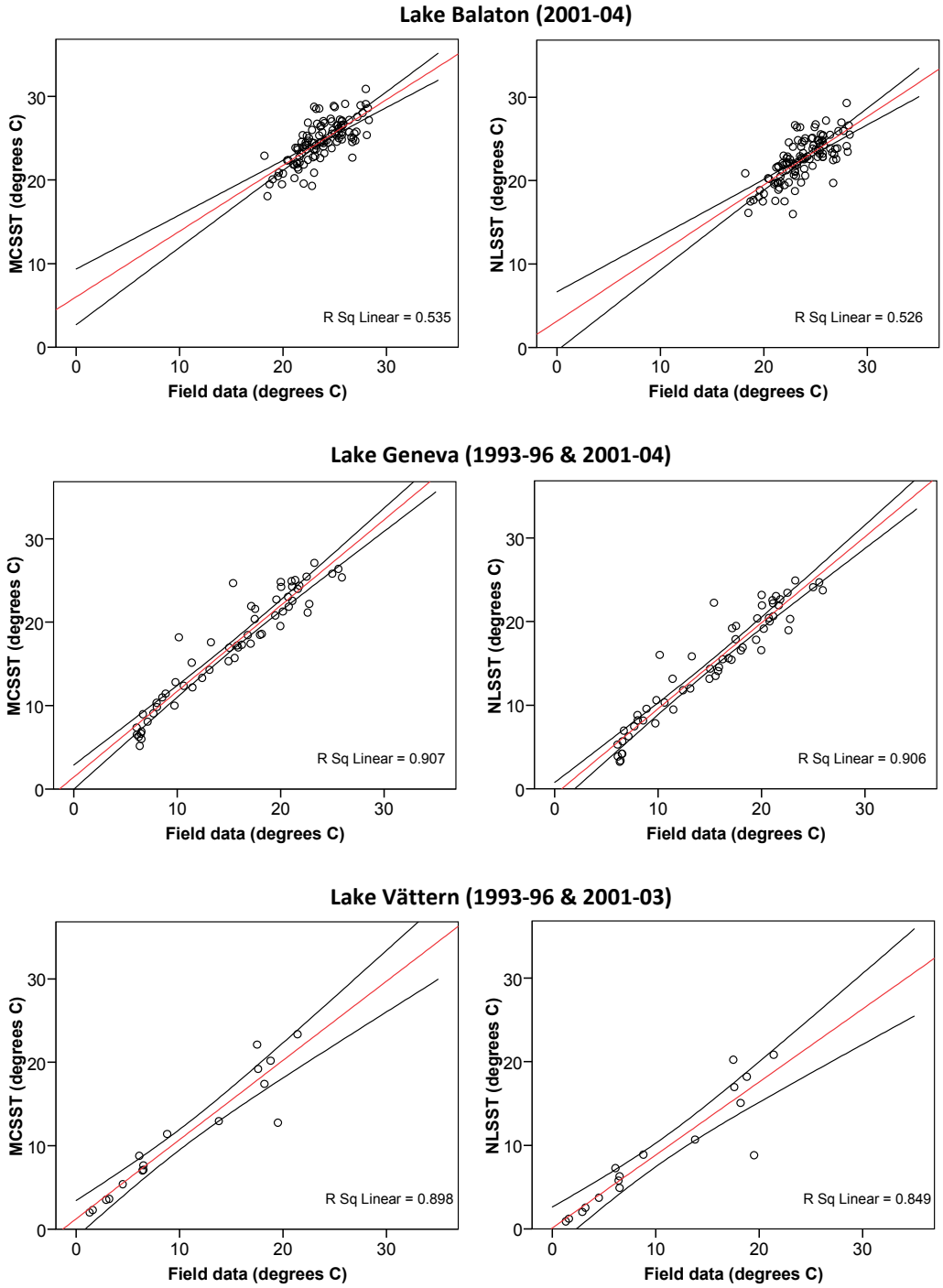

Figure 5-1: Scatter-plot between the field LST data and the NOAA AVHRR MCSST and NLSST estimates in Lakes Balaton (top), Geneva (middle) and Vättern (bottom) using data from 1993-96 and 2001-04. The red lines were determined by linear regression. The 95% confidence intervals on the mean (black lines) and the coefficient of determination (R^2) are also shown.

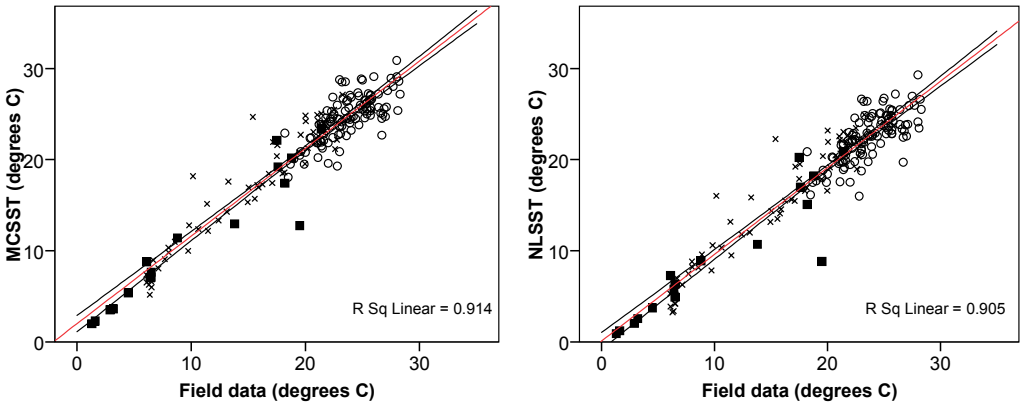

Figure 5-2: (Left) Scatter-plot between the field LST data and the NOAA AVHRR MCSST and NLSST estimates in all three lakes combined: Balaton (white circles), Geneva (crosses) and Vättern (black squares). The red lines were determined by linear regression. The 95% confidence intervals on the mean (black lines) and the coefficient of determination (R^2) are also shown.

The above results illustrate that both NOAA AVHRR MCSST and NLSST algorithms performed with high accuracy in three individual lakes and when all three lakes were combined. In conclusion, they are both suitable for the estimation of LST in large European lakes with various ecological characteristics and across different geographical areas. The latter agrees with the findings by Oesch *et al*. (2005, 2008).

In all cases, the NOAA AVHRR MCSST estimates showed equal or slightly stronger correlation with the field LST data than the NLSST estimates. In order to test the significance of differences between the two algorithms, related-samples T-tests were performed for each lake (Table 5-2). The related-samples T-tests showed that the NOAA AVHRR MCSST estimates in all three lakes were significantly different from the corresponding NOAA AVHRR NLSST estimates, with the MCSST algorithm producing higher values (by 2.11 °C in average) than the NLSST

algorithm. Oesch *et al*. (2005) suggest that the difference between the two algorithms might be related to the fact that they were developed for different regions, with the NLSST algorithm being more suitable for regions of high water vapour. In another study the NLSST was found to improve the bias compared to the MCSST, but increase the standard deviation of satellite-field data difference (Li *et al*., 2001). Due to the above issues, the NOAA AVHRR MCSST algorithm was chosen instead of NLSST for use with the rest of the data in this project.

Table 5-2: Results of related-samples T-test between the NOAA AVHRR MCSST and NLSST estimates in lakes Balaton, Geneva and Vättern in 1993-96 and 2001-04.

Lake	Descriptive statistics				*df*	*t*-statistic	p-value
	Mean (M)		Standard Deviation (SD)				
	MCSST	NLSST	MCSST	NLSST			
Balaton	24.66	22.53	2.51	2.64	109	52.914	0.000
Geneva	17.19	15.06	6.54	6.54	57	37.893	0.000
Vättern	10.98	9.08	7.17	6.78	16	10.692	0.000

The NOAA AVHRR MCSST algorithm was then calibrated using data that were not employed during the assessment of its performance. Twenty-two dates from Lake Oulujärvi were used that coincided with field data measurements. The algorithm used for the calibration was the linear regression equation between field data and AVHRR MCSST estimates (Graph 5-2, left):

$$\text{MCSSTcal [°C]} = 0.951\ (\text{MCSST}) - 0.183 \qquad (5.4)$$

The calibrated algorithm had a bias = 0.2 °C and a RMSE = 1.64 °C (Figure 5-3), which are less than those of the original MCSST.

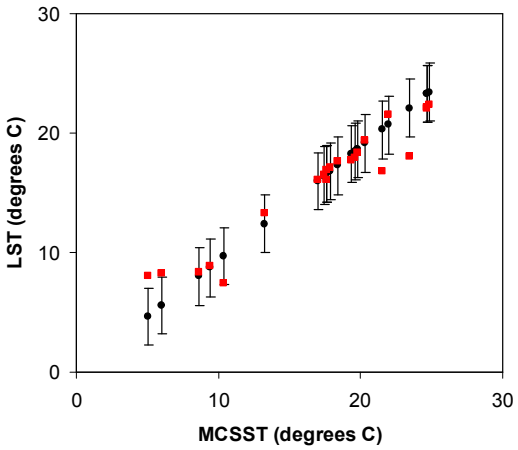

Figure 5-3: Surface temperature (black dots) estimated in Lake Oulujärvi using the MCSSTcal algorithm with the 95% confidence intervals of the mean also plotted (whiskers). The true LST field measurements (red squares) are also presented for comparison.

5.2.2 Accuracy of the Terra/Aqua MODIS SST algorithm

In lakes Geneva and Vättern the 2001-04 field LST data exhibited an extremely strong positive correlation with the Terra/Aqua MODIS SST estimates (Table 5-3; Figure 5-4). The results for the combined dataset showed there was also a very strong positive correlation between the field LST measurements from both lakes and the corresponding Terra/Aqua MODIS SST estimates (Table 5-3; Figure 5-5). The bias of the Terra/Aqua MODIS SST algorithm for the combined dataset was -0.71 ºC and its accuracy (RMSE) was 1.46 ºC, which is slightly higher than the accuracy of the NOAA AVHRR MCSSTcal algorithm. However, a smaller sample size was used for the accuracy assessment of the Terra/Aqua MODIS SST algorithm and data from eutrophic lakes were unavailable.

The above results show that the Terra/Aqua MODIS SST algorithm can produce accurate LST estimates in lakes with various characteristics and across different geographical areas. In conclusion, the algorithm was considered highly appropriate for the estimation of LST in large European lakes, which was also suggested by Oesch *et al*. (2005).

Table 5-3: Correlation of the field LST data with the corresponding Terra/Aqua MODIS SST estimations in 2001-04 in lakes Geneva and Vättern.

Algorithm	SST		
	Sample size (*n*)	**Pearson's (*r*)**	**Spearman's rho (*ρ*)**
Geneva	28	0.987(**)	0.968(**)
Vattern	12	0.992(**)	0.991(**)
Both lakes	40	0.990(**)	-

(**) Result is significant at the 0.01 level (2-tailed)

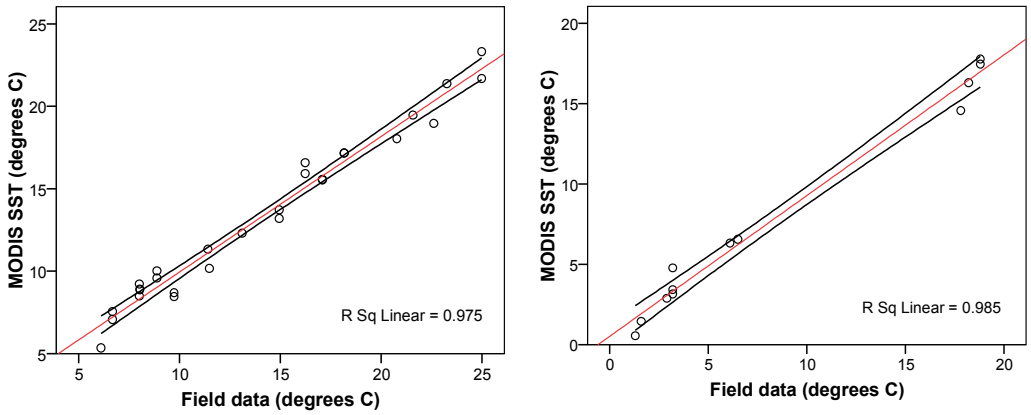

Figure 5-4: Scatter-plot between the LST field data and the Terra/Aqua MODIS SST estimates in lakes Geneva (left) and Vättern (right) in the years 2001-04. The red line was determined by linear regression. The 95% confidence internal (black lines) and the coefficient of determination (R^2) are also shown.

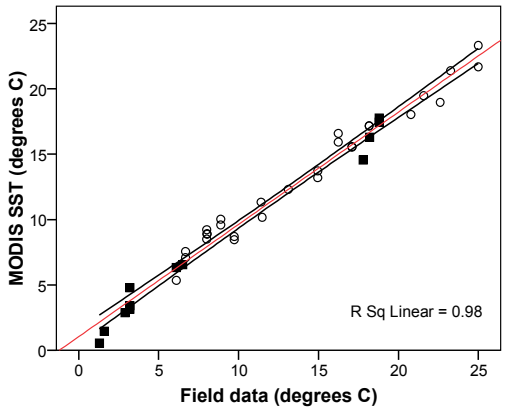

Figure 5-5: Scatter-plot between the field LST data and the Terra/Aqua MODIS SST estimates in lakes Geneva (white circles) and Vättern (black squares) combined in the years 2001-04. The red line was determined by linear regression. The 95% confidence internal (black lines) and the coefficient of determination (R^2) are also shown.

5.3 Chlorophyll *a*

Chlorophyll *a* was estimated using the Terra/Aqua MODIS OC3 algorithm in an oligotrophic (Vättern) and a mesotrophic (Geneva) lake. There were also eighteen non-standard algorithms from the published literature that were tested using data from two oligotrophic (Vänern, Vättern), one mesotrophic (Geneva) and one eutrophic (Balaton) lake.

5.3.1 Accuracy of the Terra/Aqua MODIS OC3 algorithm

The Aqua MODIS OC3 estimates in Lake Geneva contained two extreme values that were more than three standard deviations above the mean. These two values were probably caused by noise within the Aqua MODIS wavebands used on the specific dates. As a result they were removed and the reduced datasets were then used for analysis. In addition, the OC3 estimates in Lake Geneva were not normally

distributed. The same was true for the Terra/Aqua MODIS OC3 common dataset for both lakes Geneva and Vättern.

Table 5-4: Correlation of the 2001-04 field chlorophyll *a* data with the Terra/Aqua MODIS OC3 estimates in lakes Geneva and Vättern.

Algorithm	OC3		
	Sample size (*n*)	Pearson's (*r*)	Spearman's rho (*ρ*)
Geneva	23	-	0.118
Vattern	11	0.094	-0.032
Both lakes	34	-	0.391(*)

(*) Result is significant at the 0.05 level (2-tailed)

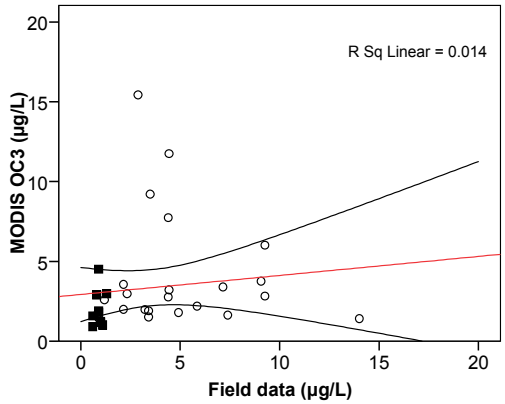

Figure 5-6: Scatter-plot between field chlorophyll *a* data and the MODIS OC3 estimates in lakes Geneva (white circles) and Vättern (black squares) combined in years 2001-04. The red line was determined by linear regression. The 95% confidence intervals (black line) and the coefficient of determination (R^2) also shown.

The field chlorophyll *a* data from lakes Geneva and Vättern were very weakly correlated with the corresponding Terra/Aqua MODS OC3 estimates (Table 5-4). The correlation improved slightly, when data from both lakes were combined for all

available years (Table 5-4; Figure 5-6). However, the correlation coefficient was still quite weak and, therefore, the Terra/Aqua MODIS OC3 algorithm was considered inappropriate for the estimation of chlorophyll *a* concentrations in lakes Geneva and Vättern.

5.3.2 Accuracy of the non-standard chlorophyll *a* estimation algorithms

In total, 22 chlorophyll *a* estimation algorithms identified from the published literature were applied to the Terra/Aqua MODIS data that were used to simulate Landsat TM, Daedaulus 1268 ATM, AISA and field spectroscopy data. Lakes Vättern and Vänern have very similar ecological characteristics and were used in a common dataset to represent oligotrophic lakes. Data from eutrophic Lake Balaton were very few ($n \leq 4$) and were only used when all four lakes were combined into a common dataset.

The outputs of each algorithm were generally coherent to each other. For some algorithms negative or unrealistically high values (>300 μg L^{-1}) appeared. However, the latter were not omitted prior to correlation analysis. In fact, the datasets of satellite estimates contained no extreme values.

Significant correlations between field data and remotely sensed estimates were exhibited in very few cases and in most cases it was noticeable how results changed depending on the sensor used (Terra MODIS or Aqua MODIS), suggesting a low degree of consistency between the two sensors when the same algorithms were applied (Tables 5-5 and 5-6). The strength of the correlations also varied between

lakes with different trophic status, suggesting that the algorithms are not transferable in lakes with different ecological characteristics (Tables 5-5, 5-6 and 5-7).

When only Terra MODIS data were used, most chlorophyll *a* estimation algorithms produced poor results (Table 5-5). No algorithm produced a significant correlation with the field data in Lake Geneva. By contrast, in lakes Vättern and Vänern three out of four algorithms proposed by Dekker and Peters (1993) performed well and the same was true for two algorithms developed by George (1997b). However, the sample size for all these datasets was rather small (n = 7). When four lakes with various characteristics were combined for Terra MODIS data, the above-mentioned algorithms performed poorly, but three other algorithms ('GeochlB32lo', 'GeochlB32hi' and 'Gitchl02') exhibited a significant correlation with field measurements.

When only Aqua MODIS data were used, the results of the non-standard chlorophyll *a* estimation algorithms were very poor in all cases for all algorithms (Table 5-6).

Finally, when the algorithm outputs for both Terra and Aqua MODIS data were combined, all but one chlorophyll *a* estimation algorithms exhibited weak correlation with the field data (Table 5-7). Only one algorithm ('Strömchla') produced promising results in lakes Vättern and Vänern.

Table 5-5: Correlation of field chlorophyll *a* data with corresponding simulated remotely sensed data (using Terra MODIS data only) for non-standard algorithms in 2001-04 in lakes Geneva, Balaton, Vättern and Vänern.

Algorithm code	Geneva			Vättern/Vänern			All four lakes		
	n	***r***	***ρ***	***n***	***r***	***ρ***	***n***	***r***	***ρ***
DlnB2jun	12	.622(*)	.063	7	**.768(*)**	**.937(**)**	19	-	.109
DchlB2jul	12	.285	.056	7	**.790(*)**	**.937(**)**	23	-	.330
DlnB2jul	12	.561	.056	7	**.792(*)**	**.937(**)**	19	-	.107
DlnB3jul	12	-	.128	7	-.003	.775(*)	19	-	-.034
BchlB123	12	.171	.231	7	-.188	.126	21	.489(*)	.401
AchlaJuly	12	.604(*)	.147	7	.387	.667	21	-	.249
AchlaDec	12	.471	.459	7	-.291	-.181	21	-.091	-.146
PchlAug	12	.260	.098	10	-.470	-.365	23	-.104	-.213
Kalchl01	12	-.260	-.098	10	-.469	-.365	23	-.105	-.213
Kalchl02	12	-.260	-.098	10	-.470	-.365	23	-.104	-.213
HchlB13	-	-	-	-	-	-	-	-	-
HchlB35	12	-.407	-.259	7	.084	-.234	21	-.198	-.095
GeochlB32lo	12	-	.203	7	-.311	-.126	23	**-**	**.620(**)**
GeochlB3lo	12	.285	.056	7	**.790(*)**	**.937(**)**	23	-	.330
GeochlB32hi	12	-	.203	7	-.313	-.126	23	**-**	**.620(**)**
GeochlB3hi	12	.285	.056	7	**.790(*)**	**.937(**)**	23	-	.330
Gitchl01	12	.607(*)	.315	10	.206	.292	22	.151	.086
Gitchl02	12	.267	.147	10	.018	.122	25	**.458(*)**	**.466(*)**
Thiemchla	12	.269	.147	10	-.494	-.365	25	-.206	-.242
Strömchla	12	.038	-.088	7	-.820(*)	-.703	22	-.236	-.273
Dallchl01	12	-	-.064	10	-.604	-.262	22	-	-.051
Dallchl02	12	-	-.064	10	-.536	-.274	22	-	-.020

n is the sample size, *r* is Pearson's coefficient and *ρ* is Spearman's rho

(**) Result is significant at the 0.01 level (2-tailed)

(*) Result is significant at the 0.05 level (2-tailed)

(-) Dataset does not follow the normal distribution or the sample size is small or unsuitable algorithm

Table 5-6: Correlation of field chlorophyll *a* data with corresponding simulated remotely sensed data (using Aqua MODIS data only) for non-standard algorithms in 2001-04 in lakes Geneva, Vättern and Vänern.

Algorithm code	Geneva			Vättern/Vänern			All three lakes		
	n	***r***	***ρ***	***n***	***r***	***ρ***	***n***	***r***	***ρ***
DlnB2jun	-	-	-	-	-	-	-	-	-
DchlB2jul	-	-	-	-	-	-	-	-	-
DlnB2jul	-	-	-	-	-	-	-	-	-
DlnB3jul	7	-.193	-.036	10	-	-.309	17	-	-.193
BchlB123	7	-.311	-.607	10	-.467	-.134	17	-.385	-.530(*)
AchlaJuly	-	-	-	-	-	-	-	-	-
AchlaDec	-	-	-	-	-	-	-	-	-
PchlAug	9	-.188	-.083	11	-.415	-.438	20	-.076	-.121
Kalchl01	9	-.188	-.083	11	-.415	-.438	20	-.076	-.121
Kalchl02	9	-.188	-.083	11	-.415	-.438	20	-.076	-.121
HchlB13	7	.509	.739	5	-.454	-.667	12	.337	.305
HchlB35	-	-	-	-	-	-	-	-	-
GeochlB32lo	7	.642	.750	5	-.550	-.600	12	.452	.308
GeochlB3lo	-	-	-	-	-	-	-	-	-
GeochlB32hi	-	-	-	-	-	-	-	-	-
GeochlB3hi	-	-	-	-	-	-	-	-	-
Gitchl01	9	-.192	-.100	11	-.382	-.627(*)	20	-	-.188
Gitchl02	9	-.159	-.100	11	-.399	-.533	20	.114	.033
Thiemchla	9	-.183	-.100	11	-.478	-.616(*)	20	-.110	-.214
Strömchla	7	-.281	-.714	10	-.523	-.758(*)	17	-.133	-.361
Dallchl01	2	-	-	6	-	-.464	8	.585	-.133
Dallchl02	2	-	-	6	-	-.406	8	.582	-.108

n is the sample size, *r* is Pearson's coefficient and *ρ* is Spearman's rho

(**) Result is significant at the 0.01 level (2-tailed)

(*) Result is significant at the 0.05 level (2-tailed)

(-) Dataset does not follow the normal distribution or the sample size is small or unsuitable algorithm

Table 5-7: Correlation of field chlorophyll *a* data with corresponding simulated remotely sensed data (using both Terra and Aqua MODIS data) for non-standard algorithms in 2001-04 in lakes Geneva, Balaton, Vättern and Vänern.

Algorithm code	Geneva			Vättern/Vänern			All four lakes		
	n	***r***	***ρ***	***n***	***r***	***ρ***	***n***	***r***	***ρ***
DlnB2jun	-	-	-	-	-	-	-	-	-
DchlB2jul	-	-	-	-	-	-	-	-	-
DlnB2jul	-	-	-	-	-	-	-	-	-
DlnB3jul	19	-	.039	17	-	-.084	36	-	-.084
BchlB123	19	.121	.281	17	-.267	-.041	38	.202	.190
AchlaJuly	-	-	-	-	-	-	-	-	-
AchlaDec	-	-	-	-	-	-	-	-	-
PchlAug	21	-.046	-.042	21	-.329	-.345	43	-	-.124
Kalchl01	21	-.046	-.042	21	-.329	-.345	43	-	-.124
Kalchl02	21	-.046	-.042	21	-.329	-.345	43	-	-.124
HchlB13	-	-	-	-	-	-	-	-	-
HchlB35	-	-	-	-	-	-	-	-	-
GeochlB32lo	19	-	-.083	12	-.025	-.074	35	-	.078
GeochlB3lo	-	-	-	-	-	-	-	-	-
GeochlB32hi	-	-	-	-	-	-	-	-	-
GeochlB3hi	-	-	-	-	-	-	-	-	-
Gitchl01	21	-.067	-.040	21	-.095	-.134	42	-	-.068
Gitchl02	21	-.037	.013	21	-.157	-.161	45	-	.293
Thiemchla	21	-.022	.013	21	-.369	-.415	45	-	-.213
Strömchla	19	-.011	-.188	17	**-.574(*)**	**-.609(**)**	39	-.142	-.240
Dallchl01	14	-	-.070	16	-.075	-.069	30	-	.181
Dallchl02	14	-	-.070	16	-.051	-.071	30	-	.209

n is the sample size, *r* is Pearson's coefficient and *ρ* is Spearman's rho

(**) Result is significant at the 0.01 level (2-tailed)

(*) Result is significant at the 0.05 level (2-tailed)

(-) Dataset does not follow the normal distribution or the sample size is small or unsuitable algorithm

Quite promising was the ‘Gitchl02’ algorithm that was developed for lakes with various characteristics and indeed its outputs were strongly correlated with field data from all four lakes when Terra MODIS data were used.

The four algorithms recommended by George (1997b) were developed specifically for low or high chlorophyll *a* concentrations. In particular, the two band ratio algorithms (‘GeochlB32lo’ and ‘GeochlB32hi’) that employ the blue and green bands were developed for less and more productive lakes respectively, but performed well with data from all four lakes ranging from oligotrophic to eutrophic when Terra MODIS data were used. The two single band algorithms (‘GeochlB3lo’ and ‘GeochlB3hi’) that employ the green band performed well in oligotrophic lakes only. Furthermore, three algorithms by Dekker and Peters (1993) that were developed for eutrophic lakes performed well in oligotrophic lakes only when Terra MODIS data were used. The same was true for the algorithm by Strömbeck and Pierson (2001) when both Terra and Aqua MODIS data were used. These results suggest that the above mentioned non-standard algorithms can be reliable in other lakes as well (apart from the ones they were developed for) and thus are potentially non site-specific.

In addition to the above, all of the non-standard algorithms were developed for specific seasons while the data used for their testing covered a wide range of months throughout the year. Specifically, the Terra MODIS data covered all months from March to November except August. The Aqua MODIS data covered all months from February to November, except May and July. This suggests that the algorithms that performed poorly are not temporally transferable, whilst this is not necessarily true for the nine promising algorithms mentioned above.

The scatter-plots between corresponding field data and the outputs of the nine promising chlorophyll *a* estimation algorithms were constructed to investigate the performance of these algorithms in more detail (Figures 5-7 and 5-8). In all cases the algorithms exhibited a high degree of scatter around the regression line, especially the algorithms 'Strömchla', 'GeochlB32lo', 'GeochlB32hi' and 'Gitchl02' (Figures 5-7F and 5-8). The 'DchlB2jul', 'DlnB2jul' and 'GeochlB3hi' algorithms produced high coefficients of determination for the linear regression ($R^2 > 0.6$), but strongly overestimated chlorophyll *a* concentrations (Figures 5-7B, C and E). The 'GeochlB3lo' algorithm was developed for oligotrophic waters and indeed showed potential in that category, but always overestimated chlorophyll *a* concentrations by a factor of 10 (Figure 5-7D). It also performed poorly when all four lakes were combined.

The 'DlnB2jun' algorithm showed potential (Figure 5-7A), but the small sample size should be taken into consideration. The same algorithm performed poorly in lakes with different trophic status and, thus, it was considered inappropriate as a transferable algorithm between sites that encompass a wide range of chlorophyll *a* concentrations. However, the algorithm showed some potential in oligotrophic lakes and should be tested further, but lack of appropriate remote sensing data in this project prohibited this specifically.

In conclusion, none of the non-standard chlorophyll *a* estimation algorithms tested with the data available in this project were able to produce highly accurate estimates of chlorophyll *a* concentrations either in separate lake categories (i.e. oligotrophic

and mesotrophic) or when all lakes were combined (oligotrophic to eutrophic) towards the investigation of a universal algorithm.

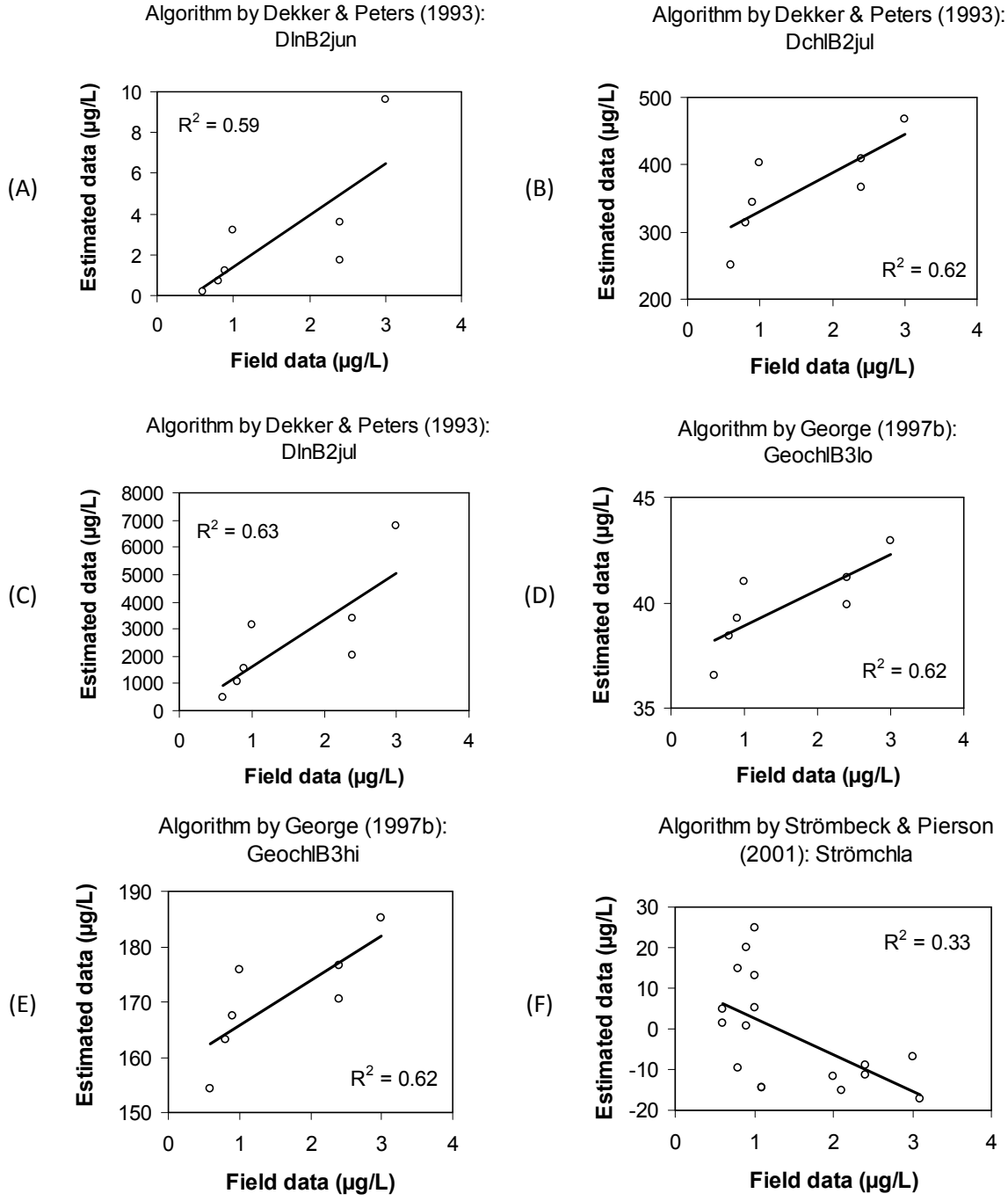

Figure 5-7: Lakes Vättern and Vänern: Scatter plots of most promising non-standard algorithms for the estimation of chlorophyll *a* using only Terra MODIS data (A-E), and both Terra and Aqua MODIS data (F).

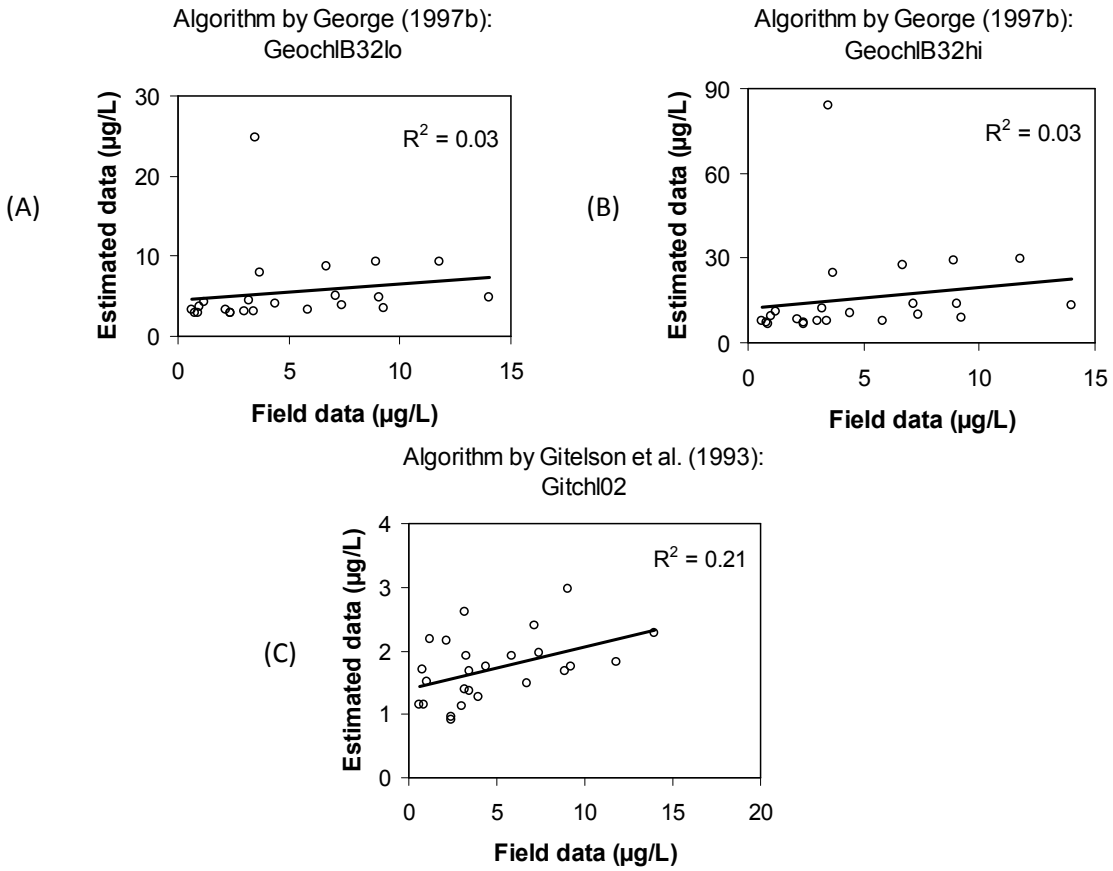

Figure 5-8: Lakes Geneva, Balaton, Vättern and Vättern: Scatter plots of most promising non-standard algorithms for the estimation of chlorophyll *a* using only Terra MODIS data.

5.4 Secchi disk depth

Five Secchi disk depth estimation non-standard algorithms were tested. In this case field data from eutrophic Lake Balaton were unavailable, so only lakes Geneva, Vättern and Vänern were used for the accuracy assessment of the algorithms.

5.4.1 Accuracy of the non-standard SDD estimation algorithms

The strength of the correlation between the field data and the outputs of the five SDD algorithms was weak in many cases. When only Terra MODIS data were used, most

algorithms exhibited promising results in Lake Geneva but only one algorithm showed strong correlation with field measurements in lakes Vättern and Vänern (Table 5-8). When all three lakes were combined all algorithm outputs exhibited weak correlation with the field data. When only Aqua MODIS data were used, no algorithm exhibited significant results in Lake Geneva and when all lakes were combined (Table 5-9). However, all four algorithms showed strong negative correlations to field measurements in lakes Vättern and Vänern. Finally, when both Terra and Aqua MODIS data were used, all algorithms performed poorly in all cases (Table 5-10).

Table 5-8: Correlation of field SDD data with corresponding simulated remotely sensed data (using Terra MODIS data only) for non-standard algorithms in 2001-04 in lakes Geneva, Vättern and Vänern.

Algorithm code	Geneva			Vättern/Vänern			All three lakes		
	n	***r***	***ρ***	***n***	***r***	***ρ***	***n***	***r***	***ρ***
DSecB3jul	12	**.789(*)**	**.802(**)**	7	.331	.536	19	.241	.599(**)
DlnSecB2jul	12	**.648(*)**	**.750(**)**	7	.810(*)	.657	19	.265	.611(**)
BSecB1	12	**.602(*)**	**.736(**)**	7	**.924(**)**	**.857(*)**	19	.156	.552(*)
ASecFeb	12	**.758(**)**	**.802(**)**	7	.272	.536	19	.308	.599(**)
SlnSDTB13	12	.531	.641(*)	7	-.003	.179	19	.101	.427

n is the sample size, *r* is Pearson's coefficient and *ρ* is Spearman's rho

(**) Result is significant at the 0.01 level (2-tailed)

(*) Result is significant at the 0.05 level (2-tailed)

(-) Dataset does not follow the normal distribution or small sample size

Table 5-9: Correlation of field SDD data with corresponding simulated remotely sensed data (using Aqua MODIS data only) for non-standard algorithms in 2001-04 in lakes Geneva, Vättern and Vänern.

Algorithm code	Geneva			Vättern/Vänern			All three lakes		
	n	***r***	***ρ***	***n***	***r***	***ρ***	***n***	***r***	***ρ***
DSecB3jul	7	-.193	.180	9	**-.842(**)**	**-.678(*)**	16	-.654(**)	-.377
DlnSecB2jul	-	-	-	-	-	-	-	-	-
BSecB1	7	-.056	.180	9	**-.813(**)**	**-.678(*)**	16	-.519(*)	-.412
ASecFeb	7	-.317	.180	9	**-.785(*)**	**-.678(*)**	16	-.667(**)	-.377
SlnSDTB13	7	-.065	.126	9	**-.871(**)**	**-.678(*)**	16	-.493	-.383

n is the sample size, *r* is Pearson's coefficient and *ρ* is Spearman's rho

(-) Dataset does not follow the normal distribution or small sample size

Table 5-10: Correlation of field SDD data with corresponding simulated remotely sensed data (using both Terra/Aqua MODIS data) for non-standard algorithms in 2001-04 in lakes Geneva, Vättern and Vänern.

Algorithm code	Geneva			Vättern/Vänern			All three lakes		
	n	***r***	***ρ***	***n***	***r***	***ρ***	***n***	***r***	***ρ***
DSecB3jul	19	.245	.549(*)	16	-.479	-.354	35	-.230	.093
DlnSecB2jul	-	-	-	-	-	-	-	-	-
BSecB1	19	.216	.504(*)	16	-.323	-.100	35	-.114	.102
ASecFeb	19	.224	.549(*)	16	-	-.354	35	-	.093
SlnSDTB13	19	.191	.433	16	-.542(*)	-.444	35	-.174	.001

n is the sample size, *r* is Pearson's coefficient and *ρ* is Spearman's rho

(*) Result is significant at the 0.05 level (2-tailed)

(-) Dataset does not follow the normal distribution or small sample size

The two algorithms by Dekker and Peters (1993) were developed for lakes with very low SDD (< 2 m), but exhibited promising results in lakes with much higher SDD values. According to the field data, in Lake Geneva the annual mean SDD in the

years 1984-2004 was 7.6 m, while the annual mean SDD in Lake Vättern was 10.9 m (1969-2003) and in Lake Vänern was 3.9 m (1973-2008). The same was true for the 'BSecB1', 'ASecFeb' and 'SlnSDTB13' algorithms. All the SDD estimation algorithms performed poorly when all lakes were combined suggesting that they are inappropriate for use in different lakes that cover a wide range of SDD values.

The scatter-plot between field data and the outputs of the promising algorithms showed a large degree of scatter around the regression line (Figures 5-9 and 5-10). The 'ASecFeb' algorithm exhibited negative results for both Terra and Aqua MODIS data (Figures 5-9D and 5-10D). The 'BSecB1' algorithm produced higher coefficients of determination in the oligotrophic lakes (Figures 5-10A and C) than in the mesotrophic lake (Figure 5-9C) but underestimated SDD in the all three cases. The 'DSecB3jul' algorithm produced the most promising results in Lake Geneva when Terra MODIS data were used (Figure 5-9A) and in lakes Vättern and Vänern when Aqua MODIS data were used (Figure 5-10B), but failed to do so when all three lakes were combined into a common dataset. The other SDD estimation algorithm by Dekker and Peters (1993) produced a very narrow range of outputs (Figure 5-9B). Finally, the 'SlnSDTB13' algorithm produced promising results in the two oligotrophic lakes when Aqua MODIS data were used (Figure 5-10E), but when all three lakes were combined for either sensor the results were poor.

In conclusion, none of the non-standard chlorophyll *a* estimation algorithms tested with the data available in this project were able to produce highly accurate estimates of SDD concentrations when all lakes were combined (oligotrophic to mesotrophic) towards the investigation of a universal algorithm. However, two algorithms

('DSecB3jul' and 'SlnSDTB13') produced promising results and should be investigated further, but lack of appropriate remote sensing data in this project prohibited this specifically.

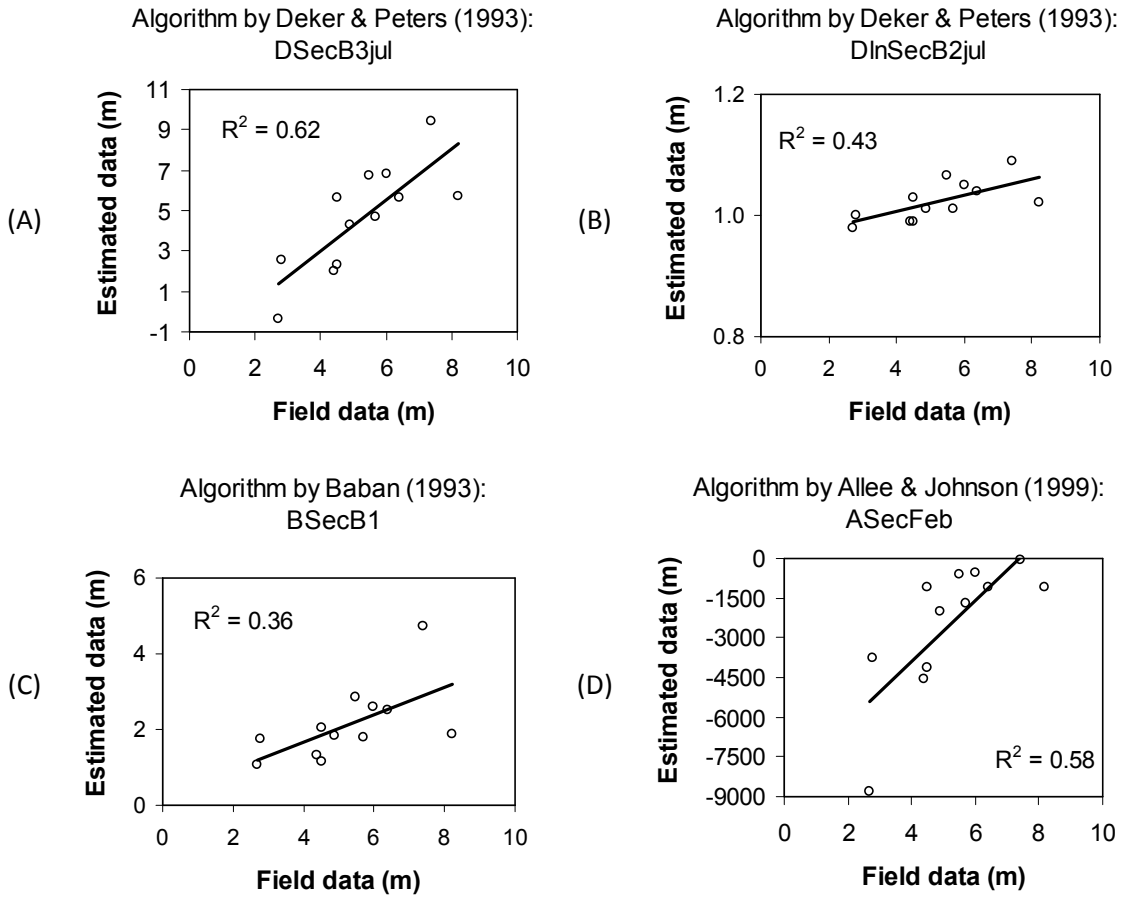

Figure 5-9: Lake Geneva: Scatter plots of promising non-standard algorithms for the estimation of SDD using only Terra MODIS data.

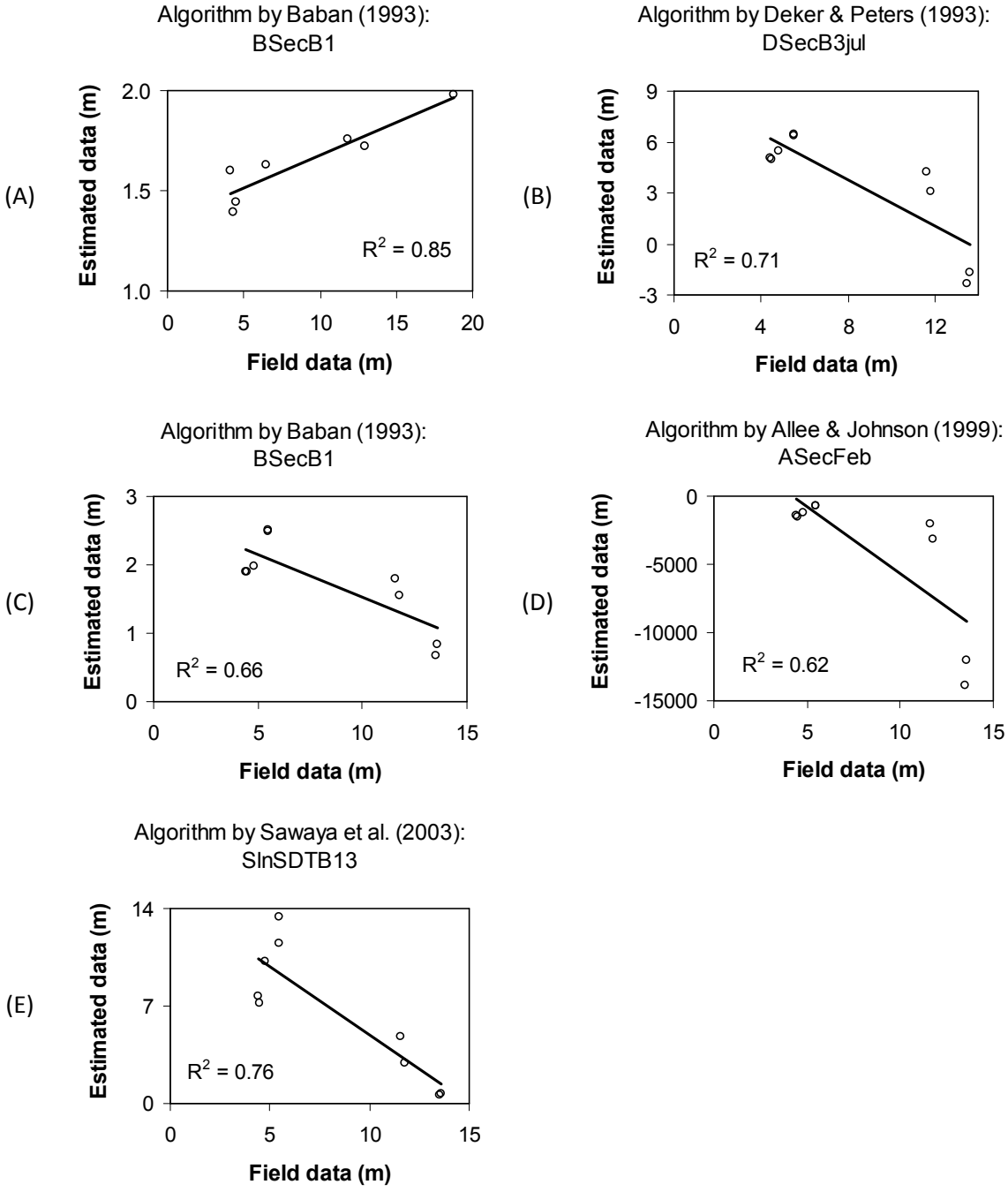

Figure 5-10: Lakes Vättern and Vänern: Scatter plots of promising non-standard algorithms for the estimation of SDD using only Terra MODIS data (A) and only Aqua MODIS data (B-E).

5.5 Discrepancy between Terra and Aqua MODIS

During the analysis of Terra/Aqua MODIS data discrepancy was observed between the outputs of the same algorithms when data from the two sensors were used. In this section the degree of disagreement between the Terra MODIS and the Aqua MODIS estimates was assessed.

5.5.1 Discrepancy between the outputs of the MODIS SST algorithm

Correlation and T-test analysis were performed to check the significance of disagreement between the Terra MODIS SST and Aqua MODIS SST estimations. The original Terra/Aqua MODIS SST dataset was divided into two subsets that represented only the estimations from either Terra or Aqua MODIS. First, the field LST data were compared to the corresponding Terra MODIS SST and the Aqua MODIS SST estimates to check for differences in the strength of correlation. Then, the Terra MODIS SST estimates were compared to the Aqua MODIS SST estimates on the same dates.

The results showed that the field LST observations were better correlated with the Terra MODIS SST estimates in both lakes than to the Aqua MODIS SST estimates for the same dates in 2001-04 (Table 5-11). However, both correlations were strong and significant. In addition, the Terra MODIS SST estimates were very strongly correlated with the Aqua MODIS SST estimates on the same dates in both lakes. In fact, an independent sample T-test showed that the difference of the means between the Terra MODIS SST (M = 13.28; SD = 5.65) and Aqua MODIS SST (M = 12.61; SD = 4.93) datasets was insignificant: $t(30) = 0.361$; $p \geq 0.01$ (2-tailed). As a result,

both sensors (with a preference for Terra MODIS) were considered appropriate for the estimation of LST.

Table 5-11: Correlation of field data with the Terra and Aqua MODIS SST in lakes Geneva and Vättern combined.

Datasets compared	Sample size (*n*)	Pearson's (*r*)	Spearman's rho (*ρ*)
Field – Terra MODIS SST	16	0.941(**)	0.921(**)
Field – Aqua MODIS SST	16	0.867(**)	0.844(**)
Terra MODIS SST – Aqua MODIS SST	16	0.961(**)	0.962(**)

(**) Result is significant at the 0.01 level (2-tailed)

5.5.2 Discrepancy between the outputs of the non-standard algorithms

The discrepancy between the algorithm outputs from the same dates when either Terra or Aqua MODIS data were used as inputs was investigated by comparing the corresponding sets of outputs for all non-standard algorithms. The datasets were not normally distributed. The correlation between Terra MODIS and Aqua MODIS chlorophyll *a* estimates was moderate ($\rho = 0.423$; $p << 0.01$ (2-tailed), $n = 68$). The same was true for the Secchi disk depth outputs ($\rho = 0.769$; $p << 0.01$ (2-tailed), $n = 24$). These results suggest a certain degree of disagreement between the Terra and Aqua MODIS data (L_{toa}, R_{toa}, nL_w and R_{rs}) that were used as inputs to the non-standard algorithms.

The MODIS sensors onboard the Terra and Aqua satellites were designed the same specifications and essentially receive the same calibration, so that the two sensors should provide highly correlated data. However, NASA scientists consider the

quality of Terra MODIS data insufficient for quantitative analysis due to a fault in the scanning mirror of the sensor (NASA Ocean Colour, 2009). Wu *et al*. (2008) have tested and confirmed the calibration consistency of three reflective solar Terra and Aqua MODIS wavebands, suggesting high agreement between the two sensors in the visible, nIR and mid IR parts of the spectrum. However, these comparisons employed non-atmospherically corrected data and ocean colour is only a very small fraction of that signal. Also, due to their different overpass time (Aqua follows Terra by approximately 3 hours), differences in the atmospheric conditions and the Sun angle may result in differences in the signal detected by the two sensors (Lillesand *et al*., 2008).

5.6 Development of new algorithms

Due to the non-transferable character of all non-standard chlorophyll *a* and Secchi disk depth estimation algorithms, the available field and remotely sensed data in this project were used for the development of new algorithms for the estimation of these two parameters. The correlation of the field data with atmospherically corrected data (remote sensing reflectance, R_{rs}, and normalized water-leaving radiance, nL_w) and non-atmospherically corrected data (at-satellite reflectance, R_{toa} and radiance, L_{toa}) was tested. Regression analysis was performed between the field chlorophyll *a* and Secchi disk depth data and the corresponding Terra/Aqua MODIS data in a mesotrophic lake (Lake Geneva) and two oligotrophic lakes (lakes Vättern and Vänern). Insufficient remote sensing data prohibited the use of a eutrophic lake in regression analysis. Regression analysis was performed for all three lakes combined for various months, to test the possibility of the development of an algorithm that is

transferable in time and space. All satellite data used in regression analysis were averaged from 9-pixel squared grids centred at the location of the stations.

Due to the discrepancy observed between the Terra and Aqua MODIS data in preceding analysis an equation using a combination of data from both sensors was not produced. Consequently, separate equations for each sensor were developed. Five types of regression models were tested; namely the linear, logarithmic, polynomial (second-order), power and the exponential model.

5.6.1 Chlorophyll *a* algorithms

First, single bands were correlated with field chlorophyll *a* measurements from the three lakes. The blue (MODIS bands 3 and 10), green (MODIS bands 4, 11 and 12), red (MODIS bands 1, 13 and 14) and nIR (MODIS band 15) parts of the spectrum were used for chlorophyll *a* as suggested in the literature (e.g. Baban, 1993; Dekker & Peters, 1993; George, 1997b; Kallio *et al*., 2001). The Terra MODIS single bands were weakly and insignificantly correlated with the field measurements for all satellite products (Figure 5-11). The same was true for the Aqua MODIS data.

Then band ratios were tested. For chlorophyll *a* the nIR/red, nIR/green, green/blue, red/blue, green/red and violet/green band ratios were used as suggested in published literature (e.g. Baban, 1993; Gitelson *et al*., 1993; Hedger *et al*., 1996; George, 1997b; Pulliainen *et al*., 2001) and all appropriate bands were combined.

Among the Terra MODIS band ratios for chlorophyll *a* only the green/blue and violet/green band combinations produced significant results. All the green/blue and

violet/green ratios were significantly correlated with the field chlorophyll *a* data when Terra MODIS R_{toa} and L_{toa} were used (Table 5-12). The correlations of the field data with the rest of the band ratio combinations for atmospherically and non-atmospherically corrected data were weak and insignificant are not presented here for the sake of brevity. For Aqua MODIS data, only one green/red band combination produced significant results for R_{toa} and L_{toa} (Table 5-13), while the correlations of the rest of the band ratios with the field data were very weak and are not presented.

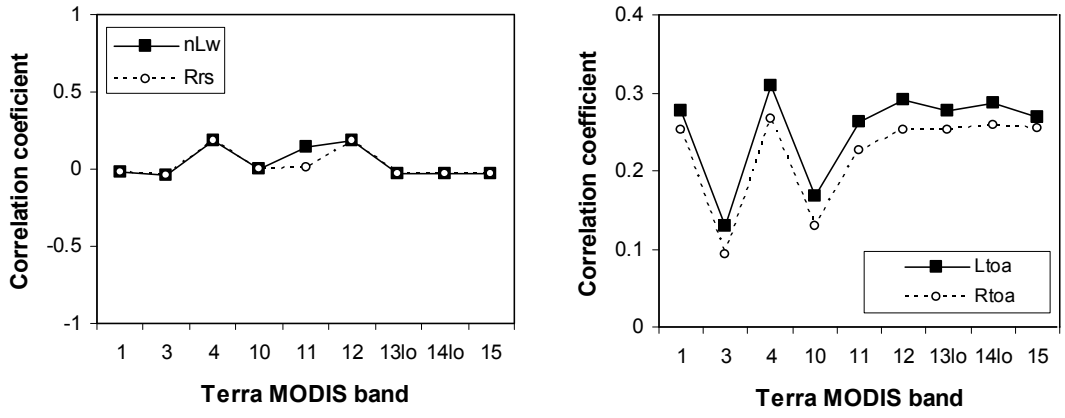

Figure 5-11: Pearson's correlation coefficient between field chlorophyll *a* measurements and Terra MODIS R_{rs} and nL_w, (left), and Terra MODIS R_{toa} and L_{toa} (right) in single bands.

A logarithmic transformation was applied to the field and satellite data to test whether it improved the correlation results. For that purpose, both the common (base 10) and the natural logarithms were applied. None of the two transformations significantly improved the correlation strength for chlorophyll *a* for either sensor, so untransformed data were used in the regression analysis.

Table 5-12: Correlation of Terra MODIS R_{toa} and L_{toa} in the green/blue and violet/green ratios of MODIS bands 3, 4, 8-12 with field chlorophyll *a* data; lakes Geneva, Vättern and Vänern (n = 30).

Ratio	R_{toa}	L_{toa}
	Pearson's (r)	**Pearson's (r)**
green/blue		
12/10	0.562(**)	0.524(**)
12/3	0.570(**)	0.538(**)
11/10	0.522(**)	0.537(**)
11/3	0.538(**)	0.542(**)
4/10	0.574(**)	0.585(**)
4/3	**0.583(**)**	**0.585(**)**
violet/green		
8/4	-0.521(**)	-0.518(**)
8/11	-0.484(**)	-0.483(**)
8/12	-0.508(**)	-0.482(**)
9/4	-0.538(**)	-0.545(**)
9/11	-0.498(**)	-0.508(**)
9/12	-0.525(**)	-0.502(**)

(**) Result is significant at the 0.01 level (2-tailed)

Table 5-13: Correlation of Aqua MODIS R_{toa} and L_{toa} in the green/red ratio of MODIS bands 1 and 4 with field chlorophyll *a* data; lakes Geneva, Vättern and Vänern (n = 23).

Ratio	R_{toa}		L_{toa}	
	Pearson's (r)	**Spearman's (ρ)**	**Pearson's (r)**	**Spearman's (ρ)**
4/1	0.472(*)	0.533(**)	0.474(*)	0.502(*)

(**) Result is significant at the 0.01 level (2-tailed)

(*) Result is significant at the 0.05 level (2-tailed)

For chlorophyll *a*, the Terra MODIS green/blue combination of bands 3 and 4 exhibited the strongest correlation coefficients with field data and was used during

regression analysis. Both R_{toa} and L_{toa} were tested, as they produced similar correlation coefficients with the field data. For Aqua MODIS data the green/red combination of bands 1 and 4 was not used because the noise in both bands was very high in all Aqua MODIS scenes available in this project (visual interpretation of the data).

Table 5-14: Regression analysis between Terra MODIS band 4/band 3 R_{toa} and L_{toa} ratio and field chlorophyll *a* data; lakes Geneva, Vättern and Vänern (n = 30).

Ratio	R_{toa}				
	Linear (R^2)	**Logarithmic (R^2)**	**Polynomial (R^2)**	**Power (R^2)**	**Exponential (R^2)**
4/3	0.340(**)	0.328(**)	**0.434(**)**	0.228(**)	0.234(**)
Ratio	L_{toa}				
	Linear (R^2)	**Logarithmic (R^2)**	**Polynomial (R^2)**	**Power (R^2)**	**Exponential (R^2)**
4/3	0.343(**)	0.330(**)	**0.447(**)**	0.226(**)	0.233(**)

(**) Result is significant at the 0.01 level (2-tailed)

The second-order polynomial model produced the best results for both R_{toa} and L_{toa} Terra MODIS data when the satellite data were regressed against field chlorophyll *a* measurements (Table 5-14). R_{toa} and L_{toa} produced similar results, but the L_{toa} data were preferred in this project as they produced higher coefficients of determination for the polynomial equation (R^2 = 0.447, $p < 0.01$, n = 30). In fact, Kallio *et al.* (2001) found that the use of at-satellite reflectance data (instead of at-satellite radiance) did not improve the accuracy of chlorophyll *a* estimation algorithms (Kallio *et al.*, 2001). The polynomial equation that employs ratio band 4/band 3 for the Terra MODIS L_{toa} data in lakes Geneva, Vättern and Vänern is given below:

$$C_{Chl\text{-}a}\ [\mu g\ L^{-1}] = 738.709\left(\frac{B_4}{B_3}\right)^2 - 755.122\left(\frac{B_4}{B_3}\right) + 195.436 \qquad (5.1)$$

where $C_{Chl\text{-}a}$ is the concentration of chlorophyll *a* and $B_{3,4}$ is L_{toa} at Terra MODIS bands 3 and 4.

The accuracy of the new chlorophyll *a* algorithm produced in this project (henceforth called the Terra MODIS Politi chlorophyll *a* algorithm (Equation 5.1)) was assessed using six scenes on dates that coincided with field measurements and were not used to develop the regression equation (Figure 5-12). The algorithm has a bias of 0.51 µg L^{-1} and its accuracy (RMSE) is 2.17 µg L^{-1}. Traditional sampling methods can usually estimate chlorophyll *a* concentrations with an accuracy of ± 0.5 µg L^{-1} in less productive lakes and an accuracy of ± 2 µg L^{-1} in very productive waters (George, 1997b), which means that the above algorithm has shown potential in lake waters.

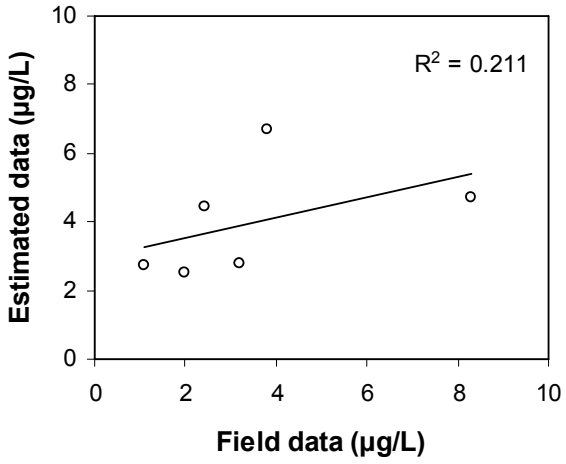

Figure 5-12: Scatter plot of field data against satellite estimations using the Terra MODIS Politi chlorophyll *a* estimation algorithm.

5.6.2 Secchi disk depth algorithms

The blue (MODIS bands 3 and 10), green (MODIS bands 4, 11 and 12) and red (MODIS bands 1, 13 and 14) wavebands were tested for correlation with Secchi disk depth measurements (e.g. Baban, 1993; Dekker & Peters, 1993; Nellis *et al*., 1998; Allee & Johnson, 1999). Three extreme values that were detected within the field SDD measuremenst were not omitted because they represent 75% of the available field measurements in Lake Vättern.

The Terra MODIS single bands were weakly and insignificantly correlated with corresponding field SDD measurements for all satellite products (Figure 5-13). The same was true for the Aqua MODIS single bands. Then band ratios were tested. The blue/red, green/red, (blue-nIR)/(red-nIR) and (green-nIR)/(red-nIR) ratios were used for Secchi disk depth as recommended in published literature (e.g. Koponen *et al*., 2002; Kallio *et al*. 2003; Sawaya *et al*., 2003; Vincent *et al*., 2004) and all appropriate Terra/Aqua MODIS bands were combined.

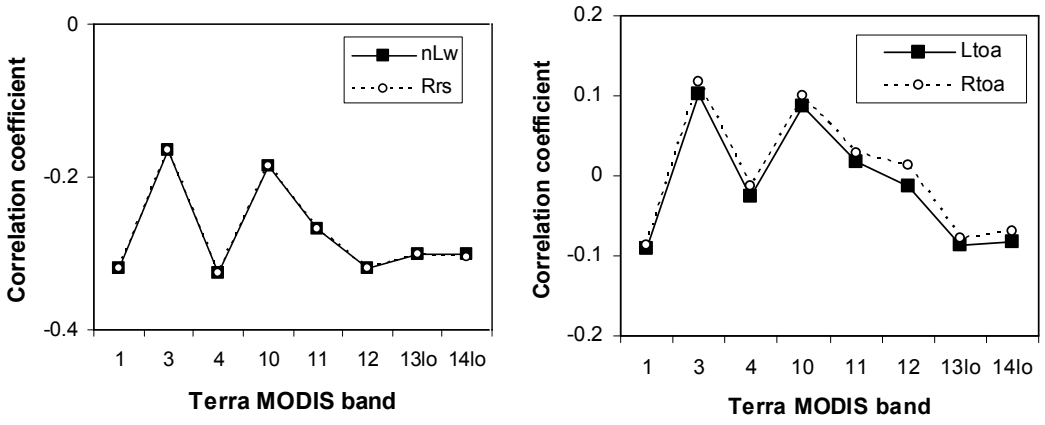

Figure 5-13: (Left) Spearman's correlation coefficient between field SDD measurements and Terra MODIS R_{rs} and nL_w, in single bands and (Right) Pearson's correlation coefficient between field SDD measurements and Terra MODIS R_{toa} and L_{toa} in single bands.

The band rations for the atmospherically corrected data were weakly and insignificantly correlated with field SDD measurements. The same was true for all combinations of the blue/red and green/red ratios when Terra and Aqua MODIS R_{toa} and L_{toa} were used. However, all of the (blue-nIR)/(red-nIR) and (green-nIR)/(red-nIR) ratios produced significantly strong correlations with the field data and are presented (Table 5-15). The Terra MODIS $\left(\frac{B_3 - B_{15}}{B_1 - B_{15}}\right)$ ratio produced the highest correlation with the field SDD data for both R_{toa} and L_{toa} and was chosen for the regression analysis.

The results of the regression analysis (Table 5-16) showed that the polynomial model produced the highest coefficient of determination for both R_{toa} and L_{toa} when compared to the other four regression models. The results were very similar between R_{toa} and L_{toa}, but R_{toa} worked slightly better ($R^2 = 0.606$, $p < 0.01$, $n = 30$) and, therefore, was chosen. In another study the use of at-satellite reflectance data (instead of at-satellite radiance) was found to improve the accuracy of turbidity algorithms (Kallio *et al*., 2001), which agrees with the findings of this project.

The polynomial equation that employs ratio $\left(\frac{B_3 - B_{15}}{B_1 - B_{15}}\right)$ for Terra MODIS R_{toa} data is given below:

$$\text{SDD [m]} = 0.071\left[\left(\frac{B_3 - B_{15}}{B_1 - B_{15}}\right)\right]^2 - 0.517\left[\left(\frac{B_3 - B_{15}}{B_1 - B_{15}}\right)\right] + 4.850 \qquad (5.2)$$

where SDD is Secchi disk depth and $B_{1,3,15}$ is R_{toa} at Terra MODIS bands 1, 3 and 15.

Table 5-15: Correlation of Terra MODIS R_{toa} and L_{toa} in the (blue-nIR)/(red-nIR) and (green-nIR)/(red-nIR) ratios of bands 1, 3, 4, 10-15 with field Secchi disk depth data; lakes Geneva, Vättern and Vänern (n = 30).

Ratio	R_{toa}	L_{toa}
	Pearson's (r)	**Pearson's (r)**
(blue-nIR)/(red-nIR)		
(3-15)/(1-15)	**0.758(**)**	**0.733(**)**
(3-15)/(13-15)	0.670(**)	0.646(**)
(3-15)/(14-15)	0.531(**)	0.657(**)
(10-15)/(1-15)	0.748(**)	0.714(**)
(10-15)/(13-15)	0.664(**)	0.632(**)
(10-15)/(14-15)	0.656(**)	0.646(**)
(green-nIR)/(red-nIR)		
(4-15)/(1-15)	0.555(**)	0.449(*)
(4-15)/(13-15)	0.521(**)	0.425(*)
(4-15)/(14-15)	0.556(**)	0.471(**)
(11-15)/(1-15)	0.637(**)	0.544(**)
(11-15)/(13-15)	0.585(**)	0.502(**)
(11-15)/(14-15)	0.603(**)	0.537(*)
(12-15)/(1-15)	0.583(**)	0.475(**)
(12-15)/(13-15)	0.543(**)	0.446(*)
(12-15)/(14-15)	0.572(**)	0.489(**)

(**) Result is significant at the 0.01 level (2-tailed)

(*) Result is significant at the 0.05 level (2-tailed)

Table 5-16: Regression analysis between Terra MODIS R_{toa} and L_{toa} in the (blue-nIR)/(red-nIR) band ratio that employs bands 1, 3 and 15 and field Secchi disk depth measurements; lakes Geneva, Vättern and Vänern (n = 30).

Ratio	R_{toa}				
	Linear (R^2)	**Logarithmic (R^2)**	**Polynomial (R^2)**	**Power (R^2)**	**Exponential (R^2)**
(3-15)/(1-15)	0.574(**)	0.525(**)	**0.606(**)**	0.421(**)	0.447(**)
Ratio	L_{toa}				
	Linear (R^2)	**Logarithmic (R^2)**	**Polynomial (R^2)**	**Power (R^2)**	**Exponential (R^2)**
(3-15)/(1-15)	0.538(**)	0.502(**)	**0.602(**)**	0.502(**)	0.524(**)

(**) Result is significant at the 0.01 level (2-tailed)

The accuracy of the new SDD algorithm produced in this project using Terra MODIS data (henceforth called the Terra MODIS Politi SDD algorithm (Equation 5.2)) was assessed using six scenes on dates that coincided with field measurements and were not used in regression analysis (Figure 5-14). The algorithm has a bias of -1.08 m and its accuracy (RMSE) is 3.99 m.

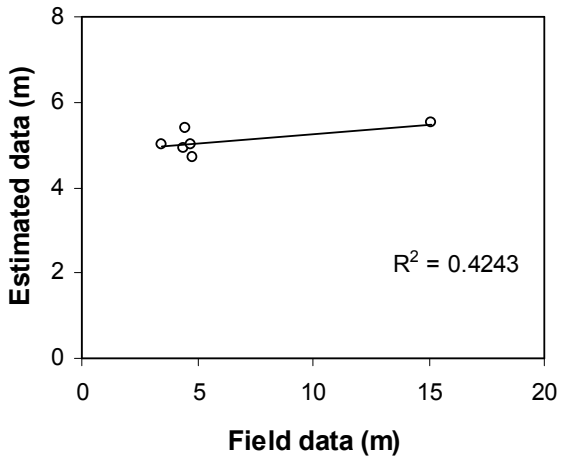

Figure 5-14: Scatter plot of field data against satellite estimations using the Terra MODIS Politi SDD estimation algorithm.

The Aqua MODIS band ratios (atmospherically and non-atmospherically corrected data) exhibited weak and insignificant results when correlated with field SDD measurements. Transformation of the data (i.e. the common and natural logarithms) improved the results only for eight band ratio combinations for Aqua MODIS R_{toa} whilst for L_{toa} the two logarithmic transformations did not improve the results of correlation analysis and are not presented. In particular, four (blue-nIR)/(red-nIR) and four (green-nIR/red-nIR) R_{toa} ratios produced strong correlations with the field data and the common logarithm produced as strong correlations as the natural logarithm (Table 5-17). The common logarithm of the Aqua MODIS R_{toa} ratio

$\left(\frac{B_{10}-B_{15}}{B_{13}-B_{15}}\right)$ produced the highest correlation coefficients and was used in regression analysis.

Table 5-17: Correlation of transformed (log_{10}, ln) Aqua MODIS R_{toa} in the (blue-nIR)/(red-nIR) and (green-nIR)/(red-nIR) ratios of Bands 3, 10-15 to transformed (log_{10}, ln) field Secchi disk depth data; lakes Geneva, Vättern and Vänern (n = 23).

Ratio	Log_{10} (R_{toa})		Ln (R_{toa})	
	Pearson's (r)	Spearman's (ρ)	Pearson's (r)	Spearman's (ρ)
(blue-nIR)/(red-nIR)				
(3-15)/(13-15)	.605(*)	.705(**)	.605(*)	.705(**)
(3-15)/(14-15)	.615(*)	.724(**)	.615(*)	.724(**)
(10-15)/(13-15)	**.691(**)**	**.622(**)**	-	.624(**)
(10-15)/(14-15)	.661(**)	.605(**)	-	.612(**)
(green-nIR)/(red-nIR)				
(11-15)/(13-15)	.670(**)	.601(**)	.670(**)	.601(**)
(11-15)/(14-15)	.645(**)	.600(**)	.645(**)	.600(**)
(12-15)/(13-15)	.640(**)	.565(**)	.639(**)	.565(**)
(12-15)/(14-15)	.620(**)	.499(*)	.620(**)	.499(*)

(**) Result is significant at the 0.01 level (2-tailed)

(*) Result is significant at the 0.05 level (2-tailed)

The results of the regression analysis for the Aqua MODIS R_{toa} (Table 5-18) showed that the polynomial model exhibited the highest coefficient of determination (R^2 = 0.544, $p < 0.01$, n = 21). The polynomial model that employs the ratio $\left(\frac{B_{10}-B_{15}}{B_{13}-B_{15}}\right)$ for the Aqua MODIS R_{toa} data is given below:

$$\log(SDD) = -1.496\left[\log\left(\frac{B_{10}-B_{15}}{B_{13}-B_{15}}\right)\right]^2 + 4.206\left[\log\left(\frac{B_{10}-B_{15}}{B_{13}-B_{15}}\right)\right] - 1.806 \qquad (5.3)$$

where log(SDD) is the common logarithm of Secchi disk depth and $B_{10,13,15}$ is R_{toa} at the Aqua MODIS bands 10, 13 and 15.

Table 5-18: Regression analysis between transformed (log_{10}) Aqua MODIS R_{toa} in the (blue-nIR)/(red-nIR) ratio that employs bands 10, 13 and 15 and transformed (log_{10}) field Secchi disk depth data; lakes Geneva, Vättern and Vänern (n = 21).

Ratio	R_{toa}				
	Linear (R^2)	**Logarithmic (R^2)**	**Polynomial (R^2)**	**Power (R^2)**	**Exponential (R^2)**
(10-15)/(13-15)	0.477(**)	0.505(**)	**0.544(**)**	0.442(**)	0.414(**)

(**) Result is significant at the 0.01 level (2-tailed)

The accuracy of the SDD algorithm produced in this project using Aqua MODIS data (henceforth called the Aqua MODIS Politi SDD algorithm (Equation 5.3)) was assessed using seven scenes on dates that coincided with field measurements and were not used in regression analysis (Figure 5-15). The algorithm has a bias of -0.74 m and its accuracy (RMSE) is 3.22 m.

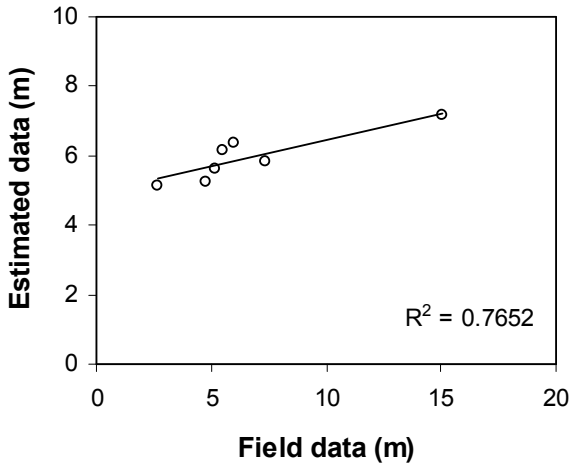

Figure 5-15: Scatter plot of field data against satellite estimations using the Aqua MODIS Politi SDD estimation algorithm.

5.7 Summary

Both NOAA AVHRR MCSST and NLSST algorithms produced highly accurate estimations of temperature and very similar predictive accuracies. The MCSST algorithm was selected for the estimation of LST from the rest of the NOAA AVHRR data available in this project as the NLSST algorithm was mainly developed for regions with high water vapour (tropical) (Oesch *et al*., 2005). Prior to its application, the NOAA AVHRR MCSST algorithm was calibrated to optimize the fit of the data of this project.

Of the other two LST-estimation algorithms considered in this project, the Terra/Aqua MODIS SST standard algorithm produced highly accurate outputs. However, due to the small length of the MODIS archive dataset and the relatively limited number of images available in this project it was not selected for further analysis. The non-standard LST-estimation algorithm was unsuitable for use with the remotely sensed data available.

The Terra/Aqua MODIS OC3 standard algorithm produced very poor results in lakes with various characteristics and was not selected for further analysis. The same was true for all the non-standard algorithms identified previously in the literature. Only the chlorophyll *a* estimation algorithm developed in this project for Terra at-satellite radiance data (Equation 5.1) was selected for application to the rest of the Terra MODIS data available in this project.

None of the SDD estimation non-standard algorithms from the literature performed well as a universal model. As a result, the two SDD estimation algorithms that were

developed in this project for Terra MODIS at-satellite reflectance data (Equation 5.2) and Aqua MODIS at-satellite reflectance data (Equation 5.3) were selected for application to the rest of the Terra/Aqua MODIS data.

In summary, one LST estimation algorithm, one chlorophyll *a* estimation algorithm and two SDD estimation algorithms were applied to the rest of the satellite data as appropriate to demonstrate the potential of remote sensing in limnological studies of wide spatial and temporal scales.

Chapter VI.

DEMONSTRATION OF THE POTENTIAL OF REMOTE SENSING IN LIMNOLOGY

6.1 Introduction

The WFD requirement to monitor lakes across wide spatial and temporal scales demands transferable algorithms to detect the spatial distribution and temporal variation in key water quality parameters. In the previous chapters candidate algorithms for estimating lake surface temperature, chlorophyll *a* concentrations and Secchi disk depth from remotely sensed data have been identified and tested. This chapter aims to apply the best performing algorithms to 23 lakes across Europe as a demonstration of the potential of remote sensing in limnological studies at wide spatial and temporal scales. NOAA AVHRR data were used here to map thermal features in large lakes, such as timings of mixing and stratification onsets, temperature maxima and minima, temporal and spatial gradients of temperature, warming and cooling trends, ice cover and ice break-up, temporal and spatial distributions of temperature and thermal circulation features. Also Terra and Aqua MODIS data were used to map chlorophyll *a* and Secchi disk depth and ecological patterns related to these two parameters. Finally, the sources of error and uncertainty, and the limitations in terms of the environmental and operational character of the methodology were identified and discussed, and thus, provided a reference for future assessments of the ecological characteristics of temperate lakes with remote sensing.

6.2 Temperature and thermal features using the NOAA AVHRR

Remote sensing data can be collected very frequently (depending on the revisit capability of the sensor used) and over long time periods (depending on the period of operation of the sensor). In the case of NOAA AVHRR, an archive of data is available dating back to 1979, providing morning day-time data over European lakes up to four times per day. In fact, when different sensors are combined (e.g. NOAA AVHRR and Terra/Aqua MODIS) for the estimation of the same parameter (e.g. LST) the temporal coverage increases up to ten images per 24 hours (Oesch *et al*., 2008). Assuming cloud conditions over the lakes are at minimum, this allows for a much shorter sampling interval than most field sampling campaigns. Field LST data collection can sometimes be limited to one measurement every few months in a year (e.g. Lake Vättern (Figure 6-1B)) or just a specific season (e.g. Lake Balaton (Figure 6-1A)) according to the needs and resources available to the data collector. However, remote sensing data offer the possibility of data acquisition throughout the entire year depending on cloud cover (Figure 6-1).

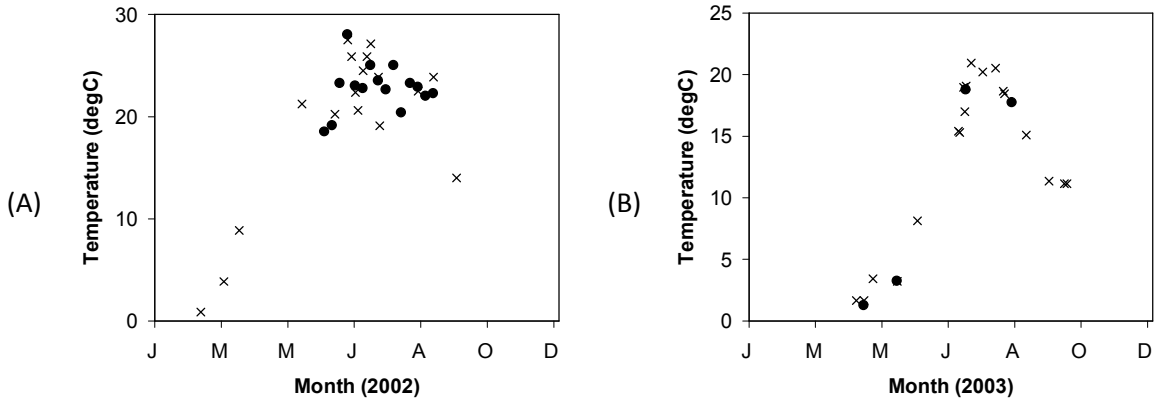

Figure 6-1: Lake surface temperature in (A) Lake Balaton (Station Siofok) in 2002 and (B) Lake Vättern (Station Jungfrun) in 2003; field LST measurements (circles) and NOAA AVHRR MCSSTcal estimates (crosses).

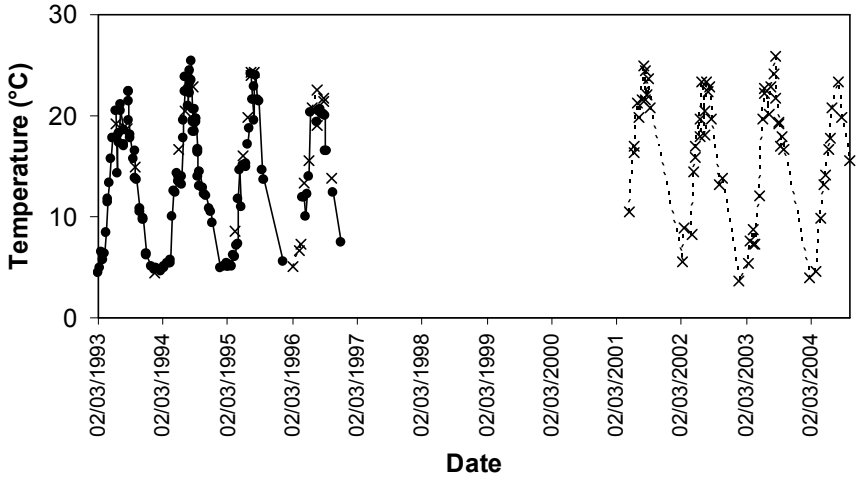

Figure 6-2: Lake surface temperature in Lake Constance (1993-2004): Field LST measurements (circles-solid line) and NOAA AVHRR MCSSTcal estimates (crosses-dotted line).

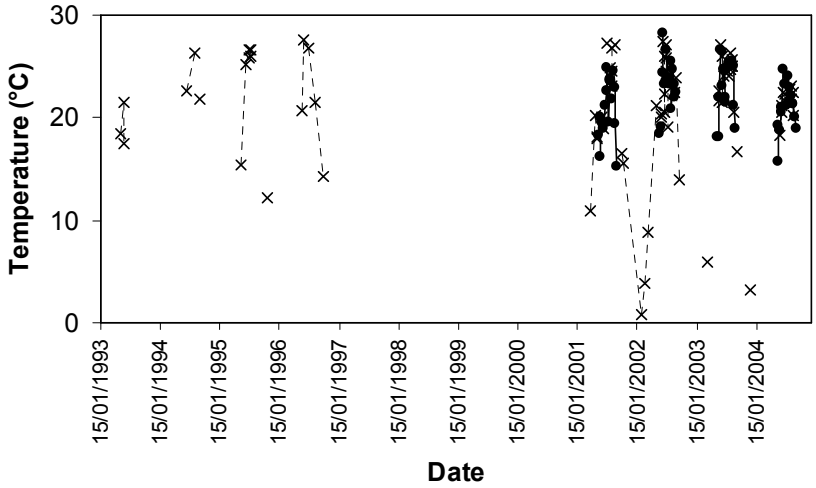

Figure 6-3: Lake surface temperature in Lake Balaton (1993-2004): Field LST measurements (circles-solid line) and NOAA AVHRR MCSSTcal estimates (crosses-dotted line).

Furthermore, remote sensing data can fill-in gaps in field sampling (Figures 6-2 and 6-3). In the case of Lake Constance, for example, field data in this project were available only up to 1997 and the remote sensing data were thus used as a continuation of the annual temporal distribution of lake surface temperature measurements (Figure 6-2). Lake Balaton is another similar example, for which

remote sensing provided information to fill-in gaps in years preceding the field sampling campaign (Figure 6-3). In this sense, remote sensing can revolutionize limnological research, which, until recently, has been based solely on field campaigns and thus restricted by issues, such as time, effort and financial resources.

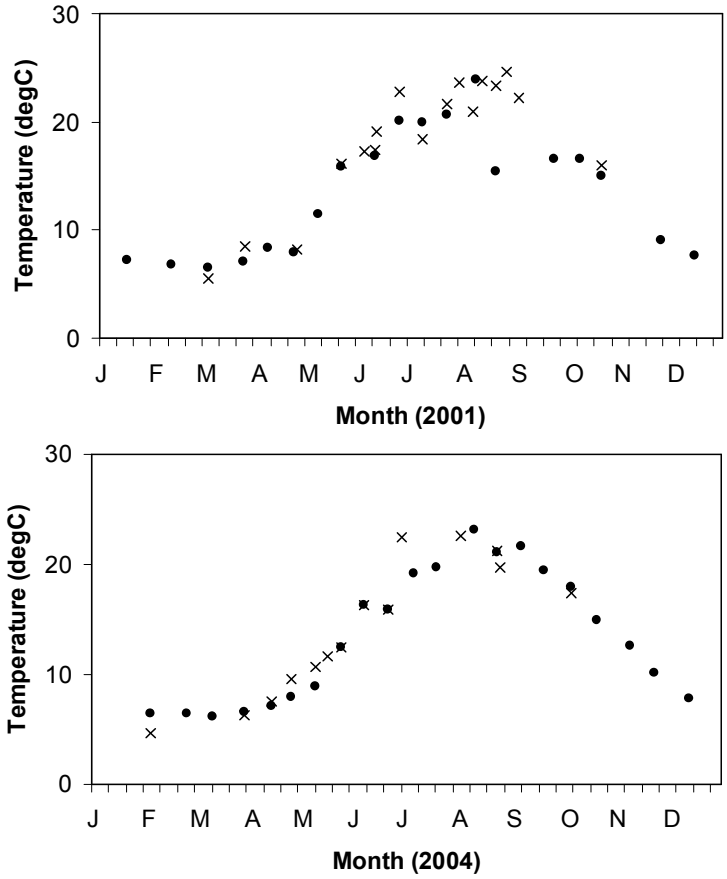

Figure 6-4: Lake surface temperature in Lake Geneva in 2001 (top) and 2004 (bottom): Field LST measurements (circles) and NOAA AVHRR MCSSTcal estimates (crosses).

For lakes where intensive and frequent sampling takes place the remotely sensed data available in this project did not provide as many estimates of LST, but were frequent enough to illustrate spatial variation (Figure 6-4). For example, field measurements

in Lake Geneva were available biweekly to monthly for all months in the years 1984-2004. NOAA AVHRR data can extend the information back to 1979 and after 2004 if the entire 30-year long NOAA AVHRR data archive is used, but the expected sampling frequencies are unlikely to be much higher due to cloud cover. Section 4.2.1 demonstrated that in Lake Geneva the average number of days with cloud coverage less than 66% are approximately 150, which results (by approximation) in an available image almost every other day. Nevertheless, if remote sensing is used as a replacement to laborious field campaigns, it will still provide LST estimates at an equivalent temporal resolution to field measurements.

Due to the high frequency of both field and satellite data available for Lake Geneva comparisons and observations could be made regarding the agreement of the two datasets in terms of the temporal patterns they exhibited. The remotely sensed estimates showed good agreement with the field data in winter, spring and autumn, whereas in summer they disagreed with the field LST data (Figure 6-4). It is likely that a certain degree of disagreement is due to the temporal gaps in either field measurements or remotely sensed estimates. What is noticeable from the temporal variability of LST as seen from the field data is that any changes are slow and gradual. However, the remotely sensed estimates suggest more abrupt changes that are probably due to the skin effect. These changes are exaggerated during the period of stratification. In winter and autumn, especially on windy days when the lake mixes and the vertical temperature gradients are relatively small, the skin effect has a smaller effect on the accuracy of the remotely sensed estimates. However, as the lake water surface warms up in late spring and summer, the surface temperature is much more susceptible to change reflecting changes in the diurnal air temperature and the

effect of wind. This will affect the estimation of the summer maximum temperature, especially when compared to field measurements taken from slightly deeper water.

6.2.1 Stratification, temperature gradients and maximum temperature

Due to irregularities in sampling depths (e.g. data used in this project were collected at 0, 0.5 or 1 m under the surface) and sampling intervals (ranging from daily to seasonal) interpolation of data is a common procedure in limnological studies when numerous past data are used for trend analysis (Livingstone, 2003). Linear interpolation may lead to incorrect estimates due to the non-linear behaviour of the parameters under consideration (especially when short-term variation is not well represented by the sampling intervals), and thus the accurate determination of the behaviour of a dynamic ecosystem such as lakes might not be feasible. However, the method allows the use of non-synchronous water quality data (Dekker *et al.*, 1993) and in this project it was applied to two different datasets (Lake Geneva and Lake Vättern) to demonstrate the advantage of coupling remote sensing with field measurements and the potential of remote sensing when used independently. Interpolation facilitated the study of thermal features, such as the onset of stratification, its breakdown and the rate of spring warming and autumn cooling that are considered of major ecological importance (Wetzel, 1975).

The dates of stratification onset and breakdown were identified using the weekly temperature gradient that was produced for Lake Geneva in 2001-04 using interpolated field and satellite data according to the following equation:

$$\text{grad}(T) = \partial T / \partial t \qquad (6.1)$$

where T is temperature in °C; ∂T is equal to the change in temperature between consecutive calendar weeks and t is the time step (in this case t = 7 days). Monday of each calendar week was used as the weekly time step. The onset of stratification was considered to coincide with the date when the weekly temperature gradient becomes greater than 1 °C and the stratification breakdown to coincide with the date from which the weekly temperature gradients are constantly negative. According to field measurements, stratification in Lake Geneva in 2002 was initiated during the week 29 April – 6 May ($\partial T/\partial t$ = 1.98 °C) and ended during the week 19 – 26 August ($\partial T/\partial t$ = -0.69 °C) (Figure 6-5). The remotely sensed estimates suggest the same dates for the onset ($\partial T/\partial t$ = 2.25 °C) and breakdown ($\partial T/\partial t$ = -0.96 °C) of stratification in the lake.

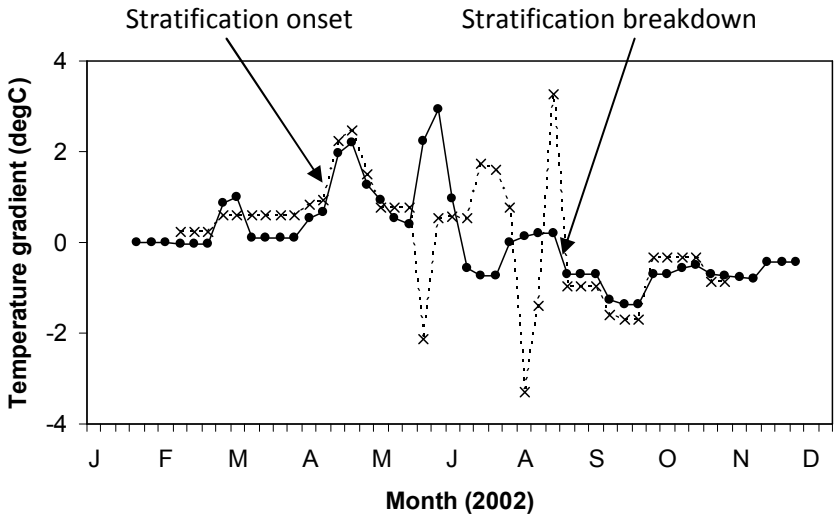

Figure 6-5: Weekly temperature gradient ($\partial T/\partial t$) in Lake Geneva in 2002: Interpolated field data (circles) and NOAA AVHRR MCSSTcal estimates (crosses).

The rate of spring warming and autumn cooling of the water surface in lakes Geneva and Vättern was determined for both field data and remotely sensed LST estimates.

Table 6-1: Mean weekly rate of spring warming (April-May) and autumn cooling (October-November) in Lake Geneva, 2001-04 using interpolated data.

Year	Spring warming (°C/calendar week)		Autumn cooling (°C/calendar week)	
	Field	MCSSTcal	Field	MCSSTcal
2001	1.05	1.03	-0.94	-0.89
2002	0.97	1.25	-0.68	-0.55
2003	1.12	1.03	-0.96	-0.99
2004	0.92	0.92	-1.08	(n/a)

Following the findings of Chapter 4 (Table 4-7), the months when temperature rose/dropped at a maximum rate in Lake Geneva were identified to be April-May and October-November respectively. As a result, the spring warming rate in Lake Geneva was produced between the first week of April and the last week of May, while the autumn cooling was produced between the first week of October and the last week of November. The comparison shows that the differences in the results were small ($\leq$ 0.28 °C) between the field and satellite datasets in the same year and also between consecutive years ($\leq$ 0.44 °C) in the same dataset (Table 6-1). In fact, the results were very similar to past trends in spring warming and autumn cooling in Lake Geneva in 1984-2000 (Table 6-2). There was insignificant ($p << 0.01$) difference between the warming/cooling rates produced from remote sensing estimates in 2001-04 and the ones produced from corresponding field data 1984-2004. Specifically, according to the satellite estimates, in 2001-04 Lake Geneva warmed by average 1.06 °C per calendar week in spring and cooled by average -0.81 °C per calendar

week in autumn. The field data showed that the same rates in 1984-2004 were 1.06 °C per calendar week in spring and -0.85 °C per calendar week in autumn.

Table 6-2: The mean weekly rate of spring warming (April-May) and autumn cooling (October-November) per year in Lake Geneva estimated from interpolated field measurements in 1984-2000.

Year	Spring warming (°C/calendar week)	Autumn cooling (°C/calendar week)
1984	0.58	-0.72
1985	1.22	-1.29
1986	1.36	-0.87
1987	1.15	-0.69
1988	1.15	-0.78
1989	1.12	-0.79
1990	1.12	-0.85
1991	0.66	-1.04
1992	1.31	-0.94
1993	1.43	-0.84
1994	1.02	-0.39
1995	1.15	-0.74
1996	0.85	-0.60
1997	0.76	-0.98
1998	1.09	-0.90
1999	1.03	-0.94
2000	1.23	-0.91
All year average	1.07	-0.84

The rate of spring warming of the water surface in Lake Vättern was produced between the first week of May and the last week of June, and the rate of autumn cooling was produced between the first week of August and the last week of September. The comparison shows that the differences were generally small (≤ 0.55

°C) between the two datasets in the same year and also between consecutive years (($\leq$ 0.48 °C) in the same dataset (Table 6-3). Field data from Lake Vättern were insufficient to produce past trends in the mean weekly rates of spring warming and autumn cooling as means of comparison.

Table 6-3: Mean weekly rate of spring warming (May-June) and autumn cooling (August-September) in Lake Vättern (Station Jungfrun) in 2001-04 using interpolated field and NOAA AVHRR data.

Year	Spring warming (°C/calendar week)		Autumn cooling (°C/calendar week)	
	Field	MCSSTcal	Field	MCSSTcal
2001	1.17	1.72	(n/a)	-0.63
2002	1.05	1.26	(n/a)	(n/a)
2003	1.53	1.27	(n/a)	-0.99
2004	(n/a)	1.36	(n/a)	-0.55

Table 6-4: Maximum lake surface temperature per year and date of occurrence in Lake Vättern (Station Jungfrun) from field and NOAA AVHRR data in 1994-96 and 2001-04 (in 1993 field and satellite data were unavailable).

Year	Field measurements*		NOAA AVHRR MCSSTcal*		Disagreement (Days)
	Max LST (°C)	Date	Max LST (°C)	Date	
1994	17.5	12 July	20.85	13 July	1
1995	19.5	21 Aug	15.65	11 July	41
1996	17.7	15 Aug	17.76	14 Aug	1
2001	17.6	17 Jul	19.88	09 Jul	8
2002	20.8	28 Aug	21.29	26 Aug	2
2003	18.8	16 Jul	20.95	21 Jul	5
2004	(n/a)	(n/a)	20.99	11 Aug	(n/a)

* Values and dates are indicative, due to low temporal coverage of both field and remotely sensed data

In Lake Vättern interpolated field measurements and remotely sensed estimates were used to produce the date when the LST maximum occurs in years when sufficient measurements and satellite images were available (Table 6-4). The degree of disagreement in the results between the two datasets was small and the estimations of the LST maximum date ranged in most cases from one day up to eight days, with the exception of one case when it was 41 days (1995). However, any disagreements were probably due to infrequent sampling (only 4 to 6 field measurements per year) and unavailability of sufficient remote sensing data over Lake Vättern that suggest low temporal sampling of the lake in summer months. Despite that, the above application highlights the advantage of remote sensing over sparse field sampling.

6.2.2 Warming and cooling trends

The above mentioned spring warming and autumn cooling rates were used to perform trend analysis in Lake Geneva. The spring warming and autumn cooling weakly mean rates were plotted for all available years for both field and satellite data from Lake Geneva (Figure 6-6). Then, linear regression was applied to these series to determine whether any evidence of long-term warming (or cooling) could be found (Livingstone & Dokulil, 2001). There was no significant trend observed in the spring warming and the autumn cooling mean rates, suggesting that despite inter-annual fluctuations, the lake warms and cools down at approximately the same rate in the period 1984-2004.

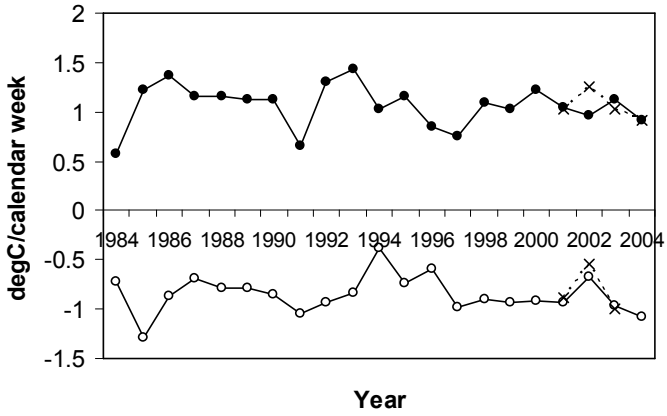

Figure 6-6: Trends in the weekly mean rates of spring warming (solid circles) and autumn cooling (open circles) calculated from interpolated field LST data in Lake Geneva in 1984-2004, and spring warming and cooling (crosses) rates calculated from interpolated NOAA AVHRR MCSSTcal LST estimates in 2001-2004.

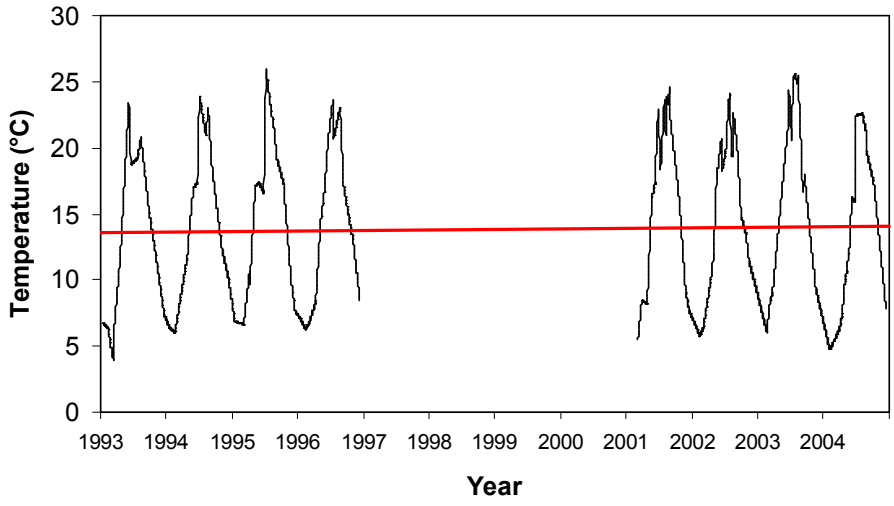

Figure 6-7A: Temporal patterns of LST in Lake Geneva in 1993-96 and 2001-04 using interpolated NOAA AVHRR MCSSTcal estimates. The red line was determined by linear regression.

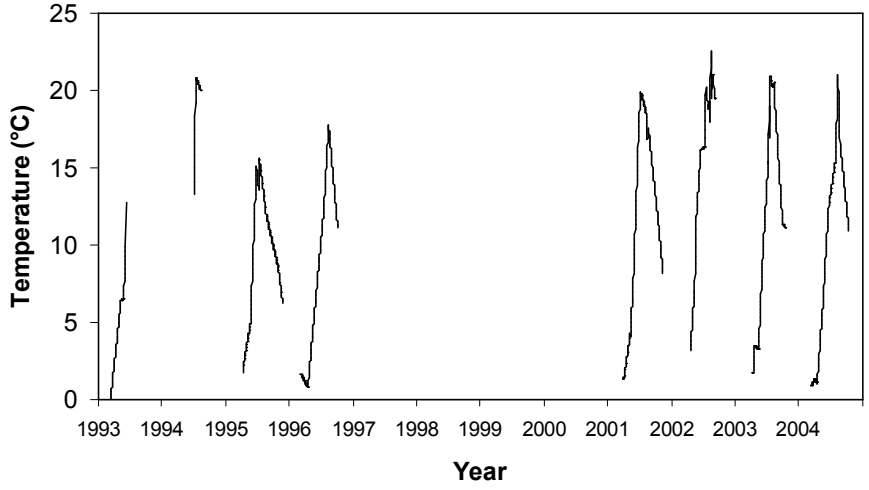

Figure 6-7B: Temporal patterns of LST in Lake Vättern (Station Jungfrun) in 1993-96 and 2001-04 using interpolated NOAA AVHRR MCSSTcal estimates.

Also, interpolated remote sensing estimates from all available years in lakes Geneva and Vättern were plotted in time series to provide information on the temporal patterns in a seasonal and annual basis (Figures 6-7A and 6-7B). For example, Figure 6-7A shows that the summer maximum temperature in Lake Geneva was higher in 1995 (25.95 °C) and 2003 (25.60 °C) than in previous and following years, which could be related with coinciding strongly positive winter NAO indices that caused mild and warm winters in 1994-1995 and 2002-2003 in Europe (CRU, 2008). Livingstone and Dokulil (2001) and Gerten *et al*. (2001) have shown that lake temperatures in European lakes can be influenced by the winter NAO index. However, further investigation of the data in relation to air temperature data is needed to conclude on the latter.

The satellite data from Lake Vättern in 1993-96 and 2001-04 were incomplete (Figure 6-7B) due to problems such as cloud cover and time delays during the data

acquisition that reduced the amount of data obtained per year. However, they demonstrate the strong potential of long remote sensing archives (when they are exploited in their full extent) for deriving information regarding seasonal and interannual patterns of lake surface temperature in European lakes.

The interpolated satellite LST estimates were used to calculate the annual mean LSTs in Lake Geneva and these data were plotted in time series. Then linear regression was applied to these data to determine whether any evidence of long-term warming (or cooling) could be found as described previously. In Lake Geneva in 1993-96 and 2001-04 there were no significant inter-annual warming or cooling trends observed in the NOAA AVHRR LST estimates (Figure 6-7A). However, similar trend analysis of annual means derived from field data in Lake Geneva in 1984-2004 revealed a significant warming trend ($p < 0.01$) in lake surface temperature (Figure 6-8). This disagreement between field and remotely sensed data suggests that either a longer archive of satellite data is required for trend analysis, or that the skin effect masks out any interannual trends in the bulk temperature of Lake Geneva. Livingstone (2003) has shown that regional climate warming in the second half of the 20^{th} century has not influenced the daily maximum (daytime) air temperatures, while the daily minimum (night-time) air temperatures have increased significantly in that time period (Livingstone, 2003). Since the diurnal temperature variability in the uppermost layers of lakes reflects the diurnal cycle of air temperature (Livingstone & Lotter, 1998), it is expected that daytime remotely sensed measurements will not show any warming trend either. In that case, night-time remotely sensed estimates would prove more informative on changes in the lake thermal structure. Oesch *et al*. (2005) have shown that night-time NOAA AVHRR

LST estimates have a higher accuracy than daytime estimates (Oesch *et al.*, 2005), which increases the potential of remote sensing in that case.

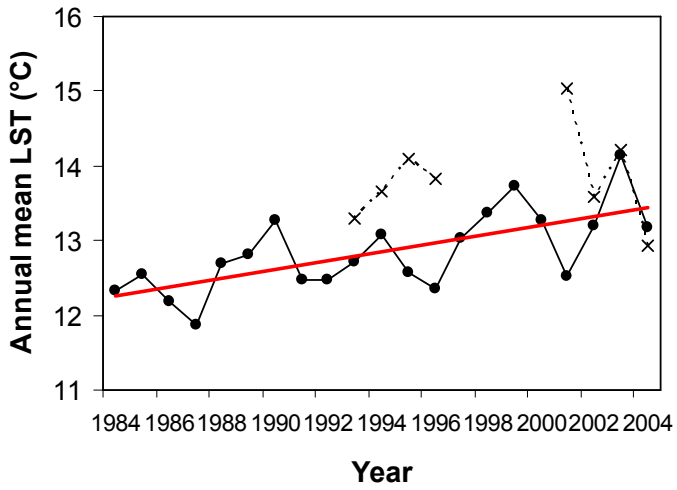

Figure 6-8: Annual means of LST in Lake Geneva in 1984-2004; field data (solid circles) and interpolated NOAA AVHRR MCSSTcal estimates (crosses). The red line was determined by linear regression.

6.2.3 Ice cover and ice break-up

In dimictic lakes in late winter and early spring temperatures rise slowly from 0 °C to 4 °C as ice starts to break-up. When the water temperature reaches 4°C it is an indicator that the water body is completely ice free and it is only after all the ice has melted that the surface temperature can increase rapidly towards the summer peak (Bussières *et al.*, 2002). The two dates/periods when the lake surface temperature is 0 °C and when it reaches 4 °C are considered important for lake ecology because they regulate the thermal regime of dimictic lakes (Bussières *et al.*, 2002). Due to lack of remote sensing data at appropriate frequencies in spring, the ice break-up start date (0 °C) could not be determined in this project. It was only possible to identify the

dates when lake surface temperature reaches 4 °C in three Scandinavian lakes by coupling remote sensing and field data.

In order to identify the timing when the lake surface water was 4 °C, the LST on the last available day with ice cover (≤ 0 °C) and immediate next available ice-free day (> 4 °C) were indentified for each lake using satellite estimates. Interpolation was then used to estimate temperature values between these two days, incorporating field measurements wherever possible to increase the accuracy of interpolation. The above technique is presented here for lakes Päijänne, Kallavesi and Vänern (Table 6-5). Lake Vänern freezes partially in winter, Lake Päijänne freezes completely between December and May, whereas information on the freezing period of Lake Kallavesi was not available in published literature (ILEC, 2010).

Table 6-5: Ice break-up completion dates (LST = 4 °C) in lakes Vänern, Päijänne and Kallavesi in the years 2001, 2003-2004.

Year	Lake	Date when LST = 4 °C
2001	Kallavesi (Station 405)	01 May
2003	Päijänne (Station 76b)	22 May
2004	Päijänne (Station 76b)	11 May
2004	Vänern (Station Tärnan)	11 May

The 4 °C occurrence dates were also identified in Lake Vättern using field data and remote sensing separately as a means of comparison between the two datasets (Table 6-6). Lake Vättern freezes partially in winter (ILEC, 2010). The results show that the identification of the date when LST = 4 °C using remotely sensed LST estimates agreed with the dates produced using field measurements. The latter was true in all

years for which sufficient field and satellite data were available and the range of disagreement varied between 0-5 days (Table 6-6).

Table 6-6: Ice beak-up completion dates in Lake Vättern (Station Jungfrun) using interpolated field data and NOAA AVHRR MCSSTcal estimates in 1993-96 and 2001-04.

Year	Field measurements (Interpolated)	NOAA AVHRR MCSSTcal (Interpolated)	Disagreement (Days)
1993	(n/a)	18 Apr	(n/a)
1994	(n/a)	(n/a)	(n/a)
1995	(n/a)	09 May	(n/a)
1996	17 May	12 May	5
2001	02 May	05 May	3
2002	24 Apr	23 Apr	1
2003	17 May	17 May	0
2004	(n/a)	03 May	(n/a)

The ice break-up completion date is the event that has been most accurately extracted with remote sensing in Canadian lakes (e.g. Wynne *et al*., 1998; Latifovic & Pouliot, 2007).

6.2.4 Thermal circulation

Contrary to point field measurements, remotely sensed data provide detailed information on the spatial variability of LST that allows the construction of thematic maps. In that way the spatial patterns of the water quality parameter across the whole surface of the lake can be studied (Allee & Johnson, 1999). Thermal features in lakes, such as thermal bars, upwelling, downwelling and river plumes, can be observed with NOAA AVHRR data (Kondratyev & Filatov, 1999; Oesch *et al*., 2008).

6.2.4.1 Thermal bars

Thermal bars insulate a warm stratified near-shore zone from a cold well-mixed and oxygenized off-shore zone and as a result they have important chemical and biological consequences (Kondratyev & Filatov, 1999). For example, surface runoff and river discharge introduce nutrients into the lake that are trapped in the stratified warm near-shore zone and increase the primary production in those areas (Wetzel, 1975). Remote sensing was successfully used to map the location and progress of the spring thermal bar in a European lake, Lake Ladoga using NOAA AVHRR thermal data (Malm & Jönsson, 1993). Due to the strong horizontal temperature gradients that occur during a thermal bar the latter can be mapped using TIR images at spatial resolution as coarse as 1 x 1 km and temperature predictive accuracies ~ 0.1 ºC (Kondratyev & Filatov, 1999).

To some extent the phenomenon of thermal bars takes place in all lakes (Wetzel, 1975). In small lakes the duration of the spring thermal bar varies from hours to days, but in deep large lakes it may last for up to 2-3 months (Wetzel, 1975; Kondratyev & Filatov, 1999). In this study, the evolution of the spring thermal bar in Lake Vänern was observed. Three NOAA AVHRR scenes from 2001-2002 show various stages of the thermal bar formation (Figure 6-9).

After winter ice cover retreats, the lake water mixes and the LST of the entire lake body is less than 4 ºC. Due to increased solar radiation in spring the shallow near-shore areas are heated more rapidly compared to the offshore deep areas (Figure 6-9A). As a result, the temperature of the former increases and summer stratification is developed, while the deeper offshore areas keep mixing and remain isothermal at

temperatures less than 4 ºC. A narrow thermal bar zone then develops and acts like a boundary convergence zone between the shallow warm and deep cold areas. Horizontal temperature gradients exist during that period and are usually much higher in the near-shore stratified zone. Water density-induced circulation is established and downwelling occurs along the nearly vertical thermal bar (isotherm of 4 ºC) of both the warm and the cold zones (Figure 6-10). Upwelling occurs in the centre of the cold zone and near the lake shore in the warm zone. In Lake Vänern the thermal bar formation correlates strongly with the bathymetry of the lake (Figure 6-11). The near-shore shallow areas with depths less than 20 m are mostly found in the south and the northeast of the lake and it is there where temperature first rises above 4 °C.

As the water continues to be heated in early May the thermal bar progresses towards the deepest parts of the lake (Figure 6-9B). A small part of the west basin and most of the northern basin (the deepest part of the lake) are still under 4 °C. The temperature gradients during that period can be as high as 17 °C. Later in May the thermal bar disappears (Figure 6-9C) and the entire lake stratifies. (Wetzel, 1975; Malm & Jönsson, 1993; Kondratyev & Filatov, 1999).

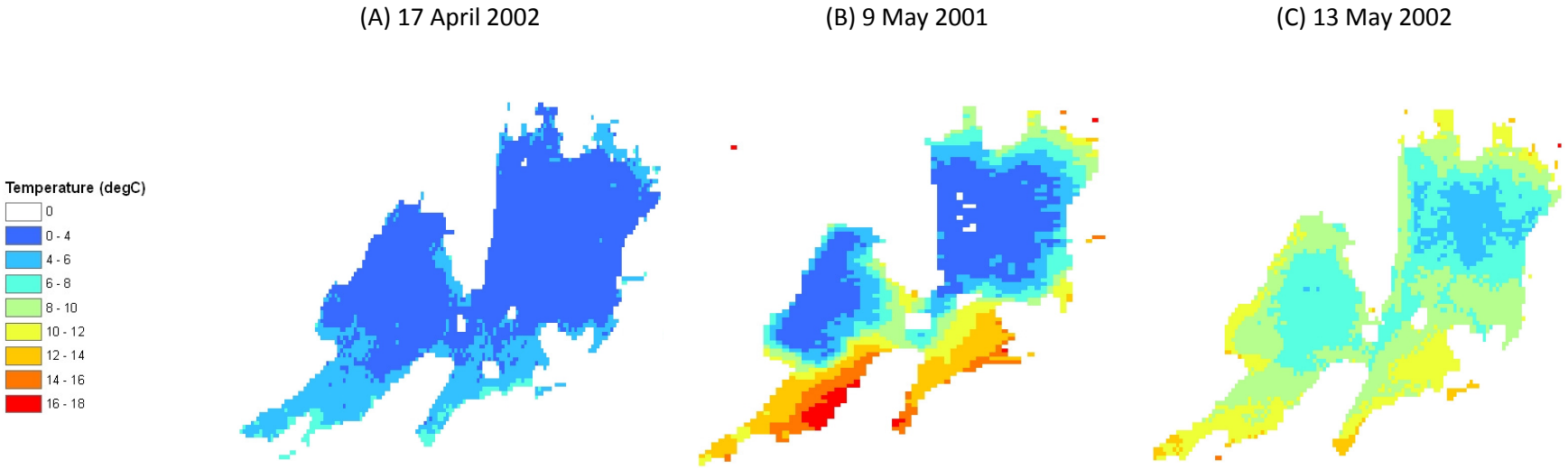

Figure 6-9: The evolution of the spring thermal bar in Lake Vänern. Dates from different years were used. The NOAA AVHRR MCSSTcal algorithm was used for the estimation of LST.

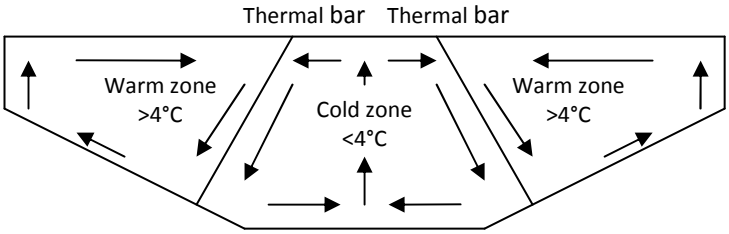

Figure 6-10: Schematic general density-induced spring circulation in a lake. Warm and cold zones with alternative upwelling and downwelling events are seen. Note the inclination of TB caused by the larger area of the cold zone near the bottom compared with that near the lake surface (Kondratyev & Filatov, 1999; p. 84).

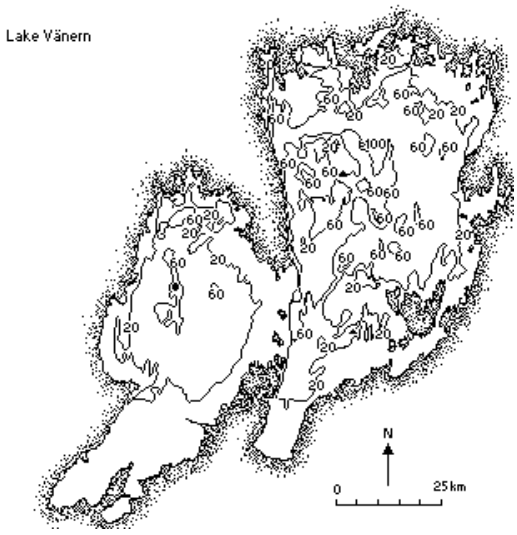

Figure 6-11: Bathymetric map of Lake Vänern (Source: ILEC, 2010).

In autumn, a thermal bar occurs in the opposite direction that is weaker than the spring thermal bar and is smoothed by the effect of strong wind-induced mixing. The shallow near-shore areas become colder and temperatures drop below 4 ºC, while the deeper offshore areas remain at higher temperatures. The autumn thermal bar

progresses towards the deeper water as the lake water cools down and finally disappears (Kondratyev & Filatov, 1999). Unavailability of sufficient data in autumn restricted the demonstration of the autumn thermal bar, but the potential of remote sensing has already been demonstrated for this application in spring-time.

6.2.5 Temporal patterns and spatial distribution of LST

Thematic temperature maps of the same lake in different months and seasons of a single year can help demonstrate the temporal patterns of the spatial distribution and variability of LST. Oesch *et al*. (2008) used NOAA AVHRR data to study permanent thermal features in Lake Geneva. They suggested that a cold zone in the centre of the lake and two warm zones appear on each side of the former during daytime in Lake Geneva and persist over time. Also, there is a cold-to-warm trend from NE to SW in the west narrow part of the lake (Oesch *et al*., 2008). Observations from year 2001 to year 2004 (Figure 6-12) suggest that in early spring (March), late spring (May) and late summer (August) a prominent cold zone (C1) in the centre of Lake Geneva and attached to the northern shore is clearly visible. Also, the two warm zones on each side of the cold zone clearly appear in the late summer image and correspond to the W1 and W2 warm cores that Oesch *et al*. (2008) described. A strong W2 warm core is also apparent in the early spring image, while the W1 warm core is less prominent on the same date. By contrast, W1 appears stronger in the late spring image and W2 is much weaker (Figure 6-12). The cold-to-warm gradient described by Oesch *et al*. (2008) in the most western part of the lake is not visible in any of the three images presented here.

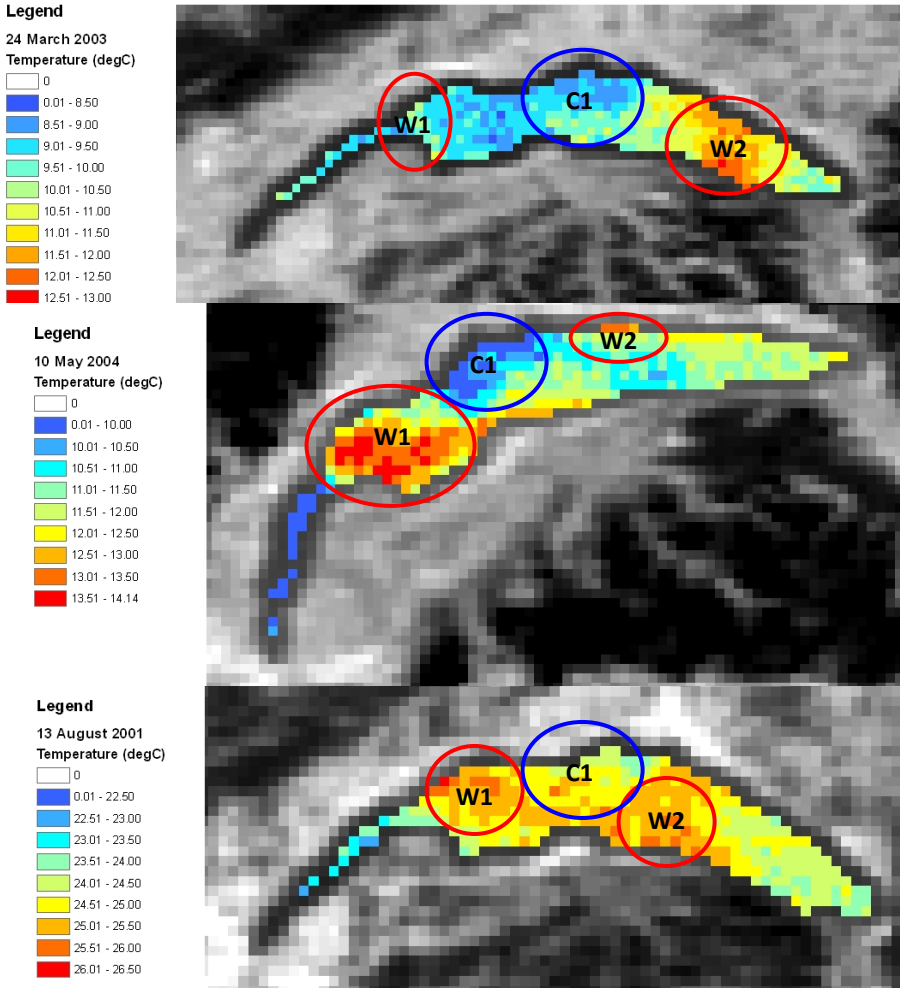

Figure 6-12: Spatial distribution of temperature in Lake Geneva: early spring (March), late spring (May), late summer (August); C1, W1-2 are permanent cold and warm cores (Oesch *et al.*, 2008).

In the case where two or more images of the same lake are available on the same day, which is not often the case with field measurements, one can also study thermal phenomena that occur at fine temporal scales of less than a day and detect differences in the spatial distribution of temperature that occur due to horizontal and vertical circulation. For each of the lakes Hjälmaren, Malaren and Oulujärvi two

NOAA AVHRR daytime images were available on 19th August 2002 with approximately 30 minutes difference between the overpasses.

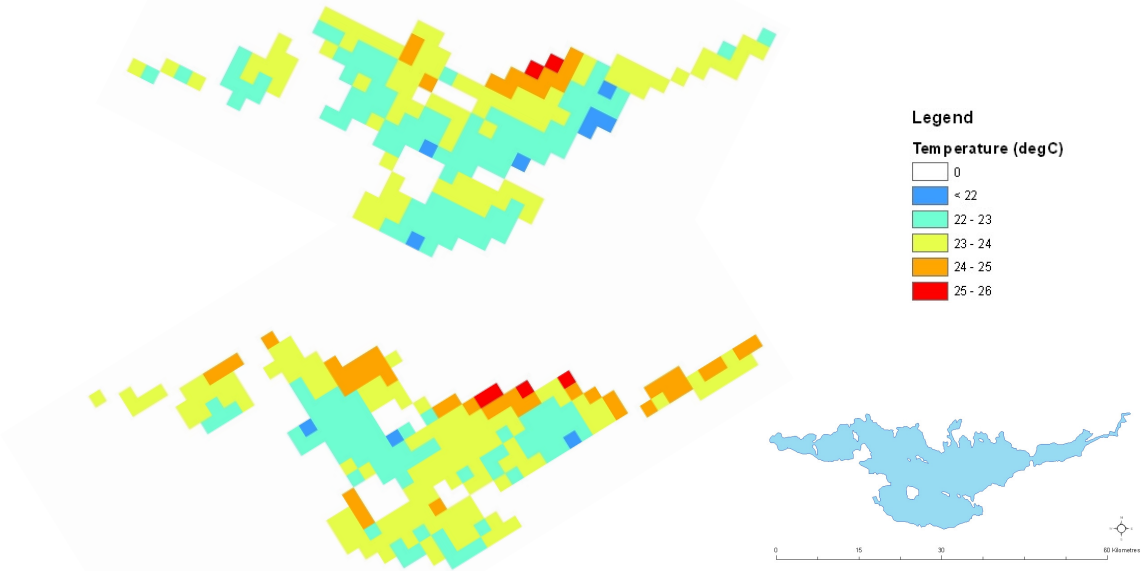

Figure 6-13: NOAA AVHRR MCSSTcal estimates in Lake Hjälmaren during two satellite overpasses within 30 minutes on 19th August 2002; (top) 1047 GMT; (bottom) 1114 GMT.

In Lake Hjälmaren the earlier image (1047 GMT) showed strong north-to-south gradients in temperature within the main lake body (Figure 6-13). Temperatures were lower (22-23 °C) in the south and increased towards the north shore where they were approximately higher by 2.5-3 °C. The same elevated temperatures along the north shore (compared to the rest of the lake surface) can be seen in the later image (1114 GMT) of the same lake, but in this image the main water body showed a more pronounced west-to-east variability in temperature. Two cold cores (22-23 °C) were located in the west and east of the main lake body and a warmer core (23-24 °C) in the centre of the lake stretching from the north to the south shore. Statistical analysis showed that the mean LST values from the entire lake surface between the two

scenes were significantly different (t = -6.48, $p < 0.01$) with the LSTs estimated for the later overpass being generally higher (Table 6-7).

Table 6-7: Statistical parameters calculated from two NOAA AVHRR scenes over Lake Hjälmaren acquired within 30 minutes on 19th August 2002; the MCSSTcal algorithm was used for the estimation of LST.

Statistical parameter	NOAA AVHRR (1047 GMT) (°C)	NOAA AVHRR (1114 GMT) (°C)
Minimum	21.55	21.62
Maximum	25.02	25.33
Range	3.47	3.71
Average	22.94	23.33
Standard deviation	0.59	0.70
Total number of pixels	210	249

In the earlier NOAA AVHRR scene over Lake Oulujärvi on 19th August 2002 (1047 GMT) the LST was generally uniform within the lake with a weak west-to-east gradient. Lower temperatures were observed in the west (17-18 °C) and higher in the east (19-20 °C) of the lake (Figure 6-14). The distribution of LST in the later NOAA AVHRR scene over Lake Oulujärvi (1114 GMT) was also fairly uniform and the same west-to-east temperature gradient was observed. Statistical analysis showed a significant difference in the mean LST values for the entire lake (t = -13.95, $p < 0.01$) with the temperatures in the later scene being relatively higher (Table 6-8).

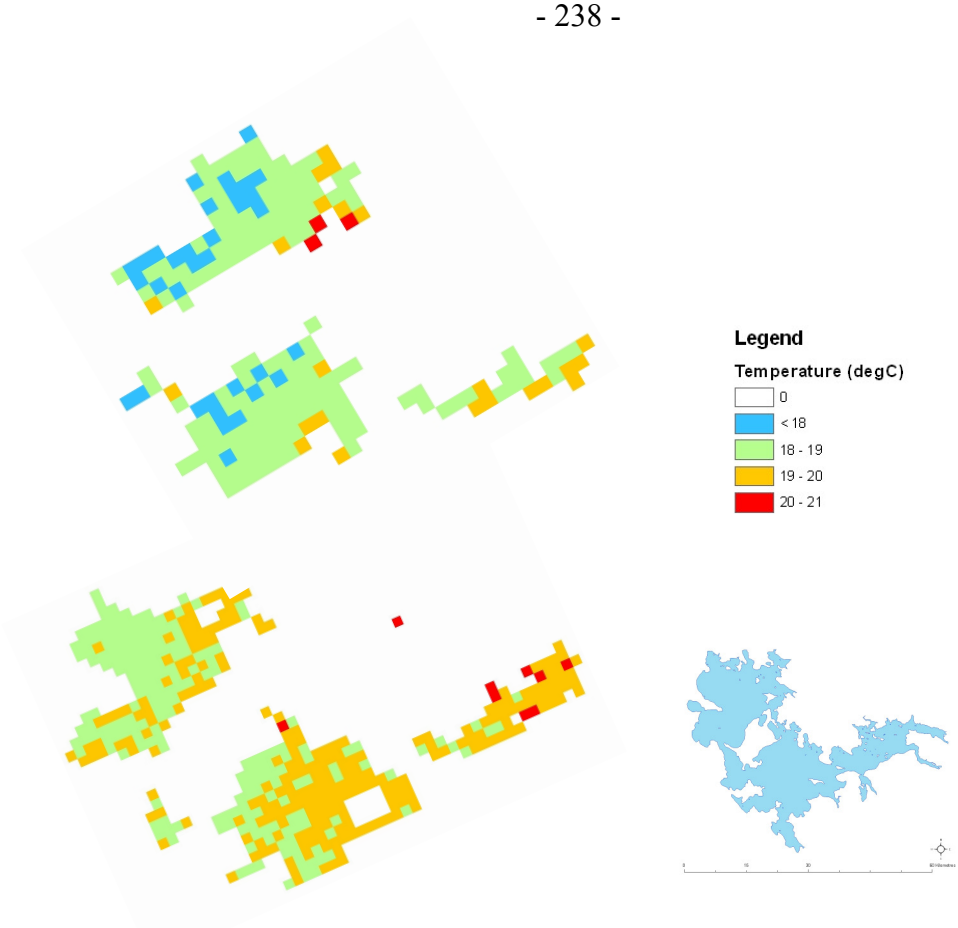

Figure 6-14: NOAA AVHRR MCSSTcal estimates in Lake Oulujärvi during two satellite overpasses within 30 minutes on 19th August 2002; (top) 1047 GMT; (bottom) 1114 GMT.

Table 6-8: Statistical parameters calculated from two NOAA AVHRR scenes over Lake Oulujärvi acquired within 30 minutes on 19th August 2002; the MCSSTcal algorithm was used for the estimation of LST.

Statistical parameter	NOAA AVHRR (1047 GMT) (°C)	NOAA AVHRR (1114 GMT) (°C)
Minimum	17.75	18.02
Maximum	20.90	20.62
Range	3.15	2.60
Average	18.50	19.04
Standard deviation	0.50	0.39
Total number of pixels	212	440

In both NOAA AVHRR images of Lake Malaren on 19th August 2002 the same west-to-east warm-to-cold temperature gradient was observed (Figure 6-15). However, in the later image the temperatures estimated by the MCSSTcal algorithm were generally higher compared to the earlier image (Table 6-9) and statistical analysis showed that the mean LST values for the entire lake surface differed significantly between the two images (t = -12.02, $p < 0.01$).

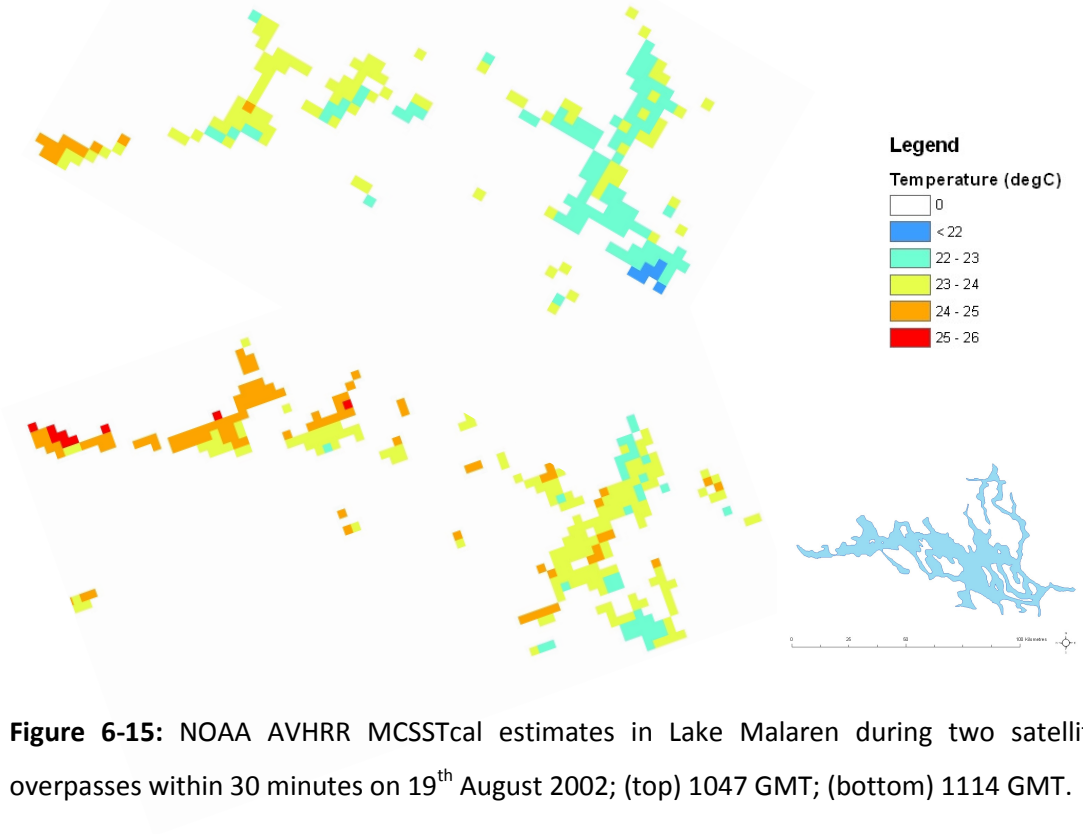

Figure 6-15: NOAA AVHRR MCSSTcal estimates in Lake Malaren during two satellite overpasses within 30 minutes on 19th August 2002; (top) 1047 GMT; (bottom) 1114 GMT.

The above observations for lakes Hjälmaren, Malaren and Oulujärvi in the late morning of a summer day showed that in all three lakes the average surface temperature rose between 0.39-0.66 °C within 30 minutes. The MCSSTcal algorithm has a predictive accuracy of ± 1.64 °C (Chapter 5, Section 5.2.1), which means that the observed difference between the two images might have been caused due to noise

within the algorithm. However, the temperature difference was consistently positive for all three lakes between the two images and thus might have occurred due to noise within the sensors (the two images derived from different NOAA AVHRR sensors that were calibrated differently).

Table 6-9: Statistical parameters calculated from two NOAA AVHRR scenes over Lake Malaren acquired within 30 minutes on 19th August 2002; the MCSSTcal algorithm was used for the estimation of LST.

Statistical parameter	NOAA AVHRR (1047 GMT) (°C)	NOAA AVHRR (1114 GMT) (°C)
Minimum	21.50	22.13
Maximum	24.96	25.65
Range	3.46	3.52
Average	23.06	23.72
Standard deviation	0.59	0.65
Total number of pixels	213	315

An advantage of remote sensing is that it covers wide spatial scales that can include more than one study site. In fact, the NOAA AVHRR with a swath width of 2400 km can cover most of the study sites of this project in a single overpass. The advantage of this is the simultaneous study of many lakes and the synoptic study of temperature distribution in lakes with various characteristics. In eastern and central European lakes estimated LST is much higher than in Scandinavian lakes in August with a clear decrease in LST as latitude increases (Figure 6-16). The difference between the second most southerly (but shallowest lake), Lake Balaton (13 August 2001), and the most northern lake of this study, Lake Inärijärvi (22 August 2001), was 14 °C.

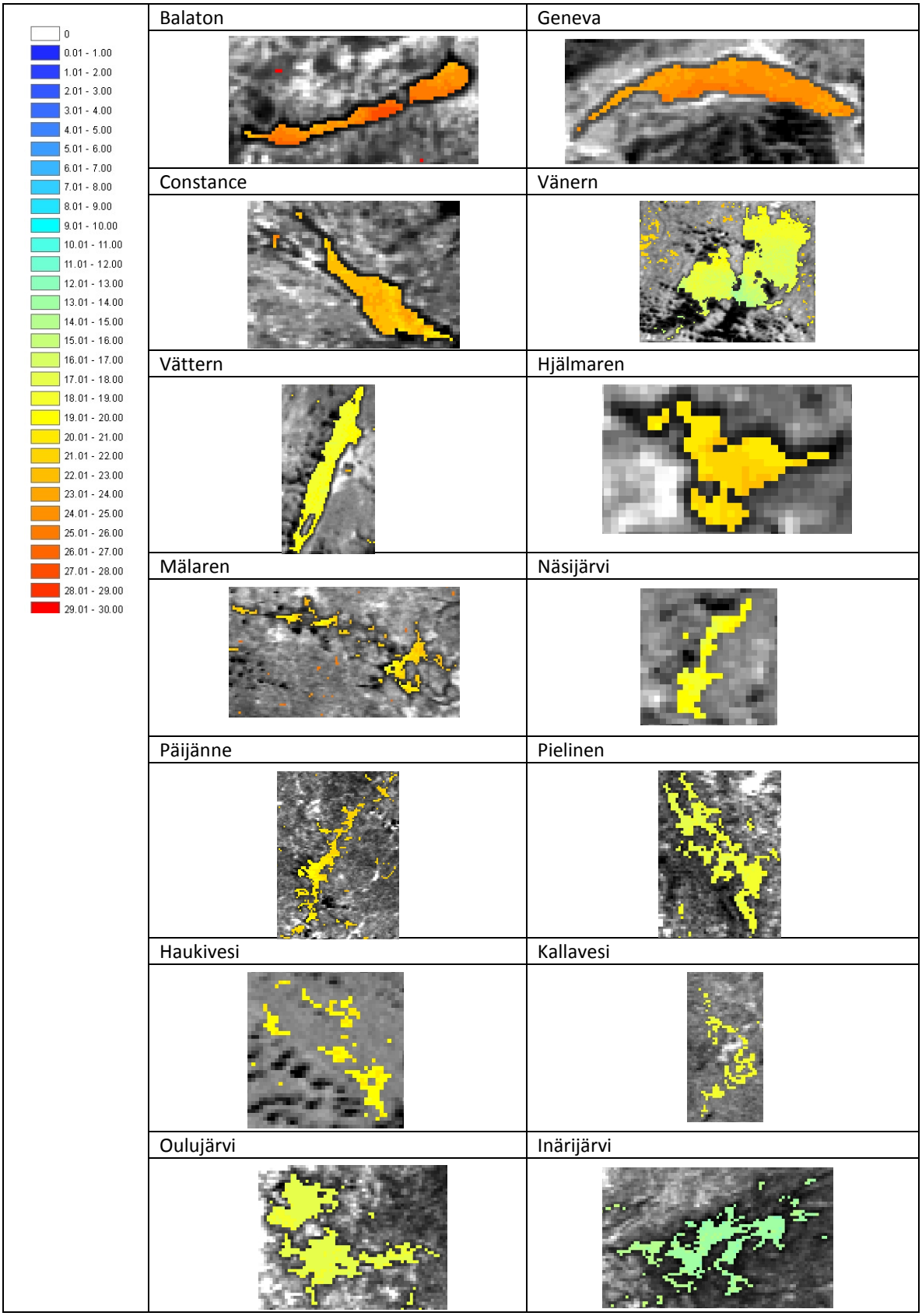

Figure 6-16: Spatial distribution of LST in fourteen large European lakes from NOAA AVHRR images acquired on various dates in August 2001.

The spatial distribution and temporal variability of LST for different dates throughout an entire year is presented for eight lakes in Appendix IV.

6.2.5.1 North-South and West-East spatial transects of LST

Spatial transects within a lake can reveal important information about the spatial variability and spatial tendencies of water quality parameters (Allee & Johnson, 1999). The north-south and west-east spatial transects in lakes Geneva and Vättern during stratification and mixing periods showed that the temperature gradients on the horizontal axis may vary considerably, depending on factors that influence the ephemeral character of surface temperature, for example wind induced circulation, partial upwellings and river plumes (Oesch *et al*., 2008). During mixing, the horizontal temperature gradients are less pronounced because the lake is under isothermal conditions (Wetzel, 1975) as seen for example in Lake Geneva in March (Figure 6-17A) and in Lake Vättern in October (Figure 6-18B) when temperature is highly uniform and the temperature gradients in both directions are very small compared to those during stratification. In July, Lake Geneva is thermally stratified and the two warm cores and the central cold core (as have been described by Oesch *et al*. (2008)) are visible and result in high temperature gradients across the lake surface from west-to-east at more than 3 °C (Figure 6-17B). In early September 2002 Lake Vättern showed a strong north-to-south temperature gradient that was equal to 4.56 °C (Figure 6-18A) and also corresponded well with the bathymetry of the lake (Figure 6-18A).

Such differences in the spatial distribution of lake surface temperature can have a pronounced effect on the aquatic life of lakes (e.g. Rajadurai *et al*., 2005; De Stasio

et al., 2009) and thus are considered ecologically important. However, it is important to highlight here once again that the above mentioned temperature gradients estimated by remote sensing reflect temperature variability of the uppermost layer of the lake and are not always representative of temperature variations that occur in layers just below the surface (Robinson, 1985; Cracknell, 1997).

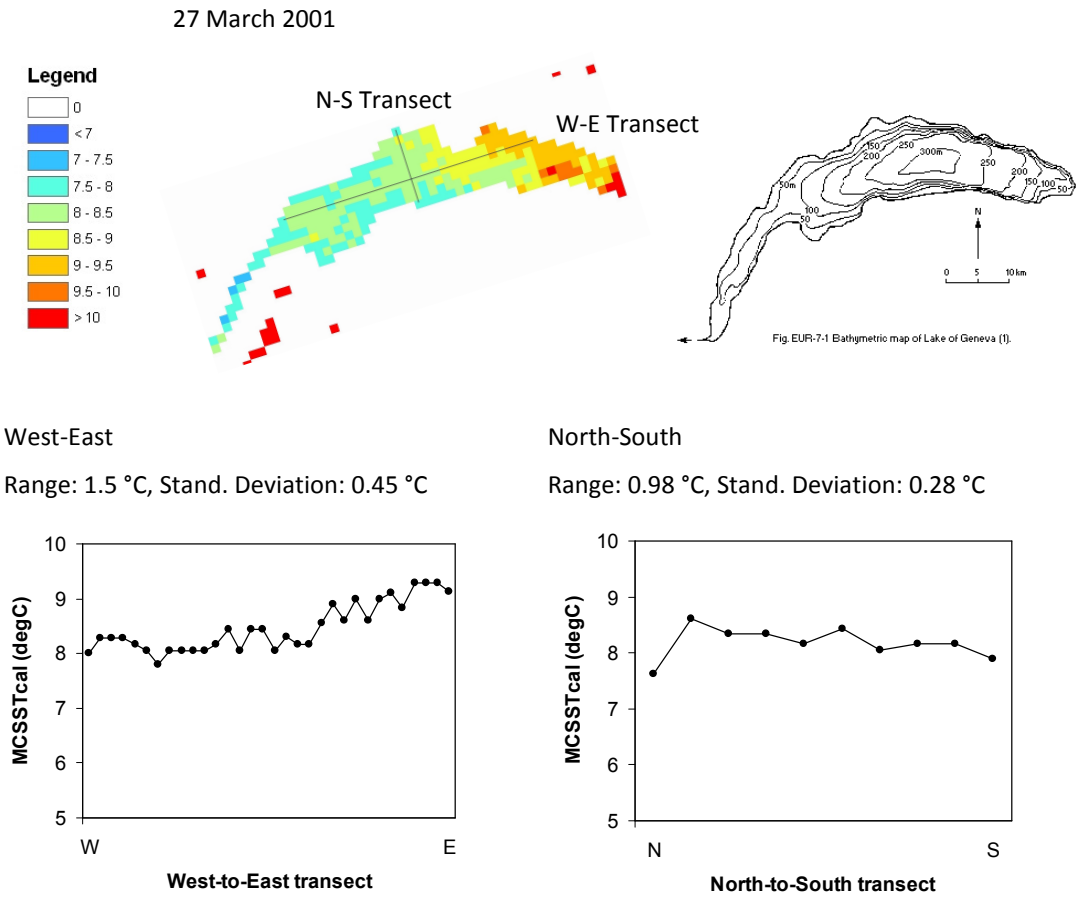

Figure 6-17A: North-South and West-East transects in Lake Geneva during mixing.

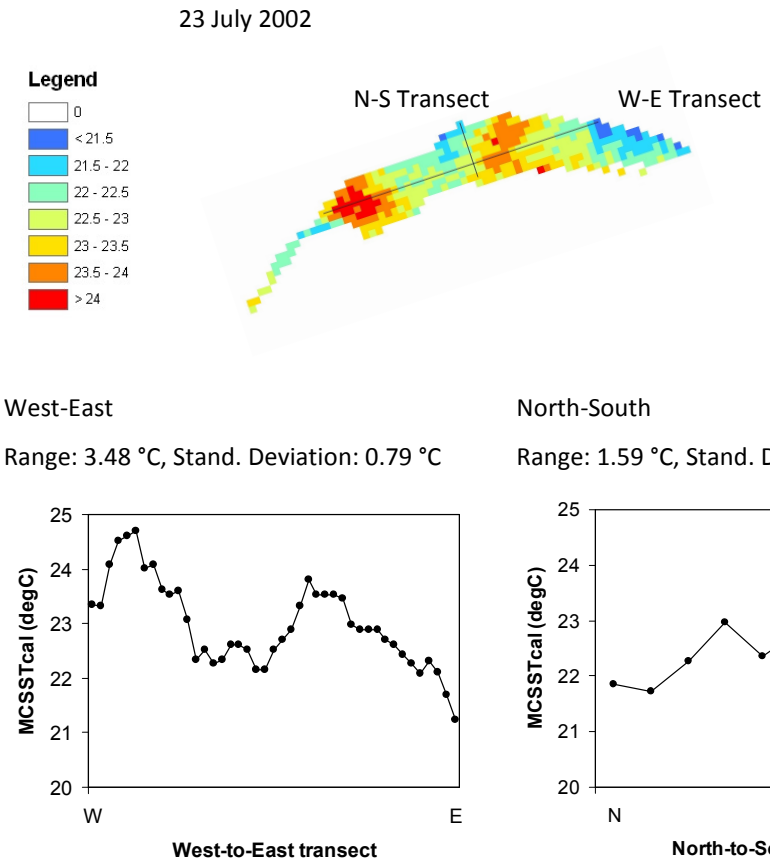

Figure 6-17B: North-South and West-East transects in Lake Geneva during stratification.

9 September 2002

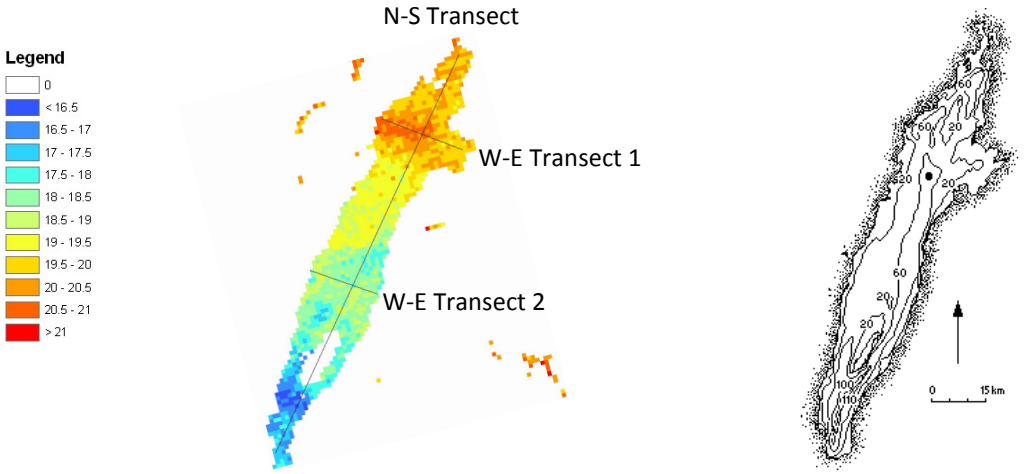

West-East 1

Range: 1.42 °C, Stand. Deviation: 0.42 °C

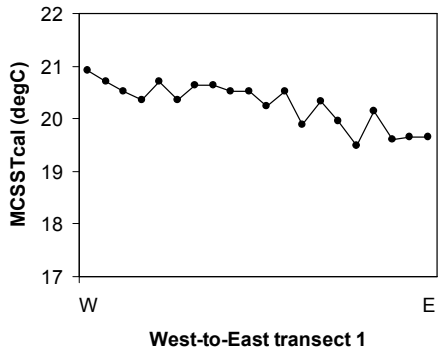

West-East 2

Range 2: 0.74 °C, Stand. Deviation: 0.20 °C

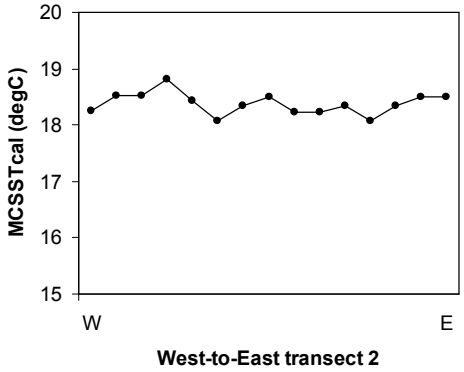

North-South

Range: 4.56 °C, Stand. Deviation: 1.15 °C

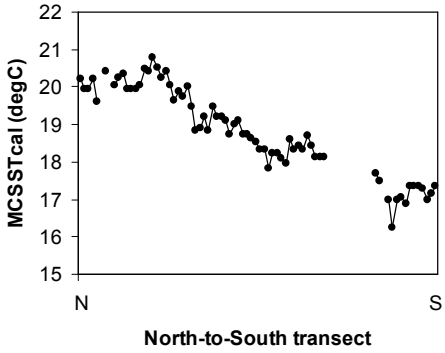

Figure 6-18A: North-South and West-East transects in Lake Vättern during stratification.

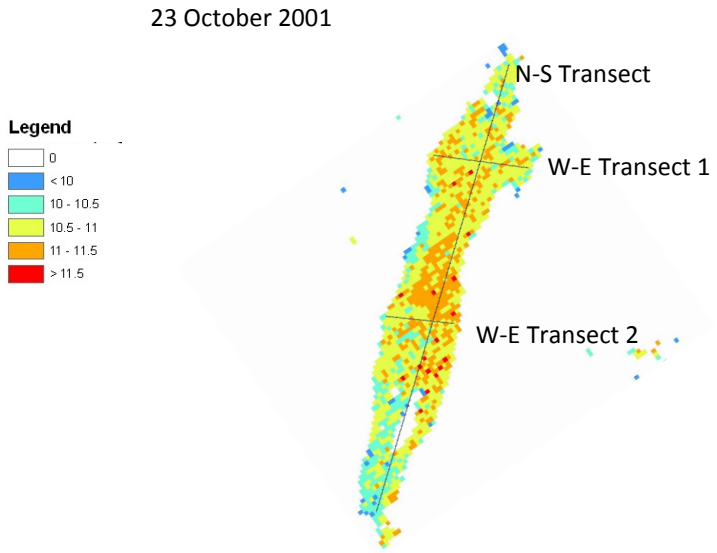

West-East 1

Range: 0.66 °C, Stand. Deviation: 0.20 °C

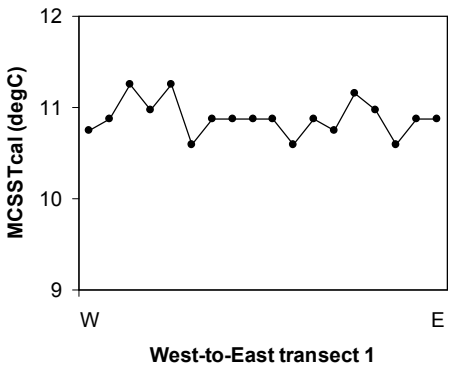

West-East 2

Range: 1.09 °C, Stand. Deviation: 0.29 °C

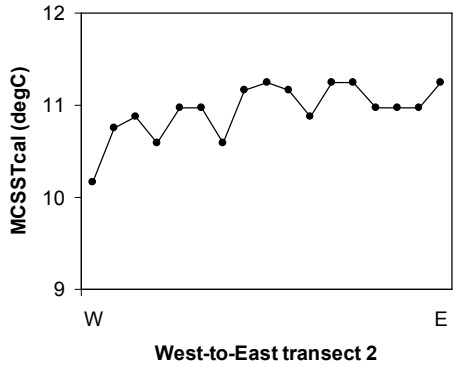

North-South

Range: 2.17 °C, Stand. Deviation: 0.43 °C

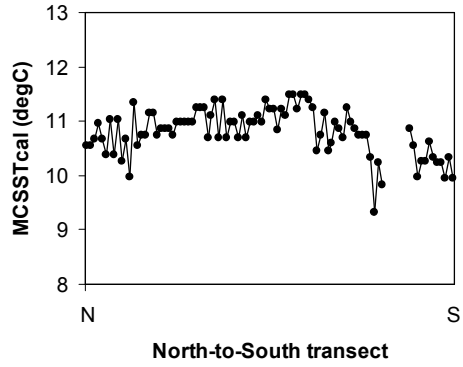

Figure 6-18B: North-South and West-East transects in Lake Vättern during mixing.

6.3 Chlorophyll *a* using Terra MODIS

There were not enough Terra MODIS data to perform analyses at similar levels of detail as for the NOAA AVHRR LST data. For example, the Terra MODIS chlorophyll *a* estimates were not sufficiently frequent to perform interpolation. In Lake Vänern in 2001-04, both field chlorophyll *a* measurements and satellite estimates were rather sparse (Figure 6-19). However, Lake Vänern is oligotrophic and the seasonal variability of phytoplankton was low in the years 2001-04 (annual range (i.e. difference between annual maximum and minimum) varied from 1.3-2.4 µg L^{-1}). The temporal variation seen in the field data was not well depicted with the remotely sensed data suggesting that the algorithm has limited potential for estimating chlorophyll *a* in oligotrophic lakes and requires improvement.

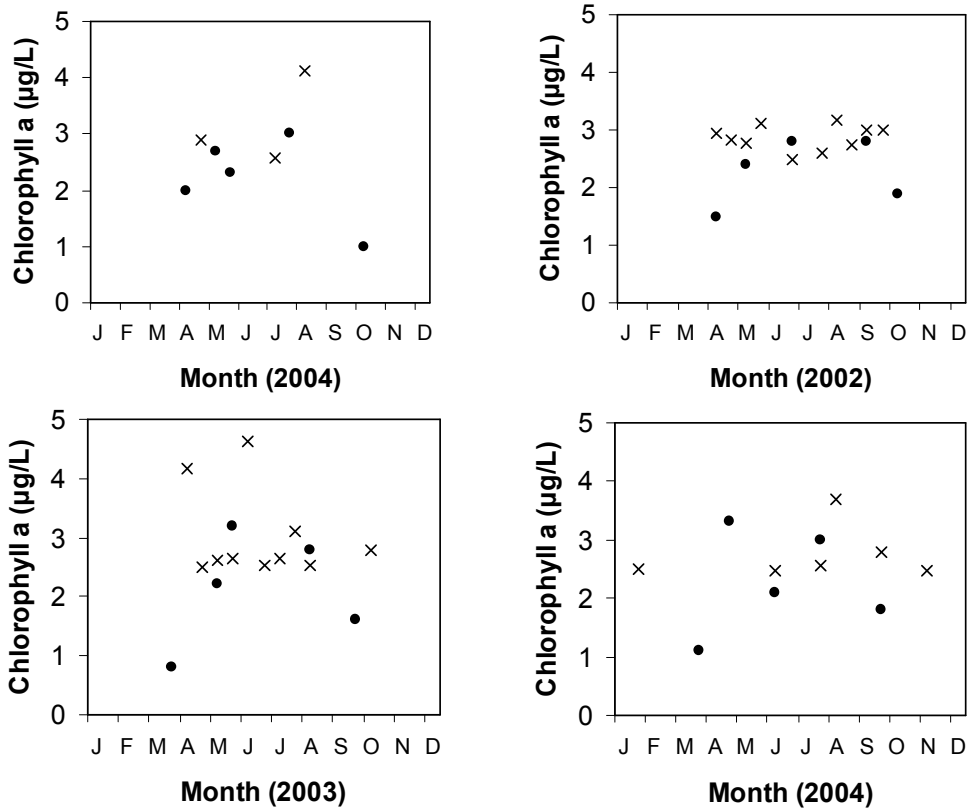

Figure 6-19: Temporal variability of chlorophyll *a* in Lake Vänern (Station Tärnan) in 2001-04; Field data (black dots) and Terra MODIS Politi chlorophyll *a* estimates (crosses).

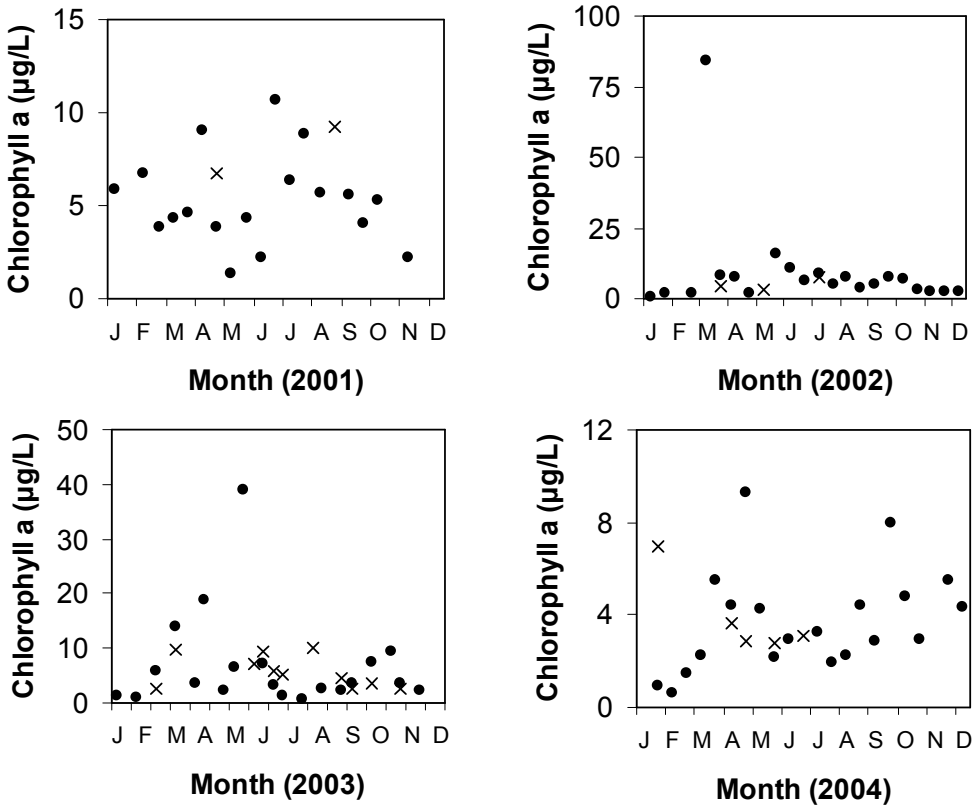

Figure 6-20: Temporal variability of chlorophyll *a* in Lake Geneva in the years 2001-04; Field data (black dots) and Terra MODIS Politi chlorophyll *a* estimates (crosses).

In Lake Geneva, chlorophyll *a* generally showed high seasonal variability in 2001-04 (Figure 6-20). In early spring 2002 and early summer 2003 the field measurements showed a large increase of phytoplankton growth that exceeded 30 µg L^{-1} and lasted less than 4 weeks in 2002 and less than 2 weeks in 2003. In fact, in 2003 a Terra MODIS Politi chlorophyll *a* estimate derived a week after the field measurement (38.95 µg L^{-1}) suggested that the phytoplankton growth had already decreased to about 7 µg L^{-1}. Despite the scarcity of satellite data, the Terra MODIS Politi chlorophyll *a* estimates in Lake Geneva did not depict well the temporal variability of field measurements on the dates available.

6.4 Secchi disk depth using Terra/Aqua MODIS

In the oligotrophic Lake Vänern, SDD showed low seasonal variability between spring, summer and autumn. In 2001-04 the available field measurements showed SDD annual ranges (difference between minimum and maximum annual SDD) between 0.7-1 m (Figure 6-21). In the same years, the Terra MODIS Politi SDD algorithm produced values with a slightly narrower range (0.41-0.88 m) than that of the field SDD measurements. The algorithm seemed incapable of capturing the seasonal variability of SDD in Lake Vänern (Figure 6-21).

By contrast, in mesotrophic Lake Geneva the seasonal variability of SDD was much higher and the SDD annual range in 2001-04 varied between 5.6-11.7 m. There were only few Terra MODIS images available to estimate SDD from, but the results showed that the algorithm seemed to perform moderately well in terms of mapping the temporal variability of Secchi disk depth on the dates available (Figure 6-22). The annual range for satellite estimates in 2001-04 varied between 0.1-2.4 m, however satellite data were not available for all seasons. In conclusion, more data are needed to investigate the full potential of the Terra MODIS Politi SDD algorithm in oligotrophic, mesotrophic and eutrophic lakes.

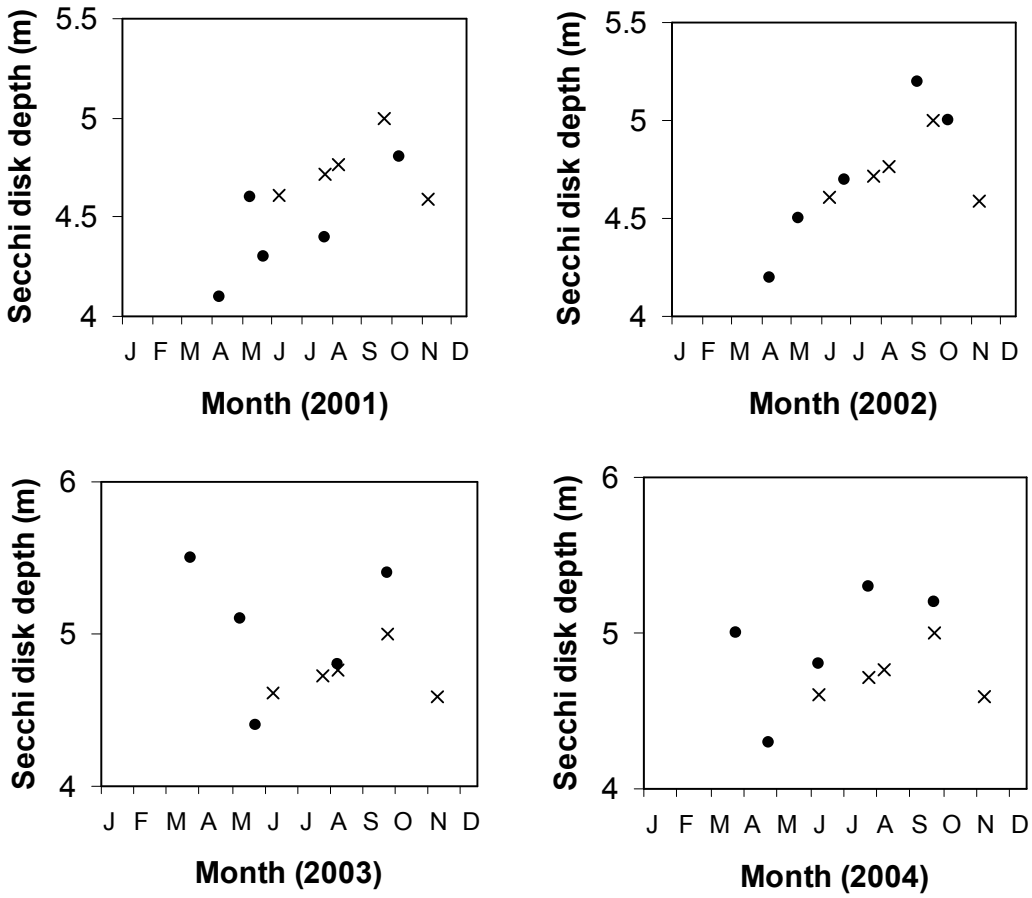

Figure 6-21: Temporal variability of Secchi disk depth in Lake Vänern (Station Tärnan) in the years 2001-04; Field data (black dots) and Terra MODIS Politi SDD estimates (crosses).

There were much more Aqua MODIS images available than Terra MODIS, but they were limited to only four study sites. Aqua MODIS images were available on each day of the second half of 2002 and the entire 2003-04 period, but most days were cloudy. Data from Lake Geneva in 2003 were used to test the potential of Aqua MODIS in mapping Secchi disk depth and the applicability of the Aqua MODIS Politi SDD algorithm.

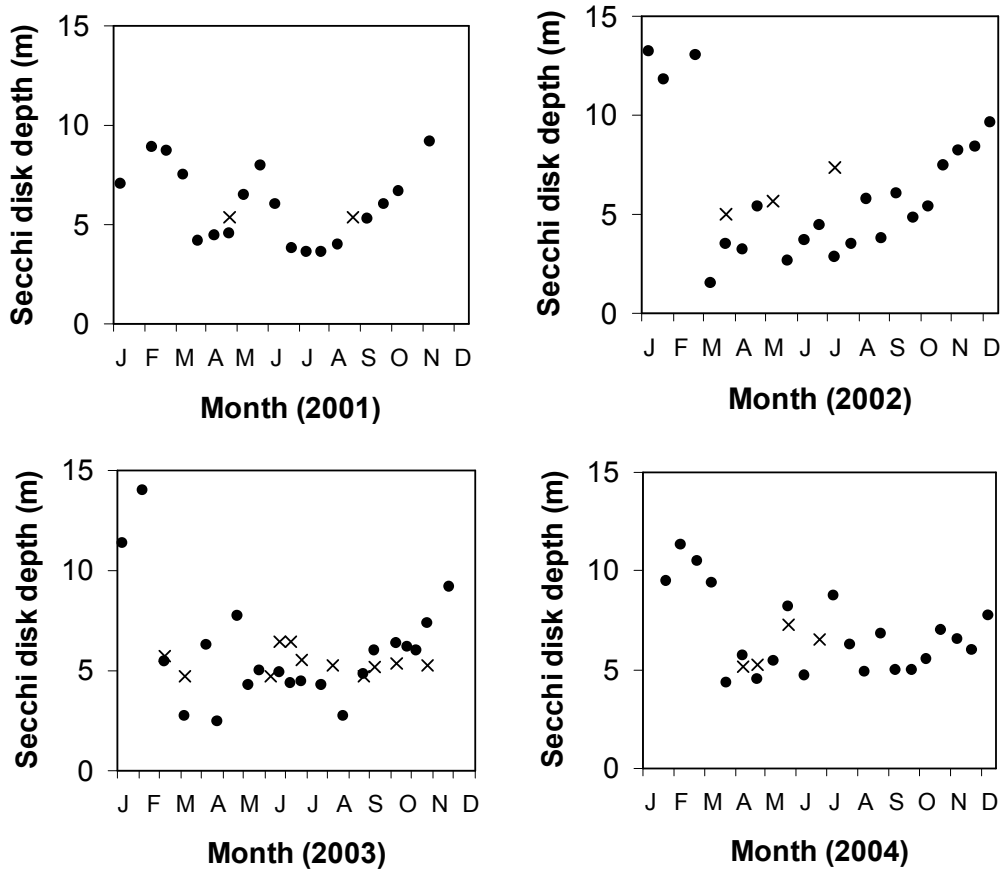

Figure 6-22: Temporal variability of Secchi disk depth in Lake Geneva in the years 2001-04; Field data (black dots) and Terra MODIS Politi SDD estimates (crosses).

The Aqua MODIS Politi SDD estimates exhibited a smaller degree of seasonal variability (4-8.8 m) than the field data (2.5-14 m) even though both field and satellite data were very frequent and covered all months and seasons (Figure 6-23). The satellite estimates were not capable to reproduce the winter SDD maxima (February SDD = 14 m, December SDD = 9.2 m) that coincided with low primary production and spring minima (March SDD = 2.7 m, April SDD = 2.5 m) that coincided with peaks in phytoplankton growth. In fact, the algorithm seemed to underestimate high values (> 7 m) and overestimate low values (< 5 m), however it seemed to perform well for intermediate SDD values of 5-7 m.

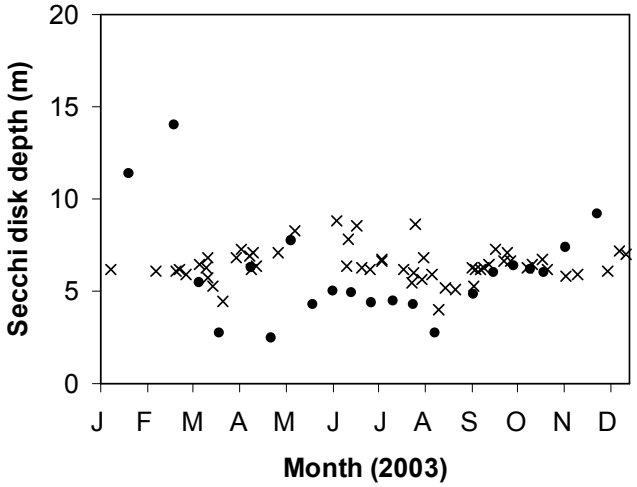

Figure 6-23: Temporal variability of Secchi disk depth in Lake Geneva in 2003; Field data (black dots) and Aqua MODIS Politi SDD estimates (crosses).

Thematic maps of the spatial distribution of SDD in Lake Geneva were created for nine cloud-free days (Figure 6-24). The thematic maps offer an important amount of information on the ecological processes that take place within the lake (Allee & Johnson, 1999). For example, Secchi disk depth is homogeneous throughout the lake during the mixing period (Livingstone, 1993) that in Lake Geneva lasts between late October and February. In March, spring turnover takes place in Lake Geneva and then stratification is established throughout spring and summer. During that period transparency is heterogeneous (Figure 6-24), depending on the spatial variability of phytoplankton, suspended sediments and particulate organic matter (Welch, 1935).

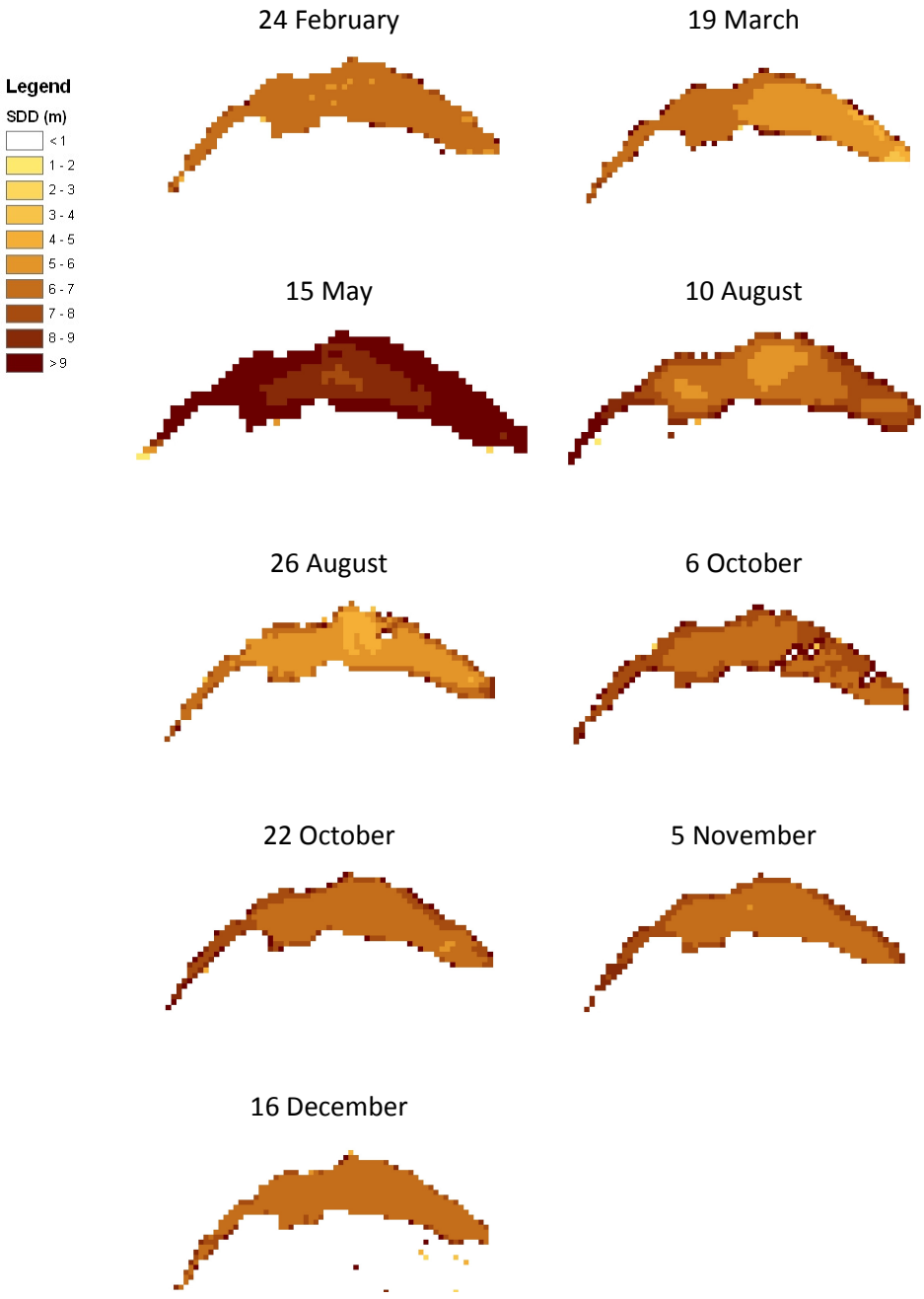

Figure 6-24: Secchi disk depth in Lake Geneva in 2003 estimated with the Aqua MODIS Politi SDD estimation algorithm.

6.5 Interactions between water quality parameters

This section presents reflections on the interactions of the three water quality parameters studied in this project because of their mutual ecological influence (Fraser, 1998). Elevated temperatures affect primary production within the lake. Studies have shown that mild winters and earlier spring warming of lakes lead to earlier phytoplankton development and peak (e.g. Adrian *et al*., 1999; Gerten & Adrian, 2000). Also, increased water turbidity limits incoming light that is available for photosynthesis by decreasing light penetration. On the other hand, increased primary production leads to higher numbers of algal cells that in turn decrease water transparency (Welch, 1935; Wetzel, 1975).

In Lake Geneva, the seasonal variability of the three parameters was plotted on the same graph for comparison (Figure 6-25). As temperature rises in spring, phytoplankton growth rates increase and three peaks occur in late March (14.01 µg L^{-1}), late April (18.80 µg L^{-1}) and early June (38.95 µg L^{-1}). The last peak is also the greatest in 2003 according to the available field measurements. In summer and early autumn, primary production decreases (< 3 µg L^{-1}). The Secchi disk depth, which is at maximum in winter during mixing (> 10 m), exhibits two minima in March (2.7 m) and April (2.5 m) that correspond to the phytoplankton peaks. During stratification in late spring, summer and early autumn, transparency is quite low (< 5 m) and increases towards winter as mixing occurs. A smaller phytoplankton peak occurs in early November and then chlorophyll *a* concentrations drop to the minimum winter values (< 2 µg L^{-1}).

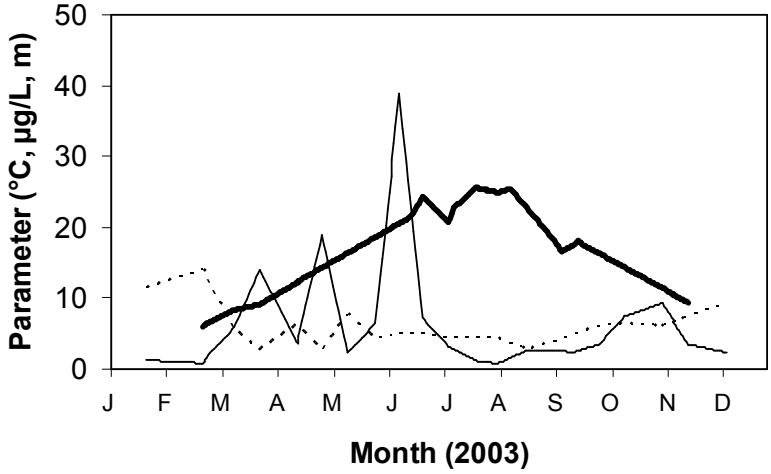

Figure 6-25: Interaction between NOAA AVHRR MCSSTcal LST estimates (thick line), field chlorophyll *a* (thin line) and field SDD (dotted line) in Lake Geneva in 2003.

SDD can be influenced by various water components, including phytoplankton, suspended sediment and organic detritus (Section 2.2.4.2). In this project, Terra MODIS data were used to demonstrate the influence of algal cells (that contain chlorophyll *a*) on SDD variations by producing thematic maps of the two parameters under consideration in two study sites. On 9th May 2001 in Lake Geneva there is a low-to-high chlorophyll *a* gradient in the main basin from southwest to northeast (Figure 6-26). High levels of primary production occur in the north-eastern part of the lake due to the inflowing River Rhône that carries nutrients into the lake basin (Oesch *et al*., 2008). The SDD estimates show higher transparency in the southwest (that corresponds to lower chlorophyll *a* concentrations) and lower transparency in the northeast (that corresponds well to higher chlorophyll *a* concentrations found in the proximity of the Rhône estuary). A similar agreement between the estimates of the two parameters was also exhibited on 16th May 2002 in Lake Constance (Figure 6-27). In Lake Constance, the River Rhein flows into the lake basin in the southeast

resulting in relatively higher nutrient concentrations and in turn increased levels of productivity in that area compared to the rest of the lake (ILEC, 2010).

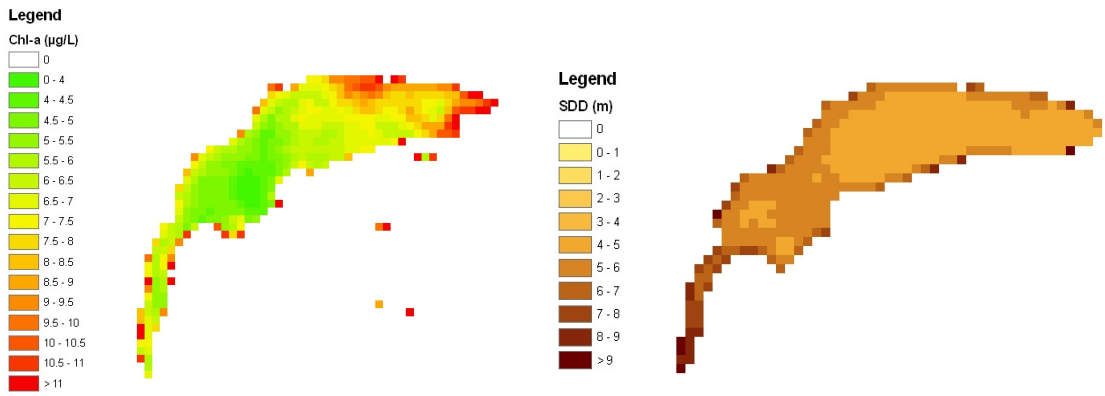

Figure 6-26: Spatial variability of chlorophyll *a* and SDD in Lake Geneva on 9th May 2001; Terra MODIS Politi chlorophyll *a* and Terra MODIS Politi SDD estimates.

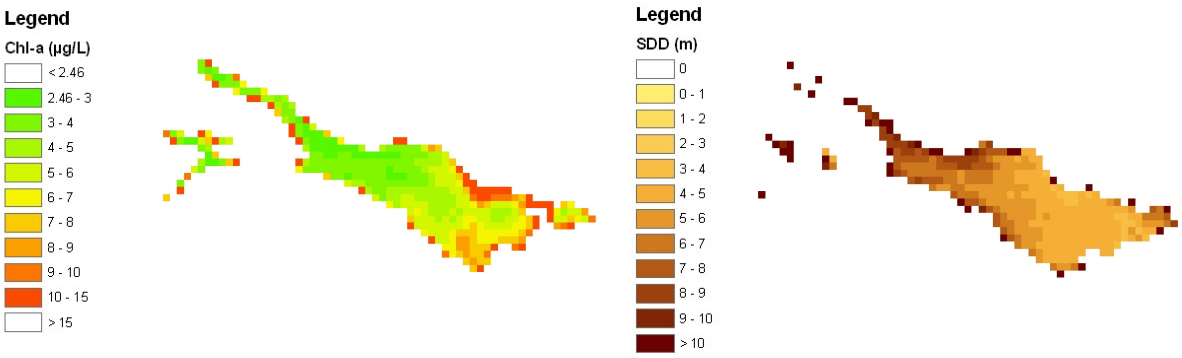

Figure 6-27: Spatial variability of chlorophyll *a* and SDD in Lake Constance on 16th May 2002; Terra MODIS Politi chlorophyll *a* and Terra MODIS Politi SDD estimates.

6.6 Sources of error and uncertainty in remotely sensed estimates

In Chapter 2 (Section 2.4.3) two sources of uncertainty (i.e. atmospheric effects and surface effects) that affect the accuracy of water quality parameter estimations were discussed. However, uncertainty and errors can also be introduced during data

acquisition and processing, and include sensor-related errors, geometric distortions, scaling issues, undetected cloud cover, mixed pixels, parameter-related uncertainty and other factors.

6.6.1 Sensor-related uncertainty

Uncertainty can be introduced because of the satellite sensor itself. For example, errors during the in-flight calibration of the NOAA AVHRR introduce uncertainty in the LST estimations of the range of 0.31 °C, whereas random thermal noise in the sensor accounts for errors around 0.05 °C (Robinson, 1985). For NOAA AVHRR data calibration is performed using measurements from floating instrumented buoys. These buoys measure water surface temperature at depths from 0.5 to 1.0 m while the NOAA AVHRR estimates skin temperature by measuring emission from the top few millimetres of the water surface (Schluessel *et al*., 1990), which suggests a certain degree of error during calibration. However, the impact of these errors depends on the application (Cracknell, 1997). In studies, where the relative differences of temperature are required, such as the study of the evolution of eddies or the location of fronts, the accuracy of calibration is less important than sensor noise. In other situations, where the average values of the water surface temperature are required and comparisons are made within different overpasses, the effective calibration of the sensor is more important (Robinson, 1985).

6.6.2 Geometric distortions

Geometric distortions are common within a remote sensing image. According to Oesch *et al*. (2008) a large scan angle (> 24°) introduces a duplication of pixels in

Terra/Aqua MODIS imagery that is identified by homogeneous horizontal stripes. This effect causes repetition of features at every 10th scan line and is called the 'bow-tie' effect (Wang *et al*., 2010). The 'bow-tie' effect was obvious in many Terra/Aqua MODIS images available in this project and it is clearly depicted in the chlorophyll *a* map of Lake Vättern on 9th May 2001 and in the SDD map of the same lake on 10th September 2002 (Figure 6-28). In smaller lakes and depending on the scan angle, this distortion can be more severe. An example is presented for lakes Geneva and Constance (Figures 6-29 and 6-30). On 4th August 2003 both lakes appear largely distorted and the same is true for Lake Constance on 7th June 2004. Fewer distortions were observed in Lake Geneva on 7 July 2003 and 7th June 2004 due to smaller scan angles (Gómez-Landesa *et al*., 2004). The 'bow-tie' effect is a well known distortion in Terra/Aqua MODIS imagery and can be corrected (e.g. Gómez-Landesa *et al*., 2004; Wen, 2008), however, the images available for this project were not geometrically corrected prior to acquisition (as discussed in Chapter 4) and as a result only the central part of the images were used where to 'bow-tie' effect is minimal (Gómez-Landesa *et al*., 2004). The latter significantly decreased the number of available data for analysis. For example, it was calculated that in 2003 there were 69 cloud-free Aqua MODIS images above Lake Geneva, 33% of which were highly distorted due to the 'bow-tie' effect.

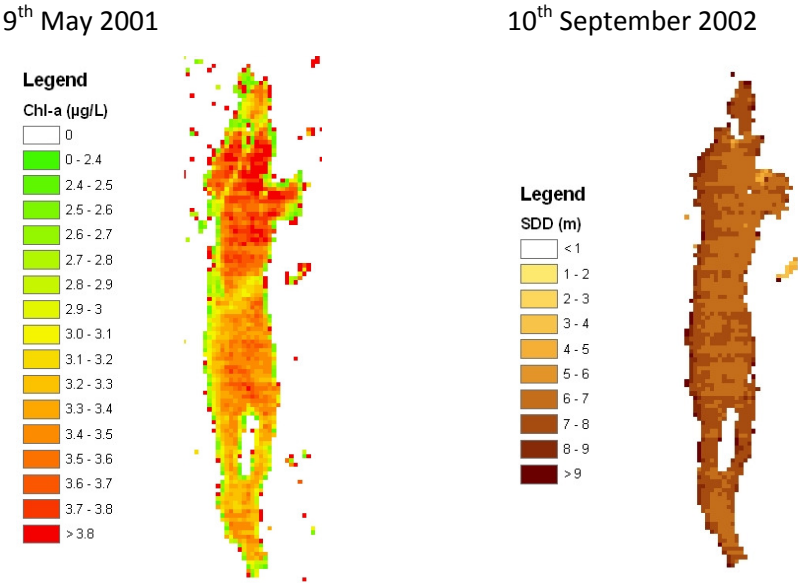

Figure 6-28: Chlorophyll *a* and SDD spatial distribution in Lake Vättern on 9th May 2001 (left) and 10th September 2002 (right); Terra MODIS Politi chlorophyll *a* and SDD estimation algorithms.

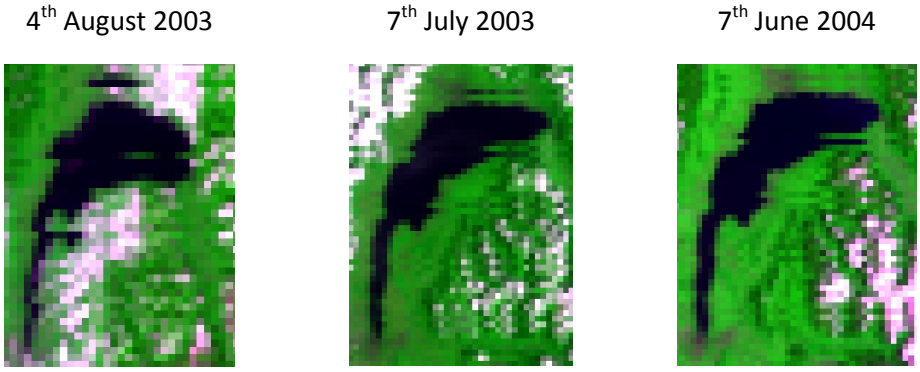

Figure 6-29: Terra MODIS RGB123 images of Lake Geneva illustrating the 'bow-tie' effect.

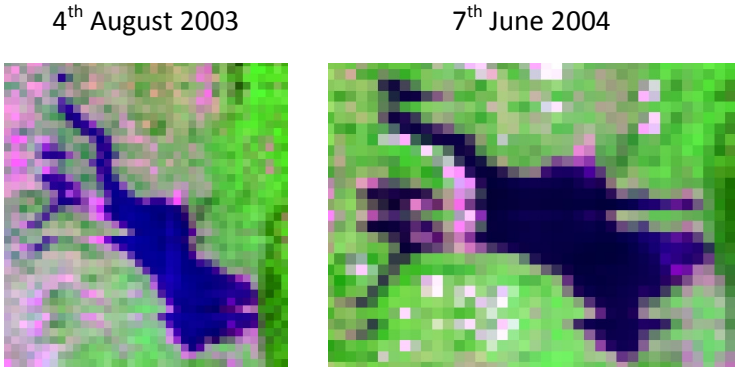

Figure 6-30: Terra MODIS RGB123 images of Lake Constance, illustrating the 'bow-tie' effect.

During geometric correction, transformations are applied to resample the image into a grid of known coordinates (Rees, 1990), but positional errors are always introduced during the process. In order to compensate for the latter, it is common in limnological remote sensing studies to use an average of values from a N x N pixel grid (where N = 2, 3, 4,…, *etc*.) centred at the location of the point field measurement. In that way the positional uncertainty of the field measurement in the image (that occurs due to errors of geometric corrections of the image) is reduced. The size of the averaged pixel grid used varies, depending on the application. Kallio *et al*. (2001), Pulliainen *et al*. (2001) and Kallio *et al*. (2003) used a 20 x 20 m averaged grid, while Kopenen *et al*. (2002) used 100 x 100 m averaged grid. George (1997b) used a 30 x 30 m averaged grid, which was large enough to minimize the variance associated with small spatial scale features, but small enough to study systematic patterns in lake waters. The use of a 90 x 90 m grid was considered most effective by Baban (1993) as it dampened noise in the data (Baban, 1993).

6.6.3 The scale issue

Each remote sensing estimate is representative of an area equal to the spatial resolution of the sensor. That means that these estimates are actually the average value or concentration of the parameter under consideration over that area. By contrast, field measurements are collected from point locations and thus uncertainty arises when these are compared to remotely sensed estimates. If there are any variations in the parameters under consideration throughout the instantaneous field of view of the sensor there will be a difference between the remotely sensed (areal) estimate and the point measurement (Cracknell, 1997). Clearly, the significance of

that difference depends strongly on the degree of spatial variability of the parameter, but studies have shown that phytoplankton biomass can vary considerably (e.g. two orders of magnitude) in 1 km^2 (Kutser, 2009).

Also, the spatial distribution of parameters such as chlorophyll *a* can be affected by water circulation features at time scales of less than a day and as a result, the temporal separation between the field measurements and the satellite overpass should be minimal (Lavender *et al*., 2004). In this project the timing of field data collection was not always known but priority was given to morning-to-early-afternoon overpasses, as this was when most field data sampling took place.

6.6.4 Cloud cover

According to Oesch *et al*. (2005) undetected cloudy pixels can be an error source in the estimates of lake water surface temperature, and the same can be true with the estimation of other water quality parameters as well. A remote sensing image that is completely cloud-free or covered by large thick clouds is easy to process and mask for clouds (Cracknell, 1997). However, it is rather common to have scattered or broken clouds. In that case it is rather important to detect and remove all cloud pixels, but also neighbouring pixels that might be contaminated by cloud scattering and cloud shadows (Oesch *et al*., 2008). The most difficult case is when thin clouds, haze or subpixel sized clouds exist that are smaller than the IFOV of the sensor used. If those cloud-contaminated pixels are not effectively removed, the satellite-derived parameter for a cloud-contaminated pixel will be different (either lower or higher) than it would be if the clouds were not there (Cracknell, 1997). An example of the latter is shown in Lake Vänern on 10th September 2002 (Figure 6-31). On that day,

there were two cloud strips located over the west basin of the lake. One of them (in the south) was successfully removed during cloud masking, but the second (in the north) was not detected resulting in cloud contaminated pixels that appeared as a strip of relatively higher chlorophyll *a* concentrations and relatively higher SDD values compared to surrounding water pixels.

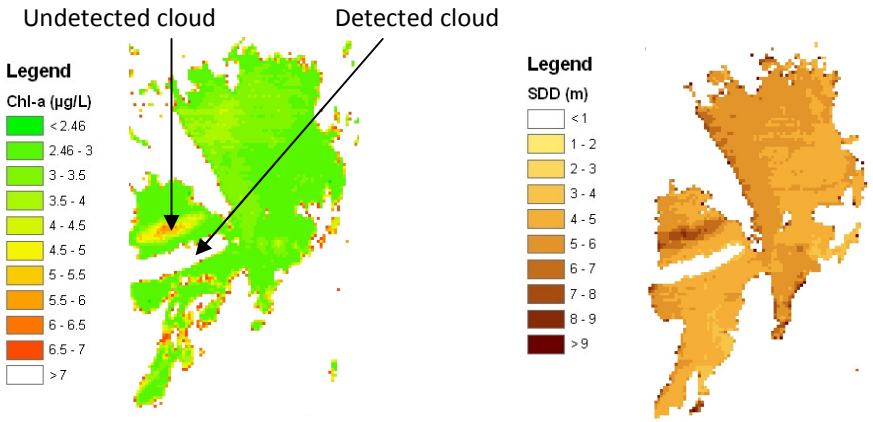

Figure 6-31: Chlorophyll *a* and SDD spatial distribution in Lake Vänern on 10th September 2002; Terra MODIS Politi chlorophyll *a* and SDD estimation algorithms.

6.6.5 Adjacency effect and mixed pixels

The adjacency effect is a phenomenon that occurs within pixels close to land-water boundaries (or any bright/dark boundary), where effectively the signal from pure water pixels is affected by scattered radiation from neighbouring land (Odermatt *et al*., 2008). The adjacency effect occurs in the visible and nIR spectral regions and is greatly influenced by the amount and vertical distribution of aerosol particles in the atmosphere (Minomura *et al*., 2001). It causes an overestimation of atmospheric radiance over the affected pixels and a subsequent underestimation of water leaving radiance (Ruiz-Verdú *et al*., 2008). However, it is very strong in near-shore areas and

decreases exponentially with distance from the shore (Minomura *et al*., 2001) and as a result the omission of near-shore pixels should account for the problem (e.g. Lavender *et al*., 2004, Bussières *et al*., 2002). The adjacency effect should be also taken into account around islands within the lakes. The adjacency effect is demonstrated here in two Terra MODIS scenes over lakes Vänern and Hjälmaren on 9th May 2001. The Politi chlorophyll *a* algorithm was applied to the scenes and the pixels adjacent to land can be easily identified; they appear red in the colour scale assigned to the maps (i.e. chlorophyll *a* concentrations greater than 3.8 μg L^{-1}) (Figure 6-32).

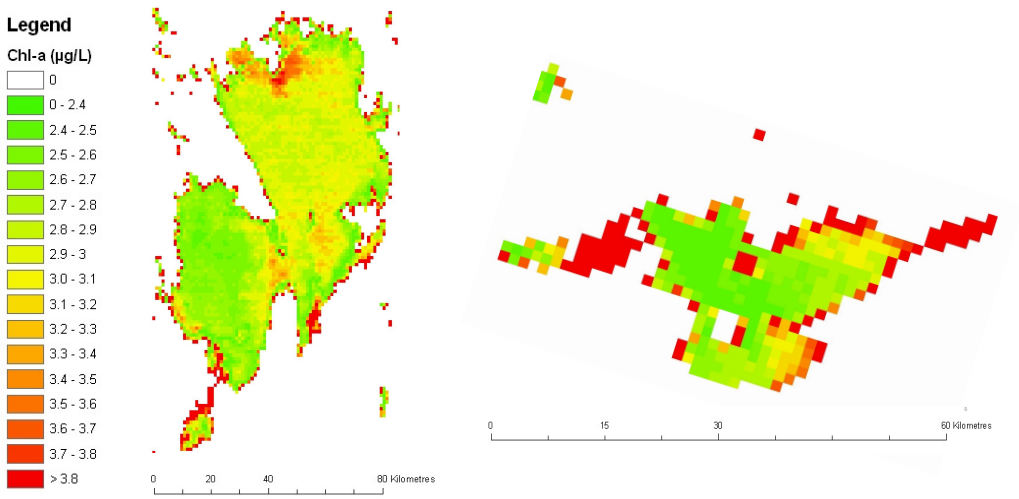

Figure 6-32: Chlorophyll *a* spatial distribution in lakes Vänern (left) and Hjälmaren (right) on 9th May 2001; Terra MODIS Politi chlorophyll *a* algorithm.

6.6.6 Parameter-related uncertainty

The remote sensing observations of water surface temperature are based on measurements of water surface emissivity, which may not be uniform across the lake body. Emissivity is influenced by wind-induced water surface roughness. For

example, Wooster *et al*. (1994) used NOAA AVHRR data to map surface temperature in a lake and found that high surface winds (> 4 m sec^{-1}) caused anomalous brightness temperature measurements and, therefore, they suggest that satellite data collected during windy days should be rejected from the analysis. Emissivity can be affected by variations in the water salinity, chlorinity and temperature, as well as by the presence of components on the water surface such as suspended sediments or pollutants (Robinson, 1985; Hepplewhite, 1989). Finally, measurements of LST are strongly affected by the satellite zenith angle, as emissivity decreases with increasing zenith angles in the same satellite image (Robinson, 1985).

The optical complexity of Case II waters makes the estimation of chlorophyll *a* concentrations and Secchi disk depth rather challenging (IOCCG, 2000). If the waveband ratio used in the estimation algorithm is also affected by other parameters apart from the parameter under consideration, then problems arise with the accuracy of the estimations (Pulliainen *et al*., 2001). For example, due to the additive effect of turbidity on the spectral signature of chlorophyll *a* in Case II waters an effective chlorophyll *a* algorithm for Case II waters should incorporate spectral wavebands that are independent of changes in turbidity, such as the nIR/Red ratio (e.g. Quibell, 1991; Gitelson *et al*., 1993; Han *et al*., 1994). Other studies have shown that the most appropriate wavelength for the estimation of chlorophyll *a* also depends on the concentration of the parameter. For example, in Case II waters shorter wavelengths in the red region are more appropriate for low chlorophyll *a* concentrations (oligotrophic and mesotrophic lakes) and longer wavelengths in the same region are necessary to map high concentrations (eutrophic lakes) (Kallio *et al*., 2001). Moreover, Dekker and Peters (1993) noted that the type of algorithm derived might be also dependant upon chlorophyll *a* concentrations and SDD values. For example,

they found that the best fit could be exponential at low to intermediate concentrations of water constituents and may approach a linear relationship at higher concentrations (Dekker & Peters, 1993), which suggests that the optimum method for the estimation of different eutrophication levels in lakes might be the development of trophic-level-specific algorithms.

Despite the above considerations, it has proved quite difficult to develop transferable chlorophyll *a* and Secchi disk depth estimation algorithms in Case II waters. Seasonal changes in the algal composition influence the algorithms developed (Allee & Johnson, 1999), because differences in the type of pigment and size of the phytoplanktonic species introduce uncertainty and potentially require different algorithms (Bennett & Bogorad, 1973; Balch *et al*., 1989). Also, chlorophyll *a* and other optically active water components in Case II waters interact in such a way that it is often impossible to separate their optical response, and thus simple algorithms that use two or three wavebands are not effective for complex Case II waters. By contrast, algorithms that use multiple wavebands designed for the estimation of more than one variable are required (IOCCG, 2000). For example, information on the amount of total suspended matter and coloured dissolved organic matter should be incorporated in the algorithms for the estimation of chlorophyll *a* concentrations to maximise their performance (Vos & Rijkeboer, 2000; Strömbeck & Pierson, 2001). Indeed, multivariate techniques have proved robust and effective in Case II waters (Tyler *et al*., 2006).

Another important (and often ignored) issue is the dependence of the water-leaving signal (i.e. remote sensing reflectance, R_{rs}) on the vertical subsurface structure of

optical parameters, such as chlorophyll *a* (e.g. Zaneveld *et al*., 2005; Kutser, 2009). Remote sensing reflectance incorporates optical information from the upper layer of water whose thickness depends upon the inherent optical properties of water (Xiu *et al*., 2008). As a result, in the case where vertical heterogeneity exists for an optical parameter in this upper layer (e.g. the presence of a subsurface chlorophyll *a* maximum (Stramska & Stramski, 2005)) variations (and errors) in the remotely sensed estimates will occur. The latter has been observed in lakes with the same surface chlorophyll *a* concentrations but different vertical structures of chlorophyll *a* (e.g. Xiu *et al*., 2008). In this project, the field measurements used to assess the accuracy of satellite estimates were collected at fixed depths of 0, 0.5 or 1 m depending on the lake. Thus, those were not necessarily representative of the vertical profile of the optical parameters under consideration. This might have introduced uncertainty to the predictive accuracy of the chlorophyll *a* and Secchi disk depth algorithms tested in this project. Uncertainty can also be introduced due to the fact that different wavelengths exhibit a different level of dependence upon vertical heterogeneity of optical parameters and thus the use of band ratios in water quality estimation algorithms can affect the predictive accuracy of the latter (Zaneveld *et al*., 2005).

6.6.7 Other factors

Lake bottom reflectance can affect the upwelling radiance measurements acquired by the satellite sensor (Robinson, 1985) and introduce errors in water parameter estimates. The latter is mostly found in clear lakes and at shallow areas. However, in turbid lakes and in sites where the Secchi disk depth is smaller than the shallowest part of the lake, this is not a problem (Kallio *et al.*, 2003). A similar effect derived

from macrophytes and other aquatic vegetation growing in shallow areas has been also highlighted in other studies (e.g. Allee *et al.*, 1999). In this study, all satellite estimates were extracted from deep open water areas to avoid uncertainty that might arise from shallow areas.

6.7 Optimal study site characteristics

The comparison of the shoreline morphological features of various lakes showed that specific lake sizes and shapes are inappropriate (or very difficult) to map with remote sensing. Generally, the presence of islands or enclosed bays is the main cause of mixed pixels within the remote sensing image. Very large lakes with a surface area much greater than 100 km^2 without islands or enclosed bays (Figure 6-33a) or with a few islands (Figure 6-33b) are optimal for remote sensing studies that use medium to coarse spatial resolution sensors. Very large lakes with many islands and enclosed bays (Figure 6-34) are more difficult to map, but still can provide an adequate number of pure water pixels to facilitate limnological studies. The same is valid for lakes with a surface area of around 100 km^2 without islands or enclosed bays (Figure 6-33c), although in this case the small number of pixels limits the study of the spatial distribution of water quality parameters. However, remotely sensed information from such lakes can be used to generate an average LST estimate for other purposes, such as the construction of time series.

(a) Very large lake (584 km^2) without enclosed bays or islands: Geneva

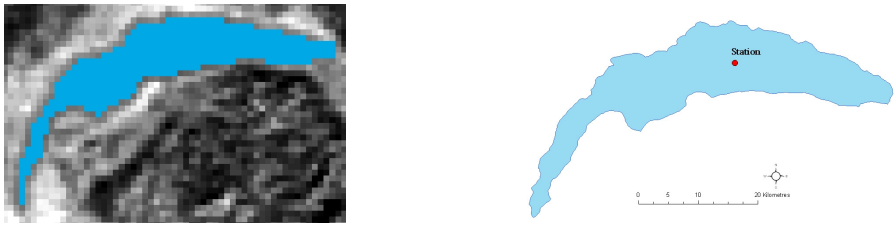

(b) Very large lake (1856 km^2) without enclosed bays, with a few islands: Vättern

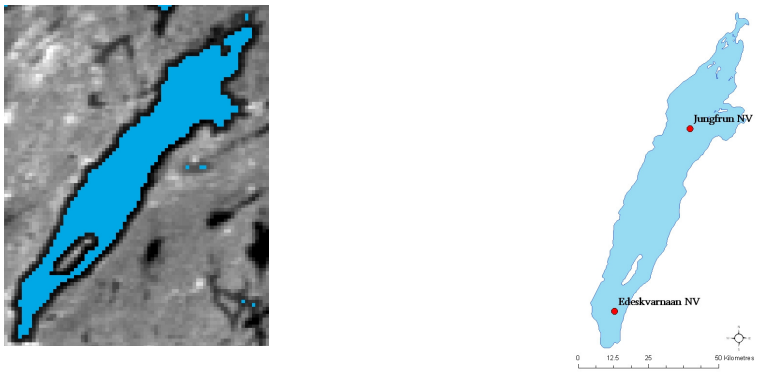

(c) Very large lake (127 km^2) without enclosed bays or islands: Tisza

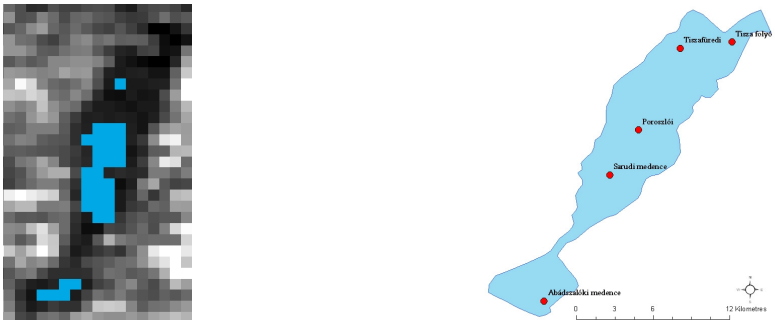

Figure 6-33: Very large lakes (> 100 km^2) without enclosed bays, with or without islands.

In lakes with surface areas less than 100 km^2 it is also the shape of the water body that affects their suitability. In Loch Lomond, that has numerous islands and a non-circular shape, yet a surface area of 71 km^2, it is rather difficult to generate pure water pixels with coarse spatial resolution sensors, such as the NOAA AVHRR

(Figure 6-35a). In that lake, all pure water pixels are limited to the southern basin, which is much wider than the northern part. In smaller lakes that have no islands, the suitability depends clearly on the surface area and the shape of the lake. In lakes Bourget (44.5 km^2) and Annecy (27 km^2) a few pure water pixels can be extracted within NOAA AVHRR scenes (Figures 6-35b and 6-35c), but that depends on the satellite zenith angle and the amount of geometric distortion in the image. Finally, Loch Leven (13.3 km^2) and Lake Müggelsee (7.4 km^2) have a circular shape that is ideal for mapping with remote sensing, but they are too small in terms of surface area and it was not able to map them with NOAA AVHRR data. The same was true for Lake Aiguebelette (5.4 km^2), which is the smallest lake studied in this project.

(a) Very large lake (1040 km^2) with enclosed bays and numerous islands: Inärijärvi

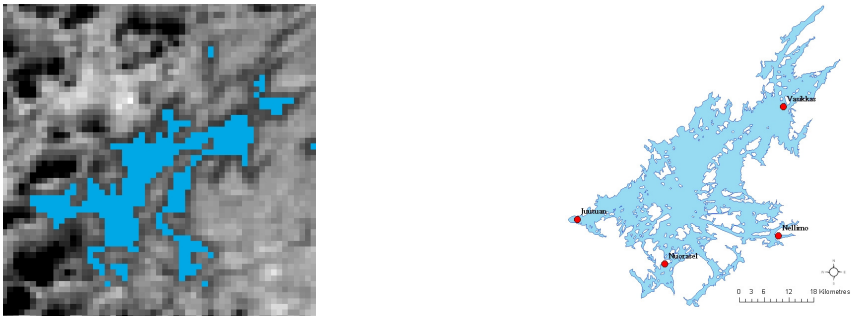

(b) Very large lake (1096 km^2) with enclosed bays and numerous islands: Mälaren

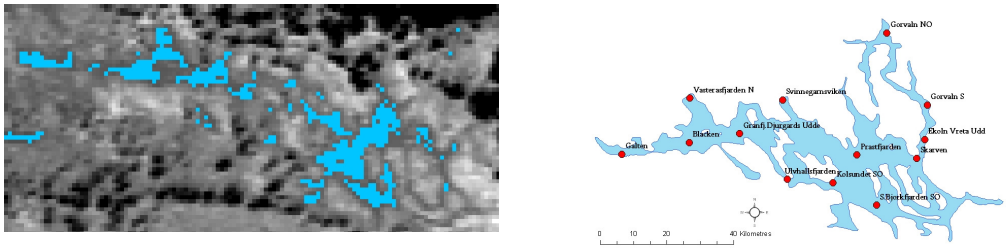

Figure 6-34: Very large lakes (> 100 km^2) with enclosed bays and numerous islands.

(a) Large lake (71 km^2) with numerous islands: Lomond

(b) Large lake (45 km^2) without islands: Bourget

(c) Large lake (27 km^2) without islands: Annecy

Figure 6-35: Large lakes (10-100 km^2) with or without islands.

There are approximately 500,000 lakes in Europe with a surface size greater than 0.01 km^2, 75% of which are located in Scandinavia and the western part of Russia (EEA, 2010). The majority of the lakes are very small (surface area < 0.1 km^2), while only 16,000 have a surface area larger than 1 km^2 and only twenty four natural lakes

have a surface area larger than 400 km^2 (EEA, 2010). The methodology proposed in this study refers to lakes with minimum surface area of 10 km^2 if they are circular and without islands to ensure at least a few unmixed water pixels can be extracted. Lakes with irregular shapes, enclosed bays and numerous islands need to be much larger for the application of medium to coarse spatial resolution data, the minimum size depending on the shape of the lake. As a result, the direct implication of the methodology proposed here is that not all European lake bodies can be studied, as small (0.01-1 km^2) and medium-sized (1-10km^2), and some of the large (10-100km^2) lakes are automatically excluded because of their relatively small size and irregular shape. However, just in Finland there are 309 lakes with a surface area larger than 10 km^2 and many of them are large enough to be suitable for remote sensing. Many of these, though, also have numerous islands, which introduce the problems of mixed land-water pixels. A satellite with a finer spatial resolution than the ones used in this project would be more appropriate for the study of lakes smaller than 100 km^2.

6.8 Optimal sensor requirements

The selection of a remote sensing instrument in limnological studies is very important, because spatial patterns and processes in ecosystems may differ, according to the resolution at which they are observed (Levin, 1992). It is impossible to study phenomena, which occur at spatial and temporal scales that are similar to or smaller than the spatial and temporal separation of the field and remotely sensed data (Lavender *et al*., 2004). For example, internal waves affect the abundance of surface phytoplankton at time-scales of less than one day (Table 6-10) and phytoplankton blooms occur at spatial scales that can be as small as a few metres (Schofield *et al*., 1999). Remote sensing instruments with temporal resolutions of more than one day

and spatial resolutions of hundreds of metres to more than one kilometre are inappropriate for the study of such phenomena. The selection of an optimum instrument also depends on the sites under consideration (Kutser, 2009). For example, large lakes exhibit much higher spatial heterogeneity in water quality parameters than small lakes (Vos *et al*., 2003).

A suitable remote sensing sensor for limnological studies should have specific spatial, temporal and spectral resolution to match the needs of the study and the scales of ecological processes within the study sites (IOCCG, 2000). The International Ocean Colour Coordinating Group (IOCCG) has recommended certain specifications for remote sensing sensors that are considered suitable in limnological studies, assuming the phenomena under consideration occur at spatial scales of approximately 30 m and temporal scales of a few hours. Specifically, the sensors require narrow spectral bands with a wide dynamic range and high signal-to-noise ratios (IOCCG, 2000). The optimal spatial resolution of a satellite instrument for lake monitoring depends on the application, but generally a large area coverage at 300-1000 m resolution provides information on large scale phenomena, whereas for more detailed studies a higher resolution (≤ 100 m) is required (IOCCG, 2000). The optimal temporal resolution also depends on the phenomenon and parameter under consideration and may vary. For example, Kloiber *et al*. (2002b) analyzed temporal trends in the water quality of 500 lakes over a period of 25 years using a total of thirteen satellite images. On the other hand, Steissberg *et al*. (2005) used twelve images from three different sensors over a period of less than two months to study partial upwelling that occurs every few days. It is difficult to identify the optimal spectral resolution because it depends on the inherent optical properties of water

which tend to be rather complex in lakes. For example, studies have shown that there is a shift in the reflectance maximum of chlorophyll *a* with varying chlorophyll *a* concentrations (e.g. Gitelson, 1992). Dekker (1993) recommends the use of wide channels in the development of algorithms for lakes encompassing a wide range of eutrophication levels, in order to cover this shift. Other studies argue that different channels should be used for varying chlorophyll *a* concentrations (e.g. Han *et al*., 1994; Hedger *et al*., 1996; George, 1997b; Kallio *et al*., 2001), assuming need for channels that cover the whole spectrum when both Case I and Case II waters are studied. Two nIR/Red ratios incorporating different narrow bands from a hyperspectral sensor have shown strong correlations with varying chlorophyll *a* concentrations (e.g. Pulliainen *et al*., 2001). Remote sensing of Case II waters should incorporate wavebands at the range recommended for Case I waters and additional wavebands below and above that range (IOCCG, 2000).

Table 6-10: Requirements and potential of satellite remote sensing measurements for the study of dynamic processes and thermal phenomena in lakes (Source: Kondratyev & Filatov, 1999; p. 128).

Process/Phenomenon	Space scales [km]	Duration of survey	Accuracy of space resolution [km]	Possibility
Macroscale circulation	10-200	1 day	1	Yes
Topographic waves	20-50	2-12 hr	10	No
Mesoscale circulation, gyres	5-20	1 day	1	Yes
Upwellings	5-20	0.5 day	0.5	Yes
Fronts	1	1 day	0.5	Yes
Internal waves	1	3-4 hr	0.5	Yes
River plumes	1	1 day	0.5	Yes
Ice fields	1	1 day	0.5	Yes
Surface waves	0.01-0.001	0.1 day	0.001	No

Many studies discuss the potential of the Envisat Medium Resolution Imaging Spectrometer (MERIS) data for the estimation of water quality parameters (e.g. Thiemann & Kaufmann, 2000; Pulliainen *et al*., 2001; Koponen *et al*., 2002; Kallio *et al*., 2003; Vos *et al*., 2003). Envisat MERIS was developed mainly for oceanographic studies with 15 wavebands from about 412.5 nm to 900 nm that are designed to provide information related to CDOM, suspended sediment, chlorophyll *a* absorption minima and maxima, and chlorophyll *a* fluorescence peaks (WDC-RSAT, 2010). The wavebands are ground-controlled and adjustable in terms of spectral resolution within a 1.25-30 nm range. Also, the sensor has the ability to collect medium-resolution data (300 m) over coastal and land areas and coarser spatial resolution data (1.2 km) over open ocean waters (Lillesand *et al*., 2008). Thiemann and Kaufmann (2000), Pulliainen *et al*. (2001) and Kallio *et al*. (2003) have all developed chlorophyll *a* estimation algorithms for AISA wavebands that coincide with Envisat MERIS channels and as a result they all suggest that the latter could be used instead in future studies. In addition, Envisat MERIS data have the potential to work well in turbid waters (Vos *et al*., 2003). However, the Envisat MERIS lacks thermal wavebands and has a shorter archive of data than Terra MODIS, being operational since March 2002.

The analysis of large scale water features requires a thorough understanding of phenomena that occur at smaller scales, which is not always feasible with satellite remote sensing. The combination of spaceborne and airborne data is a very useful approach to study simultaneously large and small scale patterns and ecological processes (e.g. Vos *et al*., 2003). In fact, a multiplatform approach has more advantages than that. It could offer a solution to the problem of cloud cover that

strongly affects the frequency of available satellite data in temperate areas (e.g. Bussières *et al*., 2002; Vos *et al*., 2003), by increasing the revisit capability. For example, the combination of sensors such as Landsat MSS and TM (Kloiber *et al*., 2002b), Landsat TM and ETM+ (Vincent *et al*., 2004) or Terra ASTER and Landsat ETM+ (Steissberg *et al*., 2005) increases the revisit capability to 8 days, instead of 16 days for each individual sensor. Sensors with more frequent revisit capabilities (e.g. Terra/Aqua MODIS) have much coarser spatial resolution. However, the combination of these sensors with a high spatial resolution sensor of less frequent revisit capability (e.g. Terra ASTER, Landsat ETM+) is considered a good solution for the study of small spatial and temporal scale lake water phenomena (e.g. Steissberg *et al*., 2005; Oesch *et al*., 2008).

6.9 Summary

The strong potential of remote sensing in limnological studies of various ecological phenomena and patterns in European lakes has been demonstrated in this chapter. Despite certain limitations, the availability of long historic satellite archives and the increasing archives from current and new satellites are key elements in studies like this when long-term temporal trends and patterns are considered. Furthermore, the development of new algorithms and the availability of new sensors that are suitable for limnological research will potentially help minimize some of the sources of error in the estimation of water quality parameters and thus increase the potential of remote sensing in limnology.

Chapter VII.

CONCLUSIONS & FUTURE RECOMMENDATIONS

7.1 Brief summary of thesis

Extensive (in volume and frequency) datasets of field measurements were obtained from various sources across Europe that covered measurements of temperature, chlorophyll *a* and Secchi disk depth at 23 European lakes covering the last 30 years. The characteristics of these lake systems were explored and similarities in the ecological behaviour of lakes within the same EU WFD ecoregion identified, thus providing the basis for the grouping of the study sites. The existence of various classification schemes represents the ecological variability and heterogeneity within and between lake bodies and the choice of a classification scheme depends on the parameters used and the research question. The classification schemes used in this project for the characterisation of the 23 study sites were based on their thermal and biological characteristics (Reid, 1961; Hickling, 1975; OECD, 1982), supplemented by abiotic information such as the mean depth, surface size and altitude of lakes, as proposed by the EU WFD (Directive 2000/60/EC, 2000). Representatives of three main lake groups that encompassed various biophysical, chemical and geomorphological characteristics were chosen to test the spatial transferability and temporal repeatability of a bank of remote sensing based water quality estimation algorithms. Then, all study sites were used for the application of the best performing algorithms. The potential of remote sensing in limnology was demonstrated and the

effect of scale and spatial resolution upon the reliable estimation of key water quality parameters was evaluated.

7.2 Achievement of research objectives

The following sections discuss the level to which the six research objectives that were stated in Chapter 1 have been achieved and completed.

Objective 1: To specify the temporal and spatial variability of the parameters under consideration in this study and, thus, to decide on the frequency of field and satellite data required

The published literature was reviewed for the temporal variability and spatial distribution of the water quality parameters studied in this project in lake waters (Chapter 2). Specifically for the 23 study sites, analysis of the field data (Chapter 3) provided detailed information on the temporal and spatial patterns and timings of ecologically important events (e.g. stratification onset, ice break-up) for each lake and each lake-group. This analysis informed decisions on the frequency (weekly to biweekly) and volume (two 4-year periods) of the satellite data that were then requested. As a result, this objective was fully achieved.

Objective 2: To identify and select appropriate methodologies and algorithms to estimate water quality parameters from remotely sensed data based upon an extensive study of published literature

The published literature was also reviewed to indentify limnological studies that employed remote sensing data to estimate water quality in lakes (Chapter 2) and the suitability of these algorithms for use with the available satellite data was tested

(Chapter 4). Also, four algorithms that are used operationally to monitor water surface temperature and chlorophyll *a* concentrations using NOAA AVHRR and Terra/Aqua MODIS data were identified. This resulted in a bank of 26 algorithms that had potential for estimating lake water quality across wide spatial and temporal scales. As a result, the second objective was also fully achieved.

Objective 3: To test the spatial and temporal transferability of predictive relationships defined at one site to other lakes across Europe and compare the results between lakes with different ecological characteristics

All suitable algorithms were applied to the satellite data as appropriate and their performance was tested to determine what water quality information could successfully be extracted from remote sensing imagery and the level of accuracy observed (Chapter 5). For this application, lakes with different ecological characteristics were used (varying from oligotrophic to eutrophic and from monomictic to polymictic) to test the spatial transferability of the algorithms, including those that were site-specific. Also, data from various years and seasons were used to test the temporal transferability of all suitable algorithms, including season-specific algorithms. The third objective was fully achieved for NOAA AVHRR as there were sufficient data from all lake types to perform the above analysis. It was found that both NOAA AVHRR MCSST and NLSST algorithms were highly correlated with field LST measurements from various lakes ($\rho = 0.89$, $p < 0.01$ in both cases).

Aqua MODIS data from eutrophic lakes were unavailable. In that case, only data from oligotrophic and mesotrophic lakes were used to test the transferability of

MODIS SST, OC3 and non-standard chlorophyll *a* and Secchi disk depth algorithms. Terra MODIS data from eutrophic lakes were insufficient (sample size ≤ 4) to test the transferability of algorithms in eutrophic lakes separately, but were used when field and satellite data from all lake types were combined into common datasets to test the transferability of non-standard chlorophyll *a* and Secchi disk depth algorithms. As a result, the third objective was not achieved for Aqua MODIS due to lack of data and was partially completed for Terra MODIS data.

Objective 4: To test the potential of NOAA AVHRR and Terra/Aqua MODIS to offer accurate estimates of the parameters under consideration within individual lakes

The potential of NOAA AVHRR and Terra/Aqua MODIS data for estimating water quality parameters in lakes was discussed in this project (Chapter 2). It was shown that NOAA AVHRR and Terra/Aqua MODIS data were capable of estimating surface temperature in European lakes when the MCSST (RMSE = 2.29 °C), NLSST (RMSE = 2.22 °C) and MODIS SST (RMSE = 1.46 ºC) operational algorithms were used (Chapter 5) and that the accuracy of these algorithms could be further improved if they are calibrated with data from the study sites (e.g. RMSE = 1.64 ºC for MCSSTcal). The potential of NOAA AVHRR MCSSTcal was further demonstrated in Chapter 6 where ecologically important events related to the thermal behaviour of lakes were identified with remote sensing, such as the stratification onset, temperature maxima and minima, temporal and spatial gradients of temperature, warming and cooling trends, ice cover and ice break-up, temporal and spatial distributions of temperature and thermal circulation features.

NOAA AVHRR data (band 1) have been used to map water quality parameters, such as total suspended matter (Prangsma & Roozekrans, 1989) but do not have appropriate spectral wavebands to be used for the estimation of chlorophyll *a* and Secchi disk depth in lakes or other water bodies (Cracknell, 1997). However, Terra/Aqua MODIS data have potential for estimating these two parameters in lake waters, but a robust methodology is still pending. This project tested the operationally used MODIS OC3 algorithm and demonstrated that it is inappropriate for Case II waters ($\rho = 0.39$, $p < 0.05$). Similarly poor results were exhibited when chlorophyll *a* and Secchi disk depth algorithms from published literature were tested (Chapter 5). However, the latter might be due to the fact that these algorithms were developed for other sensors than Terra/Aqua MODIS and/or for specific sites and seasons.

The chlorophyll *a* and Secchi disk depth estimation algorithms developed in this project from Terra/Aqua MODIS data exhibited moderate predictive accuracies (Chapter 5). This might have been due to the limited amount of data used in regression analysis, the choice of methods (e.g. multiple regression analysis might improve the predictive accuracy (IOCCG, 2000)) and/or the optical complexity of Case II waters that might require a different approach (e.g. algorithms for specific lake types, instead of a universal algorithm). Further investigation is needed to identify the reason(s) for moderate predictive accuracy before a conclusion is drawn regarding the suitability of the Terra/Aqua MODS data to estimate these two water quality parameters in European lakes. Based on the above, the fourth objective was fully achieved for NOAA AVHRR, but was partially achieved for Terra/Aqua MODIS data.

Objective 5: To investigate trends in water quality parameters for large lakes across Europe in the past 30 years and provide reasons as to why such trends have been observed

This project has demonstrated that historic thermal remote sensing data (and especially NOAA AVHRR data) can be used to identify long-term natural cycles of thermal phenomena in lakes, in order to differentiate the latter from changes caused in lakes by external factors (e.g. climatic fluctuations and anthropogenic activities) (Kondratyev & Filatov, 1999). A wider application of this could provide useful information regarding the reasons as to why observed trends occur in lakes.

However, due to delays in the acquisition of satellite data, the originally 30-year long study period was limited to two 4-year periods (Chapter 4) and consequently thermal trends in the study sites could not be studied with the appropriate detail at wide temporal scales. For example, it was shown that the NOAA AVHRR data available in this project were insufficient to perform trend analysis in Lake Vättern, whilst in Lake Geneva trend analysis produced different results between field and satellite data (Chapter 6). Moreover, the Terra/Aqua data cover a much shorter archive (since 2000) and the amount of data available for this project was small (and therefore insufficient for trend analysis) again due to delays in the data supply process. As a result, the fifth objective was only partially achieved.

Objective 6: To make recommendations as to the required sensor characteristics, data and appropriate methods to provide an operational remote sensing-based monitoring system for lakes across regional and continental scales

This project has reviewed the techniques and sensors used for the estimation and monitoring of key water quality parameters. Different platforms that have been used in limnological studies were compared, the advantages and disadvantages of various sensors were discussed and a list of the required characteristics of suitable sensors was presented (Chapter 2). At a later stage, recommendations as to the optimum study site characteristics and sensor requirements were made based on the findings of this project and the limitations and problems encountered (Chapter 6). At the end of this chapter, guidelines and recommendations to develop an effective methodology for the monitoring of water quality parameters in European lakes are provided (Chapter 7). As a result, the sixth objective was fully achieved.

7.3 Advantages of NOAA AVHRR in LST estimations

There are several advantages when the NOAA AVHRR is used to derive estimates of water surface temperatures instead of other remote sensing instruments (e.g. GOES series, Nimbus-7 CZCS, Landsat TM/ETM+, ERS ATSR/ENVISAT AATSR, microwave scanners). Even though the NOAA AVHRR has a less frequent revisit capability than geostationary satellites, it has finer spatial resolution and much better calibration (Cracknell, 1997). Also, the NOAA AVHRR thermal bands 4 and 5 have a high signal-to-noise ratio and a much longer archive than other systems (Cracknell, 1997). Landsat TM/ETM+ provide thermal data with a fine spatial resolution (60-120 m) that makes them useful for the study of small-scale phenomena in inland waters and also have the advantage of a long archive (since 1978 for thermal data), but their revisit capability is very infrequent (especially when cloud cover is considered).

The European Remote Sensing satellite (ERS-1, -2) Along-Track Scanning Radiometer (ATSR-1, -2) and Environmental Satellite (Envisat) Advanced ATSR (AATSR) are scanners that were designed to produce SST estimates of higher accuracy than the AVHRR, because they scan data from both nadir and 52° forwards of nadir, allowing corrections related to atmospheric emission and absorption (Rees, 1999). The series have been operating since 1991, allowing for a long archive of data and at the similar spatial resolution (1 km) as the NOAA AVHRR (1.1 km). However, the ATSR and AATSR data are not as easily, rapidly and/or as cheaply available as NOAA AVHRR data (Cracknell, 1997). Furthermore, the NOAA AVHRR data can produce SST maps of near-real time, which makes them operationally important in oceanographic studies (Robinson, 1985).

Estimates of water surface temperature can be derived from passive microwave sensors, but with a much coarser spatial resolution than that of the AVHRR, which makes them valuable only in continental- and global-scale environmental monitoring (Lillesand *et al*., 2008).

7.4 Advantages of Terra/Aqua MODIS in water quality estimations

The Terra/Aqua MODIS has many advantages over other remote sensing instruments that have been used in estimations of water quality parameters (e.g. Nimbus-7 CZCS, Orbview-2 SeaWiFS, Landsat TM/ETM+, NOAA AVHRR, Envisat MERIS). The Nimbus-7 CZCS and Orbview-2 SeaWiFS were originally designed for ocean colour and SST measurements and have produced very promising results. However, the Terra/Aqua MODIS has improved spectral and radiometric resolution compared to these two sensors that makes it a good candidate for the study of Case II waters.

Also, Terra/Aqua MODIS has a larger signal-to-noise ratio than Nimbus-7 CZCS. For example, the Nimbus-7 CZCS has a noise equivalent temperature difference (NETΔ) of 0.22 K at 270 K (Austin, 1993), while the NETΔ for Terra/Aqua MODIS is 0.05 K (PO.DAAC, 2010). In addition, the Nimbus-7 CZCS thermal band failed within the first year of operation (NASA Ocean Colour, 2009) and so SST estimates are not available from Nimbus-7 CZCS data.

Landsat TM/ETM+ data have been extensively used in limnological studies, largely because of their relatively fine spatial resolution and long archive (e.g. Dekker & Peters, 1993; Steissberg *et al*., 2005). However, they were not originally designed for water applications and so they lack the appropriate spectral and radiometric resolution (e.g. Dekker & Peters, 1993; Vincent *et al*., 2004; Tyler *et al*., 2006). By contrast, Terra/Aqua MODIS has nine optical and IR bands with relatively narrow spectral ranges that were specifically designed for water applications (ocean colour, phytoplankton and biochemistry) and a much finer radiometric resolution than Landsat TM/ETM+. It also has a more frequent revisit capability, but lacks the fine spatial resolution of Landsat TM/ETM+. Also, Terra/Aqua MODIS SST estimates are more accurate to NOAA AVHRR SST estimates due to the finer radiometric resolution of the former and its higher signal-to-noise ratio (PO.DAAC, 2010). The latter was confirmed by the findings of this study (Chapter 5), but the shorter data archive of Terra/Aqua MODIS is a disadvantage.

Finally, Envisat MERIS was designed mainly for coastal studies with 15 wavebands that are ground-controlled and spectrally adjustable in order to provide information on various water quality parameters (WDC-RSAT, 2010). The sensor has the ability

to collect medium-resolution data (300 m) over coastal and land areas (Lillesand *et al*., 2008) that is much finer than the 1000 m spatial resolution of the Terra/Aqua MODIS bands 8-16 which were developed for ocean colour studies (Jensen, 2000). However, the Terra/Aqua MODIS bands 1-2 with a spatial resolution of 250 m have also been used for estimating water quality parameters (e.g. Wang *et al*., 2010) and provide similar levels of spatial detail as Envisat MERIS. The main disadvantages of Envisat MERIS are that it lacks thermal wavebands and has an equally short archive of data to the Aqua MODIS, being operational only since March 2002.

7.5 Relating lake change to climate change

It is difficult to directly link changes in aquatic species (e.g. phytoplankton) to changes in environmental factors, such as climate fluctuations and nutrient availability, because there are various other forcing factors that also regulate the life cycle of such species (Wetzel, 2001). Also, the thermal structure of lakes is specific to each water body and thus, it is difficult to differentiate between the effects of regional climatic phenomena and local meteorology on the thermal characteristics of lakes unless the changes are well pronounced (Livingstone, 1997). Nevertheless, the direct response of lake water temperatures at all depths to air temperature fluctuations at regional and synoptic scales has been established (e.g. Livingstone & Lotter, 1998; Livingstone & Dokulil, 2001; Livingstone & Padisák, 2007). Even though the response of lake temperature to air temperature changes might vary seasonally and even monthly (McCombie, 1959) lake water temperature is an indicator of long-term climatic fluctuations, with a less pronounced response to short-term meteorological forcing (Livingstone, 1993).

In this study the potential of satellite data in trend analysis was demonstrated. Even though the amount of remotely sensed estimates was limited and conclusions on observed trends could not be drawn, it was demonstrated that remote sensing does provide the basis to monitor long-term trends in lake surface temperature. The long remote sensing archive at the NEODAAS DSRS was fundamental for the purposes of this project and should become a cornerstone in the implementation of international policy-related monitoring and management programmes, such as the EU Water Framework Directive. Remote sensing is a method that can be widely applied over large spatial and temporal scales and produce comparable results between lakes with various ecological characteristics. This project has demonstrated that the NOAA AVHRR MCSST and NLSST algorithms and the Terra/Aqua MODIS SST algorithm are reliable, transparent and transferable methods to monitor surface temperature in European lakes, whilst further investigation is needed for the development of robust chlorophyll *a* and Secchi disk depth algorithms from Terra/Aqua MODIS data.

7.6 Conclusions and future recommendations

The basic stages of the methodology followed in this project for the estimation of lake surface temperature from NOAA AVHRR in European lakes are presented here enriched with guidelines and recommendations for future studies (Figure 7-1). Also, the results of the chlorophyll *a* and Secchi disk depth estimation algorithms developed in this project are discussed and recommendations for future work are provided.

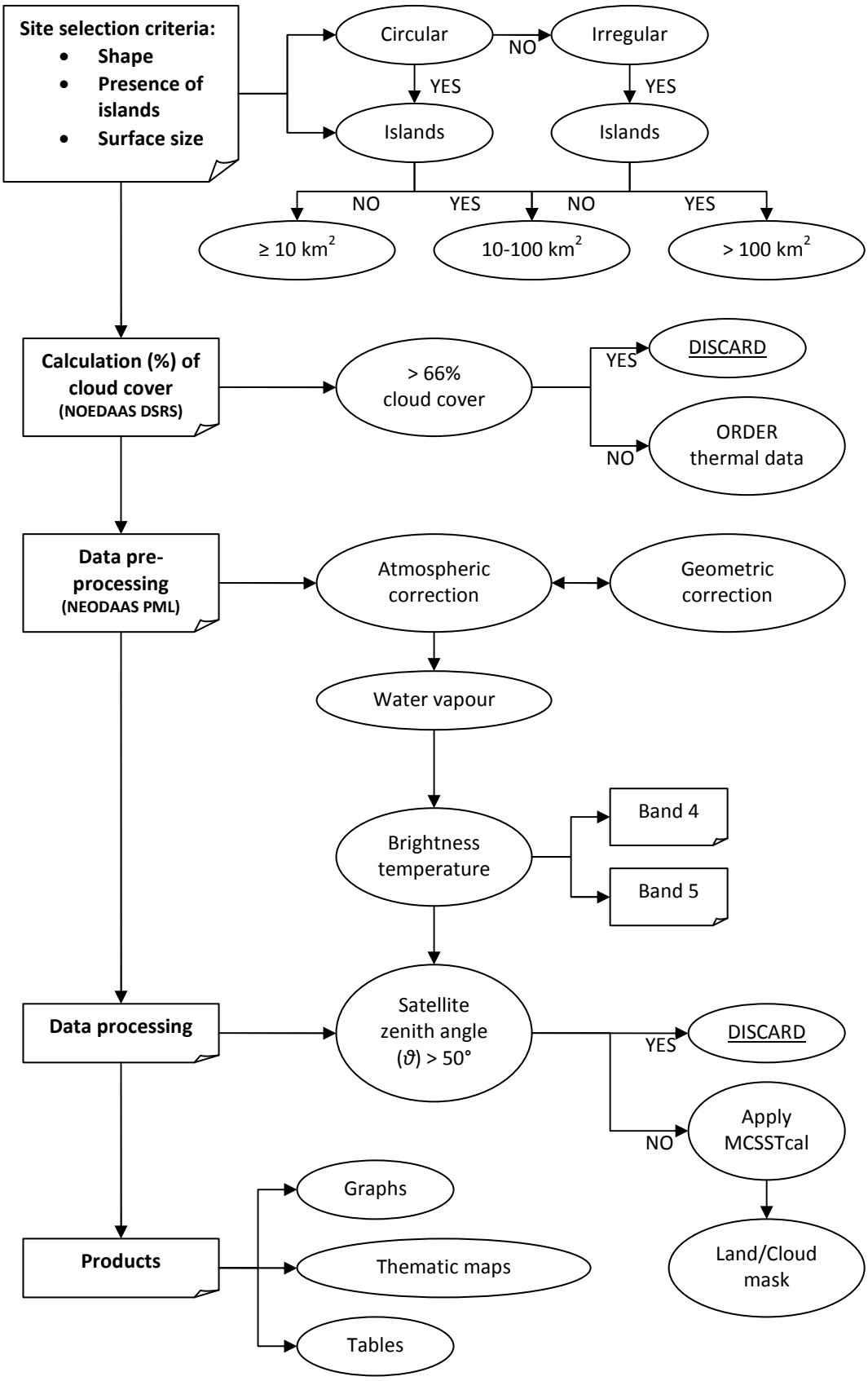

Figure 7-1: Processing chain for the estimation of LST from NOAA AVHRR data in large (≥ 10 km^2) lakes.

7.6.1 Conclusions and recommendations for the estimation of lake surface temperature from NOAA AVHRR data

The main operational limitations of the methodology proposed for the extraction of lake surface temperature from NOAA AVHRR data were (a) the shape and size of the lakes with respect to the coarse spatial resolution of the sensors and lack of georeferencing, (b) the delays during the calculation of cloud percentage and the acquisition of data, and (c) the calculation of the satellite zenith angle per lake per image.

The NOAA AVHRR has a spatial resolution of 1.1 km at nadir that allows the study of only large or very large lakes, depending on their morphology. The NOAA AVHRR scenes used in this project were not geometrically corrected to avoid spatial and numerical alterations of the scenes due to re-sampling (Personal communication with PML). Because of that, lakes with surface areas smaller than 100 km^2 were very difficult to map due to distortions. Assuming the scenes are geometrically corrected, large circular lakes (> 10 km^2) without islands have the optimum minimum size of detection in this application, while lakes of irregular shape with islands and enclosed bays need to have a surface area of approximately 100 km^2 or more to ensure a sufficient number of unmixed water pixels can be extracted for environmental analysis.

Considerable delays during the application of the cloud percentage calculation model and the data acquisition, due to the large volume of data involved and the specification of certain products needed, resulted in a considerable reduction of the

amount of satellite data received. The initial idea to exploit the entire range of the NEODASS DSRS AVHRR satellite data archive was not possible in this project because of the time-consuming nature of the pre-processing procedure. Even if the whole AVHRR archive was acquired, the non-automated data preparation and analysis that was performed by the author proved so time-consuming that this led eventually to a contraction of the original aims and objectives of the project. In addition, certain problems occurred with the data storage, since the satellite data require hard disk drives with large storing capacities and memory space. The above limitations should be taken into consideration for future studies.

The identification and removal of cloud-contaminated pixels was a very important stage of data processing and automated facilities are required for its application. In this project information about the cloud mask was provided by the NEODAAS PML, but its effectiveness was unknown as the methodology was originally designed for ocean waters (Personal communication with PML). Following that, further investigation on the accuracy of the cloud mask over inland waters is required. The incorporation of the satellite zenith angle in the NOAA AVHRR LST algorithms increases the accuracy of the algorithms by taking into account any distortions and errors in the emissivity measurement caused by differences in the satellite zenith angle (Robinson, 1985). However, the satellite zenith angle is site specific, which suggests that the algorithms cannot be applied across an entire image. The researcher believes that such a project could become operational only when the above issues have been resolved. The need for fast and reliable computing systems, updated software and automated facilities is considered a necessity. The use of automated

facilities during data analysis (e.g. application of algorithms and extractions of values from desired pixels) could also prove beneficial to projects like this in the future.

Although the full archive of the NOAA AVHRR was not exploited in this study due to data problems and time limitations, its applicability has been demonstrated. Future work could incorporate more satellite data to cover longer time periods. For example, the available 30-year long NOAA AVHRR data NEODAAS DSRS archive could be exploited in full extent in a limnological study of thermal trends and patterns in large European lakes. However, delays in the pre-processing of large amounts of satellite data (already described above) should be taken into consideration in future studies. In addition, this study demonstrated the applicability of NOAA AVHRR in estimating lake surface temperature in temperate lakes. The potential of NOAA AVHRR in tropical lakes (e.g. Wooster *et al*., 1994; Wooster *et al*., 2001) and boreal lakes (e.g. Bussières *et al*., 2002) has also been confirmed. Following that, combination of data from various continents could prove useful to test the potential of NOAA AVHRR data to monitor lake surface temperature at a global scale.

7.6.2 Conclusions and recommendations for the estimation of chlorophyll *a* and Secchi disk depth from Terra/Aqua MODIS data

Atmospherically corrected data (nL_w and R_{rs}) were weakly correlated with the field measurements available in this project, so at-satellite radiance and reflectance data were used instead. It was shown that band ratios performed better than single bands in all cases. George (1997b) has concluded that algorithms based on band ratios have an advantage in that they reduce problems caused by variations in the solar angle,

whereas single band algorithms are more sensitive to such effects. However, the combination of bands in the development of an algorithm introduces more noise (George, 1997b) and errors than when single bands are used because of spatial and temporal variations in the amount of radiation in different images (Hedger *et al*., 1996). Even though band ratios have been the basis of many algorithms, their use might be inappropriate when comparing water quality parameters in different lakes and it might be the reason of the low accuracy exhibited in the algorithms produced in this project.

Dekker and Peters (1993) recommended the use of an exponential model for low to intermediate chlorophyll *a* concentrations and Secchi disk depth values and a linear model for high values. However, in this study a polynomial model produced a better fit than other types of models, including the linear and exponential. For chlorophyll *a* data the combination of Terra MODIS Bands 3 (blue) and 4 (green) produced the best results, which agrees with the findings of other limnological studies in lakes with similar characteristics (e.g. Hedger *et al*., 1996; George, 1997b). In this study the algorithms developed were based on data from two oligotrophic and one mesotrophic lake; data from eutrophic lakes were unavailable. The chlorophyll *a* concentrations in the three lakes were always less than 10 $\mu g\ L^{-1}$ (except from one date in Lake Geneva where the chlorophyll *a* concentration was 14.01 $\mu g\ L^{-1}$) with a mean of 3.18 $\mu g\ L^{-1}$. The Secchi disk depth varied from 2.7-14 m with a mean of 6.25 m.

For Secchi disk depth a combination of three bands was used for both sensors and the algorithms incorporated a coarse atmospheric correction by subtracting a nIR band

from two visible bands. Even though in turbid lake waters the reflectance of water at the nIR wavelengths is not always zero, Koponen *et al*. (2002) found that the method improved the predictive accuracy of the algorithms. The Terra MODIS Bands 1 (red), 3 (blue) and 15 (nIR) were used and the Aqua MODIS Bands 10 (blue), 13 (red) and 15 (nIR) were used for the estimation of Secchi disk depth. It is noticeable that for both sensors the blue and red bands produced the best results, but the Aqua MODIS Bands 1 and 3 were noisy and thus, Bands 13 and 10 were used instead. The same band combination was used by others to estimate Secchi disk depth in lake waters (e.g. Kallio *et al*., 2001; Sawaya *et al*., 2003). Kallio *et al*. (2001) found that the use of reflectance data over radiance improved the accuracy of Secchi disk depth estimation algorithms. The same was true for the Terra/Aqua MODIS data used in this project. This might be based on the fact that reflectance accounts for the varying Sun-Earth distance within and between images, as opposed to radiance.

Future work should include more study sites to ensure all lake types are studied (e.g. eutrophic lakes that were under-represented in this project for Terra/Aqua MODIS data) towards the development of universal chlorophyll *a* and Secchi disk depth estimation algorithms. In addition, the investigation of the use of other sensors and/or other methods for the estimation of chlorophyll *a* and Secchi disk depth should be considered. For example, the potential of Envisat MERIS data for limnological studies has been previously suggested (e.g. Thiemann & Kaufmann, 2000; Pulliainen *et al*., 2001; Koponen *et al*., 2002; Kallio *et al*., 2003; Vos *et al*., 2003) and validation protocols for the development of MERIS lake water algorithms have been suggested (Kallio *et al*., 2007). Recent studies have shown the potential of the sensor in limnoligical studies (e.g. Odermatt *et al*., 2008a; Odermatt *et al*., 2010). The

Envisat MERIS was originally designed to measure phytoplankton and detect dissolved organic material and suspended matter (Rast *et al*., 1999) and its band configuration makes it more suitable than Terra/Aqua MODIS. The latter lacks spectral bands in the lower red (630 nm) and the red-nIR edge (700nm) which are essential for estimating chlorophyll *a* concentrations in productive waters (Kutser, 2009). In fact, limnological studies have employed the unique to MERIS waveband at 709 nm which represents the part of the spectrum where chlorophyll *a* reflectance peaks in algae-laden waters (e.g. Alikas *et al*., 2010). Furthermore, atmospheric correction schemes have been developed specifically for the use of Envisat MERIS over Case II waters (e.g. Moore *et al*., 1999) and methodologies have been suggested to account for the adjacency effect (e.g. Odermatt *et al*., 2008b). Finally, the continuity of MERIS data with the launch of the Global Monitoring for Environment and Security (GMES) Sentinel-3 sensor in 2012-13 will increase the length of the current archive and provide a good database for future lake monitoring studies.

Future studies should also prioritise the development of chlorophyll *a* and Secchi disk depth algorithms using other methods than the ones employed in this project. For example, multivariate techniques have been used for the estimation of chlorophyll *a* concentrations incorporating information from various parameters that influence the optical properties of water, such as the amount of total suspended matter and coloured dissolved organic matter (e.g. Vos & Rijkeboer, 2000; Tyler *et al*., 2006).

Another method that has been widely used in multiple remote sensing applications is the Artificial Neural Networks (ANNs) (Mas & Flores, 2008). ANNs have been used

to map chlorophyll and water quality in Case II waters (e.g. Keiner & Yan, 1998; Keiner & Brown, 1999) and have been used with Envisat MERIS data (e.g. Buckton *et al*., 1999; Schiller & Doerffer, 1999). Some of the advantages of ANNs over other remote sensing techniques are: (a) the ability to model complex and non-linear relationships between biophysical variables, (b) the fact that they are a non-parametric method and thus are not based on assumptions regarding the data (e.g. normal distribution), and (c) they can incorporate otherwise unused information (e.g. all wavebands) (e.g. Buckton *et al*., 1999; Mas & Flores, 2008).

Finally, the use of spectral libraries of inland waters with known properties could be applied to multispectral sensors (e.g. Terra/Aqua MODIS and Envisat MERIS) and thus provide a useful method for estimating water quality of optical parameters in lake waters (Kutser, 2009).

7.7 Concluding remarks

This work demonstrates a clear role for remote sensing in estimating lake water quality parameters providing that issues with sensors and algorithm transferability can be addressed. The long archive of satellite data held by the NEODAAS DSRS, coupled with sensors such as Envisat MERIS and GMES Sentinel-3, will enable future work to monitor fragile lake ecosystems at better resolutions than previously possible, providing insight into the ecological behaviour of lakes and the drivers of lake change. Effort should focus on optically complex parameters, such as chlorophyll *a* and Secchi disk depth, in order to improve current atmospheric correction techniques over inland waters and develop robust and transferable methods for the estimation of lake water quality.

REFERENCES

ADRIAN R., WALZ N., HINTZE T., HOEG S. & RUSCHE R., 1999. Effects of ice duration on plankton succession during spring in a shallow polymictic lake, *Freshwater Biology*, 41(3): 621-632

ALIKAS K., KANGRO K. & REINART A., 2010. Detecting cyanobacterial blooms in large North European lakes using the Maximum Chlorophyll Index, *Oceanologia*, 52(2): 237-257

ALLEE R. J. & JOHNSON J. E., 1999. Use of satellite imagery to estimate surface chlorophyll a and Secchi disc depth of Bull Shoals Reservoir, Arkansas, USA, *International Journal of Remote Sensing*, 20(6): 1057-1072

ARHONDITSIS G. B., BRETT M. T., DeGASPERI C.L. & SCHINDLER D. E., 2004a. Effects of climatic variability on the thermal properties of Lake Washington, *Limnol. Oceanogr.*, 49(1): 256-270

ARHONDITSIS G. B., WINDER M., BRETT M. T. & SCHINDLER D. E., 2004b. Patterns and mechanisms of phytoplankton variability in Lake Washington (USA), *Water Research*, 38: 4013-4027

ATKINSON P.M. & FOODY G.M., 2002. Uncertainty in Remote Sensing and GIS: Fundamentals, in *Uncertainty in Remote Sensing and GIS* (Edited by Foody G.M. & Atkinson P.M.), England: Wiley

AUSTIN R.W., 1993. Optical remote sensing of the oceans: BC (before CZCS) and AC (after CZCS), in *Ocean Colour: Theory and Applications in a Decade of CZCS*

Experience (Edited by Barale V. & Schlittenhardt M.), Brussels and Luxembourg: Kluwer Academic Publishers

BABAN S. M. J., 1993. Detecting water quality parameters in the Norfolk Broads, UK, using Landsat imagery, *International Journal of Remote Sensing*, 14(7): 1247-1267

BALCH W.M., EPPLEY R.W., ABBOTT M.R. & REID F.M.H., 1989. Bias in satellite-derived pigment measurements due to coccolithophores and dinoflagelattes, *Journal of Plankton Research*, 11(3): 575-581

BENNET S., 1995. *An assessment of the use of the Daedalus 1268 AADS Airborne Thematic Mapper for the study of water quality parameters in inland waters*, Unpublished MSc dissertation, University of Edinburgh

BENNET A. & BOGORAD L., 1973. Complementary chromatic adaptation in a filamentous blue-green alga, *Journal of Cell Biology*, 58: 419-435

BENNION H., HILTON J., HUGHES M., CLARK J., HORNBY D., FOZZARD I., PHILLIPS G. & REYNOLDS C., 2005. The use of a GIS-based inventory to provide a national assessment of standing waters at risk from eutrophication in Great Britain, *Science of Total Environment*, 344: 259-273

BIJAOUI J., JULLIEN S. & CAUNEAU F., 1995. Bathymetry measurement in shallow water areas using airborne spectrometers, in *Sensors and Environmental Applications of Remote Sensing*, (Edited by Askne J.), Balkema, Rotterdam, p. 311-314.

BLENCKNER T., ADRIAN R., LIVINGSTONE D.M., JENNINGS E., WEYHENMEYER G.A., GEORGE D.G., JANKOWSKI T., JÄRVINEN M., AONGHUSA C.N., NÕGES T., STRAILE D. & TEUBNER K., 2007. Large-scale climatic signatures in lakes across Europe: a meta-analysis, *Global Change Biology*, 13: 1314-1326

BONAN G., 2002. *Ecological climatology; Concepts and applications*, UK: Cambridge University Press

BUCKTON D., O'MONGAIN E. & DANAHER S., 1999. The use of neural networks for the estimation of oceanic constituents based on the MERIS instrument, *International Journal of Remote Sensing*, 20(9): 1841-1851

BURROUGHS W.J., 2001. *Climate Change, A multidisciplinary approach*, USA: Cambridge University Press

BUSSIÈRES N., VERSEGHY D. & MacPHERSON J. I., 2002. The evolution of AVHRR – derived water temperatures over boreal lakes, *Remote Sensing of Environment*, 80: 373-384

CAMPBELL J.B., 2002. *Introduction to Remote Sensing*, 3rd edition, New York: The Guilford Press, Taylor and Francis

CEN 2010, *Water quality – Guidance standard on assessing the hydromorphological features of lakes*, European Committee for Standardization (CEN), Brussels (DRAFT)

CLARK R., 1999. Spectroscopy of rocks and minerals, and principles of spectroscopy, in *Remote Sensing for the Earth Sciences, Manual of Remote Sensing Volume 3*, (Edited

by Rencz A.), 3rd edition, American Society for Photogrammetry and Remote Sensing, Canada: Wiley

CLARK-CARTER D., 2004. *Quantitative psychological research; A student's handbook*, New York: Psychology Press

CORINE 2000. European Environment Agency, CORINE Lane Cover Data: http://www.eea.europa.eu/themes/landuse/clc-download

CRACKNELL A.M., 1997. *The Advanced Very High Resolution Radiometer*, UK: Taylor & Francis ed.

CRU, 2008. Climatic Research Unit (CRU): http://www.cru.uea.ac.uk/

DALL'OLMO G., GITELSON A.A., RUNDQUIST D.C., LEAVITT B., BARROW T. & HOLZ J.C., 2005. Assessing the potential of SeaWiFS and MODIS for estimating chlorophyll concentration in turbid productive waters using red and near-infrared bands, *Remote Sensing of Environment*, 96: 176-187

DEKKER A. G. & PETERS S. W. M., 1993. The use of the Thematic Mapper for the analysis of eutrophic lakes: a case study in the Netherlands, *International Journal of Remote Sensing*, 14(5): 799-821

DEKKER A. G., VOS R. J. & PETERS W. M., 2002. Analytical algorithms for lake water TSM estimation for retrospective analyses of TM and SPOT sensor data, *International Journal of Remote Sensing*, 23(1): 15-35

DeSTASIO B.T., GOLEMGESKI T. & LIVINGSTONE D.M., 2009. Temperature as a driving factor in aquatic ecosystems, in *Encyclopaedia of Inland Waters*, Volume 2 (Edited by Likens G.E.), Oxford: Elsevier

DeSTASIO B.T., HILL D.K., KLEINHANS J.M., NIBBELINK N.P. & MAGNUSON J.J., 1996. Potential effects of global climate change on small north-temperate lakes: Physics, fish and plankton, *Limnol. Oceanogr.*, 41(5): 1136-1149

EC Guidance Document No 10, 2003. *River and lakes – Typology, reference conditions and classification systems*, Common Implementation Strategy for the Water Framework Directive (2000/60/EC), Working Group 2.3 – REFCOND, Luxembourg: Office from Official Publications of the European Communities, pp. 87

ECN, 2009. The UK Environmental Change Network (ECN) Freshwater sites: http://www.ecn.ac.uk/

EEA, 2010. European Environment Agency: http://www.eea.europa.eu/themes/water/european-waters/lakes

ELO A-R., HUTTULA T., PELTONEN A. & VIRTA J., 1998. The effects of climate change on the temperature conditions of lakes, *Boreal Environment Research*, 3: 137-150

EUROPA WFD, 2009. European Commission Water Framework Directive: http://ec.europa.eu/environment/water/water-framework/index_en.html

FEA, 2009. Finland's Environmental Administration: http://www.ymparisto.fi/

FELDMAN G.C., Dr., Oceanographer, NASA/Goddard Space Flight Centre: http://oceancolor.gsfc.nasa.gov/staff/gene/

FOLEY J.A., DeFRIES R., ASNER G., BARFORD C., *et al*., 2005. Global consequences of land use, *Science*, 309: 570-574

FRASER R.N., 1998. Multispectral remote sensing of turbidity among Nebraska Sand Hills lakes, *International Journal of Remote Sensing*, 19(15): 3011-3016

GEORGE D.G., 1997a. Bathymetric mapping using a Compact Airborne Spectrographic Imager (CASI), *International Journal of Remote Sensing*, 18(10): 2067-2071

GEORGE D.G., 1997b. The airborne remote sensing of phytoplankton chlorophyll in the lakes and tarns of the English Lake District, *International Journal of Remote Sensing*, 18(9): 1961-1975

GERTEN D. & ADRIAN R., 2000. Climate-driven changes in spring plankton dynamics and the sensitivity of shallow polymictic lakes to the North Atlantic Oscillation, *Limnol. Oceanogr*., 45(5): 1058-1066

GERTEN D. & ADRIAN R., 2001. Differences in the persistency of the North Atlantic Oscillation signal among lakes, *Limnol. Oceanogr*., 46(2): 448-455

GERTEN D. & ADRIAN R., 2002. Species-specific changes in the phenology and peak abundance of freshwater copepods in response to warm summers, *Freshwater Biology*, 47(11): 2163-2173

GIARDINO C., BRESCIANI M., PILKAITYTE R., BARTOLI M. & RAZINKOVAS A., 2010. *In situ* measurements and satellite remote sensing of case 2 waters: first results from the Curonian Lagoon, *Oceanologia*, 52(2): 197-210

GITELSON A., 1992. The peak near 700 nm on radiance spectra of algae and water: relationships of its magnitude and position with chlorophyll concentration, *International Journal of Remote Sensing*, 13(17): 3367-3373

GITELSON A., GARBUZOV G., SZILAGYI F., MITTENZWEY K-H., KARNIELI A. & KAISER A., 1993. Quantitative remote sensing methods for real-time monitoring of inland waters quality, *International Journal of Remote Sensing*, 14(7): 1269-1295

GÓMEZ-LANDESA E., RANGO A. & BLEIWEISS M., 2004. An algorithm to address the MODIS bowtie effect, *Canadian Journal of Remote Sensing*, 30(4): 644-650

GONS H.J., RIJKEBOER M. & RUDDICK K.G., 2002. A chlorophyll-retrieval algorithm for satellite imagery (Medium Resolution Imaging Spectrometer) of inland and coastal waters, *Journal of Plankton Research*, 24(9): 947-951

GORDON H.R., BROWN O.B., EVANS R.H., BROWN J.W., SMITH R.C., BAKER K.S. & CLARK D.K., 1988. A semianalytic radiance model of ocean colour, *Journal of Geophysical Research*, 93(D9): 10909-10924

HAN L., 1997. Spectral reflectance with varying suspended sediment concentrations in clear and algae-laden waters, *Photogrammetric Engineering and Remote Sensing*, 63(6): 701-705

HAN L., RUNDQUIST D. C., LIU L. L., FRASER R. N. & SCHALLES J. F., 1994. The spectral responses of algal chlorophyll in water with varying levels of suspended sediment, *International Journal of Remote Sensing*, 15(18): 3707-3718

HARDY J. T., 2003. *Climate change: Causes, effects and solutions*, UK: Wiley

HEDGER R.D., ATKINSON P.M., MALTHUS T.J. & GEORGE D.G., 1996. *Planning optimal sampling strategies for estimating the regional mean water quality in lakes*, Proceedings of the 22nd Annual Conference of the Remote Sensing Society, 11-14 September 1996, University of Durham, UK, pp: 221-228

HEEGE T. & FISCHER J., 2004. Mapping of water constituents in Lake Contance using multispectral airborne scanner data and a physically based processing scheme, *Canadian Journal of Remote Sensing*, 30(1): 77-86

HEPPLEWHITE C.L., 1989. Remote observation of the sea surface and atmosphere; The ocean skin effect, *International Journal of Remote Sensing*, 10(4-5): 801-810

HICKLING C. F., 1975. *Water as a productive environment*, UK: Redwood Burn Ltd

HIRTLE H. & RENCZ A., 2003. The relation between reflectance and dissolved organic carbon in lake water: Kejimkujik National Park, Nova Scotia, Canada, *International Journal of Remote Sensing*, 24(5): 953-967

HORNE A. J. & GOLDMAN C. R., 1994. *Limnology*, 2nd edition, USA: McGraw-Hill

HOUGHTON J., 2004. *Global Warming, The complete Briefing*, 3rd edition, UK: Cambridge University Press

HURRELL J.W., 1995. Decadal trends in the North Atlantic Oscillation Regional Temperatures and Precipitation (Updated online version), *Science*, 269: 676-679 http://www.cgd.ucar.edu/cas/jhurrell/indices.html

ILEC, 2010. International Lake Environment Committee (ILEC), World Lakes Database: http://www.ilec.or.jp/

IOCCG, 2000. Remote sensing of ocean colour in coastal and other optically-complex waters, in *Reports of the International Ocean-Colour Coordinating Group, No.3, IOCCG*, (Edited by Sathyendranath S.), Dartmouth, Canada.

IPCC, 2001. Intergovernmental Panel for Climate Change: www.ipcc.ch

JANKOWSKI T., LIVINGSTONE D.M., BÜHRER H., FORSTER R. & NIEDERHAUSER P., 2006. Consequences of the 2003 European heat wave for lake temperature profiles, thermal stability and hypolimnetic oxygen depletion: Implications for a warmer world, *Limnol. Oceanogr.*, 51(2): 815-819

JENSEN J. R., 2000. *Remote Sensing of the Environment, An Earth Resource Perspective*, USA: Prentice-Hall

KALLIO K., KOPONEN S. & PULLIAINEN J., 2003. Feasibility of airborne imaging spectrometry for lake monitoring – a case study of spatial chlorophyll a distribution in two meso-eutrophic lakes, *International Journal of Remote Sensing*, 24(19): 3771-3790

KALLIO K., KOPONEN S., RUIZ-VERDÚ A., HEEGE T., SØRENSEN K., PYHÄLAHTI T. & DOERFFER R., 2007. *Development of MERIS lake water algorithms*, Validation Protocol (WP 2.4), Version 1.0, ESRIN Contract No. 20436/06/I-LG, pp. 14

KALLIO K., KUTSER T., HANNONEN T., KOPONEN S., PULLIAINEN J., VEPSÄLÄINEN J. & PYHÄLAHTI T., 2001. Retrieval of water quality from airborne imaging spectrometry of various lake types in different seasons, *The Science of the Total Environment*, 268: 59-77

KEINER L.E. & BROWN C.W., 1999. Estimating oceanic chlorophyll concentrations with neural networks, *International Journal of Remote Sensing*, 20(1): 189-194

KEINER L.E. & YAN X.-H., 1998. A neural network model for estimating sea surface chlorophyll and sediments from Thematic Mapper imagery, *Remote Sensing of Environment*, 66: 153-165

KINNEAR P.R. & GRAY C.D., 2008. *SPSS 15 made simple*, USA: Psychology Press, Taylor and Francis Group

KLOIBER S. M., BREZONIK P. L., OLMANSON L. G. & BAUER M. E., 2002a. A procedure for regional lake water clarity assessment using Landsat multispectral data, *Remote Sensing of Environment*, 82: 38-47

KLOIBER S. M., BREZONIK P. L. & BAUER M. E., 2002b. Application of Landsat imagery to regional-scale assessments of lake clarity, *Water Research*, 36: 4330-4340

KÖHLER J., HILT S., ADRIAN R., NICKLISCH A. KOZERSKI H.P. & WALZ N., 2005. Long-term response of a shallow, moderately flushed lake to reduced external phosphorus and nitrogen loading, *Freshwater Biology*, 50: 1639-1650

KOLADA A., SOSZKA H., CYDZIK D. & GOLUB M., 2005. Abiotic typology of Polish lakes, *Limnologica*, 35: 145-150

KONDRATYEV K.Ya. & FILATOV N.N., 1999. *Limnology and remote sensing*. UK: Praxis Publishing Ltd.

KOPONEN S., POULLIAINEN J., KALLIO K. & HALLIKAINEN M., 2002. Lake water quality classification with airborne hyperspectral spectrometer and simulated MERIS data, *Remote Sensing of Environment*, 79: 51-59

KUTSER T., 2009. Passive optical remote sensing of cyanobacteria and other intense phytoplankton blooms in coastal and inland waters, *International Journal of Remote Sensing*, 30(17-18): 4401-4425

KUTSER T., PIERSON D. C., KALLIO K. Y., REINART A. & SOBEK S., 2005. Mapping lake CDOM by satellite remote sensing, *Remote Sensing of the Environment*, 94: 535-540

LAFON V., FROIDEFOND J.M., LAHET F. & CASTAING P., 2002. SPOT shallow water bathymetry of a moderately turbid tidal inlet based on field measurements, *Remote Sensing of Environment*, 81: 136-148

LakeNet, 2009. World Lakes Network: http://www.worldlakes.org/

Lake Vänern Society for Water Conservation, 2009: http://www.lansstyrelsen.se/vastragotaland/Projektwebbar/Vanern/English/

LATIFOVIC R. & POULIOT D., 2007. Analysis of climate change impacts on lake ice phenology in Canada using the historical satellite data record, *Remote Sensing of Environment*, 106: 492-507

LAVENDER S.J., PINKERTON M.H., FROIDEFOND J-M., MORALES J., AIKEN J. & MOORE G.F., 2004. SeaWiFS validation in European coastal waters using optical and bio-geochemical measurements, *International Journal of Remote Sensing*, 25(7-8): 1481-1488

LDCM, 2010. Landsat Data Continuity Mission, NASA: http://ldcm.nasa.gov/

LEVIN S.A., 1992. The problem of pattern and scale in ecology: The Robert H. MacArthur Award Lecture, *Ecology*, 73(6): 1943-1967

LI X., PICHEL W., CLEMENTE-COLÓN P., KRASNOPOLSKY V. & SAPPER J., 2001. Validation of coastal sea and lake surface temperature measurements derived from NOAA AVHRR data, *International Journal of Remote Sensing*, 22(7): 1285-1303

LICEAGA-CORREA M. A. & EUAN-AVILA J. I., 2002. Assessment of coral reef bathymetric mapping using visible Landsat Thematic Mapper data, *International Journal of Remote Sensing*, 23(1): 3-14

LILLESAND T. M., KIEFER R. W. & CHIPMAN J. W., 2008. *Remote sensing and image interpretation*, 6th edition, USA: Wiley

LIVINGSTONE D.M., 1993. Temporal structure in the deep-water temperature of four Swiss lakes: A short-term climatic change indicator?, *Verh. Internat. Verein. Limnol.*, 25: 75-81

LIVINGSTONE D.M., 1997. An example of the simultaneous occurrence of climate-driven "sawtooth" deep-water warming/cooling episodes in several Swiss lakes, *Verh. Internat. Verein. Limnol.*, 26: 822-828

LIVINGSTONE D.M., 2003. Impact of secular climate change on the thermal structure of a large temperate central European lake, *Climatic Change*, 57: 205-225

LIVINGSTONE D.M. & DOKULIL M., 2001. Eighty years of spatially coherent Austrian lake surface temperatures and their relationship to regional air temperature and the North Atlantic Oscillation, *Limnol. Oceanogr.,* 46(5): 1220-1227

LIVINGSTONE D.M. & LOTTER A.F., 1998. The relationship between air and water temperatures in lakes of the Swiss Plateau: a case study with palaeolimnological implications, *Journal of Paleolimnology*, 19: 181-198

LIVINGSTONE D.M., LOTTER A.F. & KETTLE H., 2005. Altitude-dependent differences in the primary physical response of mountain lakes to climatic forcing, *Limnol. Oceanogr.,* 50(4): 1313-1325

LIVINGSTONE D.M. & PADISÁK J., 2007. Large-scale coherence in the response of lake surface-water temperatures to synoptic-scale climate forcing during summer, *Limnol. Oceanogr.,* 52(2): 896-902

MAITLAND P. S., 1990. *Biology of fresh waters*, 2nd edition, New York, USA: Blackie

MAS J.F. & FLORES J.J., 2008. The application of artificial neural networks to the analysis of remotely sensed data, *International Journal of Remote Sensing*, 29(3): 617-663

McCOMBIE A.M., 1959. Some relations between air temperatures and the surface water temperatures of lakes, *Limnol*. *Oceanogr*., 4: 252-258

Ministry of Environmental Protection and Water Management, Hungary, 2009. Information and Guide System of the Lake Balaton and Lake of Velence: http://www.ktm.hu/balaton/lang_en/index.htm

MINOMURA M., KUZE H. & TAKEUCHI N., 2001. Adjacency effect in the atmospheric correction of satellite remote sensing data: Evaluation of the influence of aerosol extinction profiles, *Optical Review*, 8(2): 133-141

MOORE G.F., AIKEN J. & LAVENDER S.J., 1999. The atmospheric correction of water colour and the quantitative retrieval of suspended particulate matter in Case II

waters: application to MERIS, *International Journal of Remote Sensing*, 20(9): 1713-1733

MOSS B., 1988. *Ecology of fresh waters: Man and medium*, 2nd edition, Oxford, UK: Blackwell Scientific

MUMM Ocean Colour, 2009. Management Unit of the North Sea Mathematical Models; Department VI of the Royal Belgian Institute of Natural Sciences: http://www.mumm.ac.be/OceanColour/index.php

MUNASINGHE M. & SWART R., 2005. *Primer on climate change and sustainable development; Facts, Policy analysis and Applications*, UK: Cambridge University Press

NASA, 2009. POES project: http://goespoes.gsfc.nasa.gov/poes/project/index.html

NASA AMSR-E, 2010. The NASA Marshall Space Flight Centre: http://weather.msfc.nasa.gov/AMSR/

NASA Ocean Colour, 2009: http://oceancolor.gsfc.nasa.gov/

NELLIS M. D., HARRINGTON J. A. & WU J., 1998. Remote sensing of temporal and spatial variations in pool size, suspended sediment, turbidity and Secchi depth in Tuttle Creek Reservoir, Kansas: 1993, *Geomorphology*, 21: 281-293

NEODAAS DSRS, 2009. NERC Earth Observation Data Acquisition and Analysis Service (NEODAAS) Dundee Satellite Receiving Station (DSRS), University of Dundee: http://www.sat.dundee.ac.uk/

NESDIS, 2009. National Environmental Satellite Data and Information Service: http://www.class.ngdc.noaa.gov/release/data_available/avhrr/index.htm

NOAA MOST, 2009. Marine Observing Systems Team: http://manati.orbit.nesdis.noaa.gov/sst/coefficient.html http://manati.orbit.nesdis.noaa.gov/

ODERMATT D., GIARDINO C. & HEEGE T., 2010. Chlorophyll retrieval with MERIS Case-2-Regional in perialpine lakes, *Remote Sensing of Environment*, 114: 607-617

ODERMATT D., HEEGE T., NIEKE J., KNEUBÜHLER M. & ITTEN K., 2008a. Water quality monitoring for Lake Constance with a physically based algorithm for MERIS data, *Sensors*, 8: 4582-4599

ODERMATT D., KISELEV V., HEEGE T., KNEUBÜHLER M. & ITTEN K.I., 2008b. *Adjacency effect considerations and air/water constituent retrieval for Lake Constance*, 2nd MERIS/AATSR workshop, Frascati, Italy, 22-26 September 2008

OECD, 1982. *Eutrophication of water: monitoring, assessment and control*, Organisation of Economic Cooperation and Development (OECD), Paris, pp. 150

OESCH D. C., JAQUET J. M., HAUSER A. & WUNDERLE S., 2005. Lake surface water temperature retrieval using Advanced Very High Resolution Radiometer and Moderate

Resolution Imaging Spectroradiometer data: Validation and feasibility study, *Journal of Geophysical Research*, 110: C12014

OESCH D. C., JAQUET J. M., KLAUS R. & SCHENKER P., 2008. Multi-scale thermal pattern monitoring of a large lake (Lake Geneva) using a multi-sensor approach, *International Journal of Remote Sensing*, 29(19-20): 5785-5808

PADISÁK J., 1992. Seasonal succession of phytoplankton in a large shallow lake (Balaton, Hungary) – a dynamic approach to ecological memory, its possible role and mechanisms, *Journal of Ecology*, 80: 217-230

PAGE E., 2006. *Climate change, justice and future generations*, UK: Edward Elgar Publishing Limited

PALECKI M.A. & BARRY R.G., 1986. Freeze-up and break-up of lakes as an index of temperature changes during the transition seasons: A case study for Finland, *Journal of Climate and Applied Meteorology*, 25: 893-902

PEETERS F., STRAILE D., LORKE A. & LIVINGSTONE D.M., 2007. Earlier onset of the spring phytoplankton bloom in lakes of the temperate zone in a warmer climate, *Global Change Biology*, 13: 1898-1909

PITTOCK A.B., 2005. *Climate Change: Turning up the heat*, Australia: CSIRO Publishing

PO.DAAC, 2010. NASA Physical Oceanography (PO) Distributed Active Archive Centre (DAAC): http://podaac.jpl.nasa.gov/pub/documents/dataset_docs/modis_sst.html#10.

PULLIAINEN J., KALLIO K., ELOHEIMO K., KOPONEN S., SERVOMAA H., HANNONEN T., TAURIAINEN S. & HALLIKAINEN M., 2001. A semi-operative approach to lake water quality retrieval from remote sensing data, *The Science of the Total Environment*, 268: 79-93

QUIBELL G., 1991. The effect of suspended sediment on reflectance from freshwater algae, *International Journal of Remote Sensing*, 12(1): 177-182

RAJADURAI M., POORNIMA E.H., NARASHIMHAN S.V., RAO V.N.R. & VENUGOPALAN V.P., 2005. Phytoplankton growth under temperature stress: Laboratory studies using two diatoms from a tropical coastal power station site, *Journal of Thermal Biology*, 30: 299-305

RAST M., BÉZY J.L. & BRUZZI S., 1999. The ESA Medium Resolution Imaging Spectrometer MERIS – a review of the instrument and its mission, *International Journal of Remote Sensing*, 20(9): 1681-1702

REES W.G., 1990. *Physical principles of Remote Sensing*, Cambridge: Cambridge University Press

REID G. K., 1961. *Ecology of inland waters and estuaries*, New York, USA: Reinhold Publishing

REINART A. & REINHOLD M., 2008. Mapping surface temperature in large lakes with MODIS data, *Remote Sensing of Environment*, 112: 603-611

ROBINSON I.S., 1985. *Satellite oceanography, An introduction for oceanographers and remote sensing scientists*, England: Ellis Horwood Limited

RUIZ-VERDÚ A., KOPONEN S., HEEGE T., DOERFFER R., BROCKMANN C., KALLIO K., PYHÄLAHTI T., PEÑA R., POLVORINOS A., HEBLINSKI J., YLÖSTALO P., CONDE L., ODERMATT D., ESTELLÉS V. & PULLIAINEN J., 2008. *Development of MERIS lake water algorithms: validation results from Europe*, 2nd MERIS/AATSR workshop, Frascati, Italy, 22-26 September 2008

SABINS F.F., 1997. *Remote Sensing: Principles and Interpretation*, 3rd edition, New York: W. H. Freeman and Company

SAWAYA K. E., OLMANSON L. G., HEINERT N. J., BREZONIK P. L. & BAUER M. E., 2003. Extending satellite remote sensing to local scales: land and water resource monitoring using high – resolution imagery, *Remote Sensing of Environment*, 88: 144-156

SCHILLER H. & DOERFFER R., 1999. Neural network for emulation of an inverse model – operational derivation of Case II water properties from MERIS data, *International Journal of Remote Sensing*, 20(9): 1735-1746

SCHLUESSEL P., EMERY W.J., GRASSL H. & MAMMEN T., 1990. On the skin-bulk temperature difference and its impact on satellite remote sensing of sea surface temperature, *Journal of Geophysical Research*, 95: 13341-13356.

SCHOFIELD O., GRZYMSKI J., BISSETT W.P., KIRKPATRICK G.J., MILLIE D.F., MOLINE M. & ROESLER C.S., 1999. Optical monitoring and forecasting systems for

harmful algal blooms: possibility of pipe dream?, *Journal of Phycology*, 35: 1477-1496

SCHWARZ D., GROSCH R., GROSS W. & HOFFMANN-HERGARTEN S., 2005. Water quality assessment of different reservoir types in relation to nutrient solution use in hydroponics, *Agricultural Water Management*, 71: 145-166

STEISSBERG T. E., HOOK S. J. & SCHLADOW S. G., 2005. Characterizing partial upwellings and surface circulation at Lake Tahoe, California-Nevada, USA with thermal infrared images, *Remote Sensing of Environment*, 99: 2-15

STRAILE D., 2000. Meteorological forcing of plankton dynamics in a large and deep continental European lake, *Oecologia*, 122: 44-50

STRAILE D. & ADRIAN R., 2000. The North Atlantic Oscillation and plankton dynamics in two European lakes – two variations on a general theme, *Global Change Biology*, 6: 663-670

STRAMSKA M. & STRAMSKI D., 2005. Effects of non-uniform vertical profile of chlorophyll concentration on remote sensing reflectance of the ocean, *Applied Optics*, 44: 1735-1747

STRÖMBECK N. & PIERSON D.C., 2001. The effects of variability in the inherent optical properties on estimations of chlorophyll *a* by remote sensing in Swedish freshwaters, *The Science of the Total Environment*, 268: 123-137

SVÁB E., TYLER A.N., PRESTON T., PRÉSING M. & BALOGH K.V., 2005. Characterizing the spectral reflectance of algae in lake waters with high suspended sediment concentrations, *International Journal of Remote Sensing*, 26(5): 919-928

THIEMANN S. & KAUFMANN H., 2000. Determination of chlorophyll content and trophic state of lakes using field spectrometer and IRS-1C satellite data in the Mecklenburg Lake District, Germany, *Remote Sensing of Environment*, 73: 227-235

TYLER A.N., SVÁB E., PRESTON T., PRÉSING M. & KOVÁCS W.A., 2006. Remote sensing of the water quality of shallow lakes: A mixture modelling approach to quantifying phytoplankton in water characterized by high-suspended sediment, *International Journal of Remote Sensing*, 27(8): 1521-1537

UNEP, 2000. *Lakes and Reservoirs: Similarities, Differences and Importance*, United Nations Environment Programme (UNEP) International Environmental Technology Centre (IETC) Short Report 1, pp. 63

UNFCCC, 1992. The United Nations Framework Convention on Climate Change, Article 1: Definitions: http://unfccc.int/essential_background/convention/items/2627.php

US EPA, 2009. United States of America Environmental Protection Agency (EPA), Aquatic Resources Monitoring: http://www.epa.gov/nhrlsup1/arm/designpages/lakes/monitoring_lakes.htm

USGS, 2009. US Geological Survey: http://or.water.usgs.gov/grapher/fnu.html

VIDOT J. & SANTER R., 2005. Atmospheric correction for inland waters – application to SeaWiFS, *International Journal of Remote Sensing*, 26(17): 3663-3682

VINCENT R. B., QIN X., McKAY R. M. L., MINER J., CZAJKOWSKI K., SAVINO J. & BRIDGEMAN T., 2004. Phycocyanin detection from Landsat TM data for mapping cyanobecterial blooms in Lake Erie, *Remote Sensing of Environment*, 89: 381-392

VOS R. J., HAKVOORT J. H. M., JORDANS R. W. J. & IBELINGS B. W., 2003. Multiplatform optical monitoring of eutrophication in temporally and spatially variable lakes, *The Science of Total Environment*, 312(1-3): 221-243

VOS R. J. & RIJKEBOER M., 2000. *Monitoring of algal blooms in Case II waters with SeaWiFS*, XV Ocean Optics Conference, 16-20 October 2000, Monaco, paper no. 1094

WANG H., HLADIK C.M., HUANG W., MILLA K., EDMISTON L., HARWELL M.A. & SCHALLES J.F., 2010. Detecting the spatial and temporal variability of chlorophyll *a* concentration and total suspended solids in Apalachicola Bay, Florida using MODIS imagery, *International Journal of Remote Sensing*, 31(1-2): 439-453

WDC-RSAT, 2010. The World Data Centre for Remote Sensing of the Atmosphere: http://wdc.dlr.de/sensors/

WELCH P. S., 1935. *Limnology*, New York, USA: McGraw-Hill

WEN X., 2008. A new prompt algorithm for removing the bowtie effect of MODIS L1B data, *The International Archives of the Photogrammetry, Remote Sensing and Spatial*

Information Sciences, ISPRS Congress, Beijing, Volume XXXVII, Part B3b, Commission III, WG III/1

WETZEL R.G., 2001. *Limnology: lake and river ecosystems*, San Diego: Academic

WEYHENMEYER G.A., ADRIAN R., GAEDKE U., LIVINGSTONE D.M. & MABERLY S.C., 2002. Response of phytoplankton in European lakes to a change in the North Atlantic Oscillation, *Verh. Internat. Verein. Limnol.*, 28: 1436-1439

WEYHENMEYER G.A., BLENCKNER T. & PETTERSSON K., 1999. Changes of the plankton spring outburst related to the North Atlantic Oscillation, *Limnol. Oceanogr.*, 44(7): 1788-1792

WEYHENMEYER G.A., MEILI M. & LIVINGSTONE D.M., 2004. Nonlinear temperature response of lake ice breakup, *Geophysical Research Letters*, 31, L07203, doi: 10.1029/2004GL019530

WHEELER D., SHAW G. & BARR S., 2006. *Statistical techniques in geographical analysis*, London: David Fulton Publishers Ltd.

WILHELM S. & ADRIAN R., 2007. Long-term response of *Dreissena polymorpha* larvae to physical and biological forcing in a shallow lake, *Oecologia*, 151: 104-114

WILHELM S. HINTZE T., LIVINGSTONE D.M. & ADRIAN R., 2006. Long-termm response of daily epilimnetic temperature extrema to climate forcing, *Canadian Journal of Aquatic Science*, 63: 2467-2477

WOOSTER M.J., PATTERSON G., LOFTIE R. & SEAR C., 2001. Derivation and validation of the seasonal thermal structure of Lake Malawi using multi-satellite AVHRR observations, *International Journal of Remote Sensing*, 22(15): 2953-2972

WOOSTER M.J., SEAR C.B., PATTERSON G. & HAIGH J., 1994. Tropical lake surface temperatures from locally received NOAA-11 AVHRR data-comparison with *in situ* measurements, *International Journal of Remote Sensing*, 15(1): 183-189

WU A., XIONG X. & CAO C., 2008. Terra and Aqua MODIS inter-comparison of three reflective solar bands using AVHRR onboard the NOAA-KLM satellites, *International Journal of Remote Sensing*, 29(7-8): 1997-2010

WYNNE R.H., LILLESAND T.M., CLAYTON M.K. & MAGNUSON J.J., 1998. Satellite monitoring of lake ice breakup on the Laurentian shield (1980-1994), *Photogrammetric Engineering and Remote Sensing*, 64(6): 607-617

XIU P., LIU Y. & TANG J., 2008. Variations of ocean colour parameters with non-uniform vertical profiles of chlorophyll concentration, *International Journal of Remote Sensing*, 29(3-4):831-849

ZANEVELD J.R.V., BARNARD A.H. & BOSS E., 2005. Theoritical derivation of the depth average of remotely sensed optical parameters, *Optics Express*, 13(22): 9052-9061

APPENDIX I

Table: Islands and main rivers/tributaries that flow in and out of the 23 lake sites (Source: ILEC, 2009; LakeNet, 2009).

Lake	Number of islands	Size of largest island	Main inflow(s)	Main outflow(s)
Vänern	Numerous	Fågelö (50km^2)	River Klar	R. Göta
Vättern	Numerous	Visingsö (21km^2)	(n/a)	R. Motala
Mälaren	Numerous	Selaön (91 km^2),	(n/a)	
Hjälmaren	Numerous	Vinön (5 km^2)	(n/a)	R. Hyndevadsstom, Canal Hjälmare
Päijänne	Numerous	Virmailansaari (34 km^2)	(n/a)	Kalkkistenkoski, Kymijoki
Inarijärvi	> 3,000	Mahlatti (21 km^2)	(n/a)	
Pielinen	Numerous	Paalasmaa (27 km^2)	(n/a)	R. Pielisjoki
Oulujärvi	Numerous	Manamansalö (71 km^2)	(n/a)	(n/a)
Haukivesi	Numerous	Linnansaari (4.4 km^2)	(n/a)	(n/a)
Kallavesi	Numerous	Haukiniemi (5 km^2)	(n/a)	(n/a)
Näsijärvi	Numerous	Iso-Otava (1.1 km^2)	(n/a)	R. Tammeskoski
Geneva	0		(n/a)	R. Rhône
Constance	3	Reichenau (4 km^2)	R. Rhein	R. Rhein
Bourget	0		R. Leysse	Canal de Savières
Annecy	0		R. Eau Morte, R. Ire, R. Borette	R. Thiou
Müggelsee	0		R. Spree	R. Spree
Aiguebelette	2	(no name)	R. Leysse	R. Tiers
Balaton	0		R. Zala	Canal Sió
Tisza	0		(n/a)	(n/a)
Velence	0		(n/a)	(n/a)
Lomond	60*	Pier (1 km^2)	(n/a)	R. Leven
Windermere	Numerous	Belle (< 1 km^2)	R. Brathay, R. Rothay, R. Trout Beck, R. Cunsey Beck	R. Leven
Leven	6*	(no name)	(n/a)	(n/a)

*Depending on water level

Table: Catchment size and relative percentages (%) of main land use and land cover features (Source: ILEC, 2009).

Lake	Catchment size (km^2)	% of main land use/land cover features		
		Natural vegetation	Agriculture	Others*
Vänern	41,182	67.9	18.5	13.6
Vättern	4,503	62.9	26.7	10.4
Mälaren	21,460	64.5	25.4	10.1
Hjälmaren	3,575	51.9	25.4	22.7
Päijänne	25,400	87	10	3
Inarijärvi	13,400	99.9	0.02	0.08
Pielinen	12,823	83.9	6.1	10
Oulujärvi	(n/a)	(n/a)	(n/a)	(n/a)
Haukivesi	(n/a)	(n/a)	(n/a)	(n/a)
Kallavesi	(n/a)	(n/a)	(n/a)	(n/a)
Näsijärvi	(n/a)	(n/a)	(n/a)	(n/a)
Geneva	7,975	(n/a)	(n/a)	(n/a)
Constance	10,900	(n/a)	(n/a)	(n/a)
Bourget	560	(n/a)	(n/a)	(n/a)
Annecy	278	(n/a)	(n/a)	(n/a)
Müggelsee	(n/a)	(n/a)	(n/a)	(n/a)
Aiguebelette	70	(n/a)	(n/a)	(n/a)
Balaton	5,775	35	56.5	8.4
Tisza	(n/a)	(n/a)	(n/a)	(n/a)
Velence	602	(n/a)	(n/a)	(n/a)
Lomond	696	80.2	16.7	3.1
Windermere	231	(n/a)	(n/a)	(n/a)
Leven	145	(n/a)	(n/a)	(n/a)

*Include Human habitations and Industry

APPENDIX II

Maps of the study sites including the location of the field sampling station(s)

Lake Vänern (5 stations)

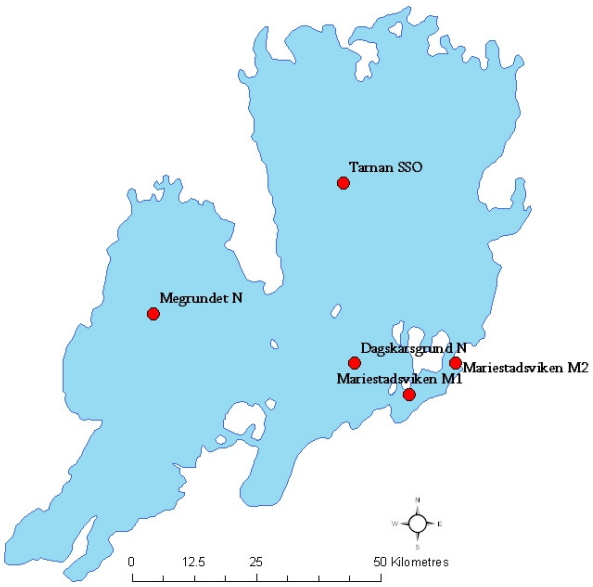

Lake Vättern (2 stations)

Lake Mälaren (13 stations)

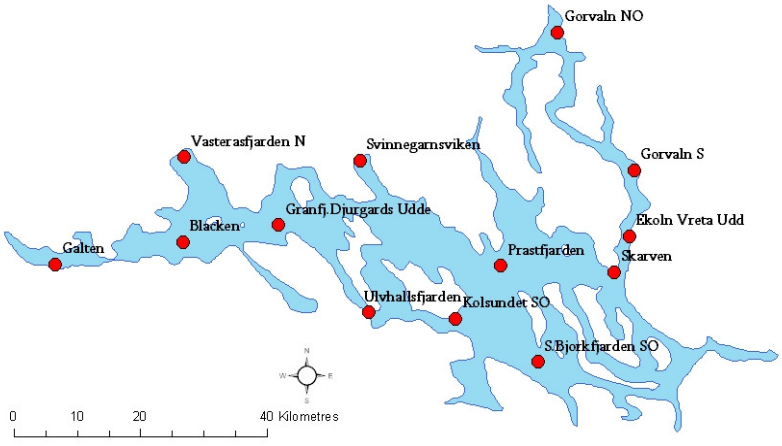

Lake Hjälmaren (3 stations)

Lake Pielinen (10 stations)

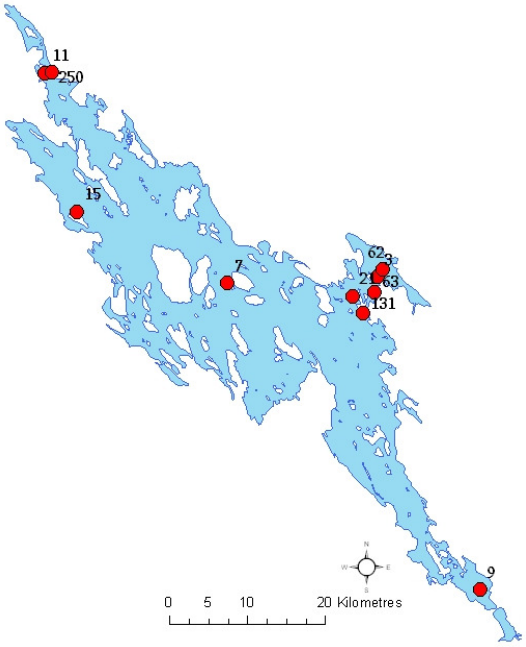

Lake Inärijärvi (4 stations)

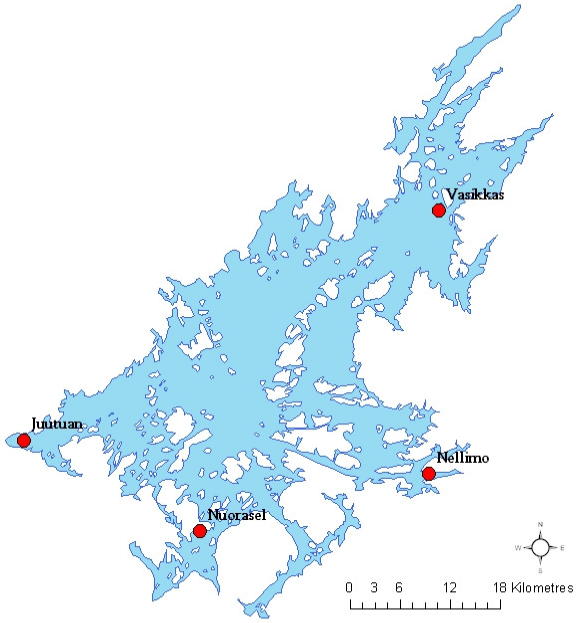

Lake Haukivesi (6 stations)

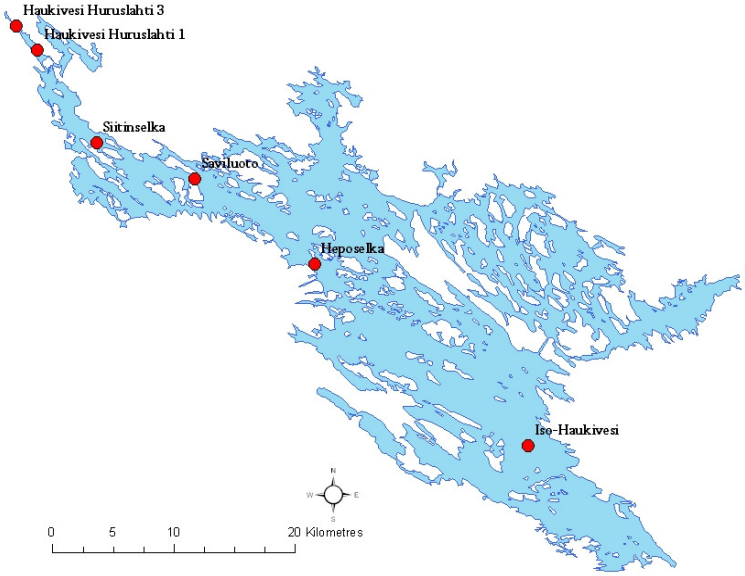

Lake Näsijärvi (6 stations)

Lake Kallavesi (7 stations)

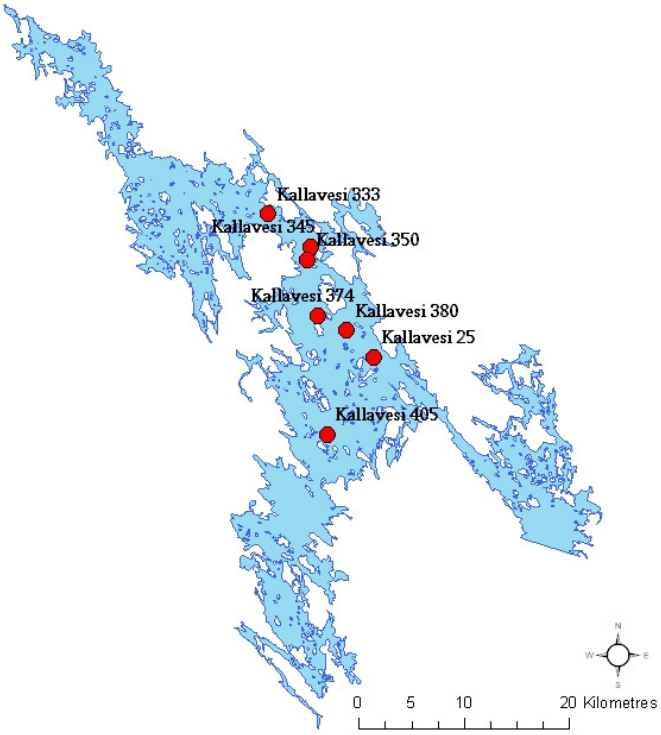

Lake Päijänne (11 stations)

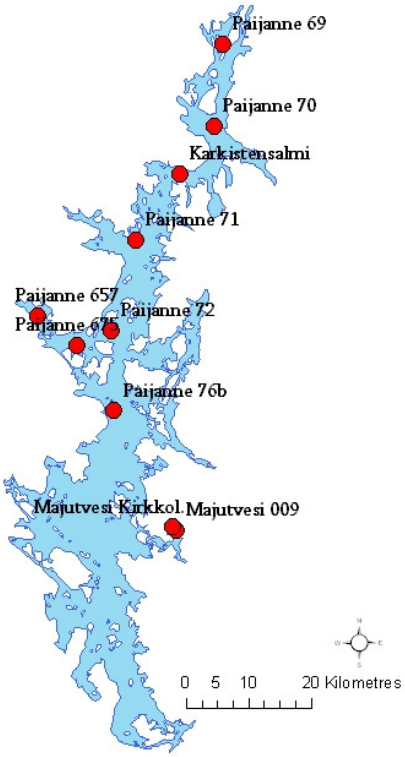

Lake Oulujärvi (7 stations)

Lake Annecy (1 station)

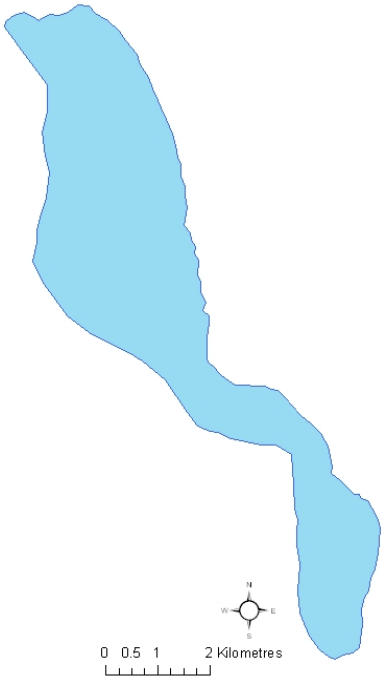

Lake Müggelsee (1 station)

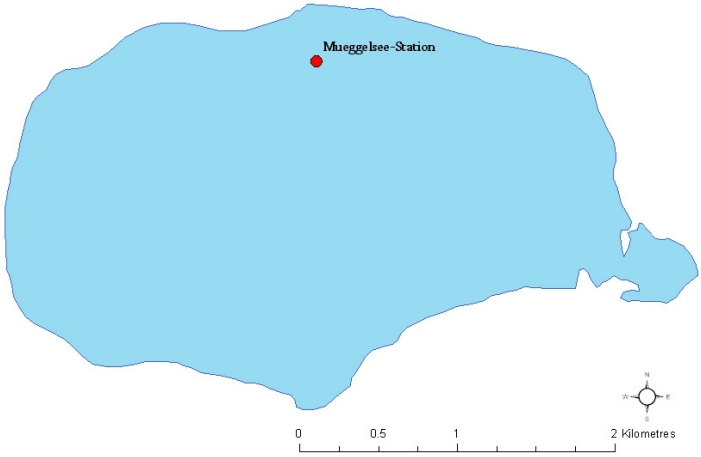

Lake Bourget

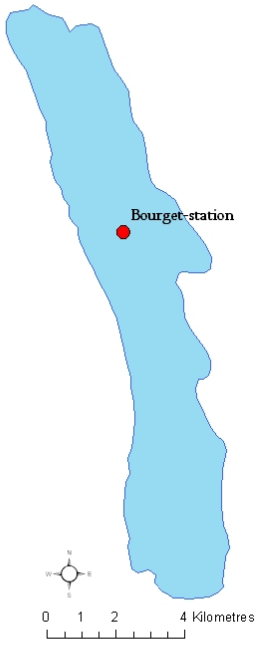

Lake Aiguebelette (1 station)

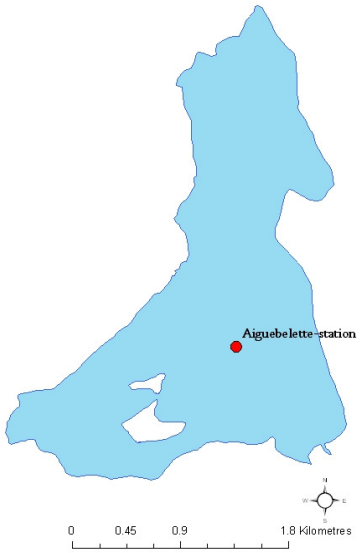

Loch Leven (2 stations)

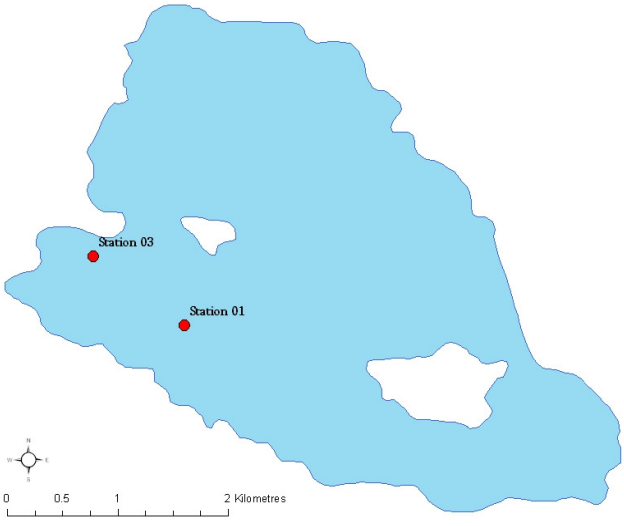

Lake Constance (1 station)

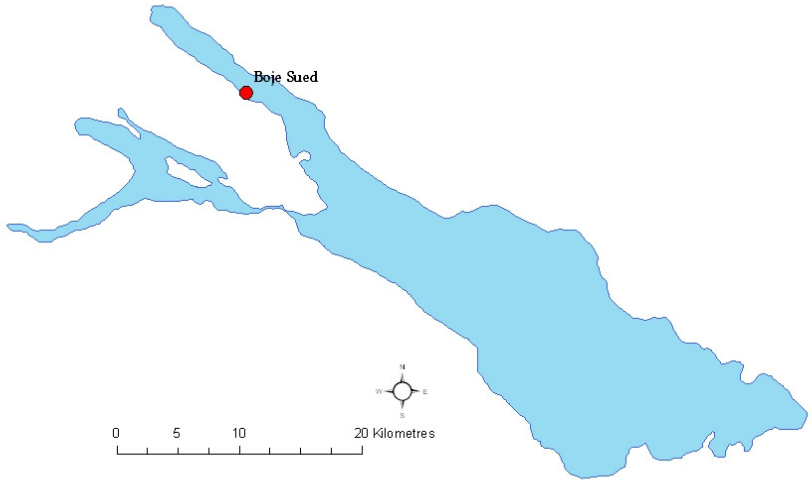

Lake Geneva (1 station)

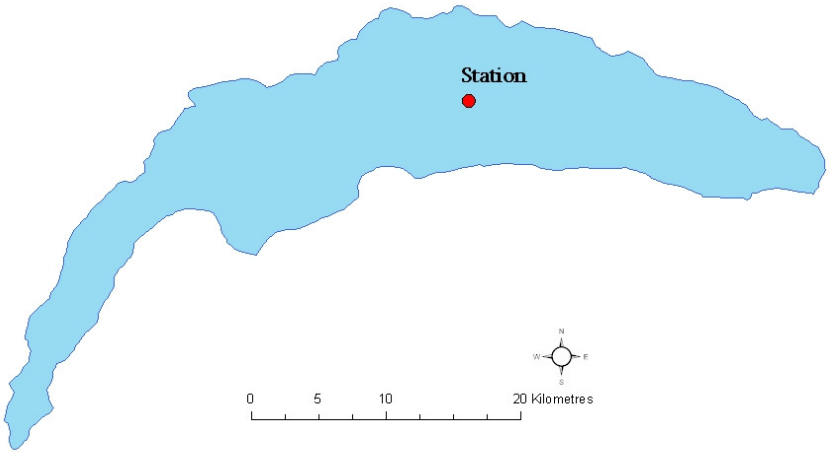

Lake Balaton (4 stations)

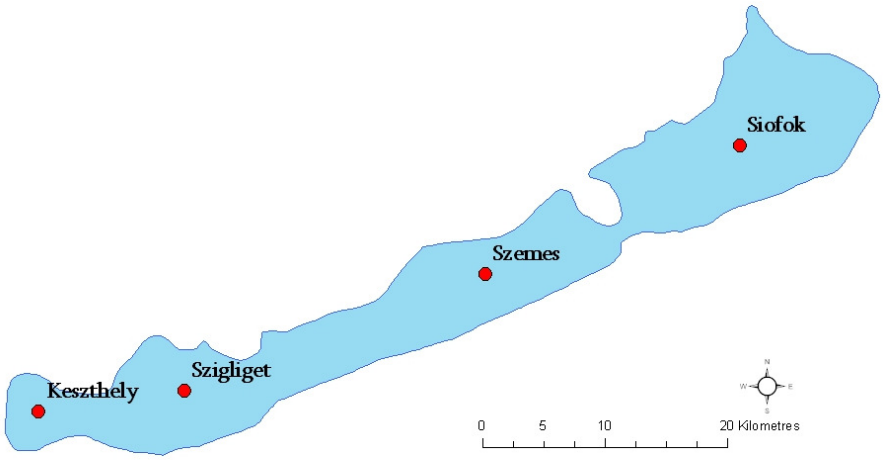

Lake Velence (3 stations)

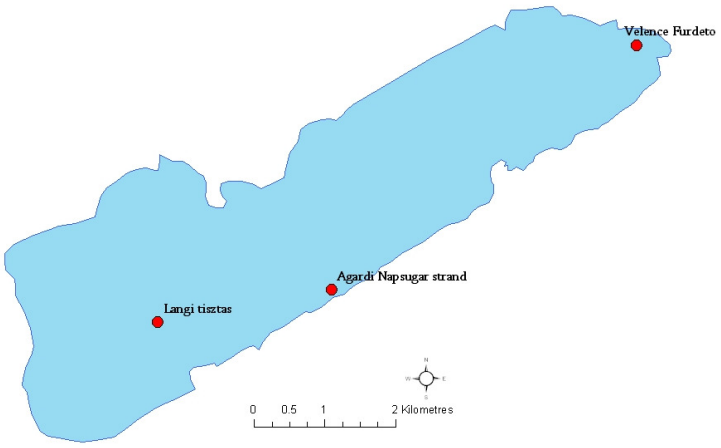

Loch Lomond (1 station)

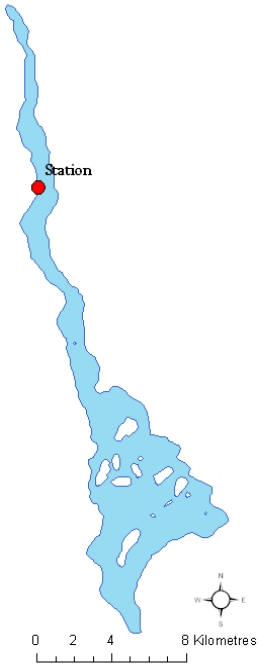

Lake Tisza (5 stations)

Lake Windermere (1 station)

APPENDIX III

Trends in seasonal temperature (calculated from monthly means) within each of the five lake groups/ ecoregions and two individual lakes

Alps: Aiguebelette, Annecy, Bourget, Constance and Geneva

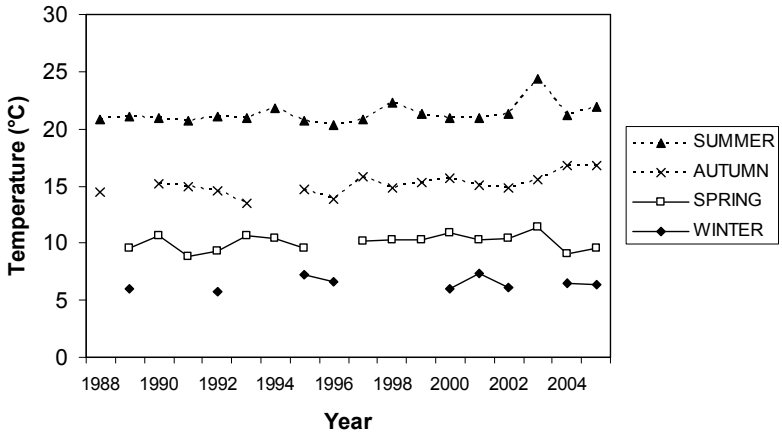

Hungarian lowlands: Balaton, Tisza and Velence

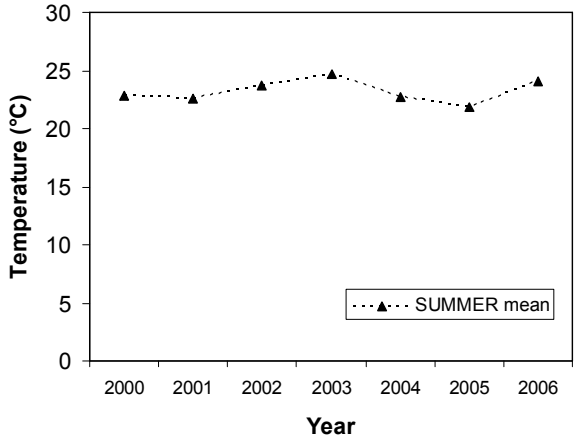

Central plains: Vänern, Vättern, Mälaren and Hjälmaren

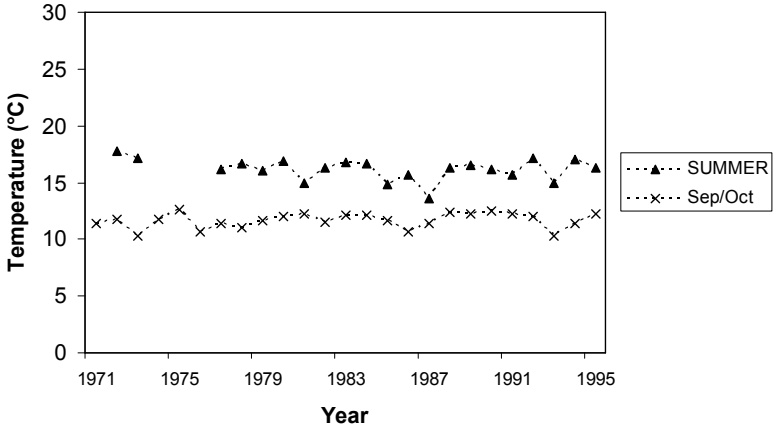

Fenno-Scandian shield: Haukivesi, Kallavesi, Oulujärvi, Päijänne, Pielinen and Näsijärvi

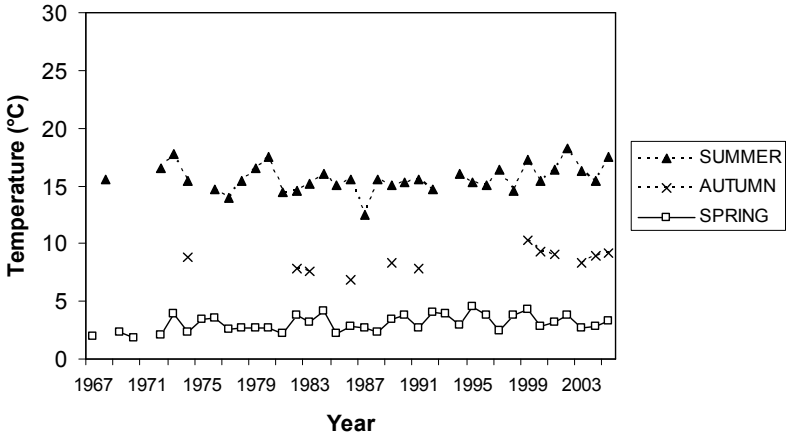

Lake Müggelsee

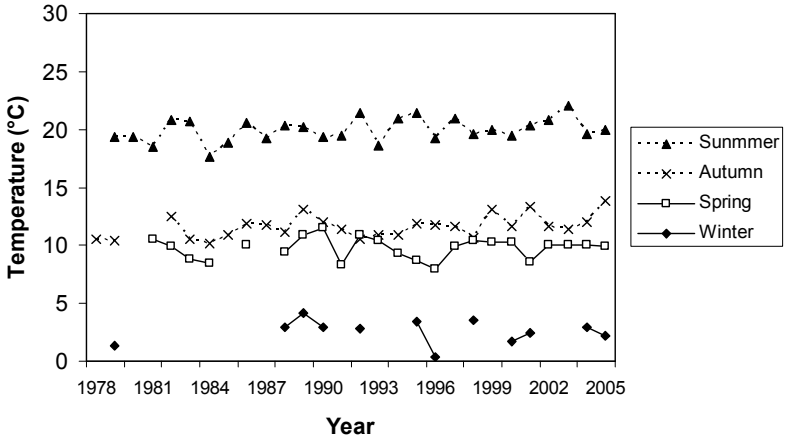

Lake Inärijärvi

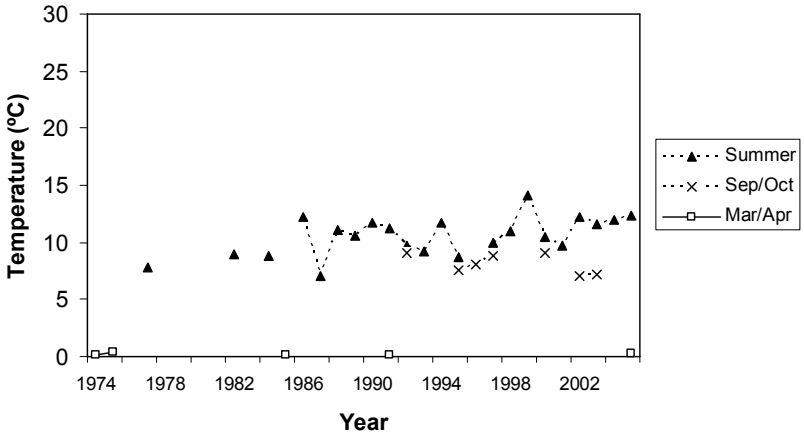

APPENDIX IV

SPATIAL VARIABILITY OF TEMPERATURE IN 2001 – Lake Geneva

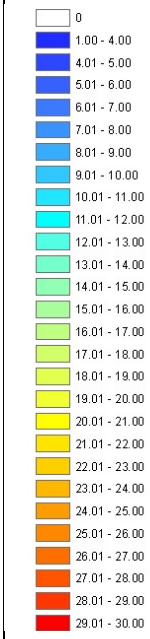

5 March

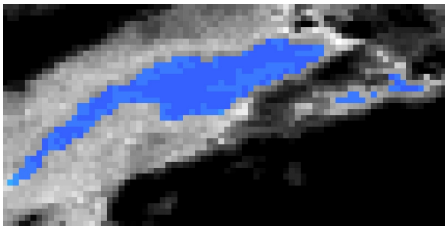

27 March

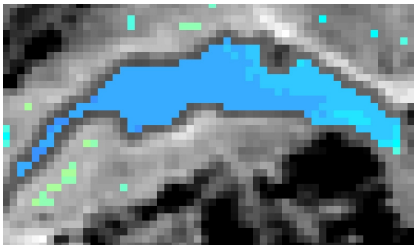

26 April

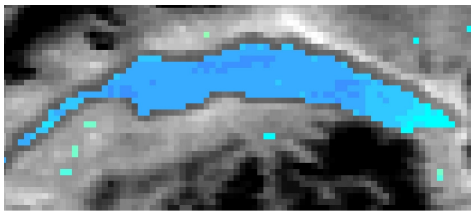

5 June

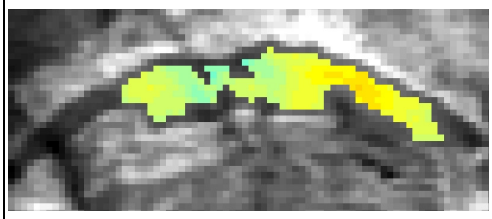

25 June

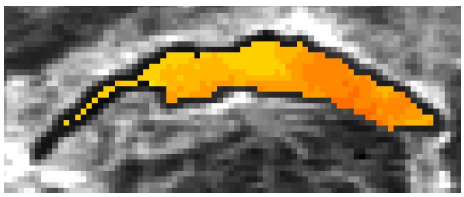

23 July

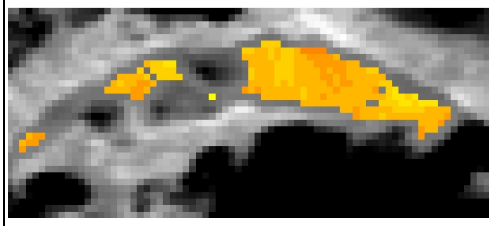

13 August

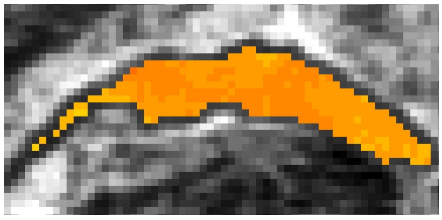

21 August

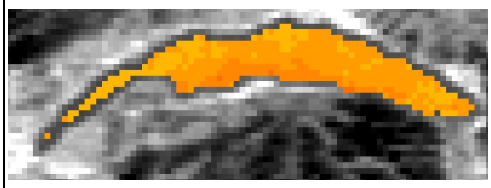

3 September

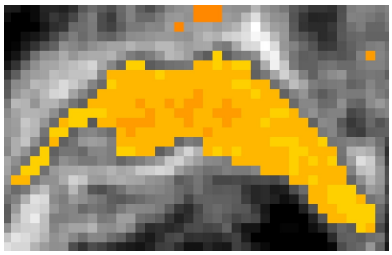

9 October

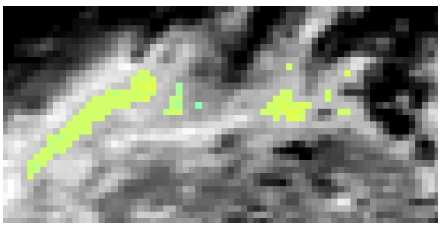

SPATIAL VARIABILITY OF TEMPERATURE IN 2003 – Lake Geneva

24 March	28 April
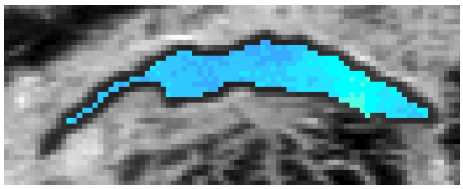	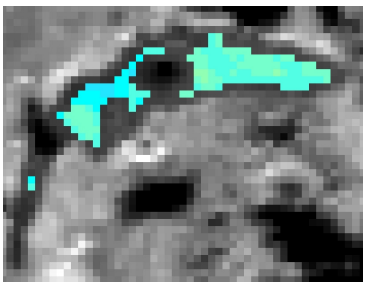
16 June	23 June
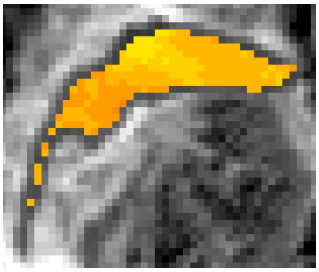	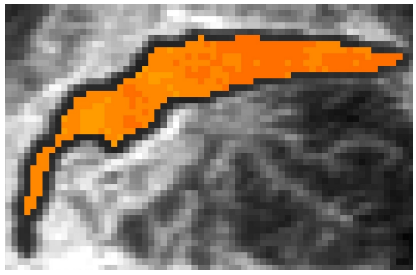
10 July	11 August
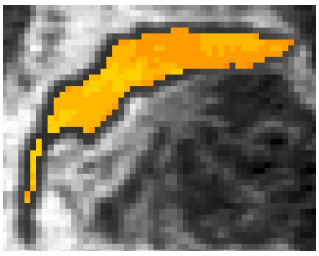	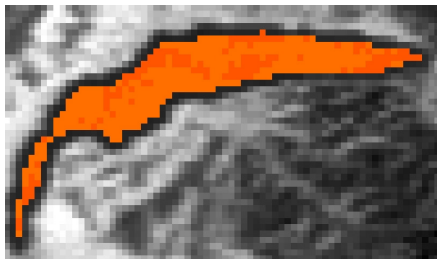
3 September	29 September
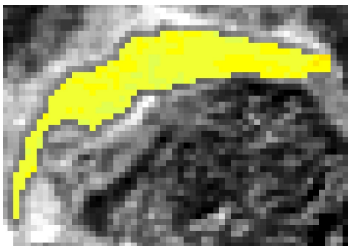	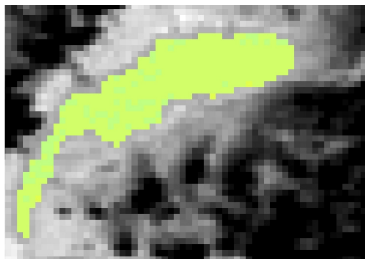
13 October	18 November
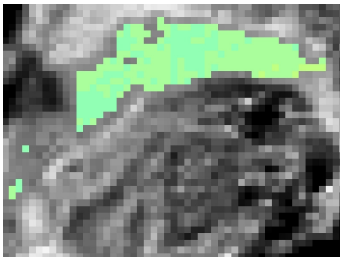	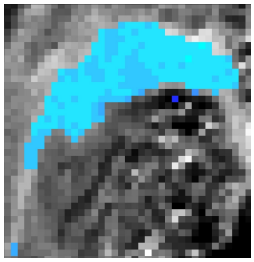

SPATIAL VARIABILITY OF TEMPERATURE IN 2001 – Lake Constance

26 April	9 May
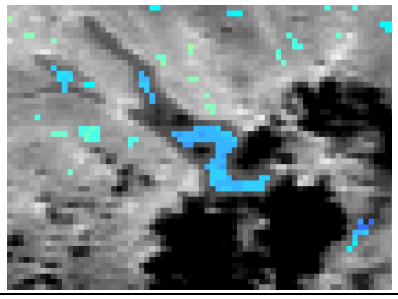	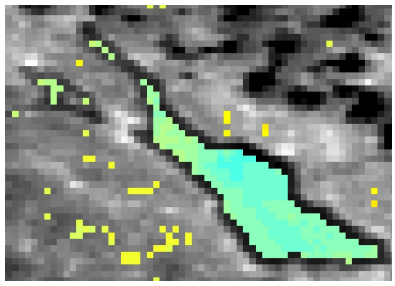
5 June	7 June
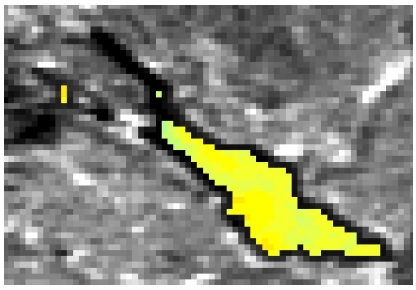	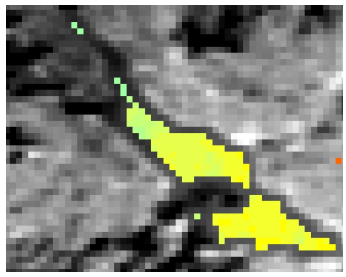
25 June	23 July
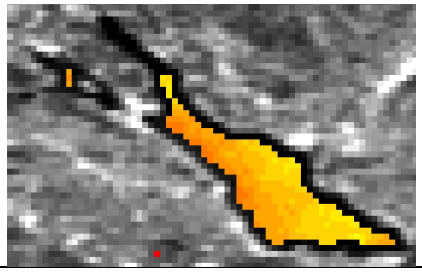	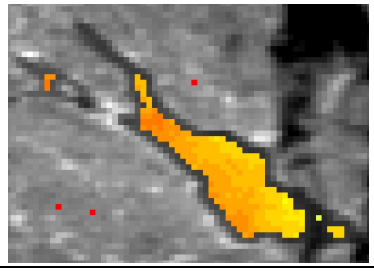
13 August	21 August
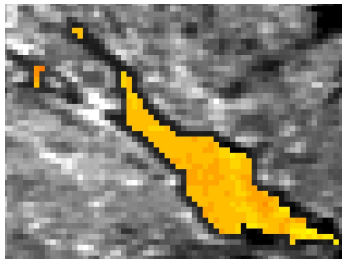	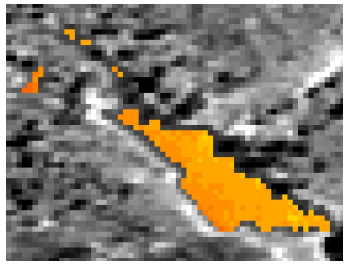
3 September	22 October
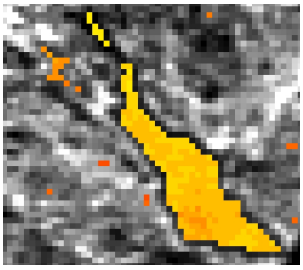	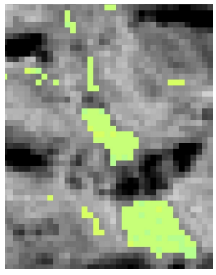

SPATIAL VARIABILITY OF TEMPERATURE IN 2002 – Lake Constance

18 March

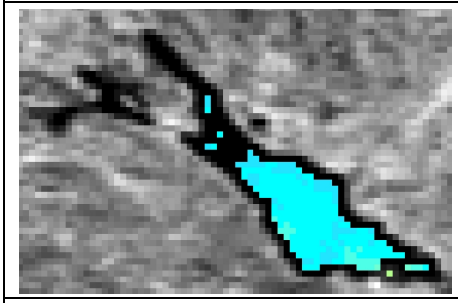

30 April

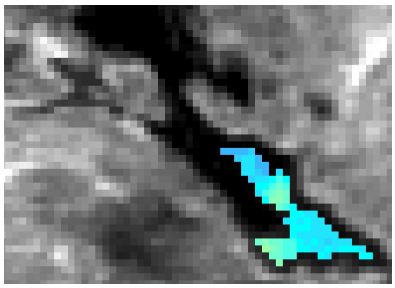

13 May

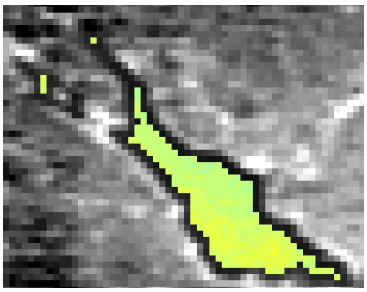

17 June

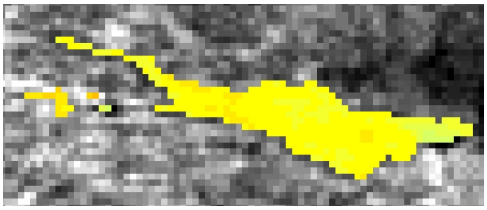

27 June

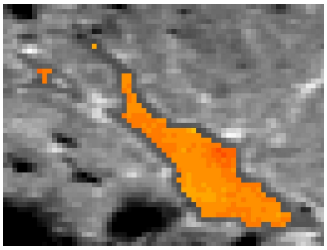

8 July

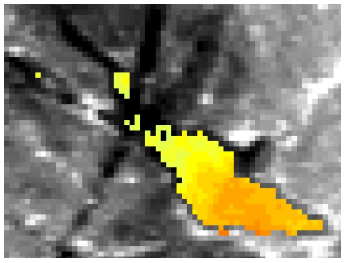

23 July

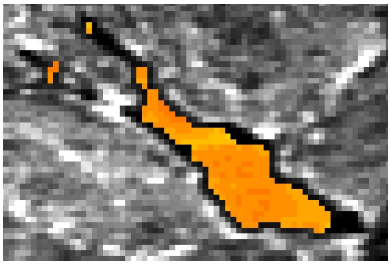

5 August

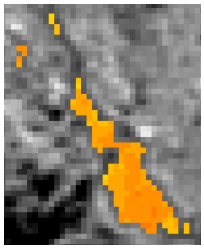

30 September

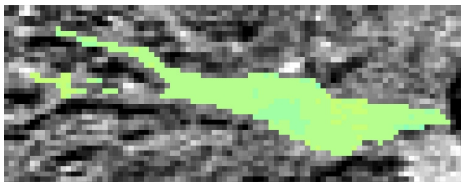

16 October

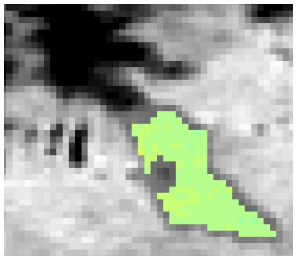

SPATIAL VARIABILITY OF TEMPERATURE IN 2001 – Lake Hjälmaren

9 May

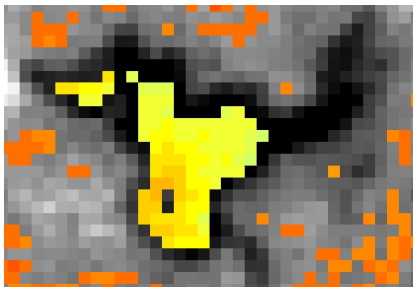

22 May

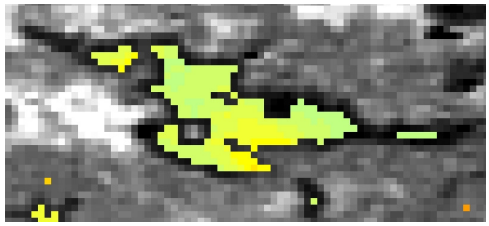

5 June

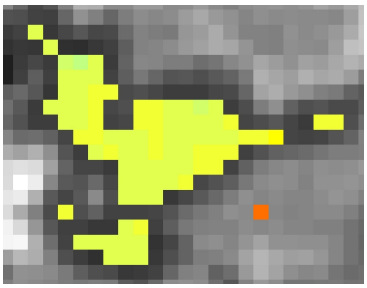

9 July

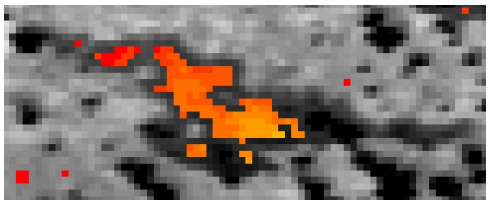

30 July

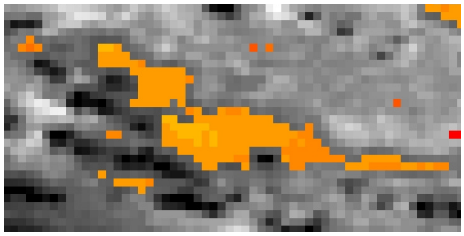

13 August

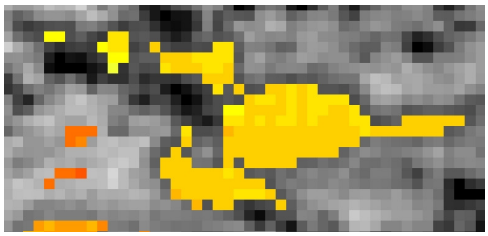

21 August

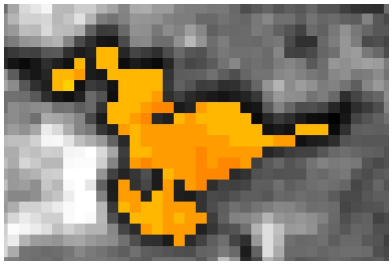

22 October

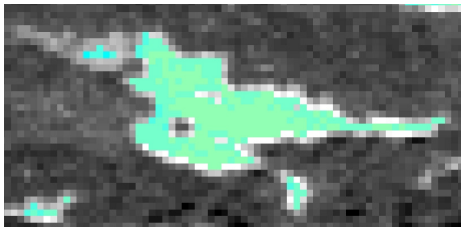

23 October

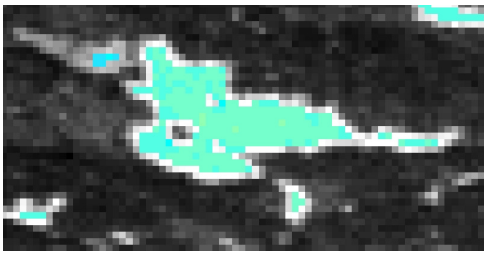

SPATIAL VARIABILITY OF TEMPERATURE IN 2002 – Lake Hjälmaren

16 May

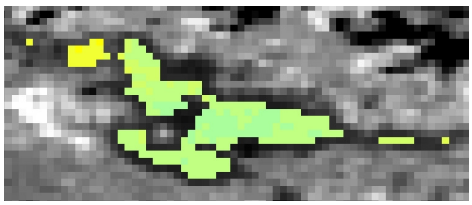

17 June

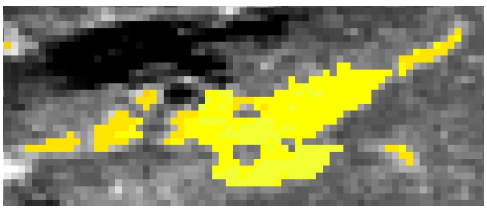

18 June

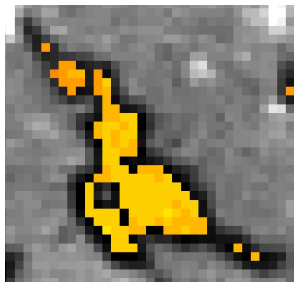

19 August (11:47 a.m.)

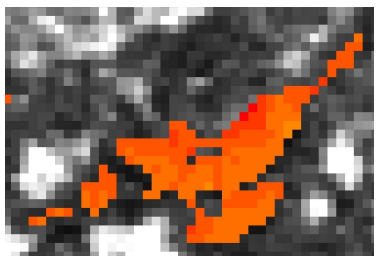

19 August (12:17 p.m.)

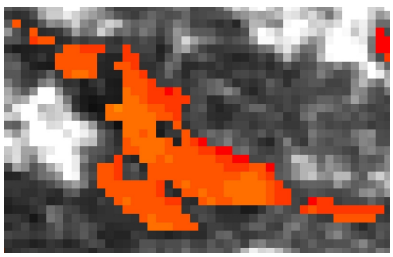

26 August

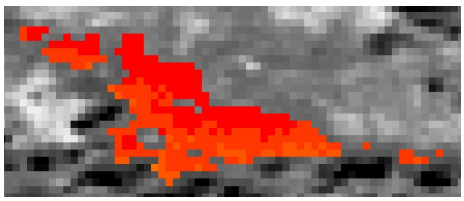

27 August

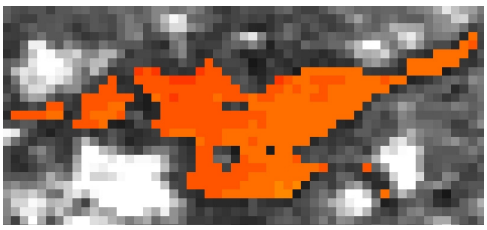

SPATIAL VARIABILITY OF TEMPERATURE IN 2003 – Lake Vänern

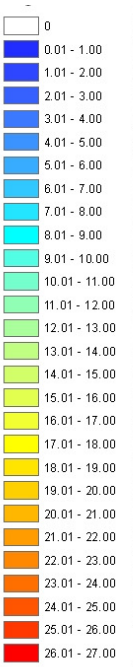

8 April

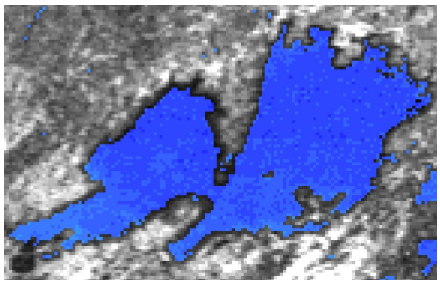

14 May

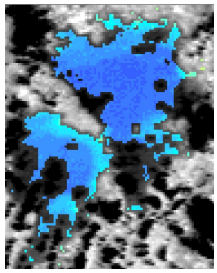

2 June

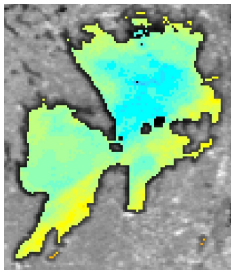

18 June

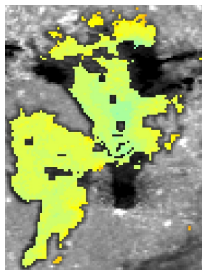

10 July

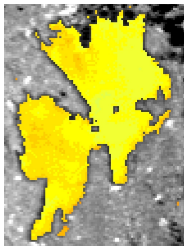

16 July

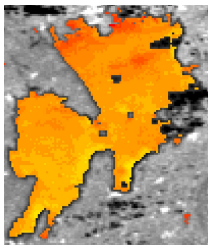

4 August

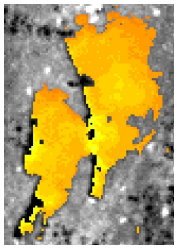

12 August

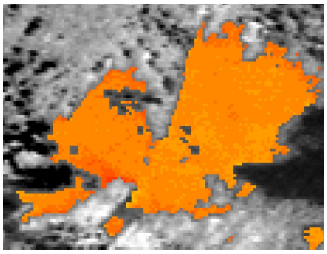

8 September

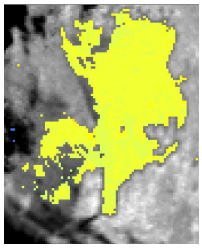

13 October

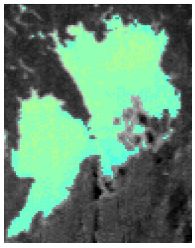

SPATIAL VARIABILITY OF TEMPERATURE IN 2002 – Lake Vänern

17 April

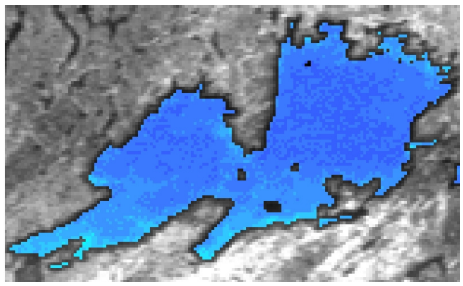

13 May

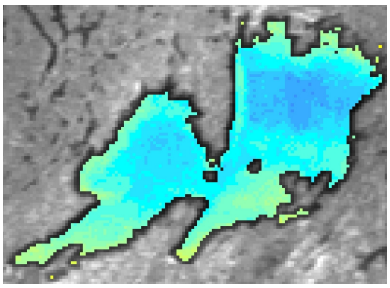

24 June

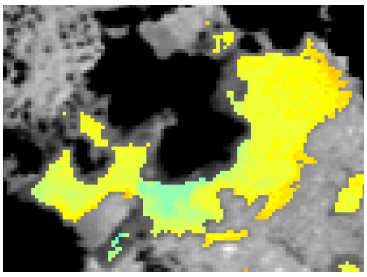

15 July

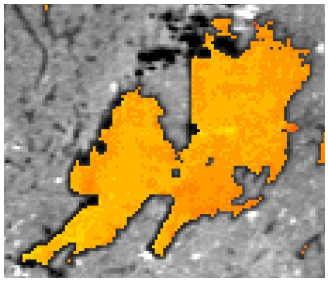

5 August

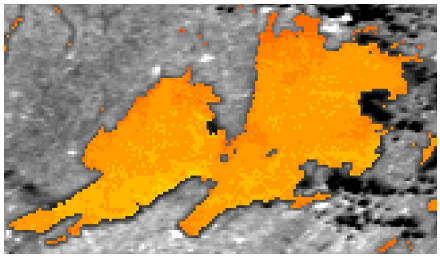

19 August (11:47 a.m.)

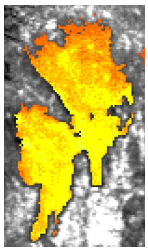

19 August (12:17 p.m.)

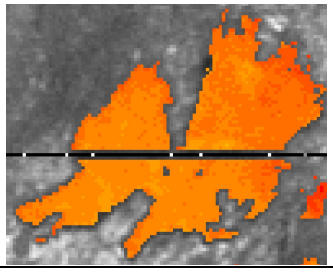

26 August

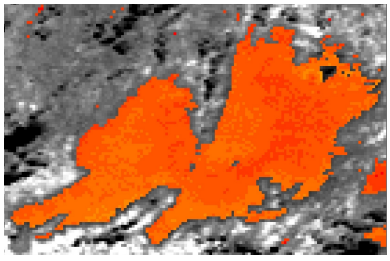

3 September

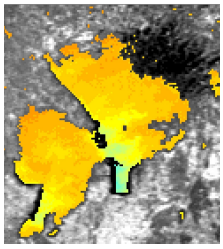

9 September

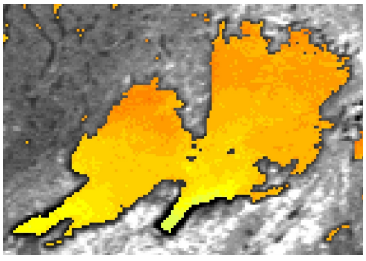

SPATIAL VARIABILITY OF TEMPERATURE IN 2002 – Lake Vättern

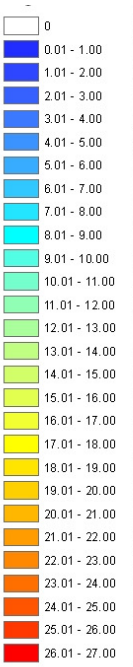

17 April

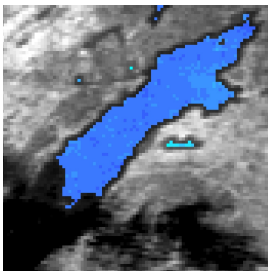

13 May

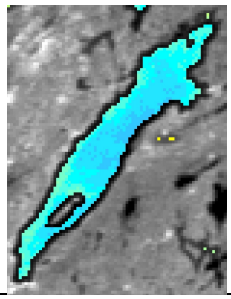

18 June

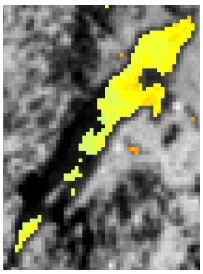

15 July

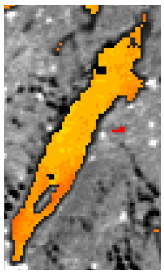

19 August (11:47 a.m.)

19 August (12:17 p.m.)

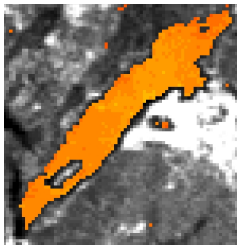

26 August

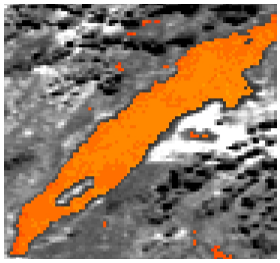

3 September

9 September

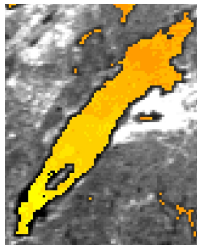

SPATIAL VARIABILITY OF TEMPERATURE IN 2003 – Lake Vättern

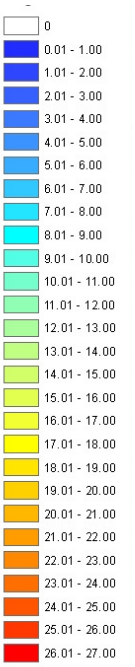

8 April	14 April
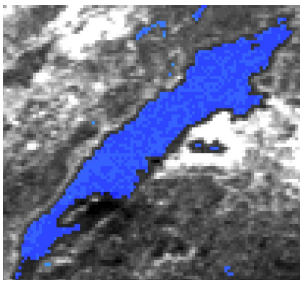	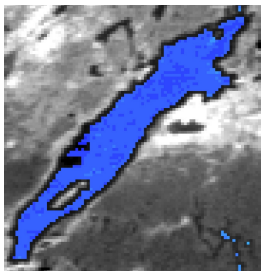
2 June	
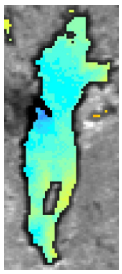	
9 July	10 July
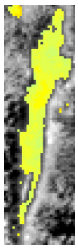	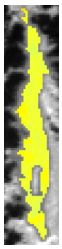
16 July	12 August
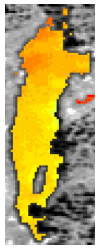	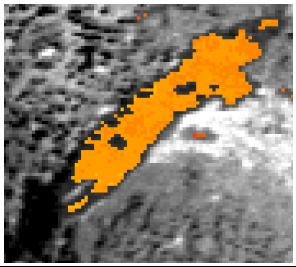
8 September	13 October
	

SPATIAL VARIABILITY OF TEMPERATURE IN 2002 – Lake Balaton

11 February

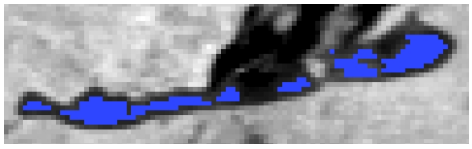

4 March

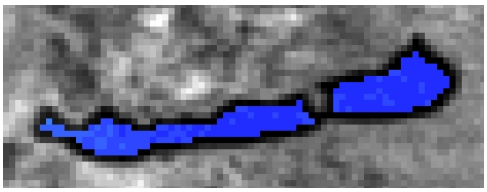

13 May

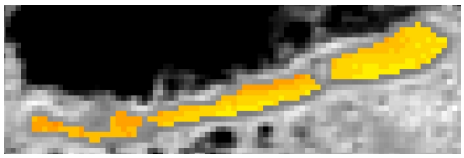

27 June

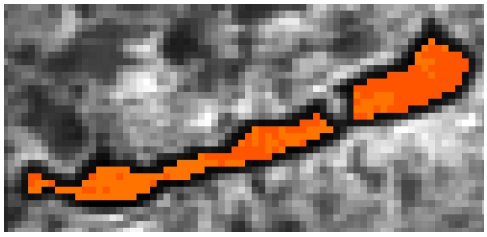

1 July

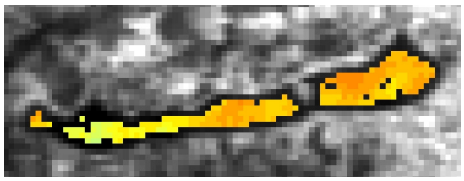

8 July

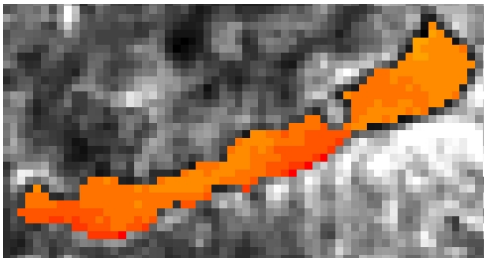

15 July

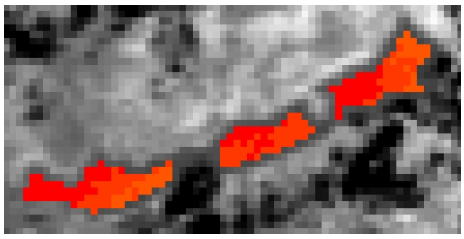

27 August

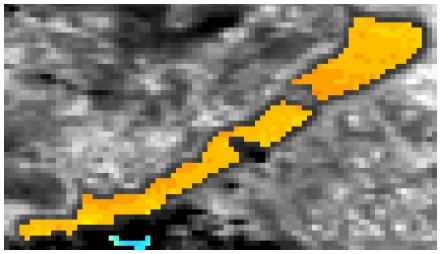

9 September

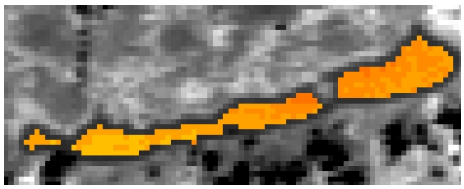

30 September

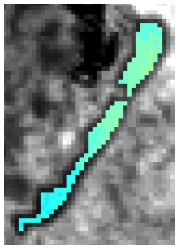

SPATIAL VARIABILITY OF TEMPERATURE IN 2001 – Lake Inarijärvi

26 June

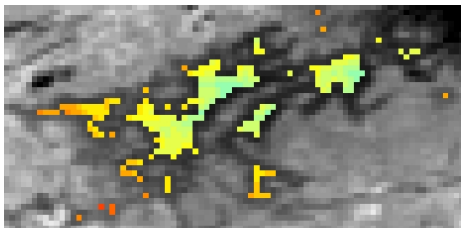

7 August

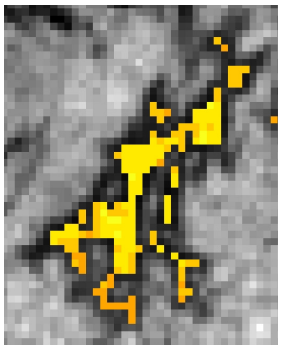

22 August

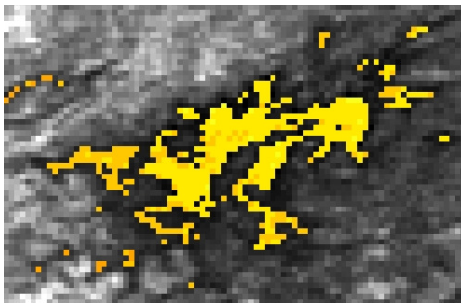

29 August

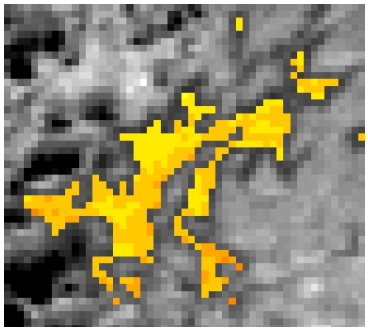

SPATIAL VARIABILITY OF TEMPERATURE IN 2001 – Lake Pielinen

8 May	16 May
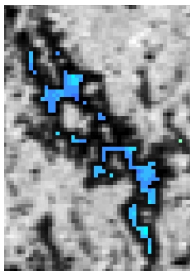	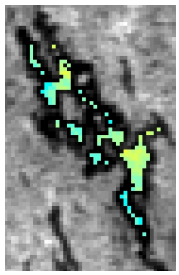
18 June	25 June
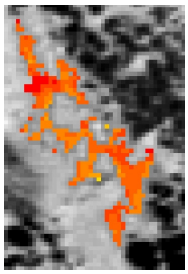	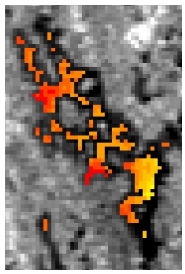
20 August	22 August
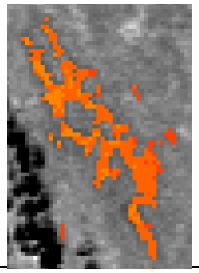	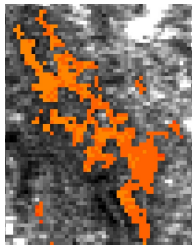
27 August	
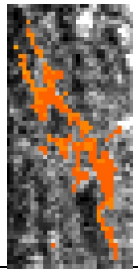	
17 September	20 September